ΠΑΝΕΠΙΣΤΗΜΙΟ ΚΡΗΤΗΣ-ΙΑΤΡΙΚΗ ΣΧΟΛΗ

ΜΕΤΑΠΤΥΧΙΑΚΟ ΠΡΟΓΡΑΜΜΑ ΚΥΤΤΑΡΙΚΗ ΚΑΙ ΓΕΝΕΤΙΚΗ ΑΙΤΙΟΛΟΓΙΑ, ΔΙΑΓΝΩΣΤΙΚΗ ΚΑΙ ΘΕΡΑΠΕΥΤΙΚΗ ΤΩΝ ΑΣΘΕΝΕΙΩΝ ΤΟΥ ΑΝΘΡΩΠΟΥ

ΔΙΔΑΚΤΟΡΙΚΗ ΔΙΑΤΡΙΒΗ

Ο ΡΟΛΟΣ ΤΟΥ ΣΗΜΑΤΟΔΟΤΙΚΟΥ ΜΟΝΟΠΑΤΙΟΥ WNT (WNT SIGNALING PATHWAY) ΣΤΗ ΡΥΘΜΙΣΗ ΤΟΥ ΠΟΛΛΑΠΛΑΣΙΑΣΜΟΥ ΚΑΙ ΤΗΣ ΚΑΡΔΙΟΜΥΟΓΕΝΟΥΣ ΔΙΑΦΟΡΟΠΟΙΗΣΗΣ ΤΩΝ ΚΑΡΔΙΑΚΩΝ ΚΥΤΤΑΡΩΝ SP (CARDIAC SIDE POPULATION CELLS)

ΟΙΚΟΝΟΜΟΠΟΥΛΟΣ ΑΓΓΕΛΟΣ

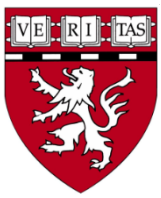

ΑΠΡΙΛΙΟΣ 2011

UNIVERSITY OF CRETE-SCHOOL OF MEDICINE

GRADUATE PROGRAM IN

CELLULAR AND GENETIC ETIOLOGY, DIAGNOSIS

AND TREATMENT OF HUMAN DISEASE

PhD THESIS

THE ROLE OF WNT SIGNALING IN THE REGULATION OF THE PROLIFERATION CAPACITY AND THE CARDIOMYOGENIC DIFFERENTIATION OF CARDIAC SIDE POPULATION CELLS (CSP CELLS).

OIKONOMOPOULOS ANGELOS

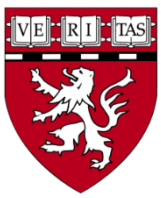

APRIL 2011

Acknowledgments

I am more than thankful to Dr. Ronglih Liao for her exceptional mentorship and guidance through a fantastic journey!

I am in debt to Dr. Vasilis Zannis for opening the door to a new world!

I am obliged to all lab members of CMRL and especially to Otmar for their valuable help!

My deepest thanks to Kostianna for her unconditional love, help, support and caring that were of vital importance from the beginning until now!!!!

There are no words to express my respect and gratitude to my parents and my siblings, Katerina and George, for their pure love and their encouragement!

Ευχαριστίες

Είμαι περισσότερο από ευγνώμων στην Δρ. Ronglih Liao για την εξαιρετική καθοδήγηση σε αυτό το φανταστικό ταξίδι!

Ευχαριστώ βαθύτατα τον Δρ. Βασίλη Ζαννή για το άνοιγμα της πόρτας σε ένα νέο κόσμο!

Θερμές ευχαριστίες σε όλα τα μέλη του εργαστηρίου της Δρ. Ronglih Liao και ειδικά στον Otmar, για την πολύτιμη βοήθειά τους!

Ιδιαίτερες ευχαριστίες στην Κωστιάννα μου, για την ανιδιοτελή και αστείρευτη αγάπη της, τη βοήθεια της, την υποστήριξη της και τη φροντίδα της, που ήταν ζωτικής σημασίας από την αρχή μέχρι τώρα!!!!

Δεν υπάρχουν λόγια να εκφράσω το σεβασμό και την ευγνωμοσύνη μου στους γονείς μου και τα αδέλφια μου, Κατερίνα και Γιώργο, για την αγνή αγάπη τους και την ενθάρρυνση τους σε κάθε μου βήμα μέχρι τώρα!

Στους γονείς μου

Contents

1. Περίληψη

Μέχρι πρόσφατα η καρδιά ενηλίκων ατόμων θεωρούνταν ως ένα μετα-μιτωτικό, τελικώς διαφοροποιημένο όργανο, χωρίς καμία ικανότητα αντικατάστασης κατεστραμμένων ή γερασμένων καρδιομυοκυττάρων. Η εύρεση ενδογενών καρδιακών αρχέγονων/πρόδρομων κυττάρων σε ενήλικα άτομα αμφισβήτησε την ανωτέρω θεωρία και ανέδειξε την ικανότητα αυτο-ανανέωσης του ενήλικου μυοκάρδιου. Ωστόσο, τα ενήλικα καρδιακά πρόδρομα κύτταρα είναι ανεπαρκή για την επισκευή του σοβαρώς τραυματισμένου μυοκαρδίου, ύστερα από έμφραγμα. Έτσι, η επιδίωξη ανεύρεσης του βέλτιστου τύπου καρδιακών πρόδρομων κυττάρων, καθώς επίσης και η προσπάθεια για την πλήρη κατανόηση των μοριακών και κυτταρικών γεγονότων που ρυθμίζουν τη μοίρα τους βρίσκονται σε εξέλιξη.

Ανάμεσα στα διάφορα καρδιακά πρόδρομα κύτταρα, τα κύτταρα του πλευρικού πληθυσμού (CSPs) αποτελούν μια ενδογενή δεξαμενή πρόδρομων κυττάρων. Τα κύτταρα CSPs προσδιορίζονται με βάση τη χαρακτηριστική ικανότητά τους να εκκρίνουν τη χρωστική Hoechst 33342. Η ικανότητα αυτή οφείλεται στη λειτουργία δύο ABC-μεταφορέων, του Abcg-2 (Bcrp-1) και του Abcb-1 (Π-γλυκοπρωτεΐνη), των οποίων η λειτουργία εξαρτάται εκτός των άλλων και από την ηλικία του ατόμου. Τα κύτταρα CSPs είναι καλλιεργίσιμα *in vitro* και μπορούν να διαφοροποιηθούν σε λειτουργικά καρδιομυοκύτταρα τόσο σε *in vitro* όσο και σε *in vivo* συνθήκες.

Στον άνθρωπο και το ποντίκι, οι πρωτεΐνες Wnt συνιστούν μια οικογένεια 19 εκκρινόμενων γλυκοπρωτεϊνών που λειτουργούν ως βασικοί ρυθμιστές διαφόρων λειτουργιών του οργανισμού κατά την ανάπτυξη, την ενήλικη ζωή και την εξέλιξη διοφόρων ασθενειών. Οι

πρωτεΐνες Wnt αλληλεπιδρούν με τους υποδοχείς Frizzled (Fzd) και τους συν-υποδοχείς LRP προκαλώντας τη μετατόπιση της β-κατενίνης στον πυρήνα, μέσω της ανασταλτικής δράσης της κινάσης GSK-3β. Η συσσώρευση της β-κατενίνης στον πυρήνα προκαλεί τη μεταγραφική ενεργοποίηση πολλών γονιδίων-στόχων, μέσω της δράσης των μεταγραφικών παραγόντων LEF/TCF. Πολλά στοιχεία δείχνουν ότι το σηματοδοτικό μονοπάτι Wnt διαδραματίζει σημαντικό ρόλο στην καρδιακή ανάπτυξη, με χρόνο-εξαρτώμενο τρόπο. Το σηματοδοτικό μονοπάτι Wnt είναι ενεργοποιημένο στο ισχαιμικό μυοκάρδιο ύστερα από έμφραγμα και αυτό είναι κρίσιμο για την ανάκαμψη της καρδιάς. Επιπλέον, ορισμένες νέες μελέτες εμπλέκουν το σηματοδοτικό μονοπάτι Wnt στην καρδιακή αναδιαμόρφωση ύστερα από ισχαιμικά επεισόδια. Επιπρόσθετα, σε ένα μοντέλο καρδιακής υπερτροφίας, αυξημένα επίπεδα β-κατενίνης βρέθηκαν εντοπισμένα στους παρένθετους δίσκους (intercalated discs) των καρδιομυοκυττάρων. Τέλος, το μονοπάτι Wnt έχει έναν πολύ καλά καθιερωμένο ρόλο ως βασικός ρυθμιστής της αυτο-ανανέωσης, του πολλαπλασιασμού και της διαφοροποίησης των εμβρυϊκών βλαστικών κυττάρων αλλά και των διαφόρων τύπων ενήλικων βλαστικών κυττάρων. Παρά την αποδεδειγμένη συμμετοχή των πρωτεϊνών Wnt στην καρδιακή ανάπτυξη, ο ρόλος τους στην ομοιόσταση των ενηλίκων καρδιακών πρόδρομων κυττάρων παραμένει άγνωστος. Ο στόχος της παρούσας μελέτης είναι να διερευνηθεί ο ρόλος του μονοπατιού Wnt στα κύτταρα CSPs.

Τα κύτταρα CSPs απομονώθηκαν από αρσενικά ποντίκια και καλλιεργήθηκαν σε *in vitro* συνθήκες και κατόπιν υποβλήθηκαν σε διάφορους πειραματικούς ελέγχους για να εξακριβωθούν οι επιπτώσεις των πρωτεϊνών Wnt στον πολλαπλασιασμό, τη διαφοροποίηση τους και την επιβίωση τους. Τα επίπεδα ενεργοποίησης του μονοπατιού Wnt στα κύτταρα CSPs μετρήθηκαν με ένα ειδικό σύστημα αναφοράς, το οποίο βασίζεται στην έκφραση λουσιφεράσης υπό τον

έλεγχο των μεταγραφικών παραγόντων LEF/TCF. Η ικανότητα πολλαπλασιασμού των κυττάρων CSPs ελέγχθηκε με συγκρίσεις αύξησης σε *in vitro* συνθήκες, με συγκρίσεις ενσωμάτωσης BrdU και με ανοσοκυτταροχημική ανίχνευση της p-H3, ύστερα από χορήγηση πρωτεΐνης Wnt3a καθώς και άλλων ρυθμιστών του μονοπατιού Wnt. Οι πιθανοί μεσολαβητές των επιπτώσεων του μονοπατιού Wnt στα κύτταρα CSPs, διερευνήθηκαν μέσω μιας προσέγγισης κέρδους και απώλειας λειτουργίας της πρωτεΐνης IGFBP3 (δεσμευτική πρωτεΐνη αυξητικού παράγοντα ινσουλίνης 3). Επιπλέον, οι *in vivo* επιπτώσεις των πρωτεϊνών Wnt στα κύτταρα CSPs, αξιολογήθηκαν μέσω κυτταρομετρίας ροής, ύστερα από ενδο-μυϊκή ένεση πρωτεΐνης Wnt3a στο τοίχωμα της αριστερής κοιλίας της καρδιάς. Τέλος, οι επιδράσεις του μονοπατιού Wnt στην καρδιακή λειτουργία αξιολογήθηκαν σε θηλυκά ποντίκια μέσω υπερηχοκαρδιογραφήματος, μετά από έμφραγμα του μυοκαρδίου (MI) και ενδο-μυϊκή ένεση της πρωτεΐνης Wnt3a στο τοίχωμα της αριστερής κοιλίας.

Στη διατριβή μου, παρέχονται στοιχεία που δείχνουν ότι το σηματοδοτικό μονοπάτι Wnt είναι απενεργοποιημένο στα κύτταρα CSPs ύστερα από έμφραγμα του μυοκαρδίου. Σε *in vitro* συνθήκες η ενεργοποίηση του σηματοδοτικού μονοπατιού Wnt μειώνει την αύξηση και τον πολλαπλασιασμό των κυττάρων CSPs. Η χορήγηση πρωτεΐνης Wnt *in vivo*, μείωσε τον αριθμό των κυττάρων CSPs, μιμούμενη τη δράση της στις *in vitro* συνθήκες. Η ενεργοποίηση του μονοπατιού Wnt στα κύτταρα CSPs, άλλαξε τα επίπεδα έκφρασης διαφόρων γνωστών ρυθμιστών του κυτταρικού κύκλου, προκαλώντας σημαντική καθυστέρηση της ολοκλήρωσης του. Επιπλέον, το μονοπάτι Wnt προκαλεί αύξηση των αποπτωτικών και μη-αποπτωτικών (νεκρωτικά) κυττάρων CSPs. Η αντι-αυξητικές επιδράσεις του σηματοδοτικού μονοπατιού Wnt στα κύτταρα CSPs διαμεσολαβούνται από την πρωτεΐνη IGFBP3. Η αυξημένη έκφραση της

πρωτεΐνης IGFBP3 μειώνει τον πολλαπλασιασμό των κυττάρων CSPs. Επιπρόσθετα, η μείωση της έκφρασης της πρωτεΐνης IGFBP3 διάσωσε την αυξηση των κυττάρων CSPs. Επίσης, παρουσιάζονται αποτελέσματα που αποδεικνύουν ότι το μονοπάτι Wnt επιδεινώνει την καρδιακή απόδοση και λειτουργία μετά από έμφραγμα του μυοκαρδίου. Η χορήγηση της πρωτεΐνης Wnt3a στην καρδιά ύστερα από επαγώγη πειραματικού εμφράγματος σε ποντίκια, αυξάνει την αναλογία του καρδιακού βάρους προς το σωματικό βάρος (στοιχείο που υποδηλώνει καρδιακή υπερτροφία), αυξάνει τις διαστάσεις της αριστερής κοιλίας, αυξάνει το πάχος του καρδικού τοιχώματος ενώ παράλληλα μειώνει την καρδιακή συστολή (cardiac contractility) και το κλάσμα εξώθησης (cardiac output).

Συνοπτικά, η παρούσα διατριβή αποκαλύπτει έναν προηγουμένως άγνωστο αντι-αυξητικό ρόλο του σηματοδοτικού μονοπατιού Wnt στα κύτταρα CSPs, καθώς επίσης έναν μη-προστατευτικό ρόλο στην καρδιακή λειτουργία κατόπιν ισχαιμικής βλάβης. Οπότε, η αναστολή της δράσης του μονοπατιού Wnt ύστερα από καρδιακή προσβολή (έμφραγμα) αντιπροσωπεύει μια ελκυστική κατεύθυνση για μελλοντικές μελέτες στον τομέα της καρδιακής θεραπείας και καρδιακής αναγέννησης.

2. Summary

Until recently the adult heart was considered as a post-mitotic terminally differentiated organ without any capacity to replace damaged or aged cardiomyocytes. The identification of endogenous adult cardiac stem/progenitor cells challenged the above concept and emphasized the self-renewal ability of post-natal myocardium. However, adult cardiac stem cells are

inadequate to repair the extensively damaged myocardium following a severe injury such as myocardial infarction. Thus, the pursuit for the optimal type of cardiac stem/progenitor cell as well as for fully understanding of the molecular and cellular events that regulate their fate is currently ongoing.

Among various cardiac stem/progenitor cells, side population cells (CSPs) represent an endogenous pool of precursors in the heart. CSPs are identified based on their characteristic ability to efflux the DNA binding dye Hoechst 33342 due to the age-dependent function of two ABC-transporters, Abcg-2 (Bcrp-1) and Abcb-1 (P-glycoprotein). CSPs are expandable *in vitro* and capable of differentiating into functional cardiomyocytes both *in vitro* and *in vivo*.

In human and mouse, Wnt proteins constitute a family of 19 secreted glycoproteins that act as key regulators in crucial functions during development, adult life and disease progression. Wnt ligands bind to Frizzled (Fzd) and low-density lipoprotein receptor (LRP) co-receptor complexes and lead to nuclear translocation of β-catenin through inhibition of GSK-3β kinase. Accumulation of β-catenin in the nucleus results in transcriptional activation of numerous target genes, through the action of transcription factors LEF/TCF.

Several lines of evidence support that Wnt signaling plays an important role in cardiac development and specification in a time dependent manner. Moreover, a number of emerging studies implicate Wnt signaling pathway in post-MI cardiac remodeling. Wnt signaling pathway is up regulated in the infracted myocardium and this is crucial for its recovery following injury. In a cardiac hypertrophy model, β-catenin was shown to be enriched in the intercalated discs of cardiomyocytes. Finally, canonical Wnt signaling pathway has a well-established role as a key regulator of the self-renewal ability, the proliferation and cell fate decisions of embryonic and

various types of adult stem cells. Despite the well-established implication of Wnt signaling in cardiac development, its role in the homeostasis of adult cardiac progenitor cells remains largely unknown. The goal of the current study is to investigate the role of canonical Wnt signaling pathway in CSP cells.

CSP cells were isolated from male mice and were cultured *in vitro* in expansion medium. They were treated with various ways to test the effects of Wnt signaling on their proliferation and differentiation. The activation status of the Wnt signaling pathway in CSPs was monitored by a lentivirus-based Wnt-reporter assay. Their proliferation capacity was tested with growth assays, with BrdU incorporation studies and with immunocytochemical detection of p-H3, following administration of purified Wnt3a protein and other manipulators of Wnt signaling. I utilized a gain and loss of function approach to investigate the role of potential mediators of the Wnt effects on the CSP cells. Moreover, the *in vivo* effects of Wnt signaling on the CSP cells were assessed through flow cytometric analysis following intra-myocardial injection of Wnt3a protein. Finally, the effects of Wnt signaling pathway on cardiac performance were assessed in female mice by echocardiography, following myocardial infarction (MI) and intra-myocardial injection of Wnt3a protein.

Herein, I provide evidence that Wnt signaling pathway is down-regulated in CSP cells in post-MI myocardium. Moreover, activation of the canonical Wnt signaling pathway decreases the growth and proliferation of CSPs. Administration of Wnt ligands *in vivo* decreased the amount of CSP cells, mimicking its own *in vitro* effects. Wnt signaling alters the expression of various well known cell cycle regulators resulting in cell cycle delay. Furthermore, Wnt signaling promotes apoptotic and non-apoptotic (necrotic) cell death in CSP cells *in vitro.* The

anti-proliferative effects of canonical Wnt signaling on CSP cells are mediated by IGFBP3 (insulin growth factor binding protein 3). Over-expression of IGFBP3 decreases the proliferation of CSPs, similarly to activation of Wnt pathway. Sh-RNA-mediated down-regulation of IGFBP3 rescues CSP cells from the anti-proliferative effects of Wnt signaling. Finally, I found that Wnt signaling deteriorates cardiac performance following myocardial infarction by altering various parameters of the cardiac architecture. Administration of Wnt3a protein in post-MI heart increased the heart weight-body weight ratio, increased left ventricular chamber dimension, wall thickness while decreasing cardiac fractional shortening and ejection fraction.

In summary, my work reveals a previously unidentified anti-proliferative role of Wnt signaling pathway in CSP cells. Moreover, I present data showing that Wnt signaling plays a deleterious role in post-MI cardiac remodeling. Thus, Wnt inhibition following ischemic cardiac injury represents an attractive direction for future studies in the field of cardiac regeneration.

3. Introduction

1. Cardiovascular diseases

The heart is an extremely efficient organ that pumps blood to sustain the metabolic needs of all tissues throughout the lifetime of an individual. In humans, the heart pumps over 6000 liters of blood, which supplies the tissues with necessary oxygen and nutrients and removes the waste products of catabolism. As expected, any major disturbance of cardiac function has a profound impact on the quality of life of an individual. Cardiovascular diseases (CVD) represent a major health problem in the industrialized world and especially in the United States. In the United States approximately 1 in 3 adults has 1 or more types of CVD [1]. Approximately 73 million adults have high blood pressure (HPD), 17 million have coronary heart disease (CHD), 8 million have suffered myocardial infarction (MI), 6 million have been diagnosed with heart failure (HF) and 0.65 to 1.3 million have some form of congenital defect [1]. In the United States, CVD represent the most common cause of death, as since 1900 (only the year of 1918 was an exception) they account for more deaths than any other major cause of death (56%) [1]. As a result the total, direct and indirect, cost of CVD in the United States, during 2009 emerged to 475 billion dollars [1]. According to latest available data, the death rate (per 100,000 individuals) related to CVD in the United States in 2009 for men and women, between the ages of 35 and 74, was 908 and 572 respectively. In Greece, in 2004 the respective numbers were 778 and 354 for men and women respectively [1].

2. Myocardial infarction and heart failure

Myocardial infarction, also known as heart attack, refers to the loss of cardiac tissue resulting from ischemia due to an occlusion of a major coronary artery. Myocardial infarction among other CVD such as hypertension, coronary heart disease, cardiomyopathies and congenital heart defects may lead to a pathological condition termed heart failure (HF). Heart failure is a clinical syndrome defined by the inability of the cardiac muscle to supply adequately the metabolic needs of all tissues. Although the etiology of heart failure is heterogeneous, this condition happens when the heart needs to pump against a very high resistance or due to a significant loss of heart muscle strength [2].

An initial diverse pathologic stimulus compromises the pumping capacity of the cardiac muscle. Subsequently, a set of compensatory responses including activation of the adrenergic nervous system, the renin-angiotensin system and numerous hypertrophic signaling cascades, is activated in order to restore the cardiac output to normal levels. All the changes in the organ geometry and the architecture of the myocardium as well as a series of cellular and molecular events, induced by the compensatory mechanisms, are generally known as cardiac remodeling. In case that the magnitude of the initial pathologic stimulus cannot be balanced by these compensatory mechanisms, there is further decline in cardiac performance, which will be followed by further potentiating of the compensatory mechanisms [3, 4]. The above events represent a vicious cycle that leads in further cardiac remodeling and eventually in heart failure and cardiac arrest (Figure 1).

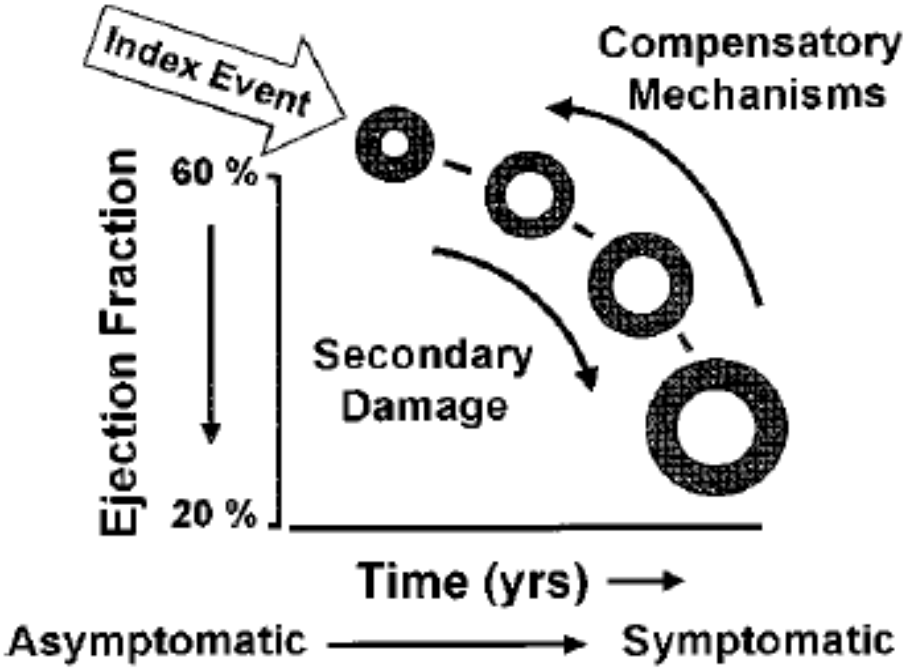

Figure 1: Schematic representation of heart failure progression. Adapted from Mann *et al,* Circulation 1999; 100:999

Recent advances in clinical assessment and management of heart failure have increased the lifespan and the quality of life of the patients. At early stages of heart failure the main therapeutic goal is the interception and the reversion of the deleterious cardiac remodeling. Various agents such as β-blockers [5], angiotensin-converting-enzyme (ACE) inhibitors, angiotensin-receptor antagonists and diuretics have been used toward this goal with considerably successful results [6]. At later stages of the disease, interventional therapeutic methods are applied, such as utilization of left ventricle assisting devices. However, despite the available therapeutic methods, patient mortality remains high [1]. Most importantly, the above pharmacological approaches do not address the primary problem associated with heart failure, which is the loss of cardiomyocytes. Currently, only heart transplantation resolves permanently

the issue of cardiomyocyte loss. Nevertheless, the shortage of donor hearts and problems related to immune rejection limit the use of this therapeutic option. Novel therapeutic strategies targeting the basis of heart failure are needed more than ever. Identification of exogenous and endogenous cardiac stem cells have emerged as promising alternative tools, in the design of cell therapy approaches for cardiac regeneration.

3. Evidence of cardiomyocyte proliferation in the adult heart

Until recently, in the cardiology field, the prevailing theory about cardiomyocyte growth was that their proliferation ceases shortly after birth. According to this model cardiomyocytes exit permanently the cell cycle and the only widely accepted way of cardiac growth is through increase in cell size (hypertrophy), and not through increase of cell number (hyperplasia) [7].

The above theory was largely based on DNA synthesis studies performed in rodents, with either BrdU or autoradiographic analysis of H^3-thymidine incorporation assays [8-10]. Soonpaa *et al* demonstrated that during mouse embryonic development the cardiomyocyte DNA synthesis index is profoundly increased and synthesis of new DNA is not linked to binucleation but to myocyte proliferation. This increased DNA synthesis rate drops gradually to undetectable levels until shortly after birth. At post-natal day 4 and until post-natal day 10 there is a second wave of DNA synthesis which is not linked to cardiomyocyte proliferation but binucleation. At post-natal day 10 and later there is no detectable DNA synthesis in cardiomyocytes [9]. Another study from the same group examined the amount of DNA synthesis in normal and injured myocardium. Measurement of H^3-thymidine incorporation revealed that the proliferation index in homeostatic conditions was approximately 0.0006% and following injury 0.008% [8]. The

above studies established the concept that the adult heart lacks any self-renewal ability and that the prevalent growth mechanism of cardiomyocytes is through hypertrophy.

Conversely, several studies of cardiomyocyte proliferation in rat hearts demonstrate considerable differences regarding the amount of DNA synthesis in adult cardiomyocytes. Different groups reported that in the rat myocardium approximately 0.2% [11], 0.45% [12], 0.70% [13], and 2.0% [14] of adult cardiomyocytes incorporated H^3-thymidine under normal or pathologic conditions. The above data suggest that in the adult rat heart, in contrast to the mouse heart, there is a considerable amount of newly synthesized DNA in post-natal cardiomyocytes. The observed differences between mice and rats could be species-dependent or they could be attributed to differences in technical and experimental approaches. Overall, these data challenge the concept of permanent inability of cardiomyocyte proliferation.

Additional evidence challenging this dogma derived from studies demonstrating mitotic figures in the nucleus of adult cardiomyocytes. Surprisingly enough, some of the earliest images of mitotic figures in the nucleus of cardiomyocytes were presented by Ring *et al* in 1950 and by Overy *et al* in 1966 (Figure 2) [15, 16]. Since then additional reports have illustrated similar images of cardiomyocytes not only residing in mitosis [10] but also undergoing cytokinesis [17]. The identification of proliferating cardiomyocytes in the adult heart (even in relatively low amount), in various species, clearly suggests that hypertrophy is not the only cardiac growth mechanism in adult organisms. Hyperplasia, the generation of new myocytes during the post-natal life of an individual, is also present and it can be studied further as it might hold therapeutic applications.

Figure 2: Mitotic figures of cardiomyocytes following ischemic cardiac injury, as documented 60 years ago. Adapted from Ring *et al*. J Pathol Bacteriol. 1950 Jan; 62(1):21-7.

4. Cardiomyocyte turn-over in the adult heart

In recent years, several elegant studies provided more evidence about the generation of new cardiomyocytes in the adult heart. Muller *et al* , using in-situ hybridization with specific probes for X and Y chromosomes, examined 21 biopsies from 13 male heart transplant recipients who received organs from female donors [18]. Totally 31.787 cardiomyocytes were examined and 0.16±0.04 % were found to be of recipient origin. The host derived cardiomyocytes were connected with gap junctions with the adjacent cardiomyocytes. Host-derived endothelial and smooth muscle cells were identified as well. Similar results were obtained by additional studies

[19-21]. However, there is a degree of uncertainty about the level of chimerism following cardiac transplantation. Glacer *et al* reported the existence of only vascular smooth muscle cells of host origin in human cardiac sex-mismatched transplants but no evidence of host-derived cardiomyocytes was provided [22]. Overall, the above data strongly imply that in the adult human heart there is a continuing process of formation of new cardiomyocytes and furthermore that there is a non-cardiac source of cells with the ability to give rise to all cardiac cell lineages.

The regenerative capacity of human and mouse adult heart under homeostatic conditions was confirmed by fate mapping studies. Bergmann *et al* estimated the mean age of the human cardiomyocytes in comparison to the actual age of the individual by taking advantage of the incorporated C^{14} in the DNA of the cells during the Cold War [23]. In unsorted nuclei (containing myocytes and non-myocytes) Bergmann *et al* demonstrated that the mean age of the heart's DNA was significantly younger than the individual itself. The DNA of the non-myocyte nuclei was substantially younger than the individual but more importantly the DNA of cardiomyocyte nuclei was also significantly younger than the actual age of the corresponding person. By excluding bi-nucleation or poly-nucleation as possible explanations of the observed differences Bergmann *et al* were able to convincingly demonstrate that there is a constant age-dependent turnover of the population of cardiomyocytes. The turnover rate is approximately 1% at the age of 20 and it progressively declines to 0.4% at the age of 75. According to this model at the age of 50, 55% of cardiomyocytes would be present from birth but 45% would have been created after birth.

Similarly, in a more recent study, Kajstura *et al,* confirmed the formation of new cardiomyocytes in the adult human heart and showed that cardiac cells (myocytes and non-

myocytes) are replaced several times during the lifetime of an individual [24]. Kajstura *et al* took advantage of the infusion of a radio-sensitizer iododeoxyuridine (IdU) in 8 cancer patients. IdU is a nucleotide-analog that is rapidly incorporated in all cycling cells and it can be used as a tool for measuring myocyte formation over time. Immuno-histochemical examination of heart samples from 8 cancer patients revealed that the fraction of IdU^+ myocytes varied from 2.5% to 46% (24% on average) in all 8 patients. Moreover, the authors demonstrated that the percentage of IdU-labeled fibroblasts was similar to that of myocytes whereas the fraction of labeled endothelial cells was 33% less compared to myocytes. By inference, an average of 22%, 20% and 13% of new myocytes, fibroblasts and endothelial cells respectively were generated per year in the hearts of the examined patients. Correspondingly, the average lifespan of these three major cardiac cell types was 4.5, 5 and 8 years, respectively. A critical point in this study is that all examined cancer patients experienced cardiac problems, which as previously documented can contribute to the amount of new myocyte formation [25]. Thus, examination of heart tissue derived from healthy donors for the presence of cycling ($Ki67^+$ and phospho-Histone $H3^+$) myocytes showed a significantly lower proliferation index. Conclusively, the above study suggests that the adult heart possesses substantial self-renewal capacity under homeostatic conditions which is enhanced by cardiac pathology like hypertrophy and heart failure.

Overall the above data represent pioneer studies that clearly demonstrate that the adult heart can no longer be viewed as a terminally differentiated organ with limited myocyte turn-over. The old dogma needs to be re-evaluated under the light of the new emerging evidence about continuous replacement of adult cardiomyocytes. Furthermore, the identification of exogenous but mainly endogenous cardiac stem/progenitor cells in the adult myocardium further

intensifies the concept that the heart possesses considerable self-renewal ability, which was previously underestimated.

5. Stem and progenitor cells

A generally accepted definition of stem cells describes them as a special cell type with the capacity to self-renew and the ability to give rise to more committed daughter cells [26, 27]. Extensive efforts have been focused on the identification of a common molecular program that controls the properties of different types of stem cells. However, until today all studies have demonstrated that there is not a universal set of genes that regulates stemness, and this unique property is regulated by rather the specific combination of numerous genes [26, 28-30]. In various organisms, stem cells reside in special microenvironments called stem cell niches [31]. The term microenvironment refers to the structural components (stem cells and supporting cells) of the niche as well as to the molecular signals derived from these cellular components [31]. The role of stem cells during development is the formation of the various tissues and organs and during adulthood their preservation through replenishment of the damaged cells.

Stem cells in embryos as well as in the adult organism can be classified according to a hierarchy model. The zygote and the descendants from the first two divisions are on top of the hierarchy. These cells can give rise to the entire embryo as well as the trophoblasts of the placenta and are thus called totipotent. Totipotent cells differentiate towards a less potent class of stem cells, which is composed of cells forming the blastocyst and a cluster of cells forming the inner cell mass (ICM). ICM cells are considered pluripotent since they are able to give rise to

cells from all the germ layers. The first and the second class of stem cells represent the so-called embryonic stem cells (ESCs) [27].

Adult stem/progenitor cells are found lower in the stem cell hierarchy model and are considered as multipotent since they can differentiate into a more limited number of cell types, depending on the tissue of origin. For example, neural stem cells demonstrate a tri-lineage differentiation capacity generating precursors of neurons, oligodendrocytes and astrocytes [32]. However, mesenchymal stem cells (MSCs) are an exception as they are able to generate cells from all three germ layers [33]. At the bottom of the hierarchy model are all the stem cells with unipotent differentiation ability. In other words, this last class of stem cells includes cells committed towards a specific cell type [34].

6. The adult heart houses endogenous stem/progenitor cells

In parallel with the sex-mismatched heart transplantation studies there have been intensive efforts in order to identify a previously unknown type of cell, the cardiac stem/progenitor cell. The newly formed myocytes, described in the mouse fate mapping studies [25] or in the human C^{14} studies [23], can either derive from the proliferation of pre-existing myocytes or by the action of exogenous or endogenous cardiac precursors.

In an elegant study, Hsieh *et al* utilized an *in vivo* inducible cardiomyocyte-specific fate-mapping approach to examine the turn-over of myocytes in adult mice. Hsieh *et al* generated a double transgenic mouse, MerCreMer-ZEG, by crossbreeding MerCreMer mice, in which the cardiomyocyte-specific α-myosin heavy chain (Myh6) promoter drives expression of a 4-OH tamoxifen- inducible Cre-recombinase, with ZEG reporter mice, in which constitutive β-

galactosidase expression is replaced by the expression of GFP upon the removal of a lox-P-flanked stop sequence. Thus, treatment with tamoxifen at any time irreversibly marks almost all cardiomyocytes with GFP expression. Using this mouse, Hsieh *et al* studied the formation of new myocytes during normal aging and following cardiac injury, under the prism that if there is generation of new myocytes the proportion of GFP^+ cardiomyocytes should be decreased. In the absence of injury (normal aging) the proportion of GFP^+ cardiomyocytes was found to be stable at various time points following the tamoxifen pulsing. However, in cardiac injury models (MI or pressure overload) the proportion of GFP^+ cardiomyocytes was found to be significantly lower in comparison to sham animals. Namely, following MI or pressure overload the fraction of GFP^+ cardiomyocytes was decreased from 82.8% in the myocardium of sham animals to 67.5% in areas adjacent to the MI, 76.6% in areas remote form the MI and 75.5% in myocardium subjected to pressure overload. The above results provide strong evidence that after a severe injury the population of adult cardiomyocytes can be replenished through the function of unknown stem or progenitor cells.

Until today, several different techniques have been applied in order to identify putative cardiac stem/progenitor cells. Although, no universal cardiac stem/progenitor cell marker has been identified, there are several well established protocols for the isolation of various cell populations that fulfill the criteria of self-renewal ability and differentiation capacity. All the endogenous cardiac stem/progenitor cell populations that have been identified in the myocardium of various organisms are described below.

7. C-kit$^+$ cardiac stem cells

Clusters of cells expressing the stem cell antigen c-kit were detected in the adult heart of several animal models (rat [35], mouse [36], dog [37]) as well as in human [38]. C-kit is a tyrosine kinase trans-membrane receptor which mediates signals through the PI3 kinase, the phospholipase C, the Src tyrosine kinase family and the $p21^{ras}$ GTP-activating protein [39]. C-kit$^+$ cardiac stem cells (CSCs) are localized in the intersticia among the cardiomyocytes with a higher density in the ventricular apex and the atria. C-kit$^+$ CSCs are negative for the expression of any lineage markers and they comprise a rather rare population (0.1%) in the adult myocardium. C-kit$^+$ CSCs are self-renewing, clonogenic and multipotent. Following appropriate stimulation c-kit$^+$ CSCs are able to differentiate *in vitro* into endothelial cells, smooth muscle cells and cardiomyocytes. Most importantly, c-kit$^+$ CSCs exhibit *in vivo* multipotent differentiation capacity. In a study by Beltrami *et al,* $2x10^5$ BrdU-labeled cells were injected in the infarct-border zone of rat myocardium following injury and their fate was tracked 10 and 20 days later [35]. A zone of BrdU$^+$ c-kit$^+$ CSCs were detected in the infarct area at both time points. The engrafted c-kit$^+$ CSCs appeared to express markers of mature cardiomyocytes, such as cardiac myosin heavy chain and connexin-43. Additionally, new vessels that incorporated the BrdU$^+$ c-kit$^+$ CSCs were detected in the regenerated myocardial area. Administration of c-kit$^+$ CSCs post-MI generated an estimated number of approximately $13x10^6$ new cardiomyocytes and subsequently it improved substantially cardiac performance, as was shown by echocardiography and hemodynamic studies. Similar results of cardiac regeneration following delivery of cardiac c-kit$^+$ cells have been reported by the same authors in several other publications [36-38].

A major advance in the field of cardiac regeneration was the identification of c-kit$^+$ CSCs in human surgical specimens [38]. Human derived c-kit$^+$ CSCs are self-renewing, clonogenic and multipotent *in vitro.* Three weeks following administration of human c-kit$^+$ CSCs to two rodent models of myocardial infarction, the engrafted cells formed chimeric rodent hearts. New cardiomyocytes, capillaries as well as arteries of human origin were detected in the rat hearts.

The identification of human c-kit$^+$ CSCs has been challenged by two recent reports. Pouly *et al* [40] reported the presence of very low numbers of c-kit$^+$ cells in various biopsies (~1 cell/mm^2). Moreover, these cells expressed the hematopoietic marker CD45. Differences among patients, biopsies and technical details could affect drastically the outcome of these experiments. Considering the potential benefits of such cells to heart failure patients, the identification and study of human c-kit$^+$ CSCs needs to be further pursued.

8. Sca-1 cells

Almost in parallel with the identification of c-kit$^+$ CSCs, a study by Oh *et al* [41] revealed the existence of Sca-1$^+$ (Stem Cell Antigen-1) progenitor cells in the adult mouse heart. Sca-1 is an 18-kDa mouse glycosyl-phosphatidylinositol-anchored cell surface protein (GPI-AP) of the Ly-6 antigen family. Although, Sca-1 is the most common marker of hematopoietic stem cells, it has been also involved in a wide variety of stem, progenitor and differentiated cells in various tissues [42]. Cardiac Sca1$^+$ cells are negative for the expression of markers of the hematopoietic lineage (CD45 and CD34) as well as for the c-kit antigen [41]. The cardiomyogenic differentiation capacity of cardiac Sca1$^+$ cells was confirmed under both *in vitro* and in *vivo* conditions. When Sca-1$^+$ cells were administered following MI they formed new

cardiomyocytes, via cell fusion dependent and independent mechanisms. In two additional reports by Wang *et al* [43] and Matsuura *et al* [44] the existence of cardiac Sca-1^+ progenitor cells was confirmed and their cardiomyogenic differentiation capacity was further demonstrated. More recently, Smits *et al* reported that the fetal and adult human heart contains a population of cardiomyocyte progenitor cells (CMPCs) that can be isolated based on the expression of the Sca-1 antigen [45]. Although the human homolog of Sca-1 has not been identified, Smits *et al* reported that utilization of murine Sca-1 antibody in human preparations leads to the isolation of a pure cell population, through probably cross-reaction with an unknown protein [45]. CMPCs can be isolated from human heart biopsies and they are readily expandable in culture. CMPCs can differentiate towards cardiomyocytes upon stimulation with 5-azacytidine or TGF [45]. Further studies are required to study CMPSs in more details and to assess their cardiac regeneration ability.

9. Cardiac Side Population cells (CSPs)

The first attempt to identify an endogenous multipotent cell population in the adult heart was carried out by Hierlihy *et al* [46] and consisted in examining whether the adult heart contains side population cells . Side population cells were originally found in bone marrow cell preparations, where they represent approximately 0.05% of the total mononuclear cells [47]. Bone marrow side population cells were found to be highly enriched in long-term repopulating hematopoietic stem cells [47]. Since then, the side population phenotype has been used as an alternative way to identify stem/progenitor cells especially in cases where there is not an established stem cell marker [48]. Until today, side population cells have been found in several

tissues like skeletal muscle, mammary gland, liver, lung, brain, retina and skin [48] and in most cases they represent a small fraction of cells enriched in stem or progenitor cells.

Hierlihy *et al* demonstrated that cardiac side population cells (CSP) comprise approximately 1% of the total cardiomyocyte-depleted mononuclear cardiac cells in an adult (8 weeks old) mouse. CSP cells do not express CD34, c-kit, Flk-2 or Thy-1.1, suggesting that they are immuno-phenotypicaly distinct from hematopoietic or skeletal muscle side population cells [46]. The authors demonstrated that CSPs possess the ability to form colonies in a methylcellulose media and when co-cultured with primary cardiomyocytes they exhibit cardiomyogenic potential, as shown by expression of connexin-43, a well-established cardiomyocyte marker [46]. Although, there is no information about the level of functional maturation (sarcomeric organization and contraction ability) of these CSP-derived cardiomyocytes [46], that was the first report suggesting that the SP phenotype can be utilized in order to identify putative cardiac precursor cells.

The existence of CSPs in the adult myocardium was subsequently reported by Martin *et al* [49]. In agreement with Hierlihy *et al*, CSP cells were negative for the expression of the hematopoietic markers CD34 and CD45 as well as the expression of the stem cell marker c-kit [49]. CSPs expressed Sca1 and approximately 10% of CSP cells were positive for the expression of the endothelial marker Tie-2 [49]. By co-culturing green fluorescence protein (GFP) expressing CSP cells with non GFP main population cells (MP), Martin *et al* detected expression of a-sarcomeric actinin in CSPs. However, the authors were unable to detect sarcomeric structures in the differentiated CSPs similarly to those reported by Hierlihy *et al*, which might suggest that the differentiation process was immature. CSP cells demonstrated high proliferation

capacity in methylcellulose medium [49], but as shown by Asakura *et al* they are unable to differentiate towards blood cell lineages [50].

Pfister *et al* [51] confirmed the existence of cardiac side population cells in the adult mouse heart (Figure 3a) and demonstrated their multipotent differentiation capacity. CSPs are expandable *in vitro* (Figure 3b) and able to differentiate into cardiomyocytes (Figure 3c-f) as well as into endothelial cells and smooth muscle cells ([51] and unpublished data). CSPs express 84±2% Sca1 and are negative for the expression of the hematopoietic markers CD34 and CD45 [51]. These results are in accordance with previous reports, establishing their non-hematopoietic phenotype. The cell adhesion molecule CD44 and the stem cell marker c-kit were also not detected in CSP cells. The absence of these markers in the protein level (not detected by FACS analysis) could be the result of proteolytic cleavage of the extra-cellular part of the proteins during the enzymatic digestion of the heart tissue [52]. Interestingly enough CSP cells express the stem cell marker c-kit in the mRNA level (unpublished data) and further experiments are required to examine its functional role. Several transcription factors such as Nkx2-5, MEF2C and GATA-4, which are required for cardiomyogenic differentiation [53, 54], were found to be expressed in CSPs [51]. A-actinin and α-myosin heavy chain (α-MHC) were not detectable confirming the undifferentiated status of freshly isolated CSP cells. CSP cells also express, in the mRNA level, smooth muscle actin (SMA) and desmin as well as the endothelial cell marker Tie-2 [51].

The cell adhesion and endothelial marker CD31 (PECAM-1, platelet/endothelial cell adhesion molecule-1) was used in an effort to further characterize CSP cells. The expression of

the CD31 antigen divides CSPs into two sub-populations. CSPs are comprised by approximately 25 % of $CD31^-/Sca1^+$ cells and 75% of $CD31^+/Sca1^+$ cells [51].

To further characterize CSP cells, Pfister *et al* tested the cardiomyogenic differentiation capacity of the two CSP subpopulations in a mono-culture and a co-culture model. $CD31^+/Sca1^+$/CSPs failed to adhere on the culture plates and they did not express any differentiation marker in both differentiation models [51]. In the mono-culture model more than 30% of $CD31^-/Sca1^+$/CSPs expressed both the muscle-specific transcription factors GATA-4 and MEF2C and at later time points they also expressed cardiomyocyte specific contractile proteins, such as troponin-I and α-sarcomeric actinin. However, the expression of these markers did not demonstrate a well organized pattern in sarcomeric structures as in mature cardiomyocytes [51].

In the co-culture model $GFP^+/CD31^-/Sca1^+$/CSPs expressed the muscle-specific transcription factors GATA-4 (64%) and MEF2C (35%). Moreover, more than 10% of the $GFP^+/CD31^-/Sca1^+$/CSP cells expressed a-sarcomeric actinin in a well-organized sarcomeric pattern, a clear indication of the formation of mature cardiomyocytes. As a further evidence of the maturation of their cardiomyogenic differentiation, $GFP^+/CD31^-/Sca1^+$/CSPs demonstrated active contraction and calcium transients in the same pace with co-cultured adult rat myocytes, as revealed by cell contractility and intracellular calcium transient assays [51]. The differentiated $GFP^+/CD31^-/Sca1^+$/CSPs cells were expressing connexin-43, an indication of functional coupling with the co-cultured adult rat cardiomyocytes.

The likelihood of cell fusion between mouse CSPs and rat cardiomyocytes was examined by utilization of a *Cre*-lox reporter system. In this experiment, $CD31^-/Sca1^+$/CSPs containing a *loxP*-flanked-Bgeo reporter were co-cultured with adult rat cardiomyocytes expressing the *Cre*-

recombinase. In the case of cellular fusion, cardiomyocyte *Cre*-recombinase would excise the *loxP*-flanked Bgeo reporter and it would initiate the expression of GFP in $CD31^{-}/Sca1^{+}$/CSPs. Blind examination of these co-cultures assays revealed no presence of $GFP^{+}/CD31^{-}/Sca1^{+}$/CSPs, suggesting that there is no cellular fusion between the co-cultured rat cardiomyocytes and the $CD31^{-}/Sca1^{+}$/CSPs [51]. Overall, the above data clearly suggest that CSPs represent a resident population of adult cardiac precursors, which are distinct from bone marrow side population cells and exhibit profound cardiomyogenic differentiation ability.

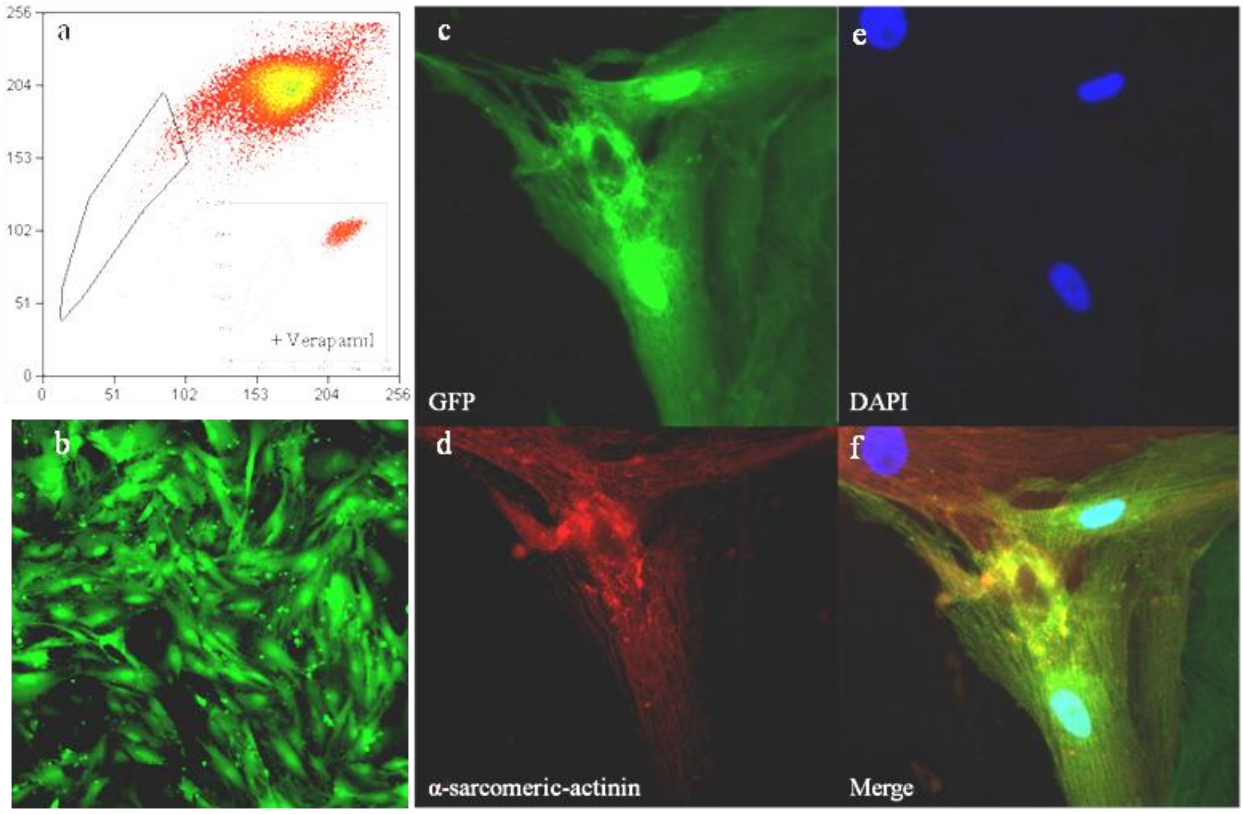

Figure 3: (a) Representative example of CSP flow cytometric analysis. Inset shows verapamil stained CSPs used as a negative control. (b) *In vitro* expanded GFP^+ CSP cells. (c-f) Expanded CSPs differentiate into cardiomyocytes when co-cultured with adult or neonatal rat cardiomyocytes. Green corresponds to GFP expression, red to α-sarcomeric-actinin and blue to the nuclei. Merged image reveals areas of co-localization of GFP and a-sarcomeric actinin (orange).

10. ABC transporters are the molecular determinants of the SP phenotype

As mentioned previously, the pioneer work of Goodell *et al* introduced the SP phenotype as a reliable marker to identify cell populations, enriched in stem cells [47]. The bone marrow side population cells (BMSPs) demonstrated equivalent transplantation ability to hematopoietic stem cells isolated based on the expression of established hematopoietic stem cell markers [55]. The SP phenotype is attributed to cells that have the ability to actively export the DNA-binding dye Hoechst 33342 (Hoechst dye) from their cytoplasm [48]. This efflux ability confers the characteristic profile of SP cells that appears in flow cytometric analysis. SP cells appear as Hoechst low cells on the side of the Hoechst high cells, the so called main population.

The SP phenotype is linked on the cellular and molecular level with the action of members of the ATP-binding cassette transporter super-family (ABC transporters) and in particular with the action of the multidrug resistance protein 1 or (Mdr1, P-glycoprotein, P-gp, Abcb1) and the breast cancer resistance protein 1 (Bcrp1, Abcg2) [56, 57]. The molecular determinant of the SP phenotype varies depending on the tissue of origin. Studies using knock-out mice of these transporters revealed significant differences in the impact of each transporter on the generation of the SP phenotype. Mdr1a/1b$^{-/-}$ mice demonstrated physiological levels of BMSP cells [57]. However, Bcpr1$^{-/-}$ mice exhibited a complete loss of BMSP cells [58]. Overall, the above data strongly suggest that the SP phenotype in the bone marrow is depended exclusively on the function of the Bcrp1 transporter. The inability of the Mdr1 transporter to compensate for the loss of the SP phenotype in the bone marrow of the Bcrp1$^{-/-}$ mice also

suggests that there is no functional overlapping and that maybe there is a tissue-dependent specificity of the function of these pumps.

Our studies focused on the identification of the molecular determinant of the SP phenotype in neonatal and adult CSPs. Previous work by Martin *et al* had suggested that similarly to BMSP, Bcrp1 is the molecular determinant of the cardiac SP phenotype. This conclusion was based on the experimental observation that the Bcrp1 inhibitor fumitremorgin C (FTC) completely abolishes the CSP phenotype, similar to verapamil [49]. To establish the role of Bcrp1 as the primary mediator of the SP phenotype in bone marrow and cardiac cells we utilized knockout mice of Bcrp1 ($Bcrp1^{-/-}$) and Mdr1 ($Mdr1a/1b^{-/-}$). As expected flow cytometric analysis of bone marrow cells from $Bcrp1^{-/-}$ mice revealed a complete lack of BMSP cells, in contrast to the analysis of cell suspensions derived from $Mdr1^{-/-}$ mice or their WT counterparts that exhibited normal levels of BMSPs. Subsequently, we examined the SP profile of cardiac cell preparations derived from adult $Bcrp1^{-/-}$ mice as well as from $Mdr1^{-/-}$ mice, in comparison to WT mice. $Bcrp1^{-/-}$ mice exhibited a clearly detectable, although significantly reduced population of CSPs.

Surprisingly, cell preparations from adult $Mdr1^{-/-}$ mice demonstrated a complete absence of CSPs, suggesting that Mdr1 is the primary determinant of the SP phenotype in adult hearts. We further verified that CSPs isolated form adult hearts express both Bcrp1 and Mdr1 but we also found that their expression levels are regulated in an age-dependent way. The expression of Bcrp1 is higher in neonatal CSPs and it is progressively decreasing during post-natal life. In contrast the expression of Mdr1 is progressively increasing with age. Thus our next step was to examine whether the same pattern applies also in the regulation of the cardiac SP phenotype. To

determine whether Bcrp1 and Mdr1 mediate the cardiac SP phenotype in an age-dependent way, CSPs from Bcrp1$^{-/-}$, Mdr1$^{-/-}$ and age-matched WT mice were analyzed at postnatal day 3 (p3), day 14 (p14), day 21 (p21) and at 8-12 weeks of age. In contrast to our observations in adult hearts, early postnatal (p3) Bcrp1$^{-/-}$ hearts demonstrated an almost complete lack of CSPs, whereas a similar number of CSPs was observed in Mdr1$^{-/-}$ and WT hearts. A gradual decrease in CSPs from p3 to adulthood was noted in WT hearts, whereas Bcrp1$^{-/-}$ samples demonstrated a gradual increase in CSPs from p3 to adult. Quite surprisingly, the opposite profile was observed in Mdr1$^{-/-}$ hearts, where the amount of CSPs progressively decreases from p3 to adulthood (Figure 4). Taken together, these data demonstrate that the CSP cell phenotype is mediated by both Bcrp1 and Mdr1 in an age-dependent fashion. In contrast to previous observations, Mdr1 represents the molecular determinant of the cardiac SP phenotype in adult hearts.

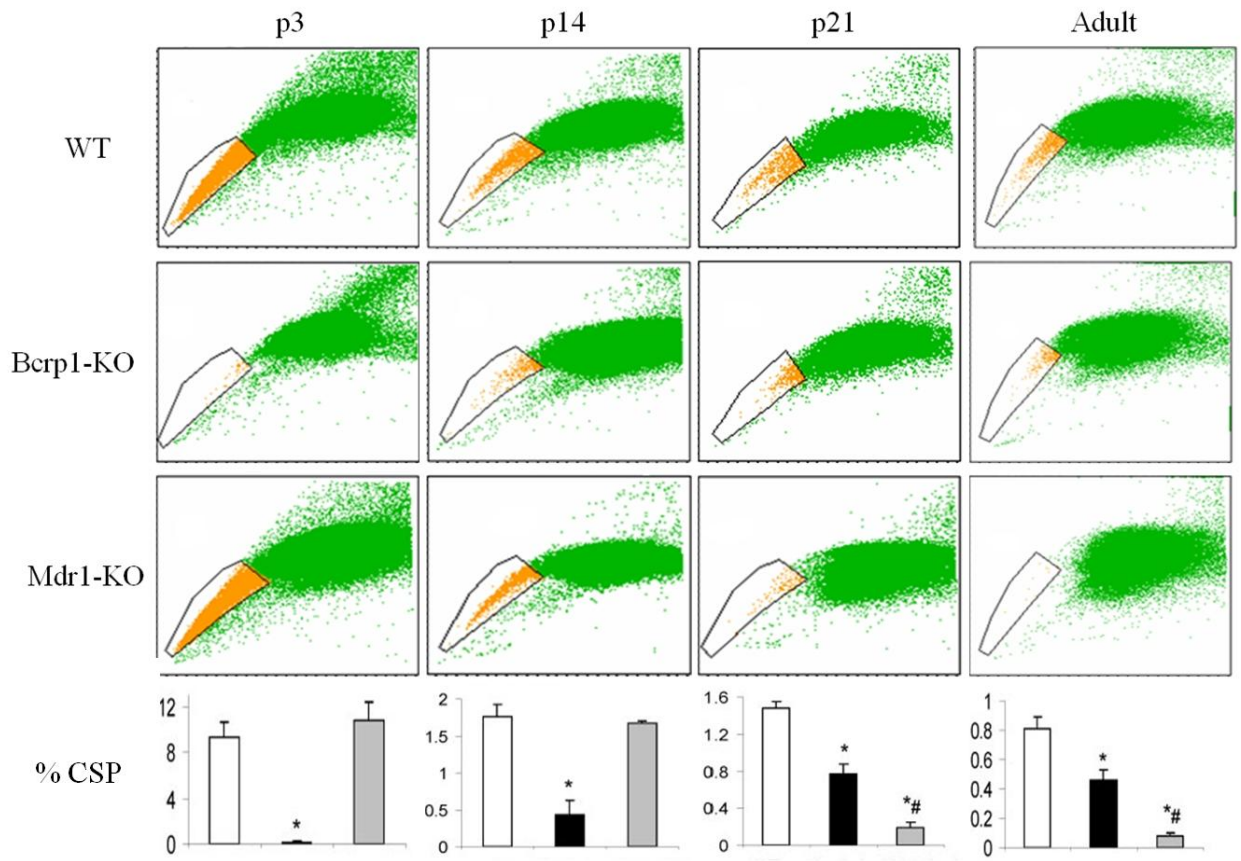

Figure 4: Brcp1 and Mdr1 represent the molecular determinant of the cardiac side population phenotype in an age dependent mechanism. At post-natal day 3 (p3) Bcrp1 mediates exclusively the Hoechst 33342 dye efflux ability of CSPs, whereas in adult mice Mrd1 is the primary transporter that exports Hoechst 33342 dye. Adapted from Pfister O., Oikonomopoulos A and Sereti K. *et al*, Circ. Res. 2008;103;825.

11. ABC transporters as protective mechanisms of stem/progenitor cells

ABC transporters comprise one of the largest protein families and are involved in the transfer of various compounds, such as drugs, toxins, sugars, amino acids, lipids, sterols, peptides, bile salts, nucleotides, endogenous metabolites and ions across the cell membranes [59,

60]. Thus, Mdr1 and Bcrp1 besides being known as the molecular determinants of the SP phenotype in various tissues, they are primarily involved in numerous biological processes, such as cell metabolism, drug resistance and cytoprotection. Bcrp1 and Mdr1 are expressed not only in side population cells but also in various types of stem or progenitor cells and until now their functional role is not fully understood [48]. Currently, there are several reports that demonstrate the cytoprotective role of Bcrp1 or Mdr1 [48, 58, 61-66].

Our studies focused on understanding the role of Mdr1 and especially Bcrp1 in cytoprotection and in proliferation of CSPs. Previous reports have implicated Bcrp1 in the proliferation capacity of cancer cells [67], so we utilized gain and loss of function approaches to study the proliferation capacity of CSPs. CSPs isolated from Bcrp1$^{-/-}$ mice exhibited decreased proliferation capacity whereas lentivirus mediated over-expression of Bcrp1 augmented their proliferation [68]. Consistently, CSPs lacking Bcrp1 demonstrated decreased expression of proliferation markers, such as Ki67 and p-H3 [68]. Furthermore, we tested whether Bcp1 exerts any cytoprotective effects on CSPs. Initially, we found that lack of Bcrp1 increases both apoptosis and necrosis in CSP cells under normal culture conditions (21% O_2) [68]. Moreover, exposure of CSPs lacking Bcrp1 to oxidative stress, induced by application of H_2O_2, further increased cell death [66]. Overall, the above results suggest that the role of Bcrp1 in CSPs is not restricted to conferring the SP phenotype through Hoechst dye efflux, but it expands in the regulation of their proliferation and survival. Additional experiments are required to dissect the molecular mechanisms that mediate the cytoprotective role of Bcrp1 in CSPs.

12. Homeostasis of CSPs under physiologic and injury conditions and the role of the bone marrow

The presence of CSP cells in the adult myocardium raises several questions about their origin, properties and functional role in the physiology and pathophysiology of cardiac muscle. Mouquet *et al* demonstrated that following MI (1 day post-MI) the CSP cell pool is acutely depleted (60%). CSP cells remain significantly reduced at 3 days post-MI but their levels returned to normal at 7 days following injury [69].

The reconstitution of CSPs resulted from two different mechanisms, the proliferation of endogenous CSPs and the mobilization of bone marrow side population cells to the heart. Under homeostatic conditions (sham operated animals) approximately 10% of the CSP cells were expressing the cell cycle marker Ki67, suggesting that a small portion of CSPs are actively cycling and the majority resides in the resting G0 phase. At 1 day post-MI, within the infarct/border zone area, there was a reduction of $Ki67^+$ CSP cells, compared to sham operated animals. However, at 3 and 7 days post-MI, approximately 20% and 25% of the CSP cells were $Ki67^+$ respectively. In the remote area, at 1 and 3 days post-MI, the amount of $Ki67^+$ CSP cells remained similar to sham animals (10%) and only at 1 week post-MI an increase in the amount of $Ki67^+$ CSPs (30%) was detected. Thus, following severe cardiac injury (MI) there is a proliferative response of endogenous CSPs, which contributes to their restoration to baseline levels approximately 1 week post-MI [69]. The molecular mechanisms and the signaling molecules mediating this response remain unknown.

Mouquet *et al* examined also the contribution of bone marrow cells in the restoration of the CSP cell pool following MI [69]. Male C57BL/6 mice were subjected to a round of lethal

irradiation, followed by transplantation of unfractionated GFP-expressing bone marrow cells. Eight weeks following transplantation, mice were subjected to MI and the contribution of GFP^+ bone marrow cells was evaluated at 1, 3 and 7 days post operation. In control (sham operation) animals the amount of GFP^+ CSP cells was less than 1%, suggesting that in the normal heart the input of bone marrow cells in the CSP pool is insignificant and the proliferation of CSPs is the primary cause force of its homeostasis. In contrast, the input of bone marrow cells to the CSP pool was elevated in post-MI myocardium. Within the infarct/border zone the amount of bone marrow derived GFP^+ cells in total CSPs, at 1, 3 and 7 days post-MI was respectively 5%, 20% and 25% [69]. On the contrary, in the remote area the amount of bone marrow derived GFP^+ cells to the CSP pool was insignificant, with less than 5% of the total CSPs being GFP^+. In parallel with the increase of the amount of GFP^+ CSPs there was a decline of the bone marrow side population cells [69].

In an effort to define the characteristics of bone marrow derived GFP^+ CSP cells, the expression of the hematopoietic marker CD45 was examined in CSPs. At 1 day post-MI approximately 50% of the GFP^+ CSPs were expressing CD45, whereas at 3 and 7 days post-MI, the fraction of $CD45^+$ cells in the GFP^+ CSPs decreased to less than 10% [69]. These results demonstrate that both the proliferation of endogenous CSP cells as well as homing of bone marrow derived cells is responsible for the restoration of CSPs following MI. The bone marrow derived CSP cells home into the myocardium and undergo an immunophenotypic conversion adopting a non-hematopoietic profile. The origin of the bone marrow derived CSP cells is unknown, although is likely that unidentified homing signals mobilize bone marrow side population cells or other hematopoietic stem cells towards the injured heart. The mobilization of

bone marrow cells to the heart after injury is in accordance with the reported contribution of bone marrow cells in the healing process of the injured myocardium [18, 70].

13. Isl-1 cells

The LIM-homodomain transcription factor islet-1 (Isl-1) has been used to identify an additional population with stem/progenitor characteristics in the myocardium. The Isl-1^+ cardioblasts progressively decrease during the neonatal life and shortly after birth relatively few are still detectable (500-600 in the heart of a 1-5-day old rat). The Isl-1 progenitors are expandable in vitro and they are able to differentiate towards functional cardiomyocytes, smooth muscle cells and endothelial cells [71], [72]. The cardiac Isl-1 progenitors represent a population that has embryonic origin and holds significant differentiation potential under appropriate conditions. However, the low percentage of Isl-1 cells in the adult heart and especially in the left ventricle constitutes an important limitation in the use of this population for cardiac cell therapy trials. This limitation could be bypassed with the use of Isl-1^+ cardiac progenitor cells derived from embryonic stem cells, through specialized culture conditions [73].

14. Cardiospheres

Another population of cardiac stem/progenitor cells isolated from human cardiac biopsies and mouse hearts was described by Messina *et al [74]*. These cells were detected within clusters of cells called cardiospheres (CSs) that are formed under special culture conditions. CSs represent a heterogeneous cell population as immunophenotypic analysis revealed the expression

of various markers of endothelial cells (KDR, flk-1 & CD31) and markers of stem cells (c-kit, Sca-1 and CD34)[74]. CSs exhibit all the fundamental properties of cardiac stem cells such as self-renewal ability and capacity to differentiate towards cardiac and endothelial cell lineages. Moreover, administration of CSs following myocardial infarction in mice resulted in improved cardiac performance and generation of myocytes and endothelial cells.

15. Epicardial progenitors

Epicardium is the outer epithelium of the heart and functions as a protective layer. The epicardial cells derive from the pre-epicardium and they play an essential role during cardiac development [75]. Until recently epicardium was considered as a source of smooth muscle cell, endothelial cell and intramyocardial and perivascular fibroblast cell progenitors [75]. However, recent fate mapping studies have challenged this idea and have suggested the epicardium is a niche of cardiac progenitors as well. Zhou *et al* established the transcription factor Wt1 as an epicardial marker since at E9.5 mouse embryos its expression was localized only in the epicardial layer of the premature heart [76]. By using two reporter-mouse lines the authors demonstrated the presence of Wt-1 derived cells in a mosaic pattern throughout the myocardium. The Wt-1 descendants were predominantly smooth muscle cells and in a lesser extent endothelial cells. Surprisingly, a proportion of the Wt-1 derived myocardial cells were expressing markers of mature cardiomyocytes as α-sarcomeric actinin and cardiac troponin T2 [76]. Similarly, Cai *et al* in a recent work demonstrated that the epicardium contains populations of not only smooth muscle cell and fibroblast precursors but also cardiomyocyte progenitor cells [77]. The authors used the expression of the transcription factor Tbx18 (an early epicardial marker) to follow the

track of epicardial cells, as it was not present in the myocardium at E10.5 [77]. However, in a recent brief communication by Christofells *et al* the epicardial specificity of Tbx18 was questioned since this transcription factor was also detected in the myocardial layer from E10.5 to at least E16.5 [78]. Despite the documented controversy of the above studies these results taken together suggest that the epicardium might have a novel role as a niche of cardiac progenitors. Further studies are required to identify reliable epicardial markers and to examine the role of these epicardial cardiac progenitors in cardiac development and in cardiac maintenance during adulthood.

16. Wnt signaling pathway

Wnt signaling pathway is one of the most well studied signaling pathways and it is remarkably conserved among various species in vertebrates and invertebrates [79]. The first components of the Wnt signaling pathway appeared with the identification of the *Drosophila* wingless (Wg) gene and its vertebrate ortholog, the int-1 oncogene [80]. Since then 19 Wnt proteins have been identified in humans and mice. Wnt ligands comprise a family of secreted glycoproteins that control cell to cell interactions during development and adulthood [81]. All Wnt proteins share some characteristic features such as a signal sequence for secretion, many glycosylation sites and several highly charged amino acids. Moreover, Wnt proteins are hydrophobic and they are associated with cell membranes and the extracellular matrix [82].

Wnt signaling is initiated at the cell membrane by the direct interaction between the Wnt ligands and the Frizzled receptors as well as various co-receptors [79]. Until today, 10 distinct Frizzled receptors and several co-receptors have been identified [83]. Based on functional assays

such as the induction of the secondary axis in Xenopous embryos and the transformation of C57 mg cells, Wnt ligands can be divided into two subgroups, the canonical Wnt-ligands and the non-canonical Wnt ligands.

Developmentally, canonical Wnt signaling is implicated with the induction of a secondary axis in *Xenopus* embryos whereas the non-canonical Wnt signaling pathway is implicated in the planar cell polarity pathway in *Drosophila*. The canonical Wnt signaling is better understood than the non-canonical pathway and they can be distinguished based on the role of β-catenin in each case. β-catenin represents a major player in the canonical branch of Wnt signaling pathway, whereas it is not involved in the non-canonical Wnt signaling cascade.

In canonical Wnt signaling, in the absence of a Wnt ligand β-catenin is constantly targeted to ubiquitination and subsequent proteosomal degradation, by the action of the so-called destruction complex. This large protein complex is composed by several proteins such as adenomatous polyposis coli (APC), glycogen synthase kinase 3β (GSK-3β), axin and CK-1 [83]. The targeting of β-catenin is achieved through CK-1 and GSK-3β mediated phosphorylation in various residues. In this case, the TCF/LEF transcription factors facilitate the recruitment of co-repressors such as Groucho, CtBP and HDACs (histone deacetylases) onto Wnt-response elements in the promoter of the various Wnt target genes [83].

In the presence of a Wnt ligand such as Wnt3a or Wnt1 the inhibitory role of CK-1 and GSK-3β is blocked and β-catenin is no longer targeted to proteosomal degradation. At the cell membrane level, Wnt ligands bind physically to the Frizzled receptor and the LRP5/6 (lipoprotein receptor-related protein) co-receptor and initiate a signaling cascade, which leads to the inactivation of the protein destruction complex. Subsequently, β-catenin is stabilized in the

cytosol and is transferred in the nucleus where it interacts with the LEF/TCF transcription factors. This interaction results in replacement of the transcriptional co-repressors with transcriptional co-activators, such as swi/SNF [83]. The final outcome is the activation of numerous genes that control diverse biological processes such as embryonic development, cell migration, cell proliferation, cell survival, cell differentiation, carcinogenesis and tumor suppression. Until today, in the various biological contexts studied there is no common set of Wnt target genes reported. Thus, the effects of the canonical Wnt signaling are tissue and cell dependent.

The non-canonical, β-catenin-independent, Wnt signaling pathway has different intracellular mediators such as c-Jun N-terminal kinase, calcium, protein kinase C, CaMK, nuclear factor of activated T-cells and the Rho or Rac GTPases [79]. Among others, Wnt5 and Wnt11 are the most representative Wnt ligands of the non-canonical Wnt signaling. Non canonical Wnt signaling is implicated in the creation of cellular polarity during embryonic development, in cell movements during gastrulation, in cardiac formation, in cardiomyogenic differentiation of cardiac progenitors and in cardiac hypertrophy [79, 83].

17. Wnt inhibitors

Wnt signaling regulates the expression of numerous target genes in various tissues during development and adulthood. The activity of Wnt signaling pathway can be also regulated by the action of several secreted Wnt inhibitors such as members of the Dickkopf1 (Dkk1) protein family, members of the frizzled-related protein family (Sfrp) as well as a membrane bound protein called Kremen which has been described as negative regulator of Wnt activity.

Dkk1 was identified in *Xenopus* embryos and is the first member of a family comprised by four proteins conserved in the genome of vertebrates and invertebrates [84, 85]. Dkk1 antagonizes Wnt signaling by preventing the formation of a functional ternary complex consisting of the LRP5/6 co-receptor, the Frizzled receptor and the Wnt ligand [84, 85]. The molecular details about the inhibitory action of Dkk1 remain unknown and currently there are two models regarding the action of Dkk1. According to the first model, Dkk1 blocks Wnt signaling by competing with Wnt ligands for binding to LRP5/6 [85]. According to the second model Dkk1 blocks Wnt activity by inducing clathrin-mediated internalization of the LRP5/6 co-receptor [86, 87]. Further insight to the second model was brought from a recent study demonstrating that Kremen acts synergistically with Dkk1 to inhibit Wnt activity [88]. According to this updated model in the absence of Dkk1, Kremen potentiates the Wnt/β-catenin signaling by maintaining LRP5/6 to the plasma membrane. In the presence of Dkk1, Kremen further potentiates the Dkk1-mediated Wnt inhibition by facilitating LRP5/6 internalization [88].

Another class of Wnt antagonists includes members of the Sfrp protein family, the Wnt-inhibitory factor 1 (Wif1) and the protein Cerberus [79, 89, 90]. The Sfrp protein family contains 8 members that form three subgroups. Sfrp1, Sfpr2 and Sfrp5 form one subgroup, Sfrp3 and Sfrp4 form a second subgroup and Sizzled, Sizzled2 and Crescent form a third subgroup that has been identified in mammals. Structural analysis showed that Sfrp proteins have two independent domains. In the amino terminal domain there is a conserved cysteine rich motif that shares great similarity with the cysteine rich domain of Frizzled proteins [79, 89, 90]. In the carboxy terminal domain there are six cysteine residues that form the NTR domain (Netrin-like domain) which is also found in other proteins such as netrin, tissue inhibitors of

metalloproteinases and others. Sfrp proteins by sequestering Wnt ligands prevent their interaction with the Frizzled receptor and are thus considered inhibitors of both canonical and non canonical Wnt signaling [79, 89, 90].

The molecular mechanism of the Sfrp/Wnt interaction has not yet been fully resolved. The apparent similarity of the cysteine rich domain between the Sfrp proteins and the Frizzled receptors led to the hypothesis that Sfrp interacts with Wnt ligands through this domain [79, 89, 90]. Additional studies showed that the NTR domain is also involved in the Sfrp/Wnt interaction and that both domains are necessary for Wnt inhibition. Currently, there is no consensus about the exact inhibitory mechanism and further studies are required in order to obtain a detailed structural map of the Wnt/Sfrp interactions [79, 89, 90].

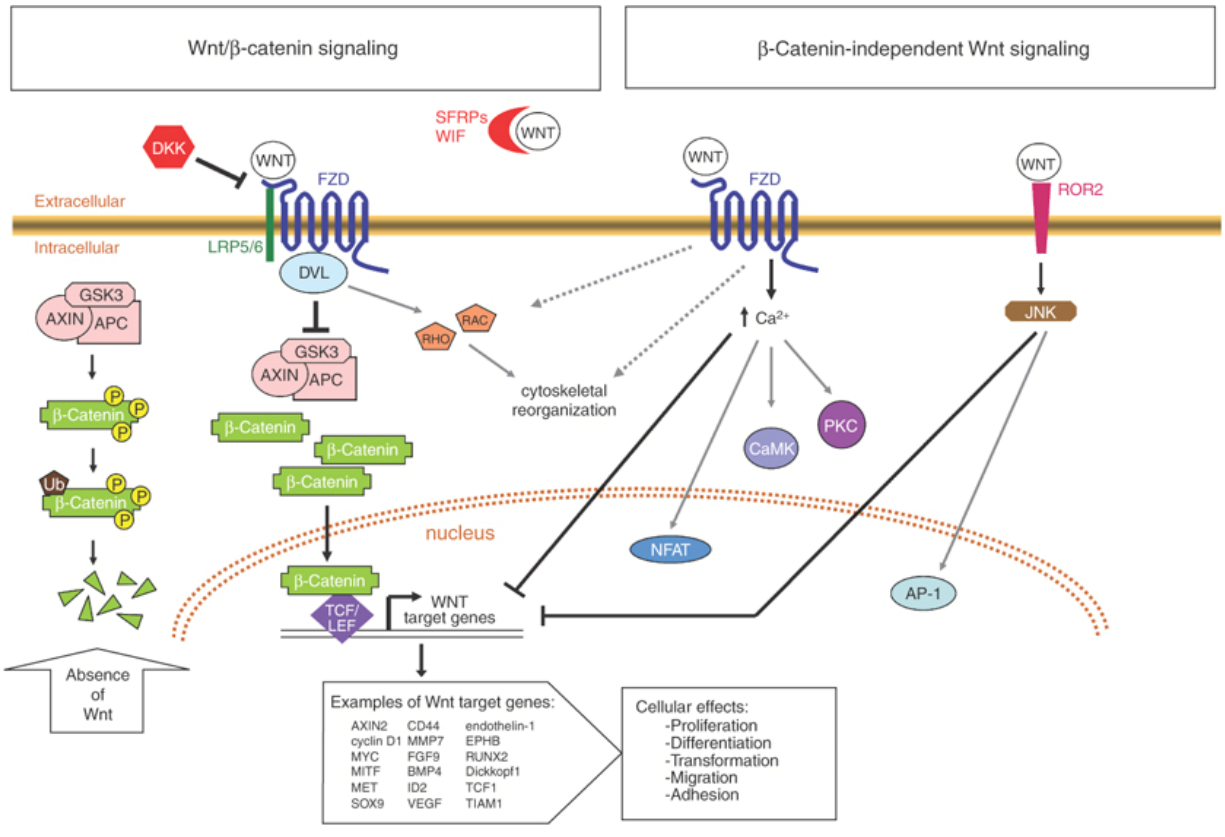

Figure 5: Representation of the canonical (β-catenin dependent) and non canonical Wnt signaling pathways. Adapted from Chien *et al*, J Invest Dermatology. 2009; 129(7):1614.

18. Wnt and stem cells

Wnt signaling has a major role during development, being involved in the formation of various organs in all species [91]. Moreover, Wnt ligands control the fate and the self-renewal properties of embryonic and adult stem cells. Several studies suggest that canonical Wnt signaling regulated the self-renewal property of embryonic stem cells and that activation of this pathway results in their expansion. On the other hand, additional studies have shown that Wnt signaling pathway regulates the differentiation properties of embryonic stem cells. Emerging evidence suggest that through a close relationship with the stem cell factor Oct3/4, Wnt signaling plays a dual role in embryonic stem cells being able to regulate both their self-renewal and differentiation.

In addition to its role as a fate determinant in embryonic stem cells Wnt signaling regulates various aspects of adult stem cells. Activation of canonical Wnt signaling pathway augments the proliferation and blocks the differentiation capacity of human mesenchymal stem cells. The role of Wnt signaling in neural progenitor cells remains elusive until today. Several reports have demonstrated that activation of this pathway increases the proliferation of neural progenitor cells. Conversely, Wnt signaling pathway is implicated also in the differentiation of neural progenitors. Similarly, the role of Wnt signaling in hematopoietic stem cells (HSCs) is

also unclear. A series of gain and loss of function approaches demonstrated that activation of the canonical Wnt signaling pathway promotes the expansion of HSCs while maintaining their self-renewal. On the other hand, recent evidence suggests that activation of Wnt signaling through similar gain of function approaches, results in impaired multi-lineage differentiation of HSCs and eventually to HSCs exhaustion. Additionally, simultaneous deletion of β-catenin and γ-catenin in HSCs did not impair hematopoiesis, suggesting that the role of Wnt signaling in this process is redundant. Overall, the above studies clearly emphasize that canonical Wnt signaling is an important regulator of the proliferation and differentiation of both embryonic and adult stem cells, but its exact role in each case is most likely context and time dependent.

19. Cardiac development and Wnt signaling

The heart is the first organ to be formed in the developing embryo following gastrulation and the establishment of the three germ layers. Defects in the formation and maturation of the developing heart result in congenital heart disease, which is the most common form of birth defect [92]. Cardiac specification occurs in a region of the anterior mesoderm called cardiac crescent, which adopts a cardiac fate in response to signals derived from the adjacent endoderm. The formation of cardiac crescent takes place at embryonic day 7.5 (E7.5) [93, 94]. The cells of the cardiac crescent migrate towards the ventral midline of the embryo where they converge, forming the linear heart tube (E8) [93, 94]. At E8.5, the heart tube undergoes a rightward looping with its posterior region moving anteriorly. As the primitive heart continues to grow the cardiac chamber starts to appear (E10.5) and finally at E14.5 following septation, the developing heart adopts it multi-chamber structure [93, 94]. The growth of the primitive heart is a

combination of the growth of myocardial cells of the heart tube and the growth of recruited cardiac precursors. Moreover, the growth and the maturation of the developing heart take place in a segmental manner [93, 94]. The development of each chamber depends on the function of a specific set of transcription factors. As an example, the basic helix-loop-helix transcription factors HAND1 and HAND2 control the formation and maturation of the right and left ventricles, respectively [93, 94].

Recent lineage tracking studies have demonstrated novel evidence about the developmental derivation of the heart [93, 95]. Two distinct populations of cardiac precursors, which might share common origin, termed first heart field (FHF) and second heart field (SHF) contribute to the formation of the four chambered heart [93, 95]. FHF progenitors are derived initially form the cardiac crescent and then they give rise sequentially to the heart tube and finally to the left ventricle and the left and right atria [93, 95]. Although there are no specific markers for the FHF progenitors they can be marked by the expression of the T-box transcription factor Tbx5 and the basic helix-loop-helix transcription factor HAND1 [93, 95]. Clonal analysis experiments performed by Kattman *et al* showed that the FHF and the SHF progenitors might originate from the same common stem cell, which can be traced by the expression of the homeobox transcription factor Nkx2.5, the VEGF receptor tyrosine kinase 1, Flk1, and probably Isl1 [96, 97].

Genetic experiments in chick and mouse embryos revealed that a distinct embryonic region, in the pharyngeal mesoderm, is the source of the SHF cardiac progenitors. The SHF progenitors migrate to the heart tube and eventually contribute to the formation of the right ventricle and the outflow track [93]. In contrast to the FHF, the SHF progenitors are better

characterized and they are marked by the expression of the Fgf10 growth factor, the basic helix-loop-helix transcription factor HAND2 and the LIM-homodomain transcription factor Isl-1 [93].

Cardiac specification is orchestrated by a complex network of transcription factors that regulate the expression of numerous cardiac myogenic factors, such as Isl1 [98]. This network of cardiomyogenic mediators includes transcription factors that belong to the families of Nk2, Mef2, Gata, Tbx and Hand [98]. Comparative genomic studies revealed that this network of transcription factors is evolutionary conserved in organisms ranging from jellyfish and nematodes to *Drosophila* and amniotes (mammals, reptiles and birds) [98]. Quite recently, Takeuchi *et al* demonstrated that Baf60c, a member of the Swi/Snf-like BAF remodeling complex, is essential for activation of the cardiac specification gene program by the above transcription factors [99]. The authors demonstrated that administration of Nkx2.5, GATA-4 and Tbx5, alone or in combinations, in cardiac mesoderm of embryos, failed to induce ectopic cardiogenesis. These transcription factors were able to promote cardiac formation in the non-cardiogenic mesoderm only in the presence of Baf60c.

The expression of the cardiomyogenic transcription factors is induced by signals derived from the adjacent regions of the cardiac-forming mesoderm [92, 100]. Intensive studies have identified several well known signaling pathways as important mediators of cardiac formation and specification [92, 101, 102]. These include bone morphogenetic proteins (BMPs), transforming growth factor proteins (TGFs), fibroblast growth factor proteins (FGFs), Sonic hedgehog proteins (Shh), Notch ligands and Wnt ligands [92, 101, 102].

The role of Wnt signaling pathway in cardiac development has been the objective in numerous studies that documented its central role in the early and late phases of heart formation

as well as in the regulation of cardiovascular progenitors. Initial experiments in Drosophila suggested a cardiac promoting role of canonical Wnt signaling but later experiments in chick and *Xenopus* embryos showed a cardiac inhibitory role. Additional perplexity was created by reports regarding the cardiac promoting role of Wnt inhibitors or conditional deletion of β-catenin in mice. The profound contradiction about the role of Wnt ligands in cardiac development was partially resolved by recent studies that suggested a time dependent role of Wnt signaling. Studies in zebrafish embryos and in embryonic stem cells indicated that the effects of Wnt signaling are strongly depended on the time of action. Namely, in the zebrafish embryos activation of the canonical Wnt signaling prior gastrulation promoted cardiac formation whereas activation post gastrulation inhibited cardiomyogenesis. The above data introduced a model of a biphasic temporal-dependent role of Wnt signaling on cardiac development.

Additional findings about the function of Wnt signaling in specific embryonic cardiac progenitor cells as well as the phenotype of Wnt-modulating transgenic animals have suggested a more complex role for Wnt signaling in cardiac development. The first step in cardiac formation is the induction and determination of the embryonic mesodermal region, where the cardiac crescent will be formed. Many lines of evidence suggest that in these very early events activation of the canonical Wnt signaling pathway in essential. Loss of canonical Wnt activity during this period causes absence of mesoderm-specific genes and ultimately inability to generate cardiac mesoderm. However, at later stages of development the role of Wnt signaling changes drastically. One of the first described populations of embryonic cardiac progenitor cells is marked by the expression of the basic helix-loop-helix transcription factor Mesp1, the expression of the tyrosine kinase Flk1 and the T-box transcription factor Brachyury (Bry), which

is a pan-mesodermal marker ($Mesp1^+/Flk1^+/Bry^+$). Recent studies demonstrated that cardiac specification of $Mesp1^+$ cells require down-regulation of the canonical Wnt signaling. Notch-mediated cardiac differentiation of Bry^+/Flk^+ cells promotes up-regulation of Wnt inhibitors, such as Sfrp1 and Sfrp5. Additional findings suggested that the canonical Wnt inhibitor Dkk1 augments the Mesp1-mediated cardiomyogenic differentiation of embryonic stem cells. Further information on the role of Wnt signaling in cardiac specification derived from studies of the function of non-canonical Wnt ligands, such as Wnt5 and Wnt11. Several reports have demonstrated that up-regulation of these non-canonical Wnt ligands is necessary for cardiac specification in the mesodermal germ layer. These data suggest that following induction of cardiac mesoderm, further specification of embryonic progenitor cells in the cardiac lineage requires inactivation of canonical Wnt signaling.

As mentioned earlier, following the formation of the linear heart tube the SHF progenitors migrate to the primitive heart and they contribute primarily to the formation of the outflow track and the right ventricle. The effects of Wnt signaling on the SHF progenitors were examined by various investigators with similar results. Activation of the canonical Wnt signaling pathway resulted in *in vitro* and *in vivo* expansion of $Isl1^+$ cells and this caused a direct effect on the formation of the SHF-derived structures. Thus, canonical Wnt signaling mediates positive effects on the proliferation of the $Isl\text{-}1^+$ SHF progenitor cells, indicating that its role varies depending on the examined cell population or the examined developmental time point.

In another series of recent studies the role Wnt signaling in the terminal differentiation of cardiomyocytes was examined. Late administration of the canonical Wnt3a ligand in embryonic stem cell culture systems blocked their cardiomyogenic differentiation. Moreover, activation of

canonical Wnt signaling in $Isl1^+$ SHF progenitor cells not only increased their proliferation, as mentioned above, but decreased their cardiac differentiation capacity.

Overall, the above studies emphasize that Wnt signaling participates actively in every phase of cardiac development, although in a very complex and not fully understood manner. Initially, Wnt/β-catenin signaling is essential for the induction of the cardiac mesoderm following gastrulation but later it is not required for the cardiac specification of the early embryonic cardiac progenitors. However, at a later time point, when the SHF progenitors emerge, canonical Wnt signaling promotes their proliferation, while during the stage of terminal differentiation of embryonic cardiac progenitors Wnt signaling seems to be inactive. Additional studies are required in order to integrate all the data in one model defining the role of Wnt signaling in cardiac development.

20. Implication of Wnt signaling in cardiovascular diseases

Wnt signaling pathway has been irreversibly linked with the onset and the progression of various types of cancer and especially colon cancer [103]. Moreover, accumulating evidence suggest that Wnt signaling pathway is implicated in the pathophysiology of numerous diseases affecting various organs in the human body such as bones, teeth, skin, brain, lungs, kidney and heart [104]. Several studies have demonstrated the importance of Wnt signaling in the cardiovascular diseases as a key player in the process of cardiac remodeling.

As mentioned previously several pathological stimuli such as hypertension or myocardial infarction can initially lead to cardiac hypertrophy and eventually to heart failure. A number of reports have investigated the role and the status of Wnt regulators in injured hearts using various

methodologies. Blanckesteijn *et al* showed that the expression of Frizzled-2, a Wnt receptor, was up-regulated following hypertrophy in rat, suggesting increased Wnt activity in this injury model [105]. Similarly, the expression levels of Frizzled-2 were also found to be up-regulated following myocardial infarction [106]. Although, increased expression of Frizzled receptors in post-MI myocardium suggests increased Wnt activity, the simultaneous presence of various inhibitors of the Wnt signaling limits their significance as markers of Wnt activation status.

Another study demonstrated that whole body Dishevelled-1 knockout mice exhibited attenuated hypertrophic response following aortic constriction, over a period of 14 days [107]. The role of Dishevelled in cardiac remodeling was further examined in additional studies resulting in conflicting results. Blankesteijn *et al* challenged Dishevelled-1 knockout mice with myocardial infarction and reported increased rates of cardiac rupture, in comparison to wild type littermates [108]. The authors also demonstrated that β-catenin was undetectable in the intercalated discs of cardiomyocytes of Dishevelled-1 knockout mice post-MI, compared to wild type mice [108]. In a more recent study, Malekar *et al* demonstrated that over-expression of Dishevelled-1 in mice accelerated cardiac remodeling and further deteriorated cardiac performance following cardiac hypertrophy, induced by aortic banding [109]. The above studies clearly suggest that Wnt signaling, canonical and non-canonical, is involved in the cardiac remodeling process. The apparent contradiction of the above investigations could be explained by the fact that two different transgenic animal models were used, either lacking or over-expressing Dishevelled-1. The results from the knockout studies suggest that Wnt signaling is essential for cardiac remodeling but as suggested by the over-expression experiments, over-stimulation of this pathway causes the opposite effect. Moreover, given that Dishevelled-1 is

implicated in both the canonical and the non-canonical Wnt pathways it is difficult to draw any conclusions about the role of each Wnt signaling branch in cardiac remodeling by these studies.

More importantly, several studies have demonstrated that GSK3β plays a major role in the hypertrophic response of the adult heart following pathologic stimuli and that it represents one of the most potent anti-hypertrophic factors described so far. Kerkela *et al* showed that deletion of GSK3β is embryonic lethal, results in severe cardiac defects and causes hypertrophic cardiomyopathy phenotype [110]. Antos *et al* demonstrated that cardiac specific expression of a constitutively active form of GSK3β abolished the hypertrophic response to chronic β-adrenergic stimulation and pressure overload [111]. Furthermore, additional reports have highlighted the negative impact of GSK3β in cardiac hypertrophy [112]. GSK3β plays a central role in canonical Wnt signaling pathway regulating the protein levels of cytoplasmic β-catenin. Haq *et al* demonstrated that the anti-hypertrophic role of GSK3β is mediated in a Wnt-independent mechanism but the exact molecular mechanisms of the protective role of GSK3β remains largely unknown [113].

The expression level of β-catenin together with its cellular localization represents one of the most reliable markers of the activation status of canonical Wnt signaling pathway [79]. Thus the role of β-catenin in cardiac remodeling has been the subject of several investigations. Haq *et al* demonstrated that stabilization of β-catenin induced cardiac hypertrophy *in vivo* and *in vitro.* Nevertheless, the authors also showed that the β-catenin stabilization was mediated by PKB recruitment, independently of Wnt signaling pathway [113]. Moreover, additional reports have indicated that cardiomyocyte-specific ablation of β-catenin attenuates the cardiac hypertrophy phenotype induced by aortic constriction [114, 115]. In disagreement with the above data,

Baurand *et al* demonstrated that cardiomyocyte-specific deletion of β-catenin promoted the hypertrophic response, induced by angiotensin II infusion [116]. Furthermore, Hahn *et al* demonstrated that adenoviral-mediated over-expression of a constitutively active form of β-catenin had an anti-apoptotic role in cardiac fibroblasts and cardiomyocytes while promoting a hypertrophic response in cardiomyocytes and a hyperplastic response in cardiac fibroblasts [117]. In the same study, administration of constitutively active β-catenin in the infarct/border zone resulted in reduced infarct size in a rat heart [117]. The above results suggest that β-catenin is involved in cardiac remodeling but its exact role depends on the nature of the pathologic stimuli and further investigation is required.

A number of additional studies have investigated the role of Wnt inhibitors such as Sfrp1 (FrzA) and Sfrp2 in cardiac remodeling. The effects of Sfrp1 in cardiac healing were tested in the settings of permanent coronary ligation and ischemia/reperfusion by Barandon *et al.* In a first report the authors demonstrated that general over-expression of the Wnt-inhibitor Sfrp1, under the control of the CMV promoter, reduced the infarct size and prevented cardiac rupture [118]. In a second report, the authors placed Sfrp1 under the control of a cardiomyocyte-specific promoter (alpha myosin heavy chain) and tested this model in the setting of ischemia/reperfusion. In this study, Sfrp-1 over-expressing mice displayed larger infarct size and worse cardiac function than control littermates [119]. The apparent contradiction in the results of the two reports is most likely attributed to the different expression pattern of Sfrp1 (universal versus cardiac) due to the use of different promoters (CMV versus α-myosin-heavy chain).

Recent reports have introduced another Wnt inhibitor, Sfrp2, as a potent regulator of the cardiac remodeling process. Initially, Mangi *et al* demonstrated that intramyocardial

implantation of genetically engineered mesenchymal stem cells ($MSCs^{Akt}$) to over-express the Akt gene decreased significantly the extent of myocardial damage caused by myocardial infarction [120]. In a follow up study of the same group, Gnecchi *et al* suggested that the beneficial effects of $MSCs^{Akt}$ in the injured heart are predominantly mediated by paracrine mechanisms and not due to donor cell-mediated cardiac regeneration [121]. Investigation for secreted $MSCs^{Akt}$-derived factors resulted in the identification of Sfrp2 as a key paracrine protein with beneficial effects on cardiomyocyte survival and cardiac function [122]. Sfrp2 was shown to play a pro-apoptotic role rescuing the cardiomyocytes in the ischemic myocardium through an unclear mechanism that is likely to involve increase of the β-catenin levels [122]. However, the beneficial role of Sfrp2 in cardiac healing after myocardial infarction was challenged by Kobayashi *et al* in a recent report [123]. The authors demonstrated that ablation of Sfrp2 is cardio-protective as Sfrp2-null mice subjected to myocardial infarction exhibited less amount of fibrosis and improved cardiac performance, in comparison to control wild type littermates [123].

Overall, the above studies provide valuable information about the function of the Wnt signaling pathway in cardiac remodeling. Both Wnt signaling cascades, β-catenin dependent and independent, are actively participating in cardiac healing following cardiac injury (cardiac hypertrophy or myocardial infarction). Despite some controversial results there is a substantial amount of data suggesting that inhibition of canonical Wnt signaling following cardiac injury might be beneficial. Additional experiments are required in order to systematically investigate the role of Wnt signaling pathway in the adult heart under physiologic and pathologic conditions.

Given the potent anti-hypertrophic role of GSK3β, it is reasonable to hypothesize that Wnt ligand-mediated inhibition of GSK3β could potentially result in deterioration of cardiac hypertrophy and improve cardiac performance.

21. Insulin growth factor binding protein 3

The insulin growth factor (IGF) signaling cascade is one of the fundamental evolutionarily conserved growth control systems during development, adulthood and disease [124]. Normal growth under the control of the IGF signaling system requires well balanced coordination between various players such as IGF-I and IGF-II, insulin, IGF receptors, IGF binding proteins (IGFBPs) and IGFBP proteases [124, 125]. The signaling cascade is initiated by the binding of IGFs to the cell membrane IGF receptors (Figure 6). The bioavailability of IGFs is tightly regulated by the action of IGFBPs, which bind and control their interaction with the IGF-receptors as well as their transport between intra- and extra-vascular spaces. The bioactivity of IGFBPs is also tightly regulated by the action of proteases such as metalloproteinases [124, 125].

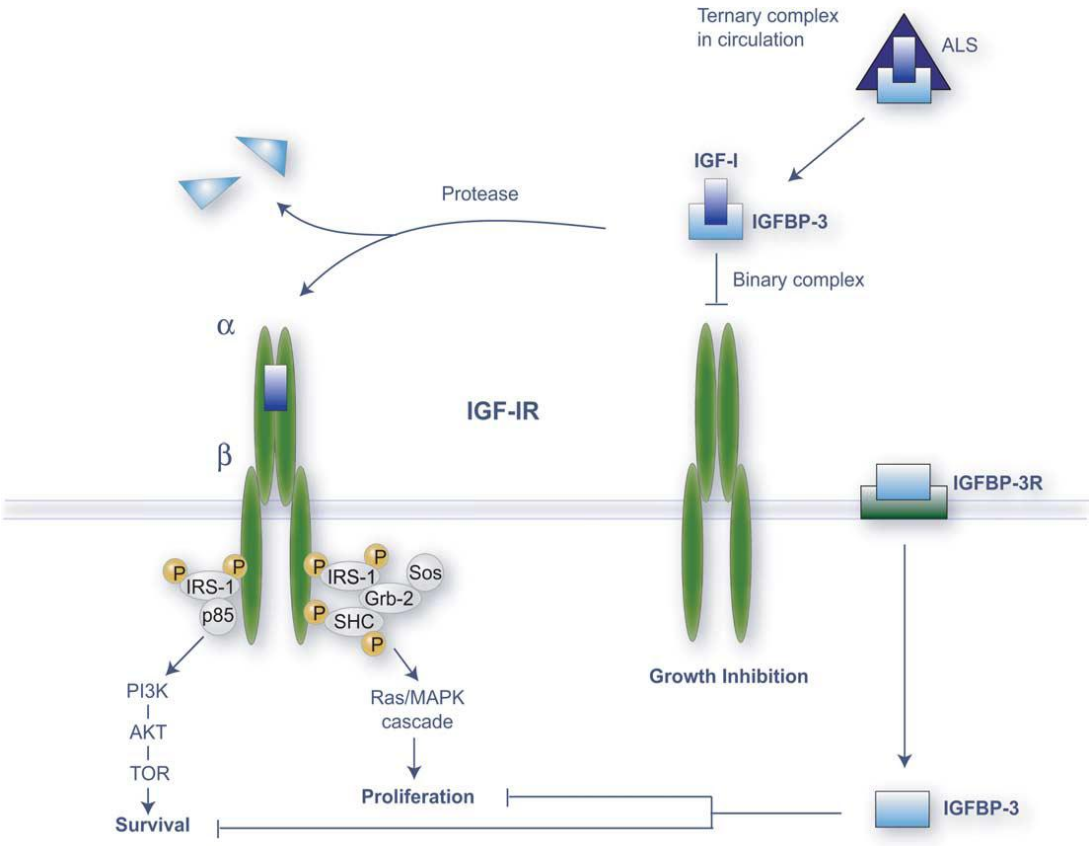

Figure 6: Schematic representation of the interactions of IGFBP3 with IGF-I and ALS, the signal transduction cascades activated by IGF-I and the IGF-dependent and IGF-independent mechanism of action of IGFBP3 through an unknown cell surface receptor. Adapted from Burger *et al*, Eur J Cancer. 2005; 41(11): 1515-27

IGFBPs represent a large family of secreted proteins consisting of six high affinity members (IGFBP 1-6) and several IGFBP low affinity proteins (IGFBP related proteins, IGFBP-rP 1-10) [125, 126]. All IGFBPs have three distinct domains, two conserved, cysteine rich, amino- and carboxy terminal domains and a non-conserved middle domain. IGFBP3 and IGFBP5 are more structurally related than the other four members [125, 126]. IGFBP-4 is the smallest member of the IGFBP protein family. IGFBP-4, similarly to other IGFBP proteins is composed by three domains. In the variable middle region of IGFBP4 there are two extra

Cysteine residues. IGFBPs contain various binding sites through which they can interact with several bio-regulators such as heparin, nuclear partners (retinoid acid receptors and others), glycosaminoglycans, fibrin, fibrinogen and most importantly IGFs [125-127].

IGFBP3 is the most abundant member of the IGFBP protein family. It is responsible for carrying more than 75% of the serum IGF-I and IGF-II in ternary complexes with ALS (acid-labile subunit), a liver derived glycoprotein [127]. IGFBP3 binds IGFs with higher affinity than the IGF receptors (IGFBPs/IGFs have a Kd of ~10^{-10}M whereas IGFs/IGF receptor has a Kd of ~10^{-8} to 10^{-9}M) [125]. IGFBP3 mediates its actions predominantly in an IGF-dependent mechanism [127].

Initially, NMR studies suggested that only the amino-terminal domain of IGFBP3 can bind to IGFs. Moreover, mutational studies using the full length cDNA of IGFBP-3 proved that the amino terminal domain is essential for IGF binding [128]. However, recent studies have shown that the carboxy-terminal domain can also bind to IGFs. The current consensus is that IGFBP3 contains IGF binding sites in both the amino- and the carboxy-terminal domains with the carboxy-terminal domain being of particular importance for the IGFBP3/IGF interaction [128]. The absence of the IGFBP3 crystal structure sustains an uncertainty regarding the detailed structure of the IGF binding pocket in IGFBP3.

Nonetheless, several reports have indicated that IGFBP3 can function also in an IGF-independent mechanism through the interaction of a currently unknown receptor and/or through nuclear action [127]. The expression levels of IGFBP3 are regulated in both the transcriptional and post-translational level. Currently, there are no reports of miRNAs or other small regulatory RNA oligonucleotides that can regulate the expression levels of IGFBP3. IGFBP3 can be post-

translationaly modified by proteolysis through various metalloproteinases as well as by phosphorylation, glycosylation and ubiquitination. The transcription of IGFBP3 can be regulated through various ways such as p53, vitamin D, hypoxia and androgen stimulation [127].

Currently, there is little evidence connecting IGFBP3 with cardiovascular diseases. In a recent report by Pucci *et al* it was demonstrated that failing human hearts had substantially higher levels of IGFBP3, in comparison to donor hearts [129]. In another study by Henson *et al,* it was shown that IGFBP3 is significantly increased in the rat heart over a period of twelve weeks following myocardial infarction [130]. In the same study, it was also shown that treatment of neonatal rat cardiomyocytes with recombinant IGFBP3 induced the expression of hypertrophic markers such as atrial natriuretic peptide (ANP) and β-myosin heavy chain (β-MHC) [130]. A potent relationship between IGFBP3 and cardiac pathophysiology was further emphasized by studies performed in IGFBP3 over-expressing mice [131]. These transgenic animals were expressing IGFBP3 under the control of the metallothionein 1 promoter (active predominantly in the liver and kidney) [131]. Although the transgenic mice were phenotypicaly normal they demonstrated selective organomegaly, as their spleen, liver and heart were significantly heavier when compared to the respective organs of wild type mice [131]. On the other hand, IGFBP3 knockout mice as well as IGFBP3-IGFBP4-IGFBP5 triple knockout mice did not demonstrate any signs of cardiac dysfunction [132]. Moreover, the triple knockout mice in contrast to single knockout mice lacking IGFBP3 or IGFBP4 or IGFBP5 demonstrated growth retardation in the adulthood and altered metabolic activity [132].

22. Goal of the study

The goal of the current study is to investigate the role of canonical Wnt signaling pathway in CSP cells as well as during cardiac remodeling in post-MI myocardium. As mentioned earlier, currently little is known about the effects of this pathway on adult cardiac progenitor cells. Moreover, the exact contribution of Wnt signaling in cardiac healing and homeostasis is still not well defined since several controversial studies have been published. In this thesis it is demonstrated for the first time that Wnt signaling is down-regulated in CSPs following myocardial infarction. Moreover, *in vivo* evidence reveals that administration of r-Wnt3a, a canonical Wnt ligand, deteriorates cardiac performance following MI. Furthermore, it is shown that activation of the canonical Wnt signaling pathway decreases the proliferation of CSPs by altering their cell-cycle progression and promotes their cardiomyogenic differentiation. Finally, this work reveals that insulin growth factor binding protein 3 (IGFBP-3) represents a main mediator of the anti-proliferative effects of Wnt signaling on CSPs, via an IGF-dependent mechanism.

4. Materials and Methods

Animals: C57BL6 and C57BL/6-Tg (ACTBGFP) 10SB/J male mice were purchased from Jackson laboratories at the age of 8-12 weeks old. Adult male (7-8 weeks old, 200 gr) and neonatal (1-2 days old) Wister rats were purchased from Charles River laboratories. All animal studies strictly adhered to the guidelines of the Harvard Medical School, the Longwood Medical Area's Institutional Animal Care and Use Committee (IACUC) and the National Society for Medical Research.

Experimental myocardial infarction (MI): MI was generated via permanent coronary ligation as previously described [133]. Briefly, C57BL/6J male mice (8-10 weeks old) were anesthetized using 65 mg/kg pentobarbital. Mice were ventilated using a standard rodent ventilator. An incision was performed between the fourth and the fifth intercostals spaces. After the pericardium was removed a descending coronary artery was permanently ligated with a silk suture. Sham-operated animals underwent an identical surgical operation without occlusion of the coronary artery. To prevent any post-operative discomfort animals received buprenorphine (0.03-0.06 mg/kg) for a period of 48 hours.

Injection of r-Wnt3a and r-SFRP-2: 400 ng of recombinant Wnt3a (R&D Systems, #1324-WN/CF) and recombinant SFRP-2 (R&D Systems, #1169-FR/CF)or vehicle were injected intra-myocardially in the left ventricular free-wall, in the absence of MI or immediately after the occlusion of the descending coronary artery. In each animal was administered a total of 10 μl of

solution, which was delivered in 3 different sites, using a 5 μl syringe (Hamilton Co, Microliter # 65).

Echocardiography: Echocardiograms were obtained at baseline (1 day prior coronary occlusion) and 7 days following MI, with a Vevo 2100 Imaging digital ultrasound system (VisualSonics). Echocardiography was performed using an 18-38 MHz linear-array transducer. Prior to echocardiography, mice were lightly anesthetized with 1% isoflurane in oxygen, the chest was shaved and the animals were placed on a heated platform in the supine position. Isoflurane concentration was reduced in order the heart rate to return to physiologic rates (>500 beats perm minute). Data acquisition was initiated with the parasternal cardiac long axis view and subsequently with a short axis view, at the level of mid-papillary muscles. Echocardiographic measurements were performed from M-mode images. All data were acquired and analyzed in a blind fashion.

Heart fixation: Mice were anesthetized by intraperitoneal injection of pentobarbital (65 mg/ml) followed by intraperitoneal administration of 100 IU/ml anticoagulant heparin. Hearts were rapidly excised and washed briefly in Krebs buffer (NaCl 137 mmol/L, KCl 4.0 mmol/L, $CaCl_2$ 1.8 mmol/L, KH_2PO_4 1.2 mmol/L, $MgSO_4$ 1.2 mmol/L, $NaHCO_3$ 24.9 mmol/L, and dextrose 11.2 mmol/L (pH 7.4)). A short cannula was connected to the aortic root to initiate retrograde perfusion by the Langerdoff apparatus. A thin cannula was pierced through the apex of the left ventricle (LV) to vent the besian drainage. A ventricular balloon was inserted into the LV through the mitral valve via an incision in the left atrium. The balloon was connected to a

pressure transducer (Statham P23Db, Gould) for recording LV pressures. Hearts were paced (Grass Instruments) with platinum wires placed on the epicardial surface of the right ventricle. Coronary perfusion pressure was held constant during the duration of the experiment at 80 mm Hg. The balloon was inflated with saline to adjust the end-diastolic pressure (EDP) to 5 mm Hg. When the end-diastolic pressure reached 5 mm Hg, hearts were arrested in diastole with KCl and were perfusion-fixed with 10% buffered formalin solution at a hydrostatic pressure of 40-50 mm Hg for 15 minutes. Hearts remained overnight in 10% buffered formalin solution at 4^{o}C. Subsequently, the balloon and the excess formalin were removed and the hearts were weighed. Hearts were imbedded in paraffin, were cut in three parts (apex, middle, base) and were analyzed by immuno-histochemistry.

Cardiac SP cell preparation: Minced cardiac tissue was digested with 0.1% collagenase B (Roche), 2.4 U/ml dispase II (Roche Molecular Biochemicals), and 2.5 mmol/L CaCl2 at 37°C for 30 minutes, filtered through 70 μm and 40 μm filters, and washed with HBSS buffer supplemented with 2% fetal bovine serum and 10 mmol/L HEPES (Sigma, #H7006, MW 238). Cardiomyocyte depleted mononuclear cell suspensions were incubated with Hoechst 33342 (5 μg/ml) (Sigma, #B2261) at 37°C for 90 minutes in Dulbecco's modified Eagle's medium (DMEM) (CellGro) (2% fetal bovine serum (FBS), 10 mmol/L HEPES) at a concentration of 10^6 mono-nucleated cells/mL. Verapamil (50 mmol/L) (Sigma, #V4629) was used as inhibitor of the Hoechst dye efflux. Cell surface antigen staining was performed at 4°C for 30 minutes using fluorochrome-conjugated monoclonal rat anti-mouse antibodies reactive to Sca-1, CD31, and

CD45 (Pharmingen). Respective isotype controls (Pharmingen) were used as negative controls. 7-Aminoactinomycin-D (7-AAD) was added to detect dead cells during FACS analysis.

FACS analysis: FACS was performed using FACSAria (Becton Dickinson, BD) equipped with triple lasers. The Hoechst dye was excited by a 20 mW UV laser (350 nm). SP cells were identified as Hoechst-low cells as previously described [65]. Phycoerythrin (PE), green fluorescence protein (GFP), and 7-AAD fluorescence were detected using a 488-nm laser. Allophycocyanin (APC) was detected using a 640-nm laser. Acquired data were analyzed using FACSDIVA software (BD Biosciences).

Immunocytochemistry for intracellular antigens (for FACS analysis): CSP cells (in vitro expanded or freshly isolated) were fixed and permeabilized at 4^{o}C for 20 minutes using the BD Cytofix/Cytoperm solution from BD Biosciences or a solution of 4% paraformaldehyde. During this fixation the suspension was mixed once or twice. Subsequently, the cells were washed twice with a BD Perm/Wash solution from BD Biosciences. The cell pellet was resuspended in 50-100 µl of the same BD Perm/Wash solution containing FITC-conjugated Ki67 antibody (Santa Cruz, 4ng/µl). Staining reactions was performed at 4^{o}C for 30 minutes in dark. Before analysis the cells were washed twice in HANK'S solution and were analyzed with BD FACSAria or Accuri C6 Flow cytometers.

Cardiac SP cells expansion and lentiviral infection for TCF-controlled luciferase assay: Freshly isolated CSPs were cultured for numerous passages in expansion medium [α-MEM culture

medium supplemented with 20% FBS (fetal bovine serum), 2 mM L-Glutamine and 1% penicillin/streptomycin (P/S)] at a density of 5-8 cells/mm^2. The culture medium was replaced every 72 hours.

CSPs from passage 3-5 were infected with the pBARL (TCF-controlled luciferase reporter) and pSL9 (Ef1-a-controlled Renilla luciferase control) lentiviruses (kindly provided by Dr. R. Moon, Washington University). CSPs were seeded the day prior to infection in a sub-confluent density (70-80% or 24-28 cells/mm2) in a 60 mm culture dish. The following day the culture medium was replaced by 3 ml viral-medium (2.9 ml of pBARL lentivirus and 50 µl of pSL9 lentivirus) supplemented with 3.6 µl [6µg/ml] of protamine sulfate (Sigma). The culture medium was replaced again 48 hours post-infection.

Production of lentiviruses: All lentiviruses were produced using HEK293-T cells (human embryonic kidney 293 cells). The day prior to transfection HEK 293-T cells were seeded in sub-confluent density (approximately 70-80%). The culture medium (DMEM low glucose, 7% FBS and 1% penicillin-streptomycin (P/S)) was renewed 2 hours prior to transfection. For the production of the GFP-over-expressing lentivirus and the IGFBP-3 and IGFBP-4 expressing lentiviruses the following mixture was prepared: the plasmid DNA of the transducing vector (GFP) (3.2µg) was mixed with the plasmid DNA of the various lentiviral components (4.0µg gagpol, 0.4µg REV, 0.4 µg TAT, 0.4µg VSVg) to a final volume of 40 µl. Subsequently, the plasmid DNA cocktail was mixed with 160 µl of DMEM (no serum or P/S and 24µl of Fugene (transfection reagent by Roche, 04709705001) to a final volume of 224µl. The final mixture was incubated for 15-45 minutes at room temperature (RT) prior to addition to the HEK293-T cells.

The next day the culture medium was replaced by CSP expansion medium and 48 and 72 hours post transfection GFP-expressing lentivirus was harvested, filtered through a 0.45µm filter to remove cellular debris, aliquoted and stored at -80^{o}C.

For the production of the pBARL, pfuBARL and pSL9 lentiviruses the following protocol was applied. The day prior to transfection HEK 293-T cells were seeded in sub-confluent density (approximately 70-80%). The plasmid DNA mixture was prepared by mixing 4µg of transducing vector (pBARL or pSL9 or pfuBARL), 8µg of packaging vector (gag-pol, pSL4), 2µg of envelope vector (pSL3), 4µg of rev plasmid with 50µl of 2.5M CaCl2 to a final volume of 500 µl (scaled up with ddH2O). 500µl of filtered 2X HBS solution of pH 7.1 [2X HBS solution: 5.6ml of 2M NaCl, 4ml of 0.5 HEPES (pH 7.0), 600µl of 0.1M Na2PO4 scaled up to 40ml with ddH2O] was added drop wise in this plasmid DNA solution. The final solution was added drop wise to the cells. 16-18 hours post-transfection fresh CSP expansion medium was added and the cells were cultured over-night. 48 and 72 hours post transfection the lentivirus-containing medium was harvested, filtered through a 0.45µm filter to remove cellular debris, aliquoted and stored at -80^{o}C.

For the production of the shRNA expressing lentivirus against IGFBP-3 and IGFBP-4 the following protocol was followed: The day prior to transfection HEK 293-T cells were seeded in sub-confluent density (approximately 70-80%). The plasmid DNA mixture was prepared by mixing 3µg of transducing vector expressing the shRNA, 3µg of envelope vector (VSVg), 0.375µg of packaging vector (dvpr8.2) with 18µl of Fugene HD and DMEM (no serum and no P/S) up to 300µl total volume. The final mixture was incubated at RT for 15-45 min and it was added to the HEK293-T cells drop-wise. The next day the culture medium was replaced by CSP

expansion medium and the cells were cultured over-night. 48 hours post-transfection the shRNA-lentivirus containing medium was harvested, filtered through a 0.45μm filter and directly applied on the target cell population (CSPs) supplemented with protamine sulfate (6μg/ml).

RNA isolation: Total RNA was extracted from various samples with different protocols depending on the experimental conditions and requirements. Total RNA was extracted from myocardial tissue using Trizol reagent (Invitrogen, 15596-018) and it was further purified using an RNeasy Mini Kit (Qiagen). Briefly, myocardial tissue was homogenized in 1 ml of Trizol using a mortar and pestle. Samples were incubated at RT for 5 minutes and subsequently 0.2ml/1ml of Trizol was added. Samples were mixed thoroughly by hand and were incubated at RT for 3 minutes. Following centrifugation at 4^{o}C for 20 minutes at 13,000 rpm, the solution was separated into three distinct phases (a lower red, phenol-chloroform phase, an inter-phase, and a colorless upper aqueous phase, where the RNA remains exclusively). The aqueous phase from each sample was transferred in a new eppendorf polypropylene tube that contained isopropanol (0.5ml/1ml of Trizol). Again all samples were mixed thoroughly by hand and were incubated at RT for 10 minutes. Samples were centrifuged at 4^{o}C for 30 minutes at 13,000 rpm. Following centrifugation total RNA was precipitated and the supernatant was carefully removed by vacuum aspiration. The formed RNA pellet was washed by adding 0.5ml of 70% ethanol and the samples were again centrifuged at 4^{o}C for 5-7 minutes at 13,000 rpm. At the last step the ethanol was again removed by vacuum aspiration and the pellet was briefly (3-5 minutes) air-dried. At this step excess of ethanol was removed by careful vacuum aspiration to avoid ethanol contamination of the samples that will inhibit further applications. The RNA pellet was

dissolved by adding RNase-free ddH2O (30 µl) and subsequently it was stored in -80^{o}C. By using the same method (addition of Trizol) total RNA was also isolated from expanded CSPs either grown on a monolayer or following trypsinization (after proliferation assays). When total RNA was harvested from adherent CSPs 1 ml of Trizol was added directly in the culture plate (60mm), following a quick wash with ice cold 1X PBS, and CSPs were homogenized by continuous pipetting. When total RNA was isolated from trypsinized CSPs, 1 ml of Trizol was added in the pellet and the cells were again homogenized by continuous pipetting. Subsequently, in both cases the above protocol was followed. Total RNA was isolated from freshly isolated CSPs by using the 'Absolute RNA Nanoprep kit (Stratagene, #400753) according to the instructions of the manufacturer.

DNase treatment: Genomic DNA was removed from all total RNA samples by using Turbo-DNA free kit (Ambion, 1907) according to the manufacturer's instructions. 2-3 units of DNase were added to each RNA sample and the samples were incubated at 37^{o}C for 30 minutes. Subsequently, DNase was inactivated by addition of a DNase inactivation reagent (provided in the kit). Samples were incubated at RT for 5 minutes under continuous mixing and then were centrifuged (4^{o}C, 3min, 13,000 rpm). Supernatant was transferred in a new RNase-free polypropylene eppendorf tube and it was stored at -80^{o}C.

RNA clean up: Total RNA isolated with the Trizol protocol intended to be utilized for qRT-PCR arrays was further purified using RNeasy Mini Kit (Qiagen, 74104) according to the manufacturer's instructions. Briefly, the volume of the RNA samples was adjusted to 700µl by

the addition of RNase-free ddH2O, cell lysis buffer and 95-100% ethanol. Following centrifugation (4^{o}C, 1min, 13,000 rpm) samples were loaded to a column. The column was washed twice and RNA samples were eluted by adding 30µl of RNase-free ddH2O and centrifuging for 1 minute at 4^{o}C at 13,000 rpm.

Reverse Transcriptase reaction: Complementary DNA (cDNA) was synthesized using the iScript cDNA synthesis kit (Bio-RAD, #170-8890) according to the manufacturer's instructions. Briefly, 0.5-1µg of total RNA was mixed with reverse transcriptase and the appropriate buffer containing random primers. The synthesis of the cDNA was performed according to the following reaction protocol: 5 minutes at 25ºC, 30 minutes at 42ºC, 5 minutes at 85 º C and an optional hold at 4 º C.

cDNA was also synthesized for the qRT-PCR based gene arrays by using the RT2 First Strand synthesis kit (Superarray, SABiosciences, #C-03) according to the manufacturer's instructions. Briefly, 0.4-1µg of total RNA was mixed with genomic elimination buffer (provided in the kit) and the reaction mixture was incubated at 42^{o}C for 5 minutes. Subsequently, the reverse transcription reaction cocktail (containing reverse transcriptase, random primers, external controls and buffer) was added to the RNA samples and the final mixture was incubated at 42^{o}C for 15 minutes. The reaction was stopped by incubation at 95^{o}C for 5 minutes. The synthesized cDNA was further diluted by adding 91µl of RNase-free ddH2O and it was stored at -20^{o}C for further use.

Quantitative Real Time Polymerase Chain Reaction (qRT-PCR) based gene array: qRT-PCR-based gene-arrays are commercially available from SABiosciences. Each 96-well plate gene-

array contains 84 genes related to the examined biological process, 5 housekeeping genes (Gusb, Hprt1, Hsp90ab1, Gapdh, Actb), 3 controls of the efficiency of reverse transcription, 3 controls of PCR efficiency. cDNA prepared from freshly isolated CSPs sorted from sham and post-MI animals was utilized to run a Wnt signaling pathway focused qRT-PCR array (#PAMM-043). cDNA prepared from CSPs treated with vehicle and Wnt3a-CM was utilized to run a cell cycle focused gene array (#PAMM-020) and a signal transduction pathway finder gene array (#PAMM-014). cDNA prepared from CSPs infected with mock and IGFBP-3 over-expressing lentivirus and with scramble and shIGFBP-3 over-expressing lentivirus was utilized to run a cell cycle focused gene array (#PAMM-020). The exact cycling program that was applied for all qRT-PCR gene arrays was the following: a) 1 cycle (1 step) at 42^{o}C for 10 minutes (activation of the hot start DNA polymerase), b) 40 cycles consisted of 1 step at 95^{o}C for 15 seconds and another step at 60^{o}C for 1 minute (annealing and prolongation of the PCR products), c) 1 cycle (1 step) at 55^{o}C for one minute (to bring all PCR products to same temperature), d) 1 cycle consisted of 80 steps starting at 55^{o}C and increasing 0.5^{o}C /step (to generate the melting curve data). Detection and record of SYBR green fluorescence from every well was set up during the annealing step of each cycle.

All qRT-PCR gene arrays were performed according to the manufacturer's instructions using a MyiQ cycler (Bio-Rad). In all cases data were acquired from 3 independent experiments and data analysis was performed as follows: Only results without apparent genomic DNA contamination and no RT inhibition were analyzed. Briefly, ΔCt values of all examined genes were obtained by subtracting the mean threshold cycle (Ct) value of 5 housekeeping genes from the Ct value of each gene. Subsequently, $\Delta\Delta$Ct values for all genes were calculated as follows:

$\Delta\Delta Ct = \Delta Ct$ experimental $-\Delta Ct$ control. Finally, fold difference of all genes was calculated based on the formula: $2^{-\Delta\Delta Ct}$. Statistical analysis was performed using the Student's unpaired t test and significant differences were identified when p value was ≤ 0.05.

qRT-PCR: cDNA produced from CSPs treated with vehicle or Wnt3a-CM was used to measure the expression of various genes by qRT-PCR. All qRT-PCR reactions were performed in a MyiQ cycler (Bio-Rad). The exact cycling program that was applied for all qRT-PCR experiments was the following: a) 1 cycle (1 step) at 95^{o}C for 3 minutes, b) 40 cycles consisted of 1 step at 95^{o}C for 15 seconds and another step at 60^{o}C for 1 minute, c) 1 cycle (1 step) at 55^{o}C for one minute, d) 1 cycle consisted of 80 steps starting at 55^{o}C and increasing 0.5^{o}C /step. Detection and record of SYBR green fluorescence from every well was set up during the annealing step of each cycle. All primers used in the qRT-PCR experiments were designed by using the Primer3 software and their specificity was examined by BLAST. The primers used for IGFBP3 are the following: forward, 5'-ATTCCAAGTTCCATCCACTCC-3' and reverse 5'-GTGTGTCCTCCATTTCTCTGC-3'. The primers used for IGFBP-4 are the following: forward, 5'- ATCCCCATTCCAAACTGTGAC-3' and reverse 5'- GATCCACACACCAGCACTTGC-3'). The primers used for GAPDH are the following: forward, 5'-TCACCACCATGGAGAAGGC-3' and reverse 5'-GCTAAGCAGTTGGTGGTGCA-3').

Production of conditioned media (CM): a) Wnt3a and Wnt5 CM: Vehicle-CM, Wnt3a-CM and Wnt5-CM were produced from L-M (TK-) cells, from L-M (TK-)-Wnt3a cells and L-M (TL-)-Wnt5 cells respectively, all purchased from ATCC. CM was produced and stored according the

manufacturer's instructions. b) Dkk-1 CM: HEK293T cells were transfected with 20 µg of fg-Dkk-1 or control plasmid (pc-DNA3.1). Plasmids were mixed with 2.5M CaCl2 and 2M NaCl, 0.5M Hepes (pH 7), 1M NaH2PO4 adjusted to a final volume of 2 ml (pH 7.1). 24 hours post transfection media was replaced to standard expansion medium. Vehicle-CM and Dkk-1-CM were harvested 48 hours and 72 hours post-transfection. Cellular debris was removed by centrifugation (5 min, 1600 rpm) and CM was stored at 4^{o}C.

Cell viability assay: Cell death of CSPs was determined by using the Annexin-V kit (Abcam, #14085) according to the manufacturer's instructions. Briefly, CSPs were treated with 25% of vehicle and Wnt3a-CM for 6 days. CSPs were trypsinized and were dissolved in 500µl of 1X Annexin-V binding buffer. Then 5µl of Annexin-V and 5µl of PI or 7-AAD were added to the cell mixture, which was incubated 5-15 minutes at RT in the dark. Cells were analyzed for Annexin-V and PI or 7-AAD staining by flow cytometry (Accuri C6 Flow cytometer).

Luciferase assay: Luciferase activity in infected CSPs was determined using dual luciferase kit (Promega) according to the manufacturer's instruction. Briefly, cell lysates were prepared from trypsinized CSPs and subsequently were used to determine the values of Firefly luciferase and Renilla luciferase using a 20/20n Luminometer (Turner Biosystems).

Proliferation assays: The proliferative capacity of CSPs was determined in expanded passage 4-6 CSPs by determining total cell number, BrdU (5-bromo-2'-deoxy-uridine) incorporation, detection of phospho-Histone-H3 and staining with PI.

Total cell number: Ten thousand CSPs from passage 4-6 were plated onto 60 mm culture dishes. CSP cell were incubated in normal expansion medium or in expansion medium supplemented with 10-30% conditioned medium derived from L-cells or L-Wnt3a cells with or without Dkk-1 or pcDNA3.1 conditioned media. In some experiments CSPs were incubated in the presence of 1-5 μM BIO. Cardiac SP cells were trypsinized and the cell number was counted using a hematocytometer at day 6. Culture medium was replaced every 72 hours.

Immunocytochemistry for phospho-histone H3: CSPs from passage 4-6 were plated and cultured in expansion medium supplemented with 25% conditioned medium derived from L-cells or L-Wnt3a cells for 5 days. Cells were washed twice with PBS, fixed with 4% paraformaldehyde solution and permeabilized with methanol. CSPs were subsequently incubated in 1% BSA solution for one hour and then stained with a primary antibody against phospho-histone H3 (Abcam) for 2 hours followed by 2 hours staining with secondary antibody (Alexa-555, Molecular probes) at room temperature. Coverslips were mounted on the slides using a DAPI-containing mounting medium (Vector Vectashield, #H-1200). Cells were visualized using Zeiss epi-fluorescent microscopy (Zeiss, Axiovert 200M).

BrdU incorporation detection: Ten or twenty thousand CSPs from passage 4-6 were plated onto coverslips in 60 mm culture dishes in expansion media supplemented with 25% conditioned medium derived from L-cells or L-Wnt3a cells for 5 days. At day 5 CSPs were pulsed with 10μM BrdU for 1 hour. Cells were labeled with a BrdU labeling kit I (Roche, 11296736001) according to the manufacturer's instructions. Coverslips were mounted on the slides using a DAPI-containing mounting medium (Vector Vectashield). Cells were visualized using Zeiss epi-fluorescent microscopy (Zeiss, Axiovert 200M).

Propidium Iodide analysis: Ten or twenty thousand CSPs from passage 4-6 were plated in 60 mm culture dishes in expansion media supplemented with 25% conditioned medium derived from L-cells or L-Wnt3a cells for 5 days. At day 5 CSPs were trypsinized and were fixed in 70% ethanol overnight. Subsequently CSPs were washed with 1X PBS (Phosphate buffered saline) and were incubated for 1 hour in PI staining solution (PBS/ 0.1% Triton-X 100/ 2μg/ml PI/ 400 ng/ml RNAse A). Cells were washed with 1X PBS and were analyzed by FACS. Data were processed by the ModFit Lt software by Verity software house.

IGFBP-3 over-expression: IGFBP-3 cDNA was excised by enzymatic digestion with XbaI and XmaI from vector pSport-6 (Open Biosystems). IGFBP-3 cDNA-fragment was blunted and subsequently ligated into lentiviral expression vector LSLV-83, which drives its expression under the constitutively active promoter EF1a. Selection of infected cells was performed by treatment with neomycin (1mg/ml) for a period of approximately 7-10 days.

IGFBP-4 over-expression: IGFBP-4 cDNA was excised by enzymatic digestion with EcoRV and XhoI from vector pSport-6 (Open Biosystems). IGFBP-4 cDNA-fragment was blunted and subsequently ligated into lentiviral expression vector LSLV-83. Selection of infected cells was performed by treatment with neomycin (1mg/ml) for a period of approximately 7-10 days.

IGFBP-3 shRNA: Five lentiviral vectors pLKO.1-puro encoding different IGFBP-3 short hairpin RNA (shRNA) (TRCN0000112125, TRCN0000112126, TRCN0000112127, TRCN0000112128, TRCN0000112129) were obtained from Open Biosystems. shRNAs TRCN0000112128,

TRCN0000112129 were found to down regulate efficiently the expression of IGFBP-3 in CSPs. Selection of infected cells was performed by treatment with puromycin (4μg/ml) for a period of 7-10 days.

IGFBP-3 mutagenesis: Lentiviral plasmid (LSLV-83) containing WT-IGFBP3 cDNA was utilized as a template for site-directed mutagenesis using the quick-change mutagenesis kit (Stratagene), according to the instructions of the manufacturer. In brief, complementary primers encoding the desired mutations (IGF-binding site and IGF-NLS-domain of IGFBP3) were annealed to the template LSLV-83-IGFBP3 plasmid and the *Pfu* polymerase was used to replicate the template, incorporating the mutated primers. The template plasmid was digested with DpnI, before bacterial transformation. The primers utilized for the mutation of the IGF binding domain are the following: IGFBP3-IGF^{mut}-sense: CCCGCTGAGGGCGGGGGGGAATGGCCGCGGG and IGFBP3-IGF^{mut}-antisense: CCCGCGGCCATTCCCCCCCGCCCTCAGCGGG. The primers utilized for the mutation of the NLS binding domain are the following: IGFBP3-NLS^{mut}-sense: GAAGAAGCAGTGCCGCCTTCCATGGACGGAGAGGCGGGCTTCTGCTGGTGTGT and IGFBP3-IGF^{mut}-antisense: ACACACCAGCAGAAGCCCGCCTCTCCGTCCATGGAAGGGCGGCACTGCTTCTTC.
The sequences of the mutated plasmids were verified by sequencing.

Western blot: Immunoblot was performed as previously described [134] . Briefly, cell pellets were re-suspended in lysis buffer (Cell signaling) supplemented with 1mM PMSF. The cell

suspension was subsequently centrifuged for 15 minutes at 13000 rpm at 4^{o}C and the supernatant transferred in a new tube. Protein concentration was measured using the Pierce BCA protein assay kit according to the manufacturer's instructions (Thermo scientific). Protein samples (30 μg) were loaded into a 4-12% SDS-polyacrylamide gel (Criterion XT, BIORAD) and were electrophoresed at a constant voltage 100 Volts. Proteins then were electrophoretically transferred to a polyvinylidene difluoride (PVDF) membrane at 15 mA overnight at 4^{o}C. The membrane was blocked for one hour with Odyssey blocking buffer (LI-COR Biosciences) before incubation with by primary antibody against IGFBP3 (Santa Cruz) or GAPDH (R&D) for 2 hours at room temperature. Membrane was washed with PBS-T (1X PBS + 0.1% Tween) before incubation with secondary antibodies (Molecular probes) for one hour at room temperature. Antibody binding was detected using the Odyssey infrared system (LI-COR).

Immunoprecipitation: 200-300μl of 2X diluted cell culture medium harvested from CSPs treated with vehicle and Wnt3a-CM was supplemented with 50 μl of protein A/G sepharose beads(Santa Cruz, sc-2003) in order to remove excess IgG. Samples were incubated at 4^{o}C while gently rolling for 30min to 1 hour. Following centrifugation (4oC, 13,000 rpm, 2 minutes) the supernatant of each sample was transferred in a new eppendorf tube and it was supplemented with 2 μg of antibody against IGFBP-3 (rabbit) or 2 μg of rabbit IgG isotype control. Samples were incubated for 3-4 hours at 4^{o}C while being gently rolled. At this point 20μl of protein A/G sepharose beads were added to each reaction mixture and samples were further incubated for 2 hours at 4^{o}C while being gently rolled. Samples were washed 5 times using 0.35ml of lysis buffer each time and finally they were resuspended in 30μl of SDS-loading buffer containing β-

mercaptoethanol (3.1 M). The next day samples were thawed in ice and then were boiled in a heat block (90-95^{o}C) for 5-10 minutes. After a brief centrifugation (4^{o}C, 13,000 rpm, 1 minute) beads were pelleted and 20μl of the supernatant were loaded on SDS-PAGE gradient gel (4-12%).

Isolation of adult and neonatal cardiomyocytes: Adult cardiomyocytes were isolated from male Wistar rats as previously described [51]. Neonatal rat ventricular cardiomyocytes (NRVM) were isolated from Wistar rats. Hearts were quickly excised from neonatal (p1-2) rats and were washed with Hank's Balanced Salt Solution (HBSS). Atria were removed and the ventricles were cut into smaller pieces and subsequently incubated in trypsin solution at 4^{o}C for 18 hours. Trypsin was inactivated by addition of pre-culture medium (DMEM, 7% FBS heat inactivated (Hyclone), 100 μM BrdU, 1.5 mM vitamin B12 and 1% penicillin/streptomycin) for 3 minutes at 38^{o}C, under constant shaking (150 rpm). Subsequently, the semi-digested cardiac tissue was further digested by collagenase solution (1 mg/ml) in a series of subsequent five digestions. The collected cardiomyocyte-containing collagenase solution was centrifuged (200g) and the pelleted cardiomyocytes were re-suspended in pre-culture medium. Following another round of centrifugation the harvested cardiomyocytes were seeded in a T75 flask for a period of one hour. The non-adherent cells were transferred in a second T75 flask and were incubated for an additional hour. Finally, the cardiomyocytes (non-adherent cells) were counted and plated onto laminin-coated coverslips. From this point forward, medium was changed every 24 hours.

Co-culture experiments: Isolated adult and neonatal rat ventricular myocyteswere seeded onto laminin-coated coverslips at a density of 300 cells/mm^2. NRVM were maintained in pre-culture medium. The pre-culture medium was replaced every 24 hours. At day 2, 10,000 GFP^+ CSPs were seeded onto the cardiomyocyte l ayer and maintained for additional 3 days. Co-cultures were incubated in DMEM culture medium supplemented with 7% FBS (heat inactivated), vitamin B12 (1.5mmoles/L), 10 ug/ml insulin, 10 ug/ml transferrin, 1% penicillin-streptomycin and 25% vehicle or Wnt3a-conditioned medium. The cardiomyogenic differentiation of CSPs was evaluated by immunocytochemical staining for a-sarcomeric actinin and measurement of the amount of a-sarcomeric actinin positive CSPs over total CSPs per field. Nuclear staining was performed by supplementation of 4, 6-diamidino-2-phenylindole (DAPI).

Immunocytochemistry: All immunocytochemical analysis was performed with cSP cells from proliferation assays or from co-culture experiments. Cells were washed twice with 1X PBS, fixed with 4% paraformaldehyde, permeabilized with methanol at-20^oC and blocked by incubation with 1% BSA for 1 hour at room temperature. Fixed cells were stained with antibodies against β-catenin (BD Biosciences) phospho-histone H_3 (Abcam), a-sarcomeric actinin (Sigma), BrdU (Roche), IGFBP-3 (Santa Cruz) and e-GFP (Invitrogen). All primary antibodies except BrdU were incubated for 2hours at room temperature. Appropriate secondary antibodies were utilized to detect each primary antibody (Alexa488 or Alexa-555, Invitrogen, Molecular probes). In all cases coverslips were mounted on the slides using a DAPI-containing medium (Vector Vectashield). Cells were visualized using Zeiss epi-fluorescent microscopy (Zeiss, Axiovert 200M).

Heat inactivation of FBS: FBS was stored in -20^{0}C. Initially FBS was thawed in 37^{o}C water-bath and then was transferred in a 56^{o}C water bath for 40 min.

Long term maintenance of expanded CSPs: Cell suspension was centrifuged at 4^{o}C for 5 min at 1500 rpm and the cell pellet was resuspended in 1 ml solution of heat inactivated FBS/DMSO in an analogy 9:1 respectively. Subsequently the cell solution was stored at -80^{o}C for 2-3 days and then stored permanently in liquid nitrogen at -150^{o}C.

Cell counting: Cell counting was performed with standard hematocytometer (LEVY hematocytometer, 0.1 MM depth, HAUSSER SCIENTIFIC). The final number of cells was calculated based on the formula: $No = \alpha * 10^3 * 10$ where α is the average number of counted cells, 10 represents the dilution factor of the cell suspension, 10^3 represents the internal factor of the hematocytometer.

Picrosirius red staining: Collagen deposition was assessed in hearts by picrosirius red staining according to standard histological protocol. Briefly, paraffin sections were dewaxed and re-hydrated through a series of 3 minute incubations in 100% xylene (twice), in 90% and 80% ethanol and water. Subsequently, the nuclei were stained with hematoxyline solution and were washed with running water. Slides were stained with 0.1% picrosirius red solution (Sirius Red dissolved in saturated solution of picric acid) for a period of one hour at room temperature. Finally, slides were stained with acidified water (twice), were dehydrated through a series of 3

minute incubations in water, 80% and 90% ethanol and 100% xylene (twice) and were mounted with coverslips.

Immunohistochemical staining protocol for macrophages: The heart sections were de-waxed and hydrated by placing them sequentially in 100% xylene, 100% ethanol, 95% ethanol, 70% ethanol and then they were rinsed with cold tap water for three minutes. Then heart sections were incubated in citrate buffer (10mM Sodium Citrate, 0.05% Tween 20, pH 6.0) in a pressure cooker for three minutes in full pressure. Heart sections were rinsed with cold tap water for three minutes. Subsequently, the endogenous peroxidase activity in the heart sections was quenched by incubation with 1% of H_2O_2 for a period of ten minutes in room temperature. The heart sections were washed with 1X PBS for five minutes in room temperature and then they were blocked by using normal goat serum (2.5%) for a period of twenty minutes in room temperature. Following blocking, heart sections were incubated with a primary antibody against the Mac-3 (2 μg/ml) in a humidified chamber in 4^oC overnight. The next day the slides were washed three times with 1X PBS and then were incubated with ImmPRESS reagent (Vector laboratories) for a period of 30 minutes. Then the slides were washed with 1X PBS, were incubated with DAB solution for 3 minutes and were immersed in hematoxyline for 2 minutes. Subsequently, the heart sections were incubated briefly with glacial acetic solution and bluing solution (NH_4OH in 70% ethanol). Finally, the heart sections were de-hydrated by sequential incubation in 70% ethanol, 95% ethanol, 100% ethanol and xylene. The slides were mounted and were analyzed by light microscopy.

Digestion with restriction endonucleases: Different amount of plasmid DNA was incubated with 2-5 units of restriction enzyme per μg of plasmid DNA, in the presence of the appropriate buffer. Bovine serum albumin was added when needed at a final concentration of 100μg/ml. The final volume of the reactions was 20-200 μl and they were incubated at 37°C for 2-3 hours.

DNA Ligation reaction: The protocol of the DNA ligation reaction depends on the edges of the DNA molecules. In case of blunted DNA fragments the reaction is incubated at 22^{o}C whereas in case of DNA fragments with protruding (sticky) ends the reaction is incubated at 16^{o}C. For each ligation reaction 100-150 ng of vector plasmid were utilized. The amount of insert for each ligation reaction was calculated by the following formula: ng insert= ng vector*(size insert/ size vector)* ratio insert/vector. The ratio insert/vector is 3/1 and 10/1 for sticky and blunt ends respectively. In all the reactions, T4 DNA ligase (1-3 units for sticky end reactions and 20 units for blunt end reactions) was utilized in the presence of appropriate buffer solution.

Small scale isolation of DNA (mini preps): 1-1,5ml of bacterial culture LB was centrifuged at 13.500 rpm for 1 minute in room temperature. The bacterial pellet was resuspended in 300 μl of P1 solution (50 mM Glucose, 25 mM Tris-HCl (pH 8.0), 10 mM EDTA (pH 8.0), RNAse 200 μg/ml)) under intense vortex. Subsequently, 300 μl of P2 solution (0.2 M NαOH και 1% SDS) were added and the samples were incubated at room temperature for 5 minutes. Then, 300 μl of P3 solution (3M potassium acetate, pH 4.8) were added and the whole sample was mixed very gently and centrifuged at full speed for 30 minutes at room temperature. The supernatant solution was transferred in a new eppendorf tube and resuspended with 750 μl of 100%

isopropanol. Plasmid DNA was precipitated by centrifugation at full speed for 30 minutes in 4^{o}C. The plasmid DNA pellet was washed with 500 μl of 70% ethanol and centrifuged again at full speed for 5 minutes in 4^{o}C. Following removal of the ethanol solution, the DNA pellet was resuspended in 50-100μl of water and its concentration was measured by a spectrophotometer (Nanodrop, Thermo Scientific).

Large scale isolation of DNA (midi preps): DNA isolation in larger scale was performed by the midi prep isolation kits (Qiagen) according to the manufacturer's instructions.

Agarose gel electrophoresis: PCR products were analyzed with agarose gel electrophoresis and they were visualized under UV light. TAE (40mM Tris-Acetate, 1mM EDTA, pH 8.0) and TBE (Tris-base 54.0 g, Boric Acid 27.5 g and EDTA 2.92 g) were used as running buffers. The concentration of the agarose used in the gels was between 1-1.5% according to the size of the PCR products.

Gel extraction: DNA isolation form agarose gel was performed using the DNA Gel extraction kit (Qiagen) according to the manufacturer's instructions.

Statistical Analysis: Statistical differences between groups were evaluated using one way Anova analysis and Student's unpaired t-test, using GraphPad Prism (Version 5.03). All data are presented as mean ± SE. A p-value ≤ 0.05 was considered statistically significant.

5. Results

1. Status of Wnt signaling pathway in the heart and CSP cells following myocardial injury

- *Wnt signaling pathway activation status in post-MI myocardium*

Wnt signaling pathway has a well established role in cardiac development regulating the initial steps of cardiac specification. However, its role in post-MI cardiac remodeling remains largely unknown and controversial. The first goal of my study was to investigate the effects of MI in the activation status of Wnt signaling pathway in post-MI myocardium. I examined separately the infarcted-border zone (left-ventricular free wall) from the remote area (septum) in order to determine probable underlying differences between these anatomically distinct regions of the injured myocardium. Myocardial samples were harvested at 1, 3 and 7 days following the surgical operation and were utilized for the isolation of total messenger RNA (mRNA). mRNA samples from both anatomical areas were used to perform a Wnt-focused quantitative RT-PCR gene array. This array allows the measurement of eighty four (84) Wnt-related genes which are involved in various aspects of Wnt signaling pathway. The 3-D diagrams in Figure 7 present the expression profile of all 84 Wnt-related genes in the infarct-border zone (A-C) and in the remote area (D-F). The gene expression profiles of Wnt-related genes in heart tissue samples derived from the infarct-border zone and the remote area were found to differ as early as 1 day post injury, relative to the respective sham controls. Namely, in the infarct-border zone the vast majority of genes were found to be significantly up-regulated whereas in the remote area most of

the genes were down-regulated. All the Wnt-related genes that were examined in the infarct/border zone and the remote area, at all time points, are listed in Tables 1A-C, 2A-C respectively.

- *Wnt signaling pathway activation status in CSPs isolated from post-MI myocardium*

The expression profiles of the Wnt-related genes in CSPs isolated from post-MI and sham animals are presented in Figure 7 (G-I). Compared to both the infarct-border zone as well as the remote area the expression profile of Wnt-related genes in CSPs is drastically different, with the vast majority of genes being down regulated. All the genes that were significantly altered in CSPs, at all time points, are listed in Tables 3A-C. Statistical analysis revealed that only casein kinase 1 delta (Csnk-1d) was down regulated at 1 day post-MI. In contrast, at later time points, several key regulators of the Wnt signaling pathway such as Fzd5, Fzd6, Tcf3 at day 3 and casein kinase 1a (Csnk-1a1) and β-catenin at day 7 are significantly down regulated. Additionally, at 7 days post-MI, Sfrp-2, a well known inhibitor of canonical Wnt signaling pathway, is significantly up-regulated. These data suggest that the Wnt signaling pathway is down regulated in CSPs post-MI. Thus, combination of the above data with previously reported data from our lab showing increased proliferation capacity of CSPs post-MI led to the hypothesis that canonical Wnt signaling down-regulates their proliferation capacity.

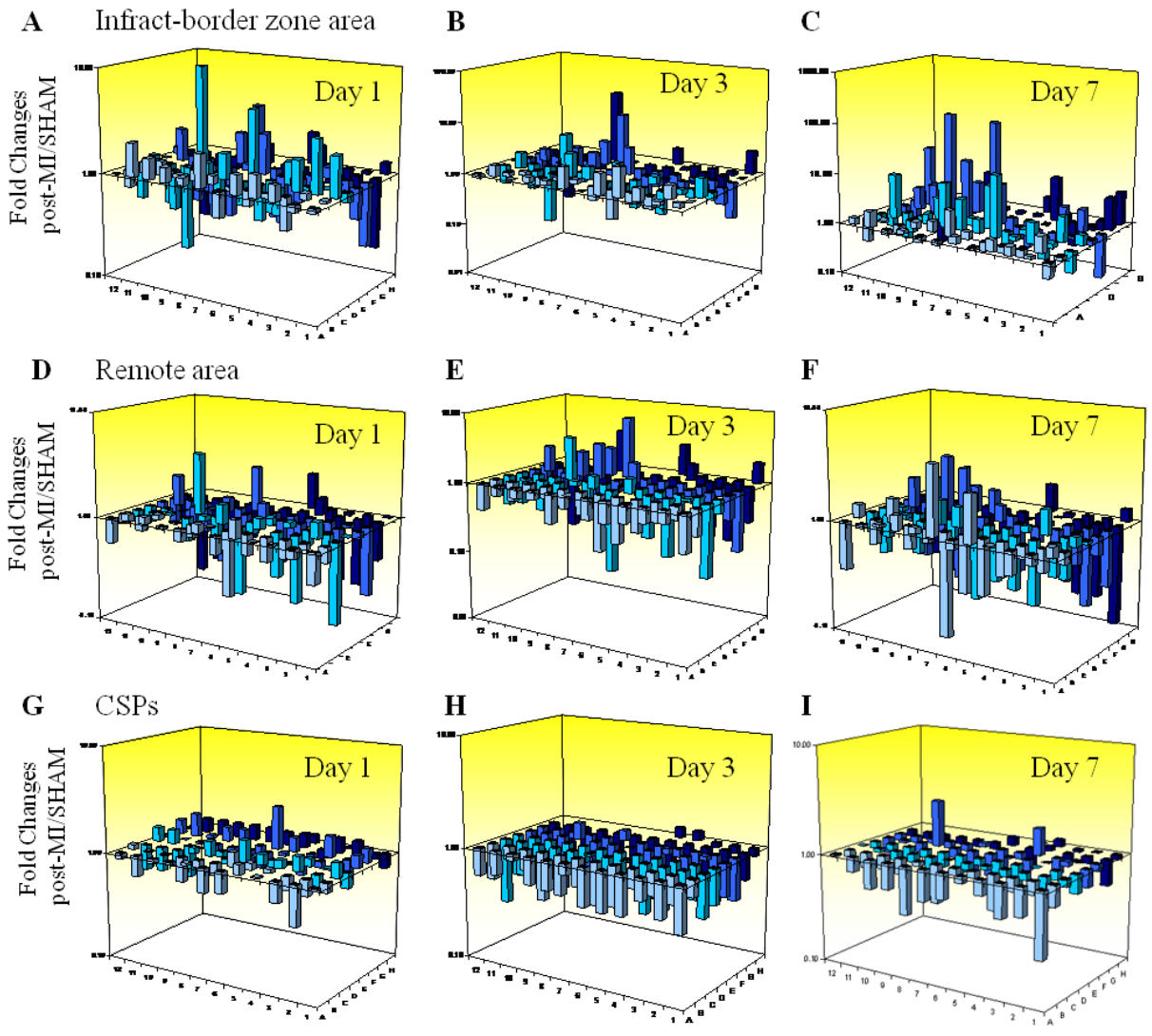

Figure 7: Expression profile of Wnt-related genes in infarcted myocardium and post-MI CSPs. 3-D diagrams demonstrate the expression profile of Wnt-related genes in infracted area (A-C), remote area (D-F) and in CSPs (G-I) at 1, 3 and 7 days post-MI (n=3). Information related to the position of each gene in the 96 well plates are available in Supplemental Table 7.

2. *Effects of canonical Wnt signaling on cardiac progenitor cells*

- *LiCl increases the proliferation of CSPs*

Initially, CSPs were treated with LiCl, a known inhibitor of GSK-3β kinase, in order to activate the canonical Wnt signaling pathway. Application of LiCl (3mM) over a period of 6 days increased the proliferation capacity of CSPs by approximately 1.70%-fold (Figure 8). In order to examine whether application of LiCl activated the canonical Wnt signaling pathway I utilized a lentivirus-expressed, TCF-luciferase reporter assay. This assay measures directly the activity of the TCF transcription factor and thus indirectly the activation of the canonical Wnt signaling pathway. Thus, CSPs were treated with LiCl, in a dose dependent manner and as a positive control conditioned medium containing Wnt3a ligands (Wnt3a-CM) was used. As shown in Figure 9, Wnt3a-CM activated robustly the TCF-luciferase reporter in CSPs by approximately 27-fold. However, LiCl did not activate the TCF-luciferase reporter assay at any dose between 3 and 10mM. Only when CSPs were treated with 15mM of LiCl the reading of the TCF-luciferase reporter was increased. Overall, the above results suggest that LiCl increases the proliferation of CSPs, through a canonical Wnt signaling independent pathway.

To examine this hypothesis I utilized a GSK-3β kinase inhibitor (GSKi) and performed similar proliferation assays to test whether blocking of GSK-3β would affect the growth of CSPs. As shown in Figure 10, treatment of CSPs with 2μM of GSKi did not alter their proliferation, whereas utilization of 10 μM of GSKi blocked significantly their proliferation, compared to vehicle treated CSPs. At day 6, treatment with 10μM of GSKi decreased the proliferation capacity of CSPs by approximately 1.7-fold and at day 9 the decrease was 3.14-fold. Thus,

blocking of GSK-3β kinase, a determining factor for the nuclear accumulation of β-catenin, limits the proliferation ability of CSPs.

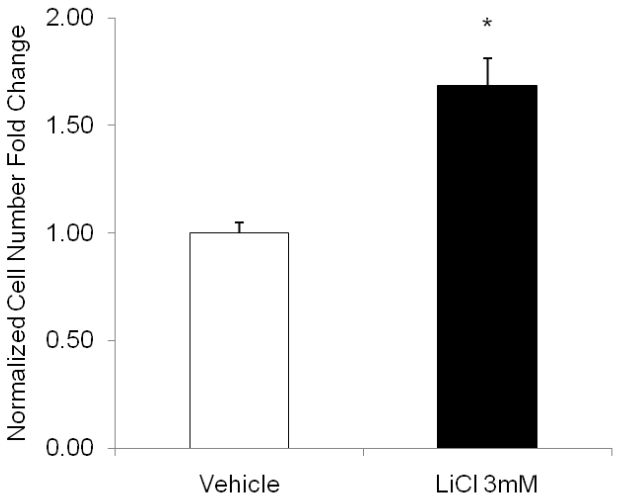

Figure 8: Proliferation assay of CSPs following treatment (6 days) with LiCl and vehicle (H_2O). Error bars show s.e. * indicates $p \leq 0.05$ for LiCl compared to vehicle.

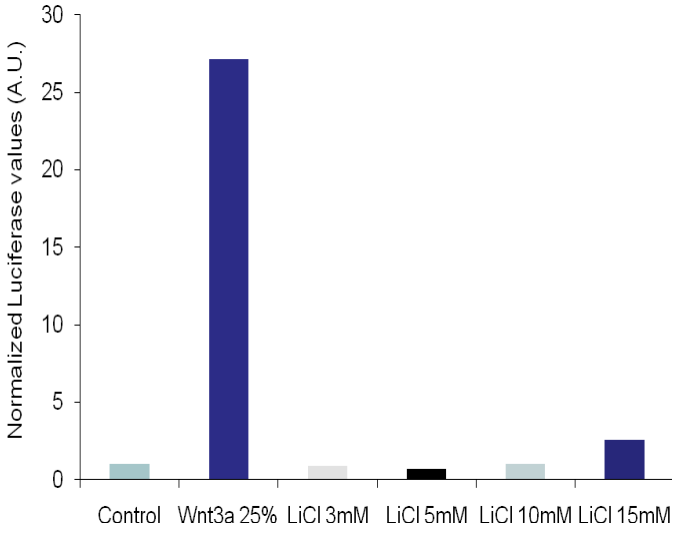

Figure 9: Luciferase assay (TCF-activity) in CSPs treated (48 hours) with Wnt3a-CM or LiCl in a dose dependent manner.

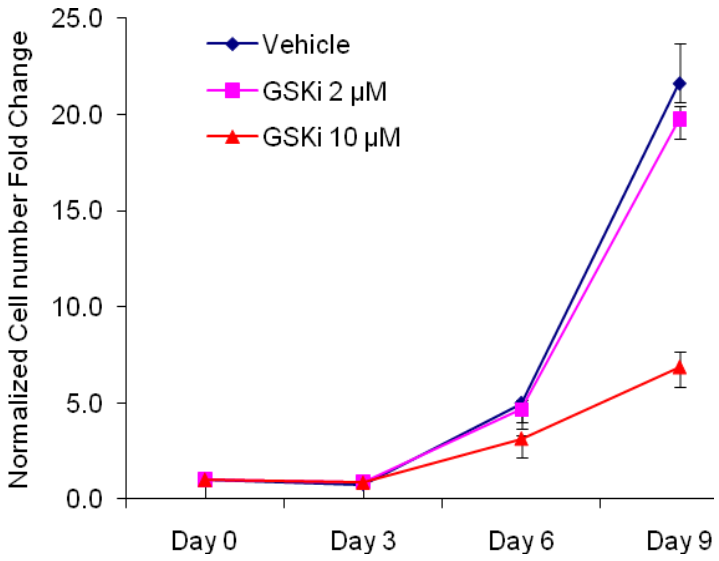

Figure 10: Proliferation assay of CSPs following treatment (6 days) with GSKi inhibitor (2 µM and 10 µM) and vehicle (DMSO). Error bars show s.e. * indicates $p \leq 0.05$ for GSKi 10 µM compared to vehicle at each time point.

- *Wnt signaling decreases the proliferation of CSPs*

My next step was to further examine the role of the Wnt signaling pathway on the growth of CSPs. I focused my attention mainly on the canonical Wnt signaling pathway and utilized various methodologies to manipulate its various members (Figure 11).

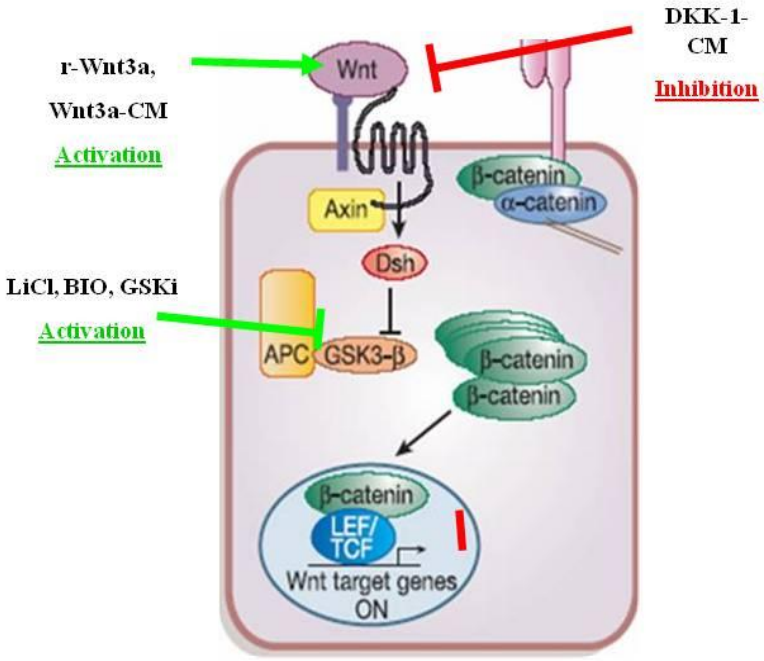

Figure 11: Graphic illustration of the canonical Wnt signaling pathway and the various ways we used to manipulate its expression.

Initially, I tested the cellular distribution of β-catenin in CSPs following treatment with Wnt3a-CM and vehicle. Nuclear localization of β-catenin was found only in CSPs treated with Wnt3a-CM in comparison with vehicle treated CSPs (Figure 12).

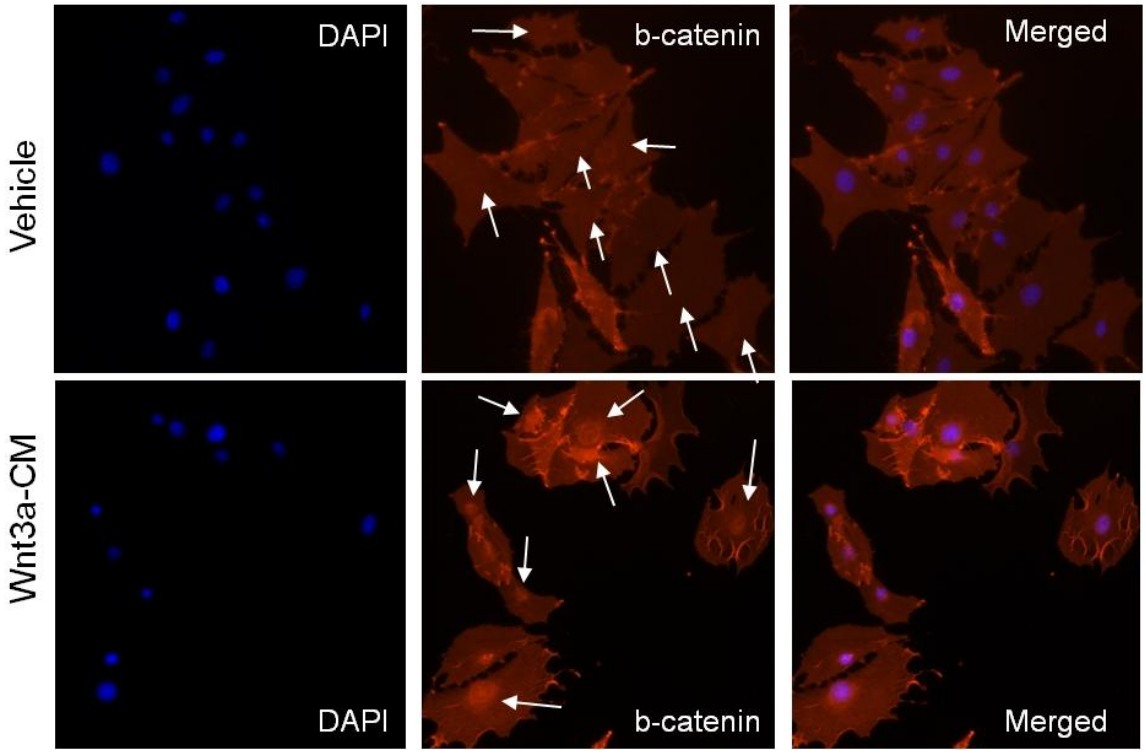

Figure 12: Nuclear localization of β-catenin is observed only in Wnt3a-CM treated CSPs. In Vehicle treated cells β-catenin is found throughout the cytoplasm. Arrows indicate nuclei.

Prior to each proliferation assay, I infected CSPs (passage 3rd-5th) with the lentivirus-mediated TCF-luciferase reporter system, in order to monitor the activation status of the canonical Wnt signaling pathway. Initially, I compared the proliferation capacity of CSPs cultured in either standard expansion medium, in the presence of 25% vehicle or in the presence of 25% Wnt3a-CM. As measured by the TCF-luciferase assay, the Wnt signaling pathway was activated in CSPs only by treatment with the Wnt3a-CM, compared to either standard expansion medium or vehicle (aproximately 70-fold) (Figure 13A). Moreover, I did not observe any difference in the activation status of the Wnt signaling pathway in CSPs cultured in either

standard conditions or in the presence of vehicle-CM. At the same time, manual count of CSPs revealed that treatment with Wnt3a-CM decreased significantly their proliferation compared to vehicle treated cells (Figure 13B). Additionally, I did not observe any difference in the proliferation nor the Wnt activition status of CSPs cultured in standard expansion medium and vehicle-CM (Figure 13A-B). The above results suggest that activation of the canonical Wnt signaling pathway decreases the proliferation capacity of CSPs.

To further investigate the effects of Wnt signaling on the growth of CSPs I performed proliferation assays with vehicle-CM or Wnt3a-CM, in increasing doses. Thus, CSPs infected with the lentivirus-mediated TCF-luciferase reporter system were treated with various doses of vehicle-CM and Wnt3a-CM, for a period of 5 days. As shown in Figure 14A, treatment with an increasing dose of Wnt3a-CM resulted in a dose dependent activation of the TCF-luciferase reporter assay (4.7-fold, 9.8-fold and 23.7-fold respectively for each dose). This was accompanied by a dose dependent decrease of the number of CSPs (2.2-fold, 3.65-fold and 6.4-fold respectively for each dose), as presented in Figure 14B.

Subsequently, I attempted to activate the canonical Wnt signaling pathway by utilizing BIO (2′*Z*, 3′*E*)-6-Bromoindirubin-3′-oxime), a potent chemical inhibitor of GSK-3β kinase. Treatment of CSPs with BIO (1μM, 2μM and 5μM) resulted in a significant increase of the TCF-luciferase activity (not in the case of 1μM), as measured by the TCF-luciferase reporter assay, compared to vehicle (DMSO) treated CSPs (3.44-fold and 98-fold respectively for 2μM and 5μM) (Figure 15A). At the same time, manual measurement of the cell number of CSPs treated with 2μM and 5μM, revealed a significant decrease of their proliferation capacity in comparison to vehicle treated CSPs (1.92-fold and 10.18-fold respectively for 2μM and 5μM) (Figure 15B).

Furthermore, I tested the effects of recombinant Wnt3a protein (r-Wnt3a) in the proliferation capacity of CSPs. Supplementation of the culture medium with r-Wnt3a ligands activated the Wnt signaling pathway as measured by the TCF-luciferase reporter assay (1.5-fold and 3.1-fold respectively for each dose) (Figure 16A). Correspondingly, Wnt3a (100ng/ml and 200ng/ml) treatment resulted in a significant decrease in the growth of CSPs (1.6-fold and 1.7 fold respectively for each dose) (Figure 16B).

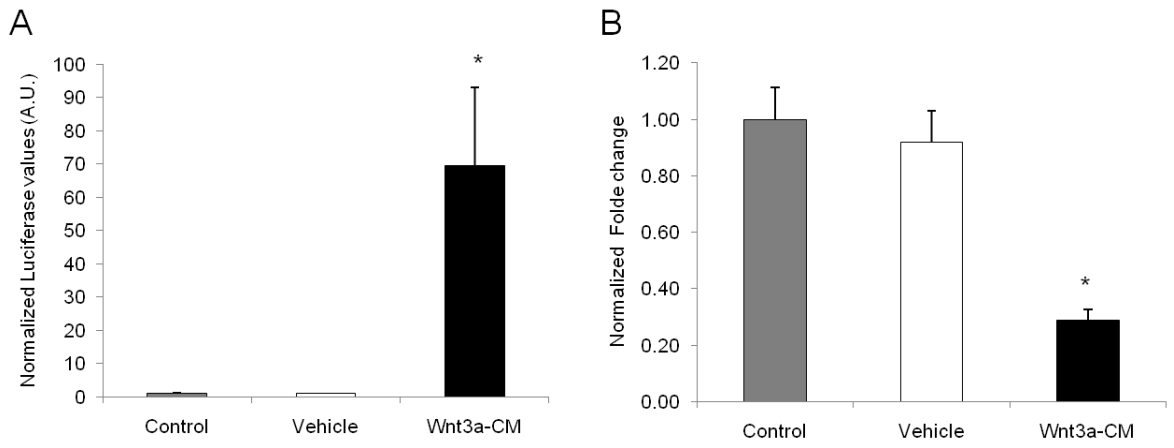

Figure 13: Effects of Wnt3a-CM on CSP cell proliferation. (A) Luciferase assay (TCF-activity) of CSPs following treatment (6 days) with Wnt3-CM (25%), vehicle medium (25%) and control expansion medium. (n=7 for all). (B) Corresponding Proliferation assay of CSPs (A.U. indicates arbitrary units). Error bars show s.e. * indicates $p \leq 0.05$ for Wnt3a-CM compared to vehicle.

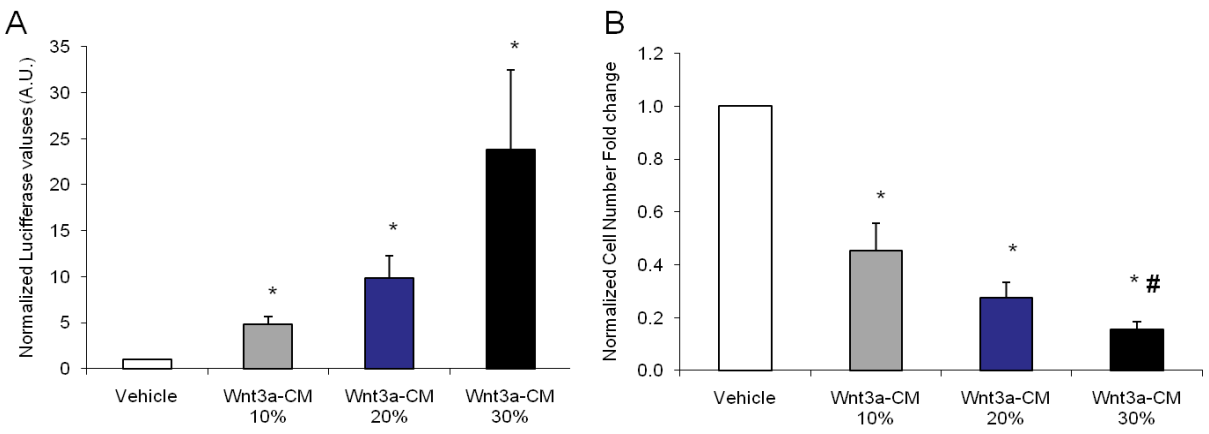

Figure 14: Dose dependent effects of Wnt3a-CM on CSP cell proliferation. (A) Luciferase assay (TCF-activity) of CSPs following treatment (6 days) with Wnt3-CM and vehicle medium in increasing doses. Vehicle represents the average in all different doses. (B) Corresponding proliferation assay of CSPs (A.U. indicates arbitrary units). Error bars show s.e. * indicates $p \leq 0.05$ for all samples compared to vehicle, # indicates $p \leq 0.05$ for Wnt 10% vs Wnt 20%.

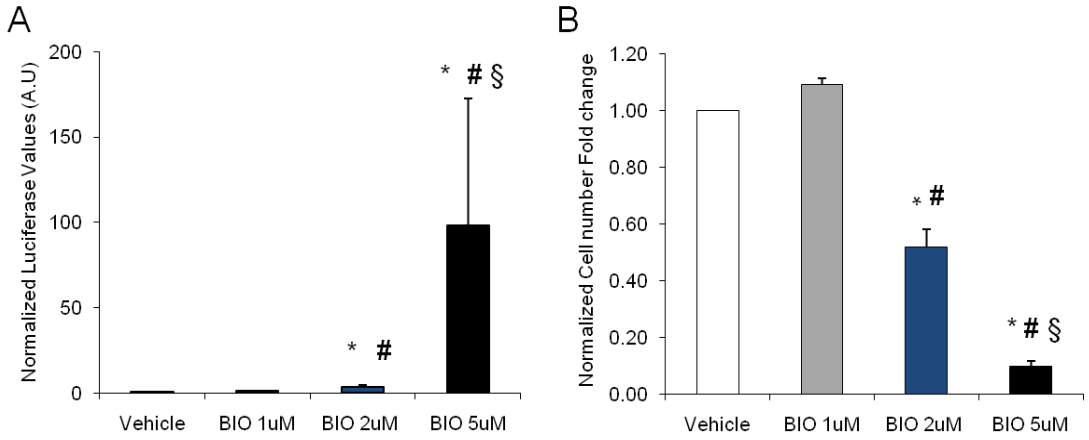

Figure 15: Effects of BIO on CSP cell proliferation. (A) Luciferase assay (TCF-activity) of CSPs following treatment (6 days) with BIO and vehicle (DMSO) (n=6 for all). Vehicle represents the average in all different doses. (B) Corresponding proliferation assay of CSPs (n=6) (A.U. indicates arbitrary units). Error bars show s.e. * indicates $p \leq 0.05$ for all samples compared to vehicle, # indicates $p \leq 0.05$ for BIO 1µM vs BIO 2µM, § indicates $p \leq 0.05$ for BIO 2µM vs BIO 5µM.

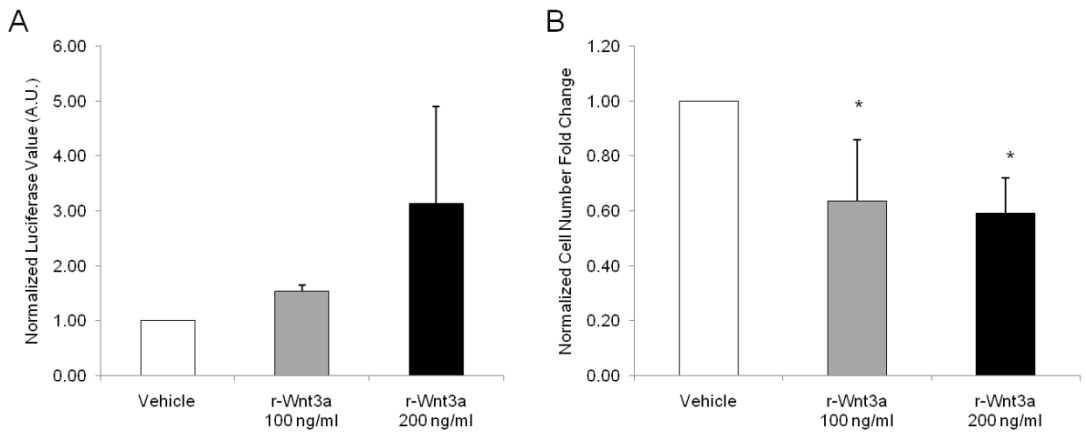

Figure 16: Effects of r-Wnt3a on CSP cell proliferation. (A) Luciferase assay (TCF-activity) of CSPs following treatment (6 days) with r-Wnt3a (100 ng/ml and 200ng/ml) and vehicle (n=6 for all). Vehicle represents the average in all different doses. (B) Corresponding proliferation assay of CSPs (n=6) (A.U. indicates arbitrary units). Error bars show s.e. * indicates $p \leq 0.05$ for all samples compared to vehicle.

- *Dkk-1 partially inhibits the anti-proliferative role of Wnt3a ligands*

To examine in more details the inhibitory effects of canonical Wnt signaling pathway on the proliferation of CSPs I utilized Dickkopf-1 (DKK-1), a Wnt signaling inhibitor, to block the activation of the pathway. DKK-1 was supplemented in the form of conditioned medium (DKK-1 CM) in two doses (20% and 30%) in the presence of either vehicle-CM or Wnt3a-CM. Addition of 20% and 30% of Dkk-1-CM alone did not significantly affect the activation status of Wnt signaling pathway in CSPs, neither their growth characteristics, in comparison to vehicle-CM treated cells. As expected, treatment of CSPs with 20% of Wnt3a-CM activated the Wnt signaling pathway (40.48-fold) and decreased their proliferation capacity, in comparison to vehicle-CM treated cells (12.49-fold) (Figure 17A). Treatment with both Wnt3a-CM and 20%

or 30% of DKK-1-CM decreased gradually the activation of Wnt signaling pathway (6.59-fold and 10.00-fold respectively), as measured by the TCF-luciferase reporter system compared to the respective controls (Figure 17A). This was accompanied by respectively increased proliferation of the CSPs (4.49-fold and 7.10-fold) compared to the corresponding controls (Figures 17B). Overall, the above data clearly demonstrate that Wnt signaling pathway decreases the proliferation capacity of CSPs and this anti-proliferative phenotype can be partially rescued by DKK-1.

Moreover, I attempted to completely prevent the activation of Wnt signaling pathway by the Wnt3a-CM through the utilization of DKK-1-CM. Thus, I treated CSPs, which were infected with the lentivirus-mediated TCF-luciferase reporter assay, with various doses of DKK-1-CM (10-40%) in the presence of 20% of vehicle or Wnt3a-CM. As expected, supplementation of Wnt3a-CM resulted in a profound activation of the Wnt signaling pathway, as measured by the TCF-luciferase assay, compared to treatment with vehicle-CM (Figure 18). Administration of DKK-1 in a dose dependent manner did not alter the activation status of the Wnt signaling pathway in vehicle-CM treated CSPs (Figure 18). Interestingly, dose dependent treatment with DKK-1-CM resulted in a gradual decrease of the activation status of the Wnt signaling pathway. However, it was not possible to reduce the activity of the Wnt pathway to levels similar to the vehicle-CM treated CPSs.

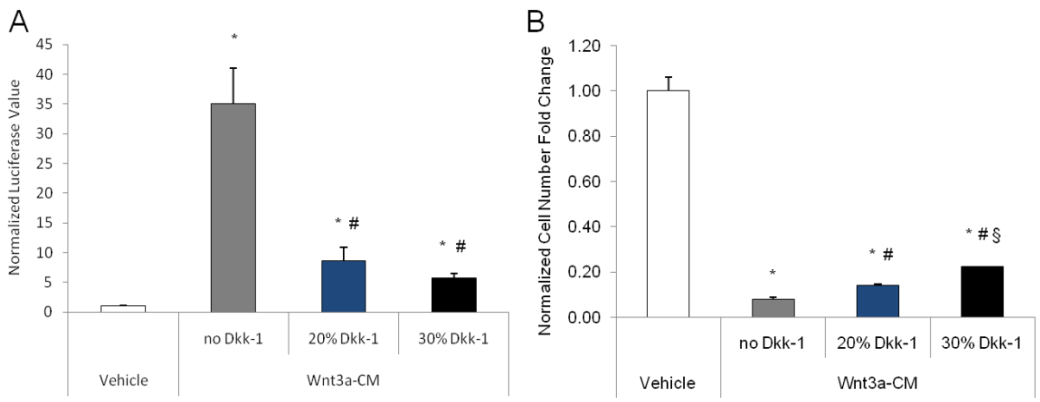

Figure 17: Dose dependent effects of Dkk-1 on CSP cell proliferation. (A) Luciferase assay (TCF-activity) of CSPs following co-treatment with Wnt3a-CM (20%) and Dkk-1-CM (20% & 30%) and vehicle medium (n=3). Vehicle represents the average in all different doses. (B) Corresponding proliferation assay of CSPs (n=3). (A.U. indicates arbitrary units). Error bars show s.e. * indicates $p \leq 0.05$ for all samples compared to vehicle, # indicates $p \leq 0.05$ for 20% Wnt3a-CM vs Wnt3a-CM/20% Dkk-1-CM and Wnt3a-CM/30%Dkk-1, § indicates $p \leq 0.05$ for Wnt3a-CM/20% Dkk-1-CM vs Wnt3a-CM/30% Dkk-1-CM.

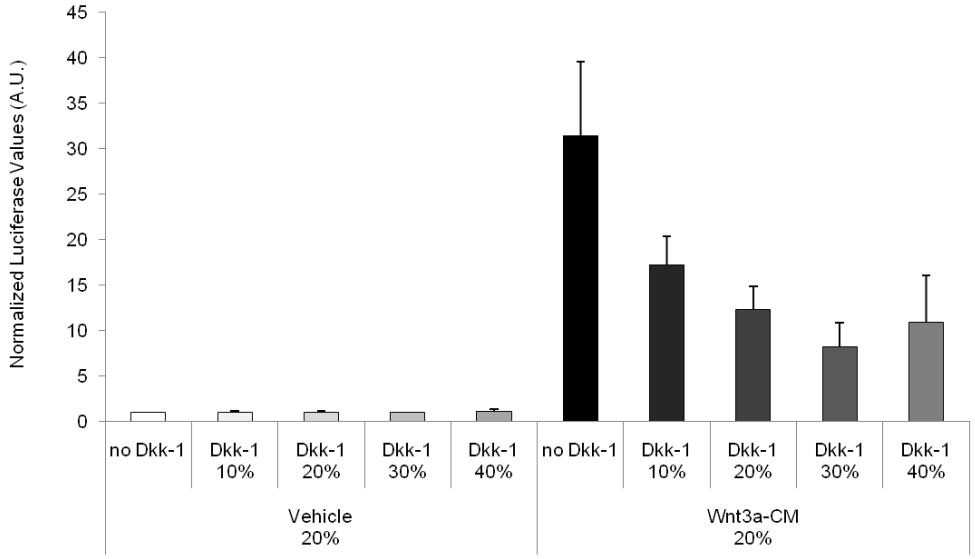

Figure 18: Dose dependent effects of Dkk-1 on the activation status of Wnt signaling pathway in CSPs (n=2). Error bars show s.e.

- *Effects of Wnt signaling on other cardiac stem/progenitor cells*

Subsequently I examined whether the anti-proliferative effects of Wnt signaling are restricted only in CSPs. I treated mouse derived c-kit$^+$ stem/progenitor cells (kindly provided by Dr. P. Anversa) with 25% vehicle-CM and Wnt3a-CM and measured their proliferation after 5 days. C-kit$^+$ cells were infected with the lentivirus mediated TCF-luciferase reporter in order to monitor the activation status of the Wnt signaling pathway. Treatment with Wnt3a-CM resulted in activation of the Wnt pathway (approximately 53-fold) as evidenced by the TCF-luciferase assay, in comparison to vehicle-treated cells (Figure 19A). Correspondingly, manual cell counting of the c-kit$^+$ cell number following 5 days of Wnt3a-CM treatment revealed a significant decrease in their proliferation capacity (2.2-fold) when compared with vehicle-CM cells (Figure 19B).

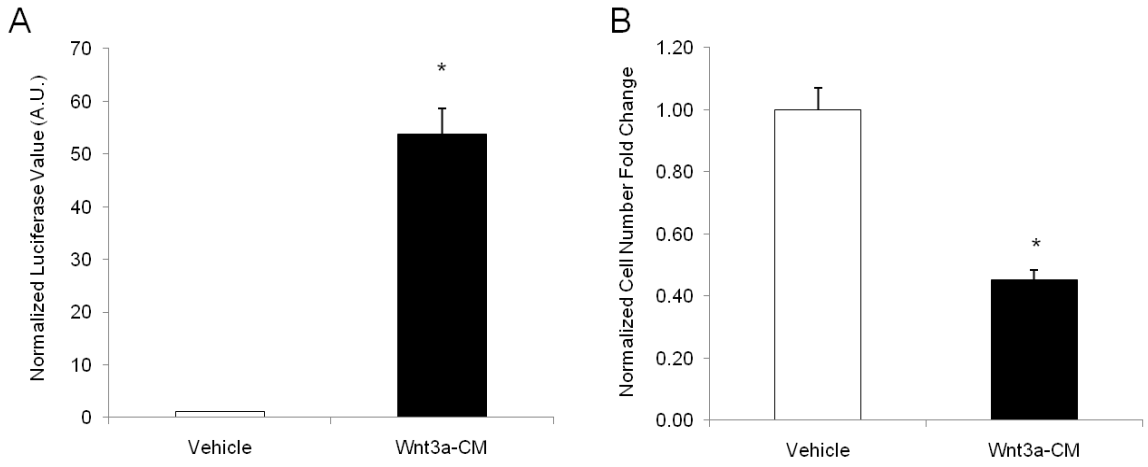

Figure 19: Effects of Wnt signaling on the proliferation of c-kit$^+$ cardiac progenitor cells. (A) Luciferase assay (TCF-activity) of c-kit$^+$ cardiac progenitor cells following treatment (6 days) with Wnt3-CM (25%) and vehicle (25%) medium (A.U. indicates arbitrary units). (B) Corresponding proliferation assay (n=3 for all). Error bars show s.e. * indicates $p \leq 0.05$ for Wnt3a-CM compared to vehicle.

- *Effects of Wnt signaling on non-cardiac cells*

Subsequently, I examined the effects of the Wnt3a-CM on a cell population of non-cardiac origin such as HEK-293 cells (Human Embryonic Kidney 293 cells), which were also stably transfected with the lentivirus TCF-luciferase reporter system, in order to monitor the activation status of the Wnt signaling pathway. Supplementation of 25% of Wnt3a-CM resulted in activation of the canonical Wnt signaling pathway by approximately 8-fold while their proliferation capacity was increased by 1.3-fold (Figure 20A-B). Thus, activation of the Wnt signaling pathway in HEK-293 cells produced different results suggesting that the anti-proliferative effects in cardiac progenitors are not universal but cell type dependent.

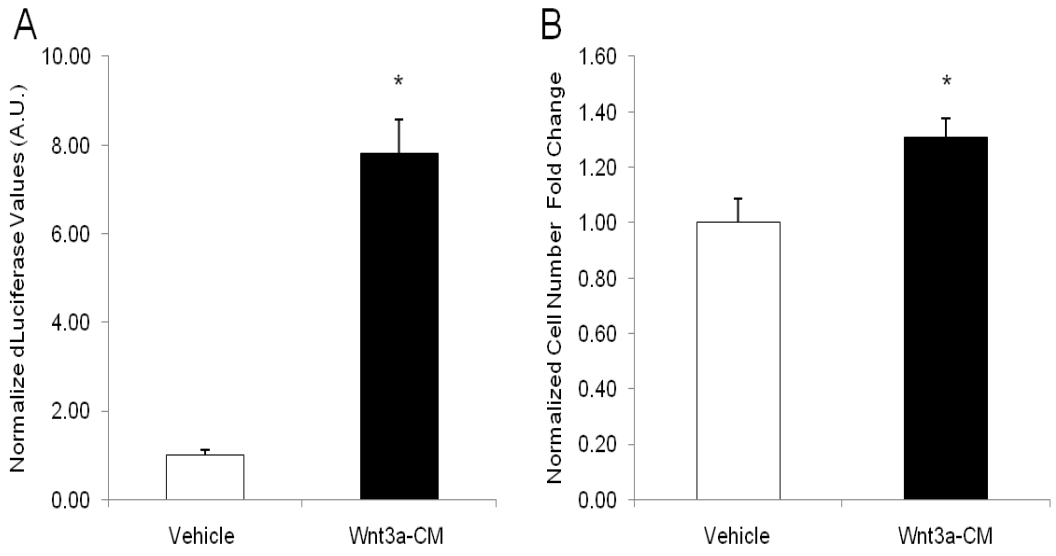

Figure 20: Effects of Wnt signaling on the proliferation of HEK-293 cells. (A) Luciferase assay (TCF-activity) of HEK-293 cells following treatment (6 days) with Wnt3-CM (25%) and vehicle (25%) medium (n=3 for all). (B) Corresponding proliferation assay of HEK-293 cells (A.U. indicates arbitrary units). Error bars show s.e. * indicates $p \leq 0.05$ for Wnt3a-CM compared to vehicle.

3. Effects of canonical Wnt signaling on the survival of CSP cells

My next goal was to determine the effects of the Wnt signaling pathway on the survival of CSPs. CSPs were treated with 25% of vehicle-CM and Wnt3a-CM for a period of 6 days and the cell death was determined by staining with Annexin-V and 7-AAD. As presented in Figures 21A-C, administration of 25% of Wnt3a-CM increased significantly (3.47-fold) the amount of Annexin-V^+ cells (apoptotic) (2.75%) compared to vehicle-CM treated cells (0.79%). Similarly, treatment with Wnt3a-CM increased (3.80-fold) the amount of Annexin-V^+/7-AAD^+ cells (8.78%) in comparison to vehicle-CM treated cells (2.31%). Overall, in Wnt3a treated samples the total amount of dead cells (12.53%) was significantly higher (3.99-fold) than in vehicle treated cell (3.13%). In Figures 21D-E are presented representative examples of the flow cytometric analysis of the staining of CSPs for 7-AAD and Annexin-V.

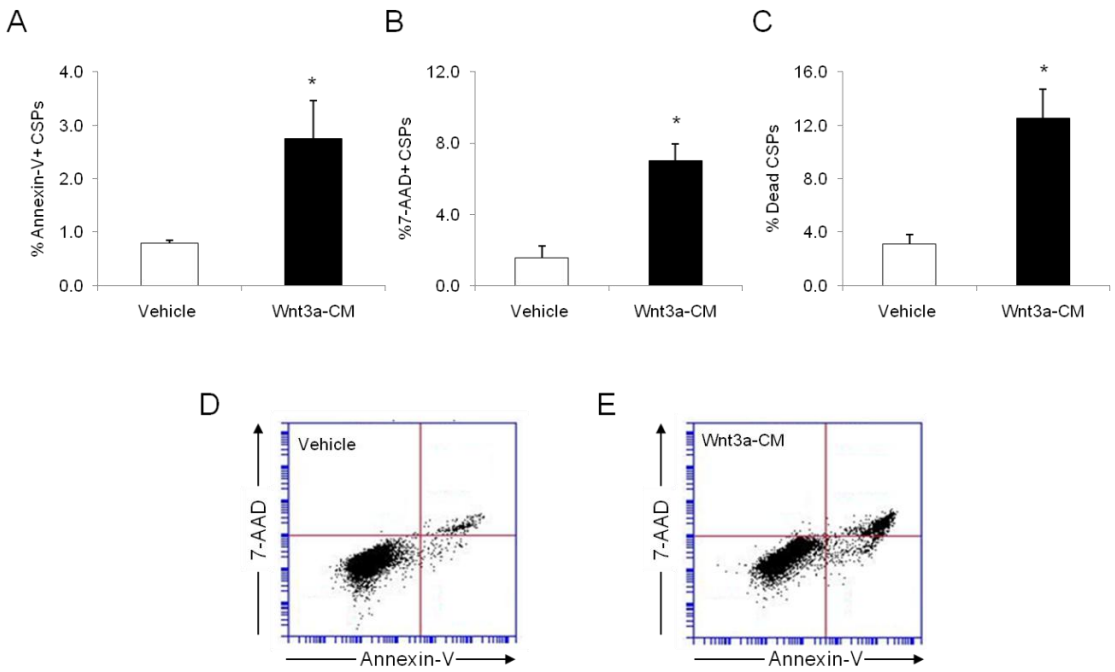

Figure 21: Cell death analysis of CSPs following treatment (6 days) with Wnt3a-CM and vehicle. (A) Apoptotic cell death (n=4), (B) Necrotic cell death (n=4), (C) Total cell death (n=4), (D & E) Representative flow cytometric analysis of Annexin-V and 7-AAD staining. Error bars show s.e. * indicates $p \leq 0.05$ for all samples compared to vehicle.

4. Effects of canonical Wnt signaling on cell cycle regulation of CSP cells

- *Activation of the canonical Wnt signaling pathway delays cell cycle progression in CSP cells*

The next step was to investigate the effects of canonical Wnt signaling on the cell cycle properties of CSPs. The hypothesis to be tested was that Wnt signaling might affect the distribution of CSPs in the various cell cycle phases, favoring an accumulation of the cells

towards the early, non proliferative, G0/G1 cell cycle phases. By utilizing various well established methodologies, such as BrdU incorporation assay, immunocytochemical detection of the phosphorylated form (Serine 10) of histone-H3 (p-H3), propidium iodide (PI) staining and gene expression analysis I studied the cell cycle profile of CSPs.

Initially, CSPs were incubated for a period of 5 days in the presence of 25% of vehicle-CM and Wnt3a-CM. At day 5, they were pulsed for a period of one hour with 10 mM of BrdU and subsequently they were fixed and analyzed for the presence of incorporated BrdU molecules. Immunocytochemical analysis of the BrdU-pulsed CSPs revealed that Wnt3a-CM-treated cells incorporated BrdU at a significantly lower rate (4.57-fold decrease) in comparison to vehicle-CM treated cells (23.82% versus 5.27% respectively) (Figure 22A). The above data clearly demonstrate that activation of the canonical Wnt signaling decreases the amount of CSPs entering the S-cell cycle phase. Figures 22B-C show representative examples of the immunostaining for BrdU in both experimental conditions, in low and high magnification power.

p-H3 is a cell proliferation marker that is expressed in cells that reside in the late-G2 (Gap-2) and predominantly in M (Mitosis) cell cycle phases [135]. CSPs were treated with vehicle-CM or Wnt3a-CM for a period of 5 days. Immunocytochemical analysis revealed a significant lower amount (4-fold) of p-H3^{+} cells following Wnt3a treatment in comparison to vehicle-CM treated cells (7.9% versus 2.05% respectively) (Figure 22D). Figures 22E-F demonstrate representative examples of the immunostaining for p-H3 in CSPs following each experimental treatment, in low and high magnification power. Hence, activation of Wnt signaling pathway causes a decrease in the number of CSPs residing in the late cell cycle phases.

Next, the overall cell cycle profile of CSPs was further analyzed by propidium iodide (PI) staining. Flow cytometric analysis revealed that administration of Wnt3a-CM resulted in a substantial increase in the amount of cells residing in G0/G1-phases in comparison to vehicle-CM treated cells (67.9% versus 52.6% respectively). Conversely, in CSPs treated with Wnt3a-CM, the proportion of cells residing in S-phase (21.0%) and in G2/M-phases (11.0%) was significantly decreased in comparison to vehicle-CM treated cells (32.5% and 14.8% respectively) (Figure 22G). Representative examples of the PI staining experiments in CSPs are presented in Figures 22H-I.

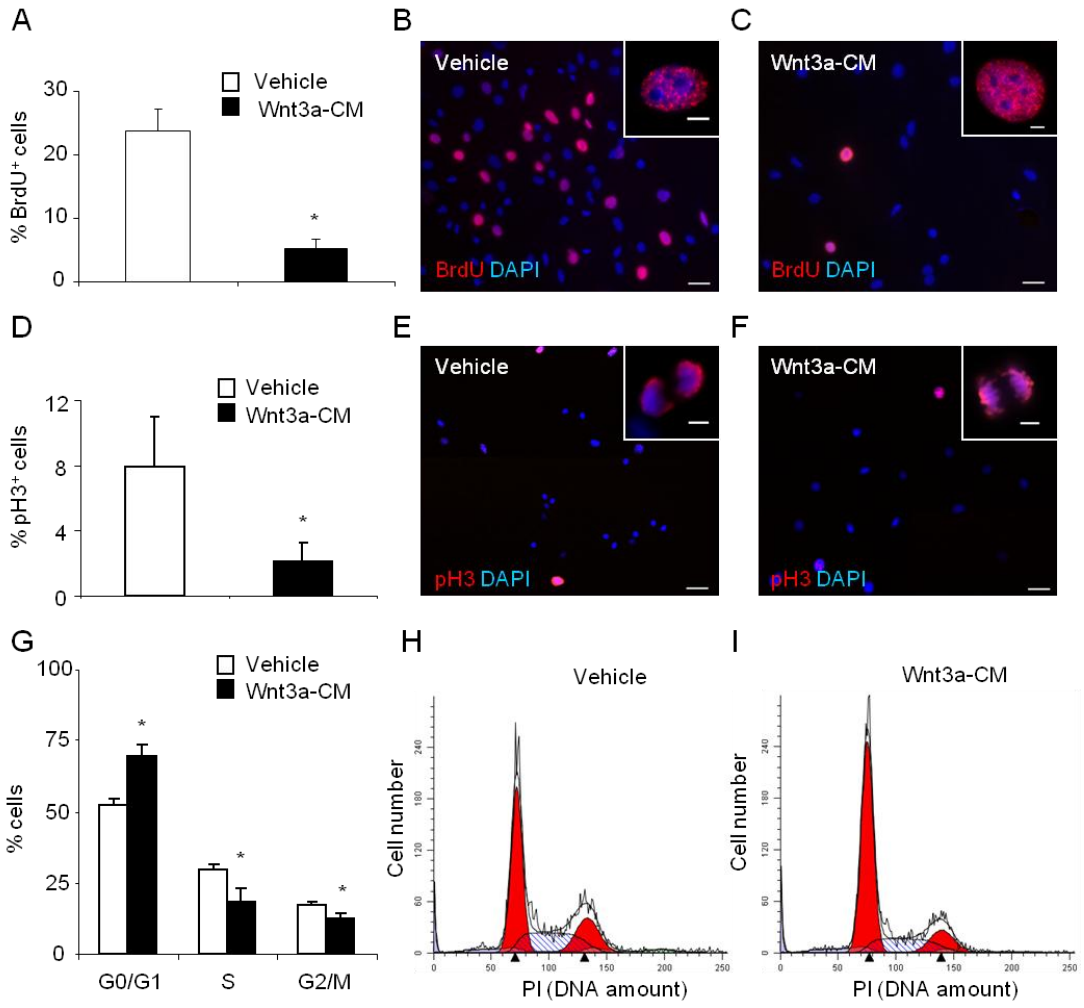

Figure 22: Activation of canonical Wnt signaling pathway in CSPs delays the progression of their cell cycle. (A) Treatment of CSP cells for 5 days with 25% vehicle or Wnt3a-CM results in a reduced number of CSP cells with incorporated BrdU (n=5) as well as CSP cells expressing pH3 (n=4) (D) compared to vehicle treated cells. Representative examples of the immunocytochemical analysis for BrdU and for pH3 respectively, in low and high magnification, are shown in images B, C and E, F respectively. (G) PI analysis revealed that treatment of CSP cells for 5 days with 25% vehicle or Wnt3a-CM results in an increase of cells in G0/G1 cell cycle phases and a decrease of the amount of cells in S and G2/M cell cycle phases, in comparison with vehicle treated cells. Representative examples of the PI analysis are presented in images H and I. * indicates $p<0.05$. Error bars show s.e.

marker which is found in all the phases of the cell cycle but not in the G0 phase [136]. Once more, CSPs were treated with vehicle or Wnt3a-CM and 5 days later were analyzed for the presence of Ki67 marker. Flow cytometry analysis of Wnt3a-CM and vehicle treated CSPs revealed no difference in the percentage of $Ki67^{+}$ cells in both experimental conditions (90.7% versus 89.4% respectively) (Figures 23A-B). Thus, the amount of quiescent CSPs in normal culture conditions is approximately 10% and Wnt signaling does not change this proportion. By combining the data from the experiments with PI staining and Ki67 immunostaining the total cell cycle profile of CSPS, including the G0 cell cycle phase can be estimated (Figure 23C). Overall, the above data demonstrate that activation of the canonical Wnt signaling pathway modifies the cell cycle profile of CPSs towards a less proliferative status.

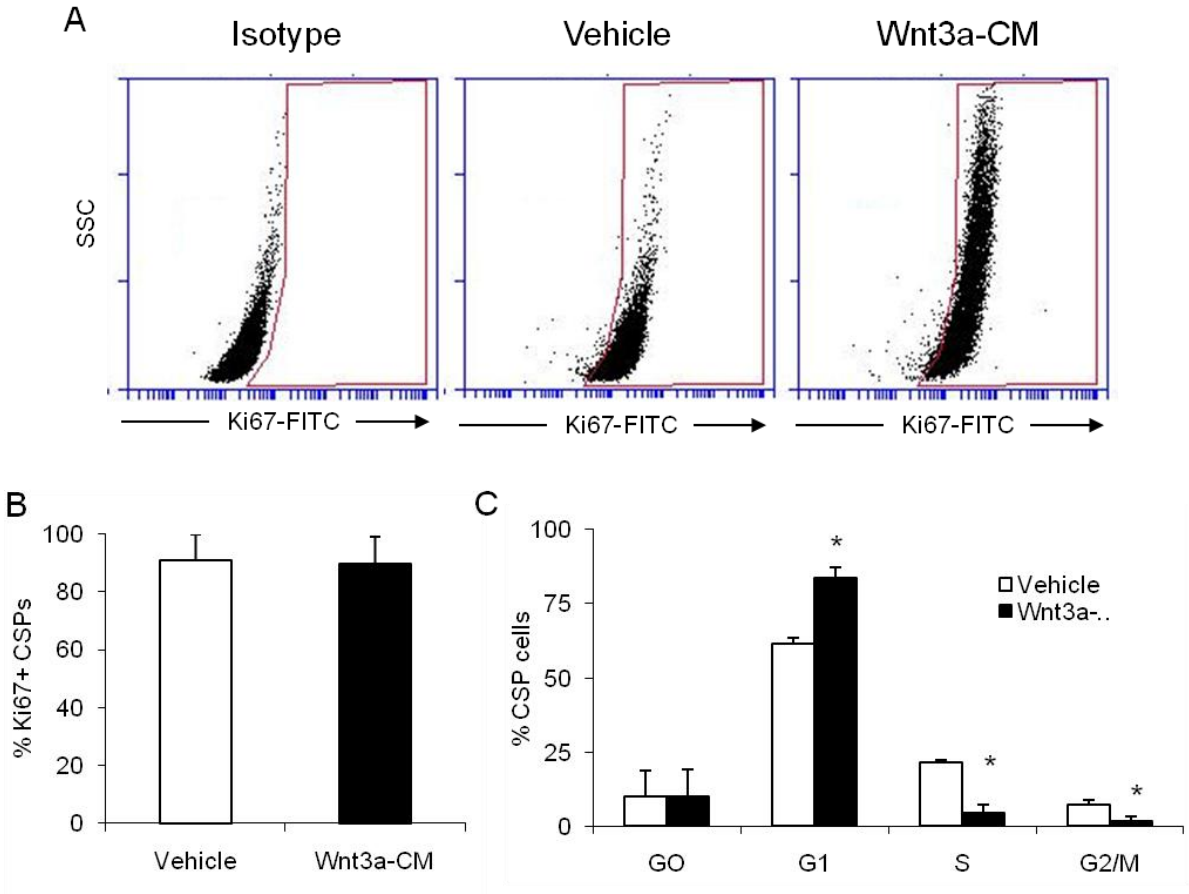

Figure 23: Effects of Wnt signaling pathway on Ki67 expression. (A) Representative examples of flow-cytometric analysis of Ki67 expression in CSPs following treatment (5 days) with Wnt3a-CM and vehicle medium (n=6 for all). (B) Ki67 expression in CSPs. (C) Cell cycle distribution of CSPs following treatment (5 days) with Wnt3a-CM and vehicle medium. Error bars show s.e. * indicates $p \leq 0.05$ for Wnt3a-CM compared to respective vehicle.

- *Effects of canonical Wnt signaling pathway on gene expression of cell cycle regulators*

After identifying substantial differences in the cell cycle profile of Wnt3a-CM treated CSPs, the regulation of their cell cycle was examined in more detail. I utilized a qRT-PCR gene array to measure the expression of various (84) cell cycle related genes, following treatment with vehicle and Wnt3a-CM at different time points (8 hours and 48 hours). I was especially interested in the earliest time point (8 hours) as it might reveal critical molecular events that influence the progression of the cell cycle of CSPs.

Treatment of CSPs with Wnt3a-CM for a period of 8 hours affected several well known cell cycle regulators. The 3-D diagram in Figure 24A shows the expression profile of all examined cell cycle regulators at this specific time point. Note that the expression of the vast majority of the examined genes did not change. Additional information about all the genes that were analyzed with the cell cycle gene array can be found in Table 4. Further analysis of the gene array results revealed that only 5 genes were significantly altered in Wnt3a-CM treated cells in comparison to vehicle-CM treated cells. Cdkn2a (p16) and Gadd45a were both significantly up-regulated by approximately 2.00-fold and 1.50-fold respectively (Figure 25).

Conversely, Brca2, Ki67 and Pcna were all significantly down-regulated by approximately 3.80-fold, 2.9-fold and 1.25-fold respectively (Figure 25). The above results demonstrate that treatment with Wnt3a-CM in CSPs, for a short period of time, causes alteration in the gene expression of crucial regulators of the cell cycle progression.

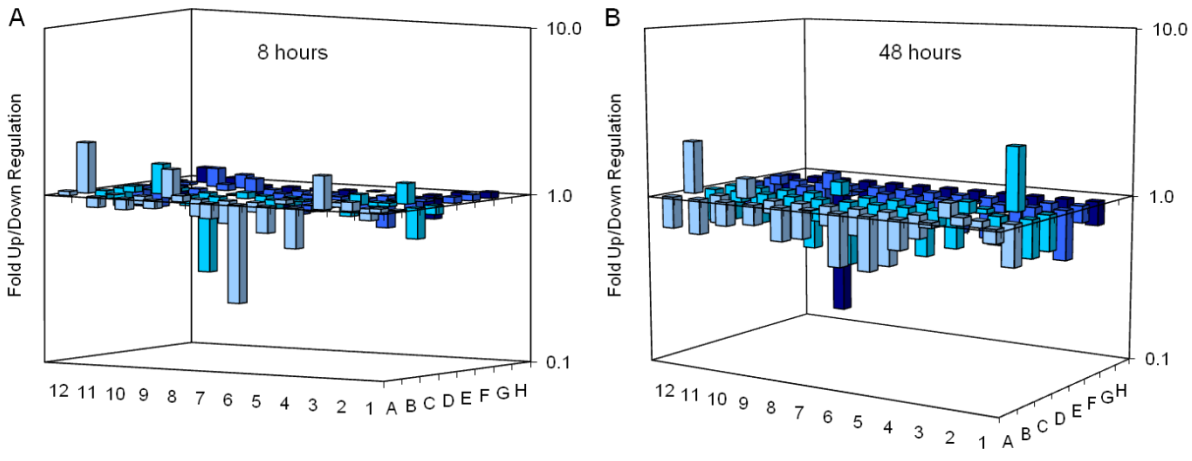

Figure 24: 3-D plots of the expression profile of cell cycle-related genes in CSPs following Wnt3a-CM treatment for (A) 8 hours and (B) 48 hours (n=3 for all).

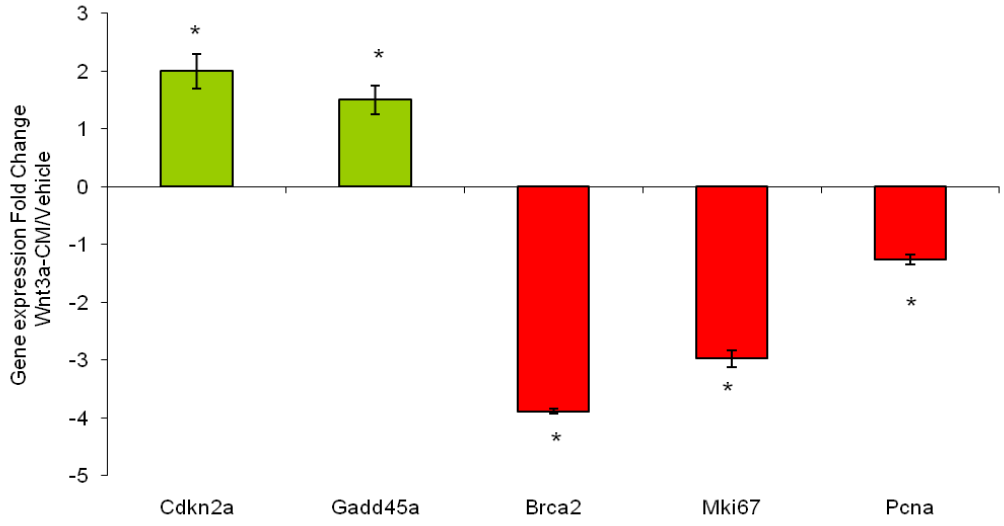

Figure 25: Diagram of fold changes in the expression cell cycle-related genes in CSPs following treatment with Wnt3a-CM for 8 hours (n=3 for all). Error bars indicate s.e. * indicates $p \leq 0.05$ for Wnt3a-CM compared to vehicle.

Moreover, incubation of CSPs with Wnt3a-CM for a period of 48 hours, resulted in substantial decrease in the expression level of numerous cell cycle related genes, compared to vehicle-CM treated CSPs. The 3-D diagram in Figure 24B, demonstrates the expression profile of all examined cell cycle regulators at this later time point. It is apparent that more genes are altered by the experimental treatment and that the vast majority of the examined genes are down-regulated, in contrast to the expression profile at 8 hours. Overall 33 out of 84 genes were significantly altered and among those only 2 were up-regulated. Similarly with the earlier time point, the expression of Cdkn2a (p16) was significantly increased (2.04-fold). Moreover, Itgb1 (integrin beta 1, fibronectin receptor beta 1) was also significantly up-regulated (2.33-fold) in Wnt3a-CM treated CSPs in comparison to vehicle-CM treated cells. A full list of all the genes that were examined in Wnt3a-CM treated CSPs is presented in Table 4. Here are presented those with particular importance in the progression of the cell cycle as CDK4 (-1.63%), CDC25a (-1.44-fold), Ccnf (-2.04-fold), Brca-1(-2.04-fold), Brca-2 (-2.02-fold), Ccnb1 (-1.55-fold), Mcm2 (-2.06-fold), Mcm3 (-1.63-fold), Ki67 (-2.17-fold), PCNA (-1.55-fold) and c-myb (-1.95-fold). Overall, the above results strongly suggest that the canonical Wnt signaling inhibits the proliferation of CSPs by delaying their cell cycle progression through altering the expression of numerous regulators.

- *Wnt signaling pathway increases the cell size of CSPs*

Microscopic observation showed that activation of the canonical Wnt signaling pathway increases the cell size of CSPs (Figures 26A-D). Quantification of the cell area of CSPs following treatment with Wnt3a-CM revealed an approximate 70% increase in cell size, compared to vehicle treated cells (0.019mm^2 versus 0.01mm^2 respectively) (Figure 26E).

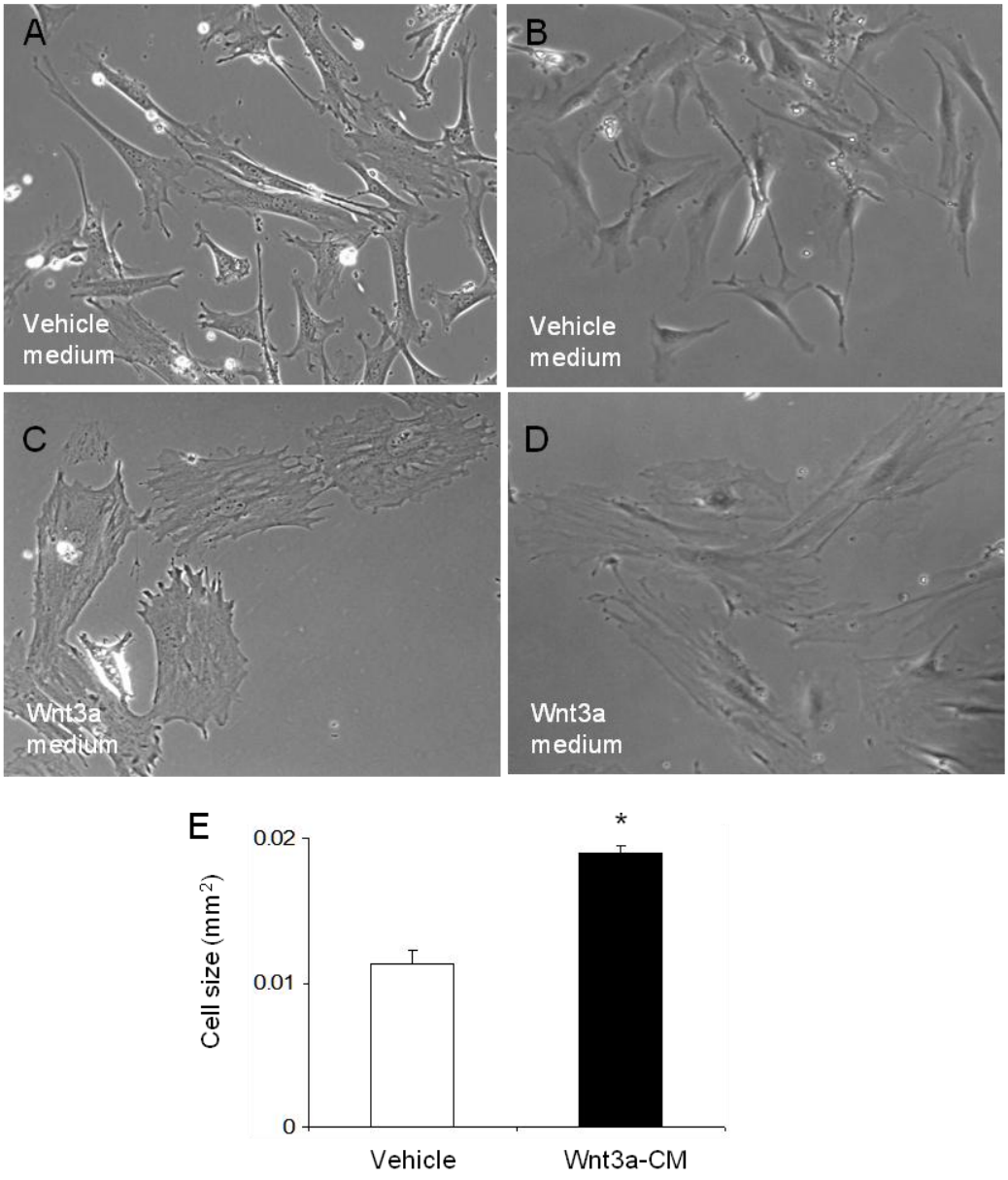

Figure 26: Effects of Wnt3a-CM on the cell size of CSPs. Representative images of CSPs (A-B) treated with vehicle medium and (C-D) CSPs treated with Wnt3a-CM medium. (E) Quantification of the effects of Wnt signaling pathway on CSP cell size (Vehicle n=13, Wnt3a-CM n=17). Error bars indicate s.e. * indicates $p \leq 0.05$.

Subsequently, I measured the effects of Wnt signaling on the cell size of CSPs over a period of 3 days. At day 1, no changes were observed on the size of CSPs by Wnt3a treatment and all the cells were equally distributed among the various sizes, as shown in the frequency analysis diagram (Figure 27A). However, at day 2, the first changes in cell size started to appear as 18% more vehicle treated CSPs had smaller size than 0.010 mm^2 in comparison to Wnt3a-CM treated cells (Figure 27B). Moreover, 15% more Wnt3a-CM treated CSPs had larger size than 0.052mm^2 (Figure 27B). At day 3, 32% more vehicle treated cells had smaller size than 0.010 mm^2 in comparison to Wnt3a-CM treated cells (Figure 27C). Furthermore, 27% of Wnt3a-CM treated CSPs had larger size than 0.052 mm^2 (Figure 27C). These results clearly suggest that activation of the Wnt pathway in CSPs increases their size in a time dependent manner.

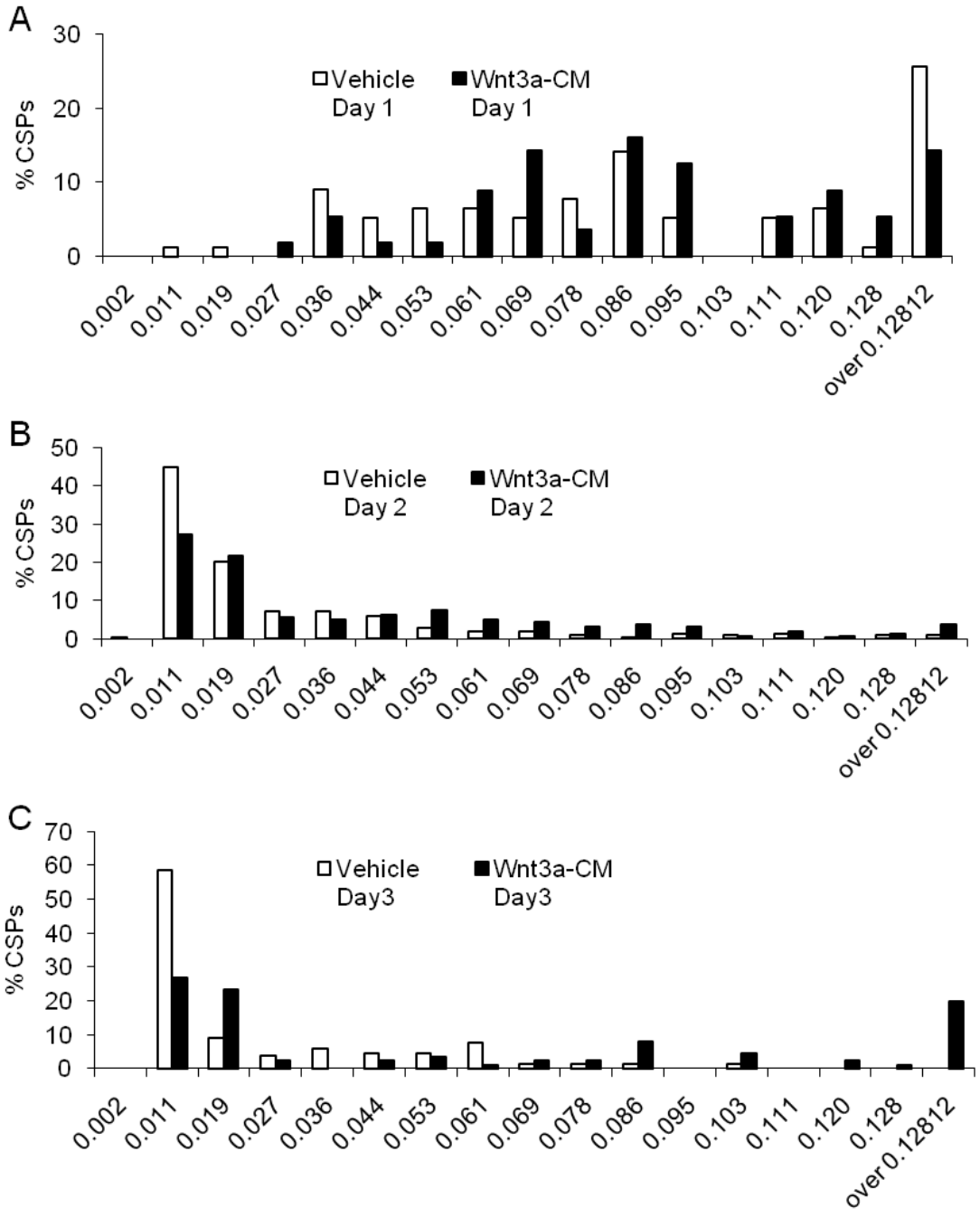

Figure 27: Frequency analysis of the various sizes of CSP cells following treatment with Wnt3a-CM (25%) and vehicle medium for (A) 24 hours, (B) 48 hours and 72 hours (C).

Similar results were obtained when CSPs were treated with recombinant Wnt3a (r-Wnt3a) protein (100ng/ml and 200 ng/ml). Supplementation of r-Wnt3a ligand in the culture medium of CSPs resulted, on average, in an approximate 1.8-fold increase in the cell size of CSPs, compared to vehicle treated cells (0.019 mm^2 versus 0.036 mm^2 and 0.034 mm^2 respectively) (Figure 28A-D). Further analysis of the distribution of CSPs at different sizes 3 days following treatment revealed that, 27% more vehicle treated cells were smaller than 0.015 mm^2 compared to r-Wnt3a-treated CSPs (Figure 28E). Respectively, 13% (100 ng/ml) and 17% (200ng/ml) more r-Wnt3a-treated CSPs had larger size than 0.0525 mm^2, compared to vehicle treated cells (Figure 28E). Both doses of the r-Wnt3a protein changed similarly the size of CSPs and they did not demonstrate any dose dependent effects.

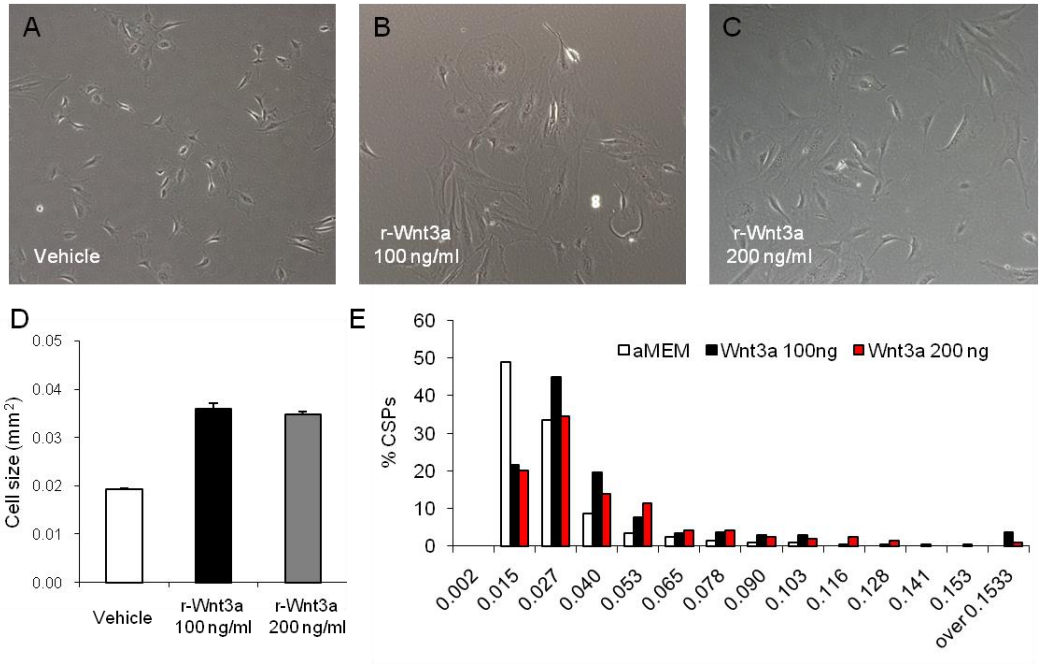

Figure 28: Effects of r-Wnt3a on the cell size of CSPs. Representative images of CSPs treated (48 hours) with (A) vehicle medium (B) r-Wnt3a 100 ng/ml and (C) 200 ng/ml r-Wnt3a (n=2 for all). (D) Quantification of the effects of r-Wnt3a protein on CSP cell size. (E) Frequency analysis of the various sizes of CSP cells following treatment with r-Wnt3a.

GSK-3β kinase, and studied its effects on the cell size of CSPs, in different doses. Application of BIO increased the size of CSPs by approximately 1.5-fold (1μM) and 1.9-fold (3μM), compared to vehicle (DMSO) treated cells (Figure 29A-C). Further analysis of the distribution of CSPs in the various sizes revealed that 55% more vehicle-treated CSPs had smaller size than 0.014 mm^2 compared to BIO treated cells (both doses of BIO). Respectively, 14% (1μM) and 25% (3μM) of BIO treated CSPs had bigger size than 0.0525 mm^2, compared to vehicle treated CSPs (Figure 29D).

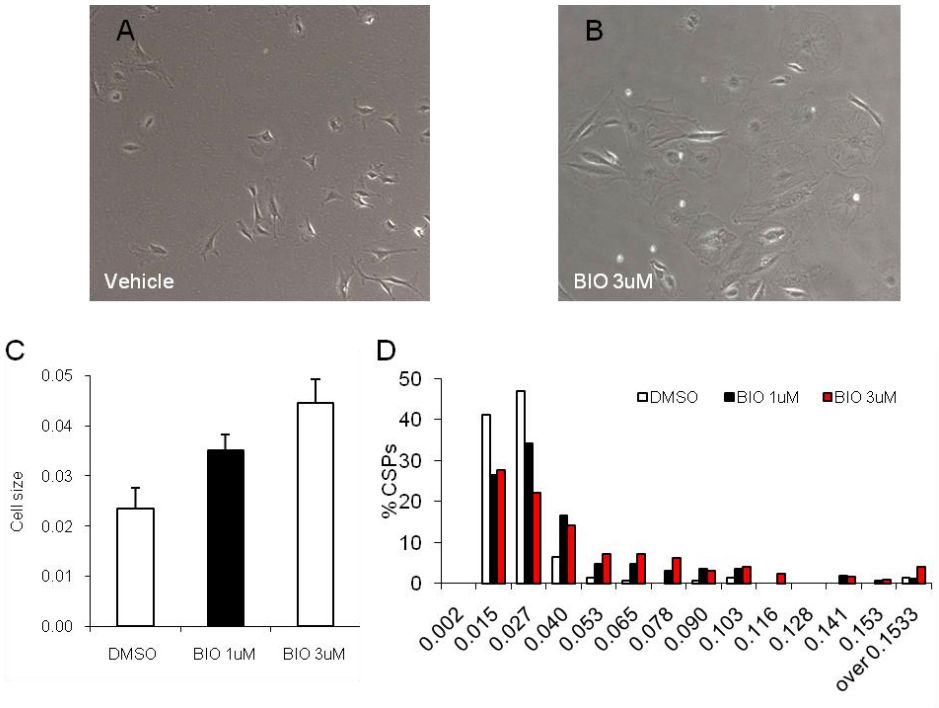

Figure 29: Effects of BIO on the cell size of CSPs. Representative images of CSPs treated (48 hours) with (A) vehicle medium (B) 3μM BIO (n=2 for all). (C) Quantification of BIO effects on CSP cell size. (D) Frequency analysis of the various sizes of CSP cells following treatment with BIO.

- *Wnt signaling promotes the cardiac differentiation of CSPs*

Subsequently, I investigated the role of Wnt signaling pathway on the cardiomyogenic differentiation of CSPs. Differentiation assays were performed based on our established co-culture system [65] utilizing either adult rat ventricular cardiomyocytes or neonatal rat ventricular cardiomyocytes (NRVM). When CSPs were co-cultured with adult cardiomyocytes, treatment of Wnt3a conditioned medium resulted in an approximate 3-fold increase of the amount of CSPs expressing α-sarcomeric actinin, in comparison to the vehicle-CM treated CSPs (5.18% versus 1.64% respectively) (Figure 30G). Similarly, when CSPs were co-cultured with neonatal cardiomyocytes, application of Wnt3a-CM resulted in approximately 2-fold increase of CSPs expressing α-sarcomeric actinin, compared to vehicle-CM treated cells (2.90% versus 1.56% respectively) (Figures 30I). Representative examples of differentiated CSPs following treatment with vehicle or Wnt3a-CM are presented in Figures 30A-F.

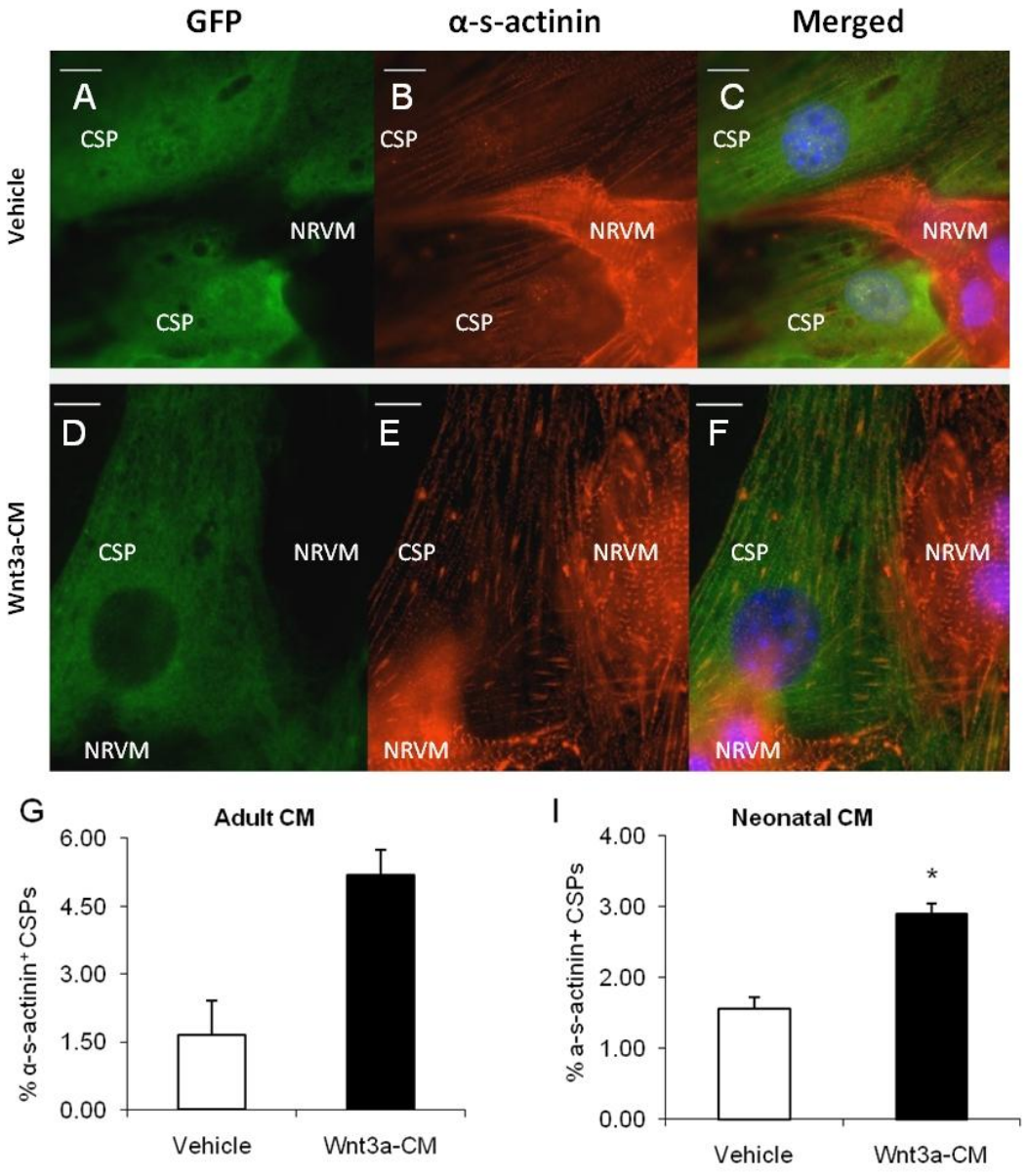

Figure 30: Effects of Wnt signaling on cardiomyogenic differentiation of CSPs. (A-F) Representative images of vehicle treated CSPs (A-C) and Wnt3a-CM treated CSPs (D-F) in co-culture with NRVM. GFP expression (green) identifies CSPs, α-sarcomeric-actinin (red) is characteristic of NRVM and differentiated CSPs. Nucleus is stained with DAPI (blue). Merged images show areas of co-localization of GFP and a-sarcomeric actinin (orange). (G-I) Quantification of CSP cell differentiation in co-culture with adult (n=2) (G) and neonatal (I) NRVMs (n=5), in comparison to vehicle treated cells. Error bars show s.e. * indicates $p<0.05$.

- *Effects of Wnt signaling pathway on neonatal cardiomyocytes*

All the differentiation experiments were performed using a well established co-culture protocol of our lab, in which CSPs are plated onto a layer of previously seeded neonatal rat ventricular cardiomyocytes (NRVM). Thus, the next step was to examine the effects of the Wnt signaling pathway on the neonatal cardiomyocytes. Consequently, NRVMs were pulsed with 10μM of BrdU and they were treated with 30% vehicle-CM or 30% Wn3a-CM for a period of 48 hours. The proliferation capacity of NRVMs was measured through immuno-staining and detection of the incorporated BrdU through fluorescence microscopy. As shown in Figure 31A treatment with Wnt3a-CM did not change significantly the amount of mono-nucleated NRVMs that incorporated BrdU in comparison to vehicle-CM treated cells (29.20% versus 23.20% respectively) (Figure 31B). Similarly, there was no change in the amount of Wnt3a-CM treated bi-nucleated NRVMs that incorporated BrdU, compared to vehicle-CM treated cells (31.70% versus 31.09% respectively). Overall, there was no change in the amount of total nuclei with incorporated BrdU in both experimental treatments (30.45% versus 27.17% respectively) (Figure 31C).

The above results were supplemented by measurement of the ratio between the total numbers of cells and the microscopically examined area (cell #/area in mm^2). No significant difference was observed in the ratio of vehicle-CM and Wnt3a-CM treated mono-nucleated and bi-nucleated NRVMs (176 versus 216 and 45 versus 44 respectively).

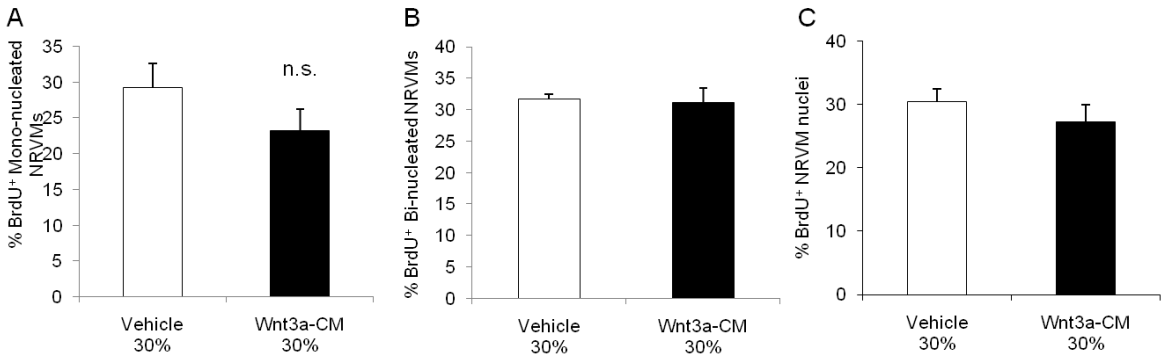

Figure 31: Effects of Wnt signaling pathway on NRVM proliferation. Quantification of the mono-nucleated NRVM (A), bi-nucleated NRVM (B) and total nuclei (C) that incorporated BrdU following Wnt3a-CM (30%) treatment, compared to vehicle treated cells (n=3 for all). Error bars indicate s.e. n.s indicates $p > 0.05$ for Wnt3a-CM treated NRVM vs respective controls.

Subsequently, I examined the effects of the activation of Wnt signaling pathway on NRVMs, via a different approach. NRVMs were treated with BIO (3μM) and were pulsed with 10μM of BrdU for a period of 48 hours. The amount of NRVMs with incorporated BrdU was determined through immuno-fluorescence microscopy. As shown in Figure 32A application of 3μM BIO changed significantly the proportion of mono-nucleated NRVMs that incorporated BrdU in comparison to vehicle (DMSO was utilized as a solvent of BIO) treated cells (50.55% versus 36.96% respectively). There was no difference in the amount of $BrdU^+$ NRVMs between the standard culture conditions (control) and the vehicle culture conditions (DMSO) (34.99% versus 36.96% respectively). Moreover, there was no alteration in the amount of BIO treated bi-nucleated NRVMs that incorporated BrdU, compared to vehicle (DMSO) and control cultured cells (39.32%% versus 42.64% and 45.89% respectively) (Figure 32B). Overall, there was a significant increase in the amount of total nuclei of NRVMS with incorporated BrdU when they

were treated with BIO, in comparison to vehicle (DMSO) and control treated cells (48.22%% versus 39.80% and 37.15% respectively) (Figure 32C).

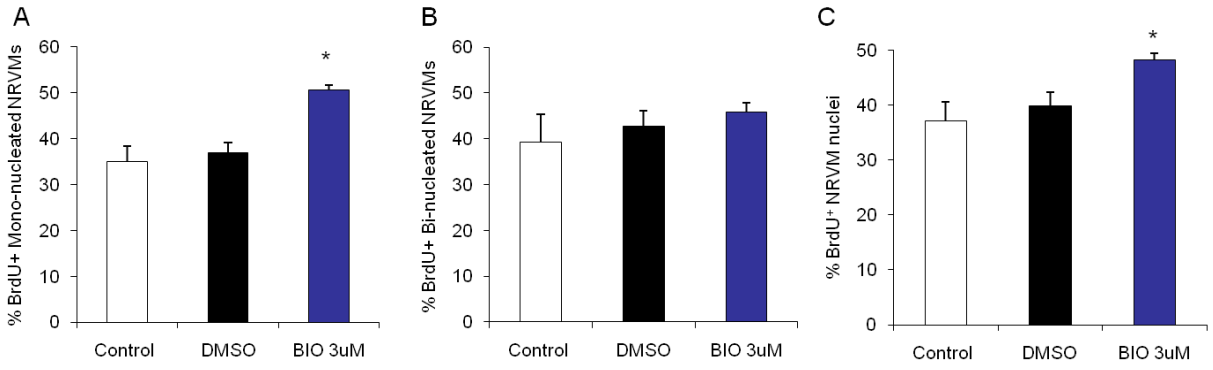

Figure 32: Effects of BIO on NRVM proliferation. Quantification of the fraction of mono-nucleated NRVM (A), bi-nucleated NRVM (B) and total nuclei (C) that incorporated BrdU following treatment with BIO, in comparison to vehicle treated cells (n=3 for all). Error bars indicate s.e. * indicates $p<0.05$ for BIO compared to vehicle.

The above data by measuring the ratio between the total numbers of cells and the microscopically examined area (cell number/area in mm^2). No substantial difference was observed in the ratio of vehicle (DMSO) and BIO treated mono-nucleated and bi-nucleated NRVMs (91.75 versus 103.12 and 25.23 versus 25.94 respectively). However, there was a significant difference in the ratio between the cell number and the examined area in the case of control cultured and vehicle (DMSO) or BIO treated cells for both mono-nucleated and bi-nucleated NRVMs (36.06 versus 59.93 and 56.84 respectively for mono-nucleated and 13.38 versus 25.23 and 25.94 respectively for bi-nucleated respectively).

The ratio of mono-nucleated versus bi-nucleated cells remained unchanged independent of the experimental treatment (Control, Vehicle (DMSO), BIO, Vehicle-CM and Wnt3a-CM) (Figure 33).

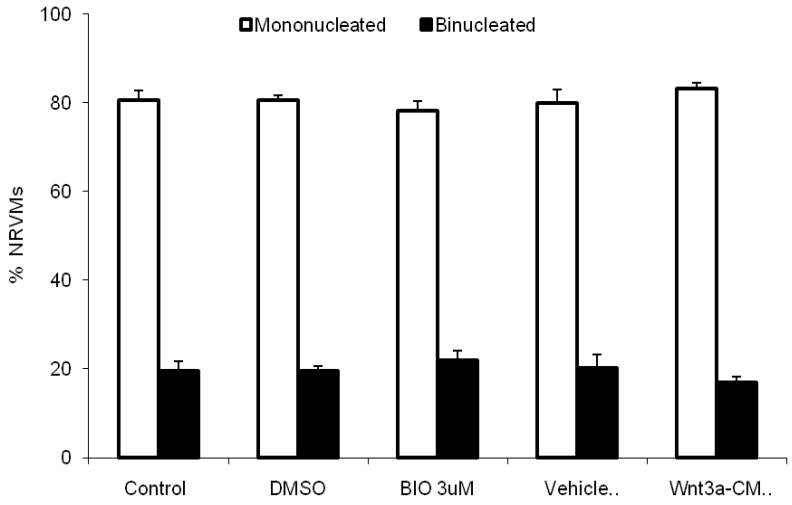

Figure 33: Effects of Wnt signaling pathway on the ratio of mono-nucleated to bi-nucleated NRVM (n=3 for all). Error bars indicate s.e.

Finally, I also examined the effects of Wnt signaling pathway on the size of mono-nucleated NRVMs. Measurement of the area of each NRVM, following application of vehicle-CM and Wnt3a-CM, revealed no difference between the two experimental groups. The average size of vehicle-CM treated cells was 867.74 μm^2 and the average size of the Wnt3a-CM treated NRVMs was 1016.28 μm^2 (Figure 34A). Similarly, there was no difference in the average value of the perimeter of NRVMs in each experimental treatment (164.22 μm versus 181.43 μm). Moreover, activation of the Wnt signaling pathway through treatment with BIO did not significantly affect the size of mono-nucleated NRVMs. Measurement of the area of each

NRVM, in standard culture conditions or following application of vehicle (DMSO) and BIO (3μM), revealed no difference between all the experimental groups. The average size of NRVMs in standard culture conditions was 1051μm^2 , following treatment with vehicle (DMSO) it was 1054μm^2, and following application of BIO it was 929μm^2 (Figure 34B). Similarly there was no difference in the average value of the perimeter of NRVMs in each experimental treatment (standard culture 161.25μm, vehicle (DMSO) treated 176.76μm and BIO treated 169.78μm).

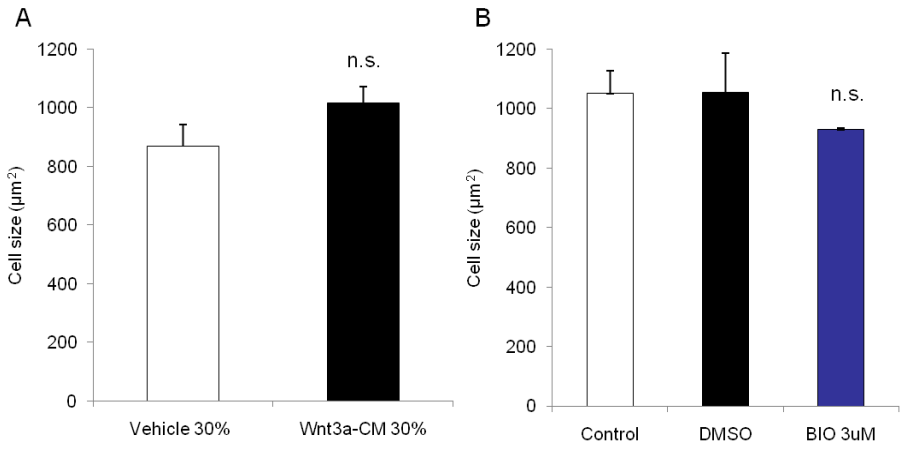

Figure 34: Effects of Wnt signaling on the cell size of NRVM. Quantification of the cell size of NRVM following treatment with Wnt3-CM (30%) (A) and BIO (B) (n=3 for all). Error bars indicate s.e. n.s indicates $p > 0.05$ for Wnt3a-CM treated or BIO treated NRVM compared to respective controls.

5. IGFBP3 is an essential mediator of the anti-proliferative effects of Wnt signaling on CSPs

- *IGFBP3 is up-regulated in CSPS following activation of the Wnt signaling pathway*

In order to identify potential mediators of the effects of Wnt signaling pathway on CSPs I used a RT-PCR-based array, which includes 84 genes involved into several signaling pathways (Pathway Finder). In this series of experiments, I used mRNA from CSPs treated with vehicle-CM and Wnt3a-CM for a period of six days. The expression profile of the examined genes that were expressed in CSPs is presented in the 3-D diagram (Figure 35). All the examined genes including those with negligible or no expression are listed in Table 5. Despite the fact that many genes were up-regulated in CSPs following treatment with Wnt3a-CM, only a handful of genes (9 out of 84) were significantly up-regulated (Figure 36). Namely, Ei24 (1.92-fold), Hspb1 (1.92-fold), Tmepai (6.88-fold), Lef-1 (8.52-fold), Cdnk2a (9.11-fold), Tcf-7 (9.81-fold), Fas (10.14-fold), Wnt2 (13.94-fold) and IGFBP3 (43.44-fold) were all up-regulated following treatment with Wnt3a-CM for a period of 6 days.

Among all the examined genes, IGFBP3 was noticeably up-regulated (over 40-fold). To further examine the expression pattern of IGFBP3, I performed a time-course analysis of its expression in CSPs that were treated with Wnt3a-CM for different periods of time. qRT-PCR analysis revealed that IGFBP3 was up-regulated in CSPs treated with Wnt3a-CM at 24 hours (4-fold), 48 hours (7-fold) and 72 hours (7-fold), in comparison to vehicle-CM treated cells (Figure 37). The expression of IGFBP3 was also progressively increased in a time dependent manner in

the vehicle-CM treated CSPs. IGFBP3 was also up-regulated in the protein level as shown by immnunoblot analysis of cell extract and harvested cell culture medium (Figure 38A-B).

Subsequently I examined the effects of BIO on the expression of IGFBP3. Treatment of CSPs with 2μM and 5μM of BIO increased the expression of IGFBP3 in the gene level (only when 5μM were used) and in the protein level (in both cases) (Figure 39 A-B). Overall, the above results clearly suggest that activation of the Wnt signaling pathway increases the expression of IGFBP3 in a time dependent manner.

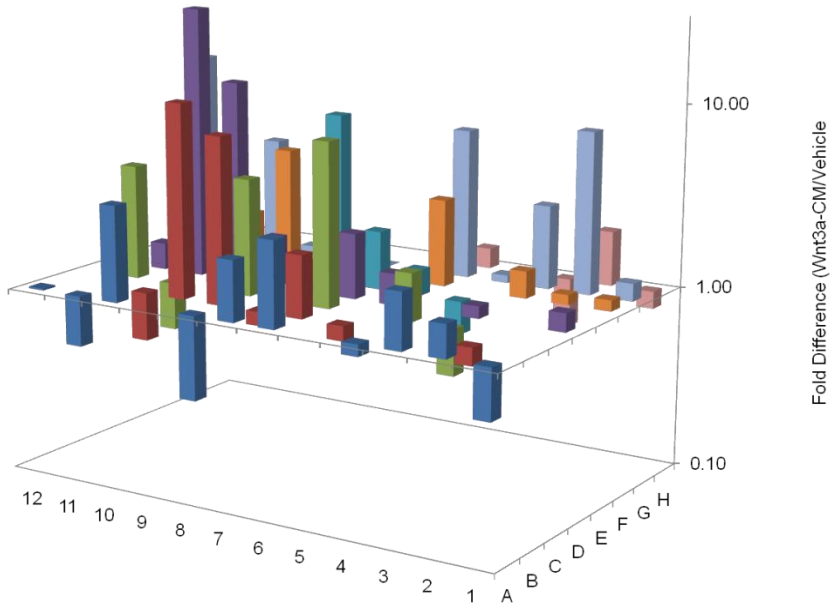

Figure 35: 3-D plot of the expression profile of the genes examined with pathway-finder array in CSPs following treatment with Wnt3a-CM (25%) or vehicle (6 days) (n=3).

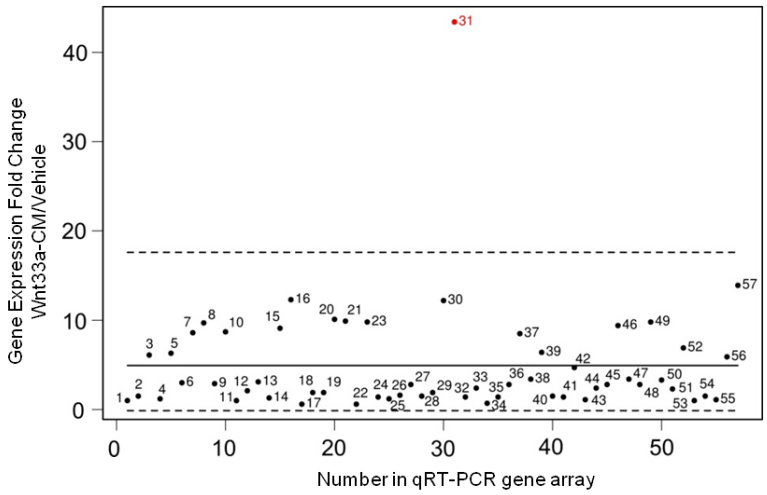

Figure 36: Scatter plot analysis of gene expression fold changes of all genes examined in the pathway-finder array, in CSPs following treatment (6 days) with Wnt3a-CM or vehicle (n=3 for all). Solid line represents the average value of the fold changes of all genes and dashed lines represent values of 2 standard deviations above and below the average. In red, gene #31 corresponds to IGFBP3.

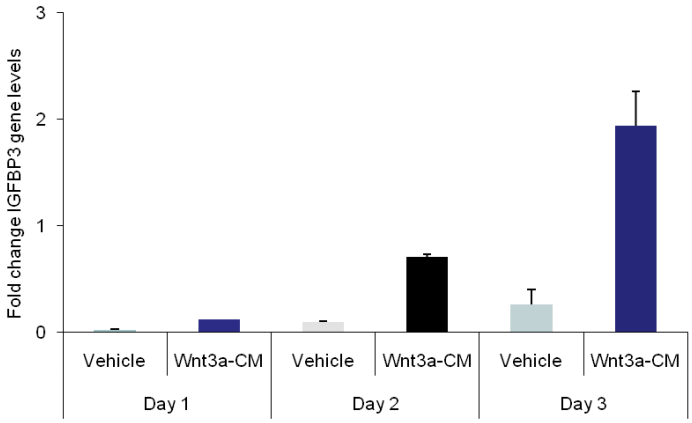

Figure 37: Gene expression analysis of IGFBP3 in CSPs treated with Wnt3a-CM (25%) or vehicle medium for 1 Day, 2 Days and 3 Days (n=3 for all). Error bars indicate s.e. * indicates $p \leq 0.05$ for Wnt3a-CM compared to vehicle, # indicates $p \leq 0.05$ for Vehicle Day 1 vs vehicle Day 2, § indicates $p \leq 0.05$ for Vehicle Day 2 vs vehicle Day 3.

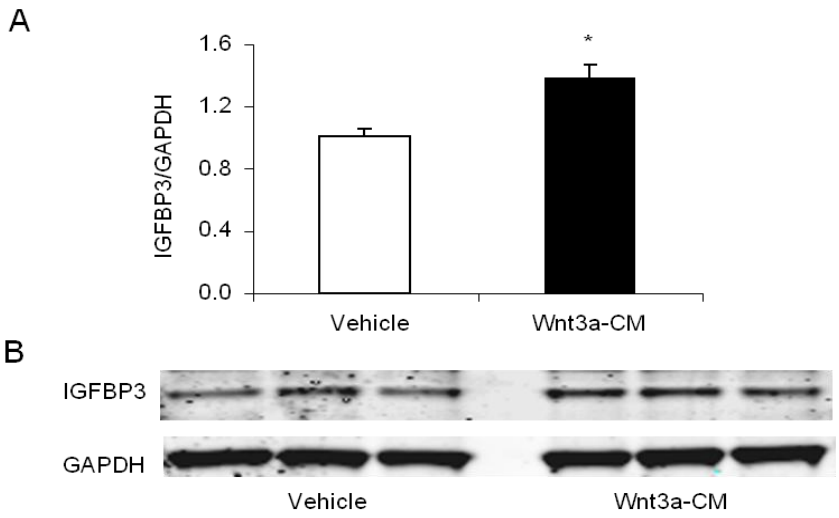

Figure 38: Western blot analysis of IGFBP3 protein expression in CSPs. (A) Quantification of IGFBP3 protein levels in cell extract of CSPs treated (48 hours) with Wnt3a-CM (25%) or vehicle medium (n=3 for all). (B) Representative immunoblot analysis of IGFBP3 protein in CSPs. Error bars indicate s.e. * indicates $p \leq 0.05$ for Wnt3a-CM compared to vehicle.

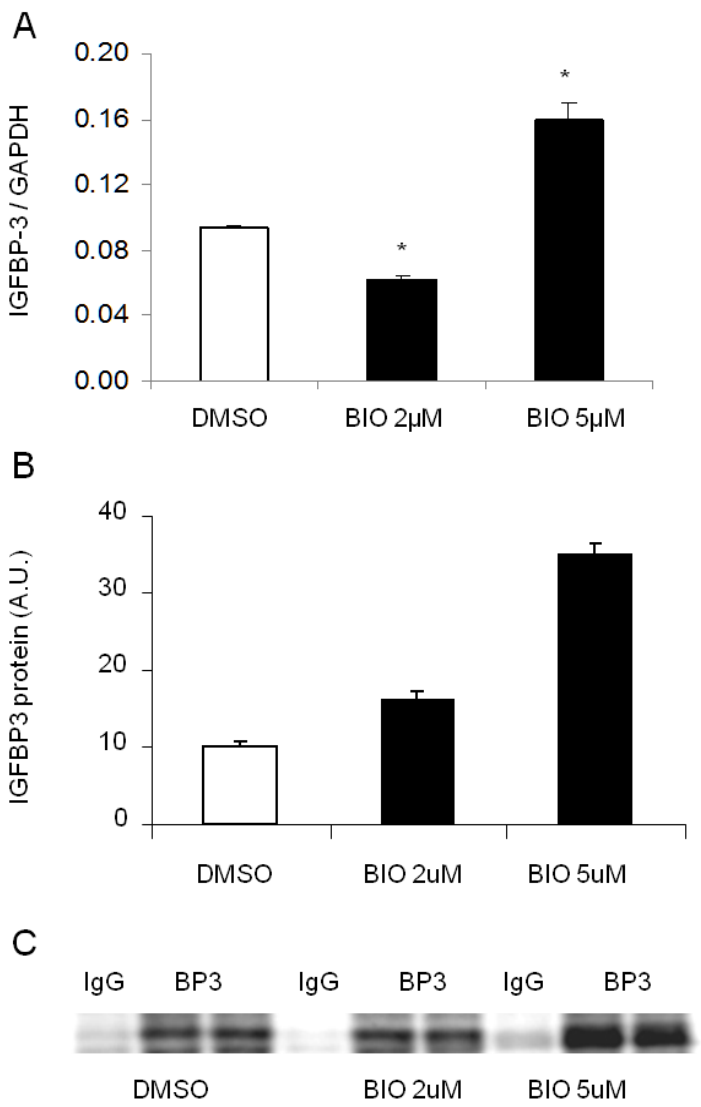

Figure 39: IGFBP3 protein expression in CSPs following treatment of BIO (72 hours). (A) qRT-PCR of IGFBP3 gene expression analysis (n=3). (B) IGFBP3 protein analysis (n=2). (C) Immunoprecipitation analysis of IGFBP3 protein expression in cell culture medium harvested from CSPs. Error bars indicate s.e. * indicates $p \leq 0.05$ for BIO compared to vehicle.

- *Role of IGFBP3 in the proliferation capacity and cell cycle status of CSPs*

To assess the question whether IGFBP3 is involved in the anti-proliferative actions of Wnt signaling pathway I followed a gain and loss of function approach. Initially, I created a lentivirus construct that over-expresses mouse IGFBP3 under the control of the constitutively active Ef1a promoter (Figure 40A). Infection of CSPs with the IGFBP3 over-expressing lentivirus increased its expression by approximately 100-fold as determined by qRT-PCR assays (Figure 40B). Immunocytochemical analysis of CSPs infected with mock (empty) and IGFBP3 over-expressing lentivirus revealed a significant increase also in the IGFBP3 protein levels (1.42-fold) (Figure 40C). Interestingly enough, the intra-cellular IGFBP3 was found to be primarily localized in the nucleus of CSPs (Figure 41).

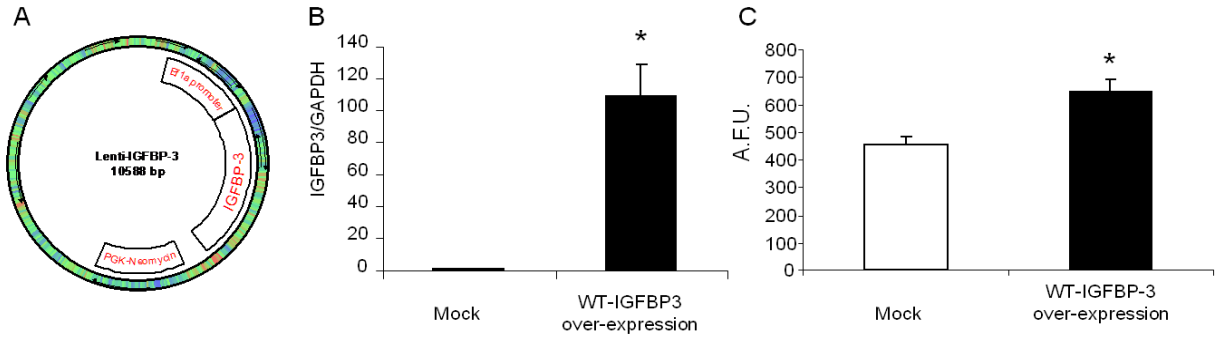

Figure 40: Lentivirus-mediated IGFBP3 over-expression. (A) Schematic illustration of IGFBP3 lentivirus construct. (B) Quantification of IGFBP3 gene expression levels in mock- and IGFBP3 infected CSPs (n=3 for all). (C) Quantification of IGFBP3 nuclear protein expression in mock- and IGFBP3 infected CSPs, measured by fluorescence microscopy (A.F.U. stands for arbitrary units). Error bars indicate s.e. * indicates $p \leq 0.05$ for IGBFP3 over-expression compared to mock.

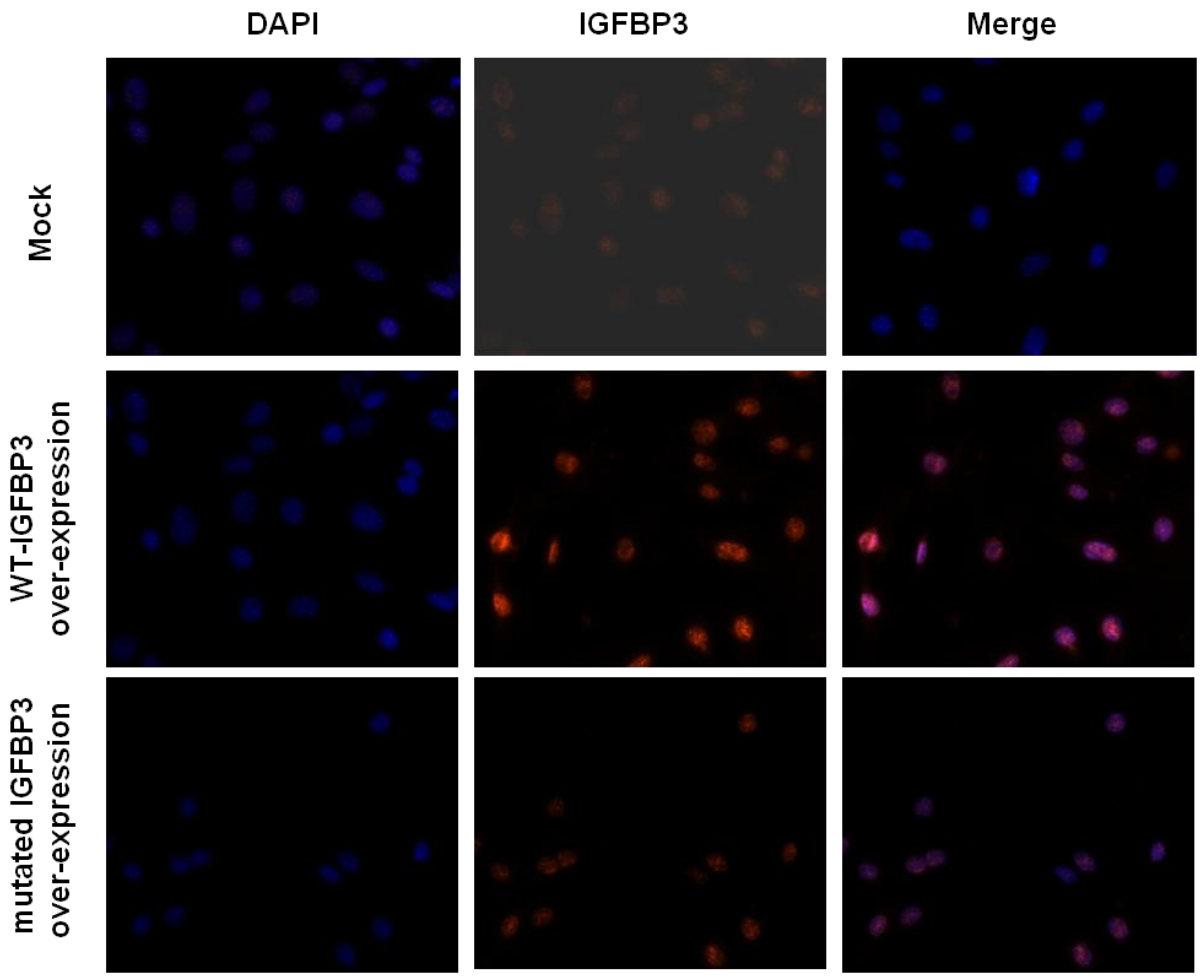

Figure 41: Representative images of IGFBP3 nuclear protein expression in CSPs following infection with mock-, WT-IGFBP3 and IGFBP3^{mNLS} lentivirus. Blue represents the nucleus (DAPI) and red represents IGFBP3.

Lentivirus-mediated over-expression of IGFBP3 decreased significantly the proliferation capacity of CSPs (2.63-fold), in comparison to mock-infected CSPs (Figure 42). Furthermore, I tested the effects of increasing doses of isolated recombinant IGFBP3 protein on the proliferation of CSPs. Treatment of CSPs with r-IGFBP3 resulted in decreased proliferation (1.5-fold) only at

the highest dosage (800 ng/ml) (Figure 43). Overall the above data suggest that IGFBP3 acts as negative regulator of the proliferation of CSPs.

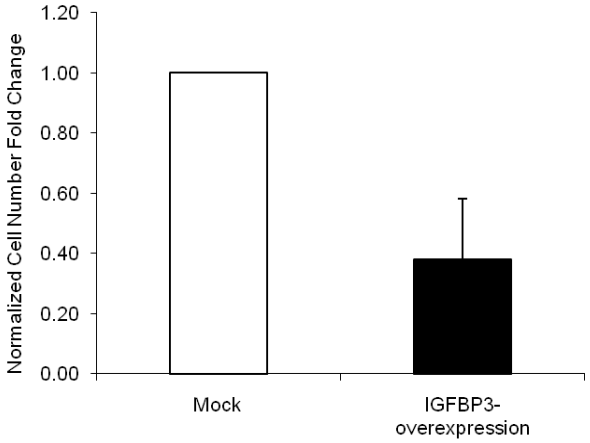

Figure 42: Effects of lentivirus mediated over-expressed IGFBP3 on the proliferation of CSPs. Puromycin-selected CSPs (mock and IGFBP3-over-expressing) were seeded ad day0 and their numbers were measured 5 days later. Error bars show s.e. * indicates $p \leq 0.05$.

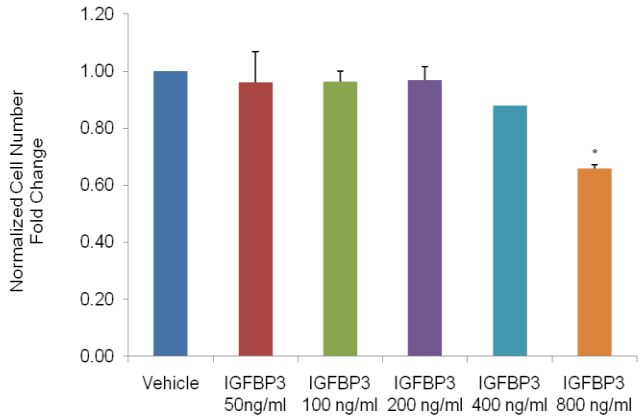

Figure 43: Effects of r-IGFBP3 protein on the proliferation of CSPs. Proliferation assay of CSPs following treatment (6 days) with IGFBP3 (dose dependent) (vehicle n=4, 50ng/ml n=2, 100ng/ml n=2, 200ng/ml n=3, 400 ng/ml n=1 and 800 ng/ml n=2). Error bars show s.e. * indicates $p \leq 0.05$.

Subsequently, I examined the cell cycle profile of CSPs following lentivirus mediated over-expression of IGFBP3 in comparison to mock infected cells. I utilized the same cell cycle focused qRT-PCR gene array as mentioned above. The expression profile of all cell-cycle related genes, which were expressed in CSPs, is presented in the 3-D diagram (Figure 44). All the examined genes including those with negligible or no expression are listed in Table 6. Among all altered genes following treatment with Wnt3a-CM only a few were significantly changed. Specifically, Brca-1 (-2.91-fold), Mcm2 (-2.42-fold), Rad21 (-1.57-fold), Rbl1 (-1.85-fold), Trp53 (-1.72-fold) and Camk2a (2.2-fold) (Figure 45).

Finally, I evaluated the effects of canonical Wnt signaling pathway and IGFBP3 over-expression on the expression of the various cell cycle regulators. The fold changes of all examined cell-cycle focused genes, obtained from the cell cycle arrays of Wnt3a-CM treated cells and IGFBP3 over-expressing cells were directly compared. This method revealed that approximately 79% of the cell-cycle related genes (66 genes out of 84) are regulated similarly by the two experimental treatments. Approximately 21% of all genes (18 genes out of 84) were differentially regulated by the two treatments (Figure 46). An analytical table of the comparison of the fold changes of each cell cycle array (Wnt3a treatment and IGFBP3 over-expression) can be seen in Table 6. Overall, the above data strongly suggest that IGFBP3 represent a primary mediator of the anti-proliferative action of Wnt signaling pathway in CSPs.

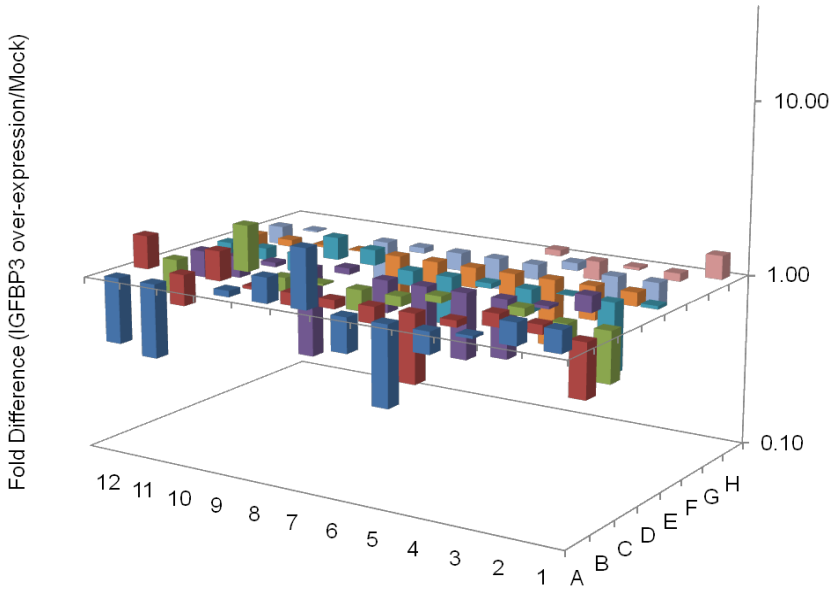

Figure 44: 3-D plots of the expression profile of cell cycle-related genes in CSPs following treatment mock and IGFBP3 over-expression (6 days) (n=3 for all).

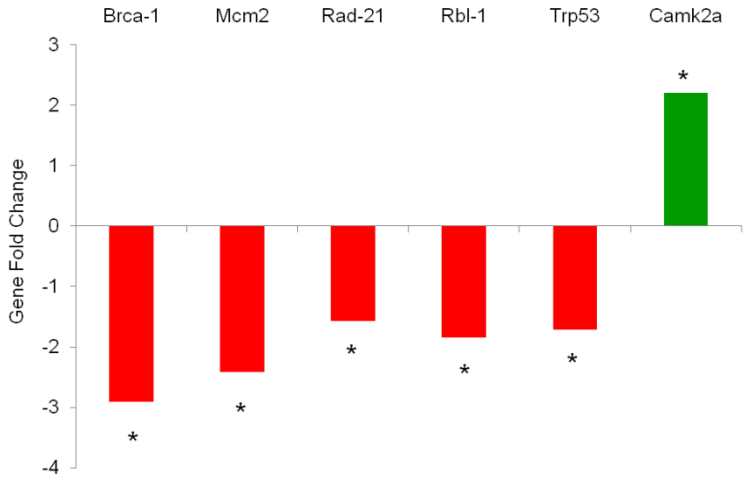

Figure 45: Fold changes of the expression of cell cycle-related genes in CSPs following infection with mock or IGFBP3 lentivirus (6 days) (n=3 for all). Error bars indicate s.e. * indicates $p \leq 0.05$ for IGFBP3 compared to mock.

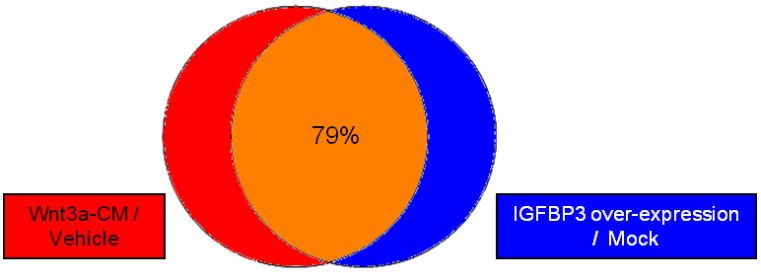

Figure 46: Direct comparison of the fold changes of all examined cell-cycle related genes, obtained from the cell cycle arrays of Wnt3a-CM treated cells and IGFBP3 over-expressing. Approximately 79% of the cell-cycle related genes are similarly regulated by the two experimental treatments.

- *Ablation of IGFBP3 blocks the anti-proliferative role of Wnt signaling in CSPs*

Subsequently, in order to further dissect the role of IGFBP3 in CSPs following activation of the Wnt signaling pathway, I utilized a lentivirus encoding a shRNA against IGFBP3 to down-regulated its expression. After testing several sequences targeting IGFBP3 in CSPs I selected a shRNA oligo (sh-IGFBP3) that was able to down-regulate IGFBP3 protein levels by approximately 70%, in comparison to scramble shRNA (scramble) infected CSPs (Figure 47). Scramble and sh-IGFBP3 infected CSPs were treated with 25% vehicle or Wnt3a-CM and their growth was assessed 5 days later. As expected, treatment of scramble infected CSPs with Wnt3a-CM decreased their proliferation (2-fold), in comparison to vehicle-CM treated cells (Figure 48). However, in shIGFBP3 expressing CSPs, treatment with Wnt3a-CM did not decrease their proliferation, in comparison to vehicle-CM treatment. The above data strongly suggest that IGFBP3 represents an important mediator of the anti-proliferative effects of Wnt signaling pathway in CSPs (Figure 48).

Subsequently, I compared the changes in the expression profile of the cell cycle-related genes (included in the cell cycle gene array) between scramble- and sh-IGFBP3-infected CSPs, which were treated with either vehicle-CM or Wnt3a-CM. In all samples 9 genes demonstrated negligible expression levels and they were excluded from the analysis. In the scramble-infected CSPs 35 out of the 75 (47%) examined cell-cycle related genes were altered (up- or down-regulated) by more than 2-fold due to treatment with Wnt3a-CM. Whereas, in the sh-IGFBP3-infected CSPs only 12 out of the 75 examined cell cycle regulators (16%) were altered by more than 2-fold following treatment with Wnt3a-CM. Thus, consistent with our observation in the proliferation assay, the expression profile of cell cycle related genes, in response to the Wnt3a treatment, was normalized in IGFBP3 shRNA infected CSPs (Figure 49). Overall, the above loss-of-function experiments strongly support the necessity of IGFBP3 as a critical mediator for the anti-proliferative effects of Wnt3a in CSPs.

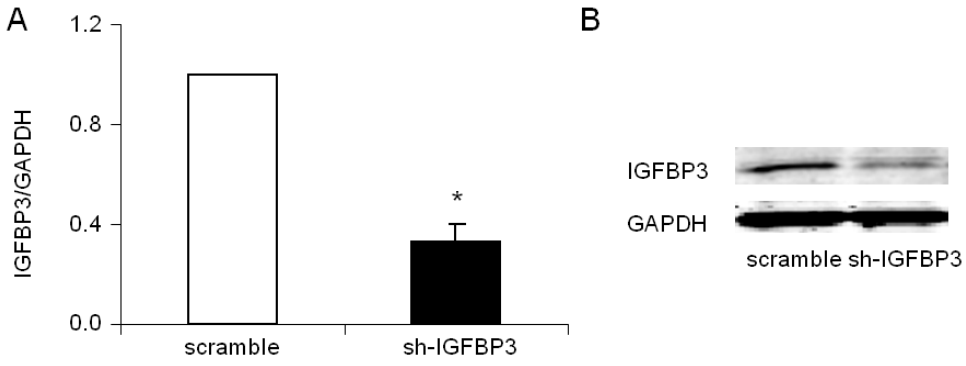

Figure 47: A) sh-IGFBP3 down-regulates IGFBP3 protein levels by approximately 70%, in comparison to scramble scramble infected CSPs. Error bar indicates s.e. * indicates $p \leq 0.05$ B) Representative immunoblot analysis of IGFBP3 protein expression in scramble- and shIGFBP3 expressing CSPs.

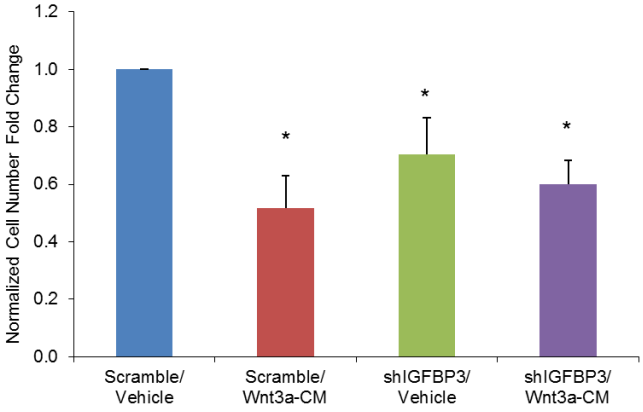

Figure 48: Down-regulation of IGFBP3 rescues CSPs from the Wnt-mediated anti-proliferative action. Scramble-infected and shIGFBP3-infected CSPs were treated (6 days) with Wnt3a-CM (25%) and vehicle medium. Error bars indicate s.e. * indicates $p \leq 0.05$ for all samples vs Vehicle.

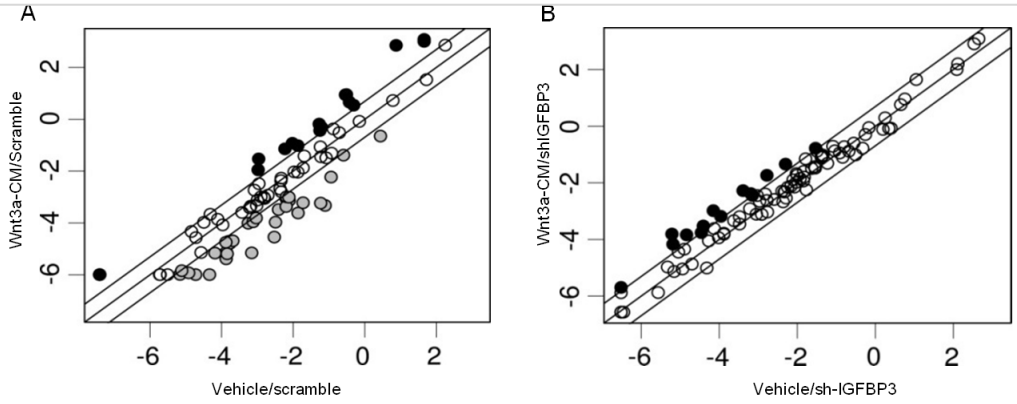

Figure 49: Scatter plot analysis of the fold changes of cell cycle related genes in CSPs which were infected with sh-Scramble and sh-IGFBP3 following treatment with Wnt3a-CM or vehicle medium respectively. Down-regulation of IGFBP3 expression in CSPs reverses the Wnt-mediated changes in the expression of cell cycle related genes (B) observed in scramble-infected CSPs (A). The outer diagonal lines indicate 2-fold changes; full black circles represent Wnt-induced up-regulated genes, full grey circles represent Wnt-down-regulated genes and empty circles represent genes with equal expression in both groups.

- *IGFBP3 exerts its anti-proliferative effects via an IGF-dependent manner*

IGFBP3 is an abundant circulating IGF-binding protein and acts as a modulator of cell survival, cell proliferation and cell metabolism via IGF-dependent and IGF-independent mechanisms. To address the question whether IGFBP3 exert its effects via IGF-dependent or -independent manner, I performed side-directed mutagenesis to generate two mutant forms of IGFBP3. It has been reported that IGFBP3 exerts some of its IGF-independent functions through its nuclear localization [127]. Thus, the nuclear localization sequence of IGFBP3 ($IGFBP3^{mNLS}$) was mutated by replacing 5 amino acids, KGRKR, with 5 non functional amino acids, MDGEA (Figure 50). Similarly, in the second mutant ($IGFBP3^{mIGF}$) the IGF-binding site of IGFBP3 was inactivated by substituting 2 conserved leucine residues by 2 glycine residues (Figure 50).

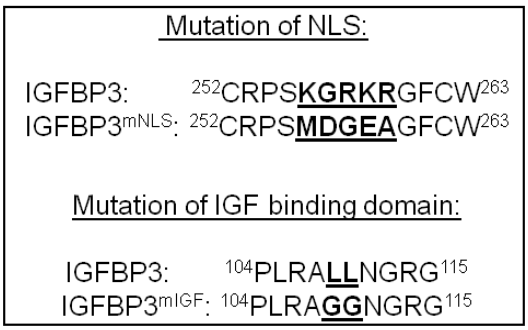

Figure 50: Schematic illustration of the mutated forms of IGFBP3.

Both mutated forms ($IGFBP3^{mNLS}$ and $IGFBP3^{mIGF}$) were used in order to examine the role of IGFBP3 in the growth of CPSs. CSPs infected with $IGFBP3^{mNLS}$ demonstrated decreased proliferation capacity in comparison to mock-infected CSPs. CSPs infected with $IGFBP3^{mNLS}$ demonstrated also a mild but not significant increase in their proliferation rate

relative to IGFBP3-infected cells (Figure 51). In contrast, to IGFBP3 and IGFBP3^{mNLS}, IGFBP3^{mIGF} resulted in a significant increase of CSP cell proliferation (Figure 51). CSPs infected with the IGFBP3^{mIGF} lentivirus exhibited a significant increase in their growth compared to mock-infected cells. Overall, the above data suggest that following treatment with Wnt3a ligands sequestration of IGF-I by IGFBP3 is required to mediate its anti-proliferative effects whereas its nuclear localization is not.

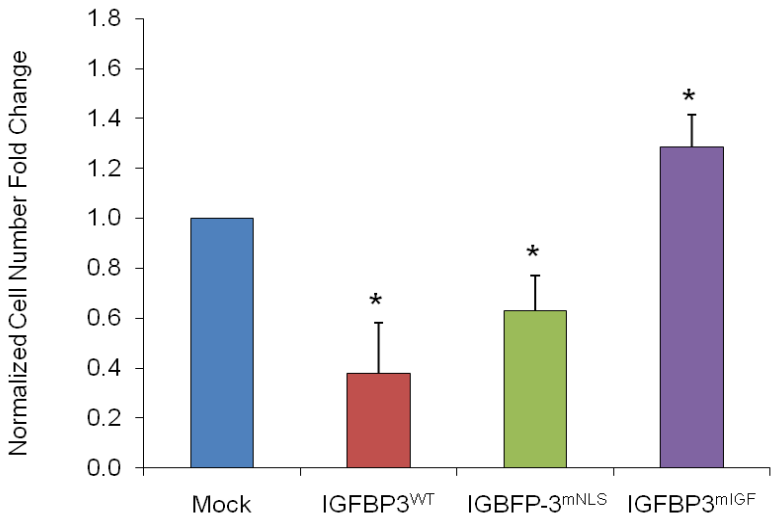

Figure 51: IGFBBP3 decreases the proliferation of CSPs via IGF-dependent mechanism. Proliferation assays of CSPs infected with mock-lentivirus (n=5), IGFBP3^{WT}-lentivirus (n=5), IGBFP-3^{mNLS}-lentivirus (n=4) and IGFBP3^{mIGF}-lentivirus (n=3). Error bars show s.e. * indicates $p<0.05$ of all samples to vehicle.

- *<u>Effects of IGFBP3 on the cardiomyogenic differentiation of CSPs</u>*

IGFBP3 represents a major mediator of the anti-proliferative effects of Wnt signaling pathway on CSPs as shown by the gain and loss of experiments. Therefore, I sought to

examine the role of IGFBP3 on the cardiomyogenic differentiation of CSPs. CSPs were treated with 800 ng/ml of either mouse or human origin recombinant IGFBP3 for a period of 3 days, in our established co-culture protocol. The cardiomyogenic differentiation of co-cultured CSPs was evaluated through immuno-fluorescence staining for the presence of α-sarcomeric-actinin, a marker of mature cardiomyocytes. Blind scoring of co-cultures treated with mouse (1. 45%) and human (1.51%) originated IGFBP3 revealed a non significant decrease in the amount of GFP^+ α-sarcomeric-$actinin^+$ CSPs compared to vehicle (2.10%) (Figure 52). Representative examples of differentiated (GFP^+ α-sarcomeric-actinin+) CSPs, in low and high magnification, from each experimental condition are presented in Figure 52.

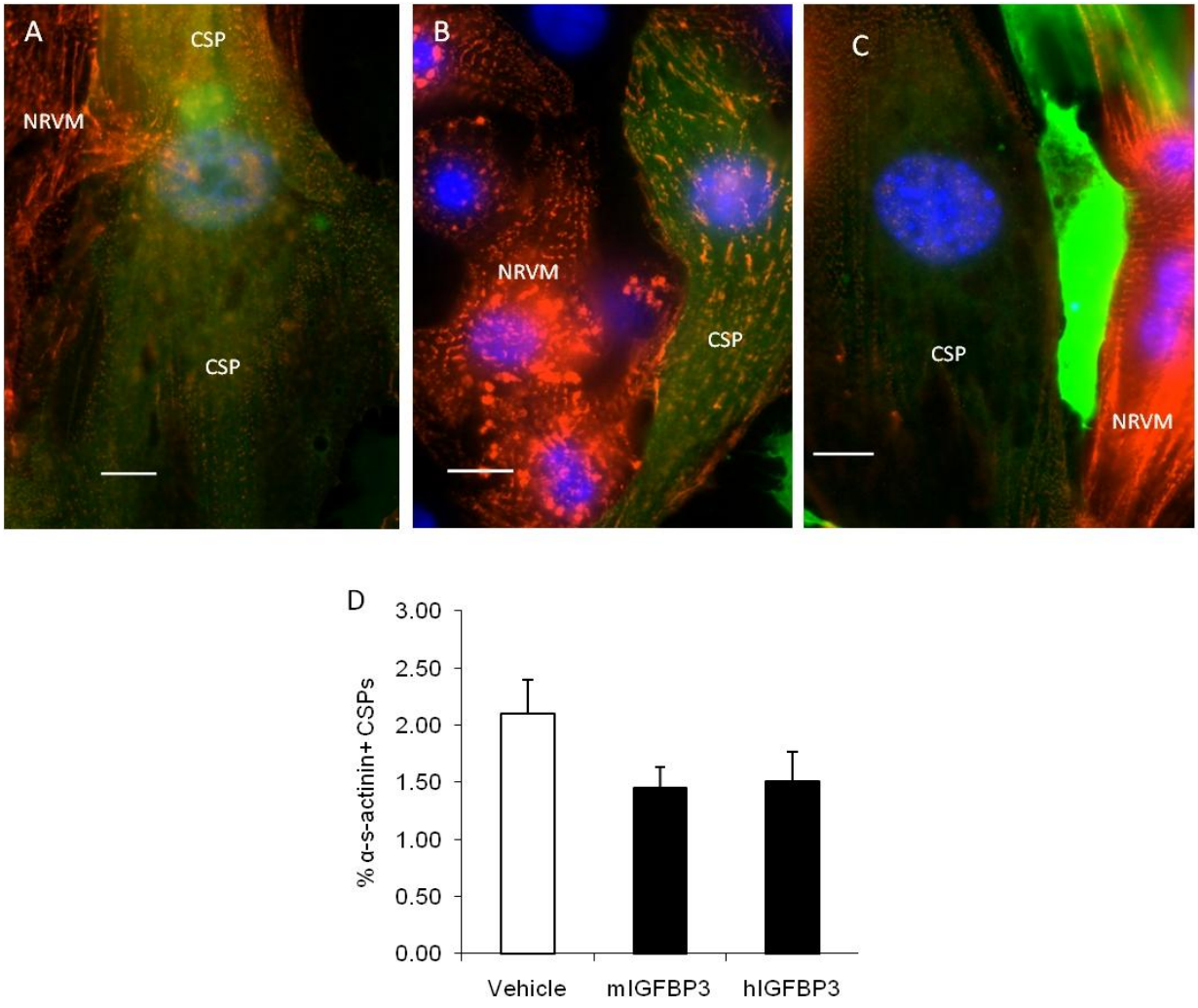

Figure 52: Effects of IGFBP3 on cardiomyogenic differentiation of CSPs. (A-C) Representative images of vehicle (PBS) treated CSPs, mouse derived IGFBP3 (mIGFBP3) (B) and human derived IGFBP3 (hBP3) (C) treated CSPs, in co-culture with NRVM. GFP expression (green) identifies CSPs, α-sarcomeric-actinin (red) shows NRVM and differentiated CSPs. Nuclei are stained with DAPI (blue). Diagram presents quantification of CSP cell differentiation. Error bars show s.e.

- *IGFBP3 does not affect the survival of CSPs*

IGFBP3 regulates the proliferation as well the survival of various types of cells. Therefore I tested the effects of IGFBP3 on the survival of CSPs by supplementing the culture medium with 800 ng/ml of recombinant mouse IGFBP3 (r-IGFBP3) for a period of 5 days. Cell death was assessed by Annexin-V and propidium iodide (PI) staining. Treatment of CSPs with r-IGFBP3 did not alter the amount of dead cells as measured by either Annexin-V or PI in comparison to vehicle treated cells (Figure 53).

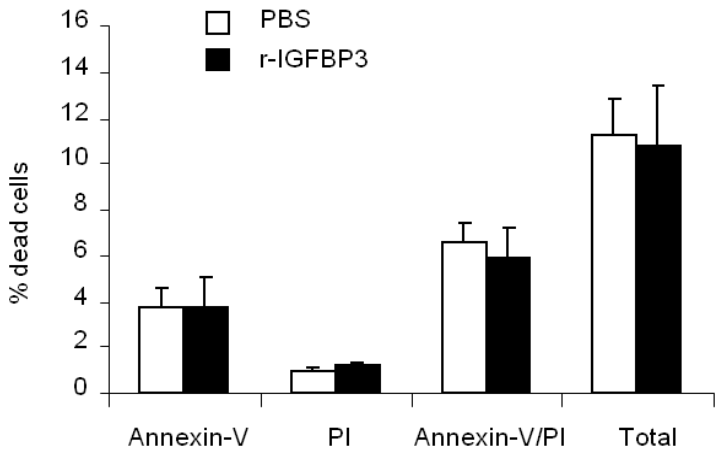

Figure 53: Cell death analysis of CSPs following treatment (6 days) with r-IGFBP3 protein

- *Expression levels of IGFBP3 in post-MI myocardium*

In parallel with the studies in CSPs, we examined the expression of IGFBP3 in post-MI cardiac tissues. mRNA samples were harvested from the infarct-border zone and the remote area at 1, 3 and 7 days post-infarction. In the infarct-border zone, IGFBP3 was found to be

significantly up-regulated acutely after MI (day 1) and it remained elevated at both later time points (day 3 and day 7) (Figure 54A). The expression of IGFBP3 in the remote area was significantly elevated 1 day following injury, it remained up-regulated until day 3 and its expression returned to baseline levels at day 7 (Figure 54B).

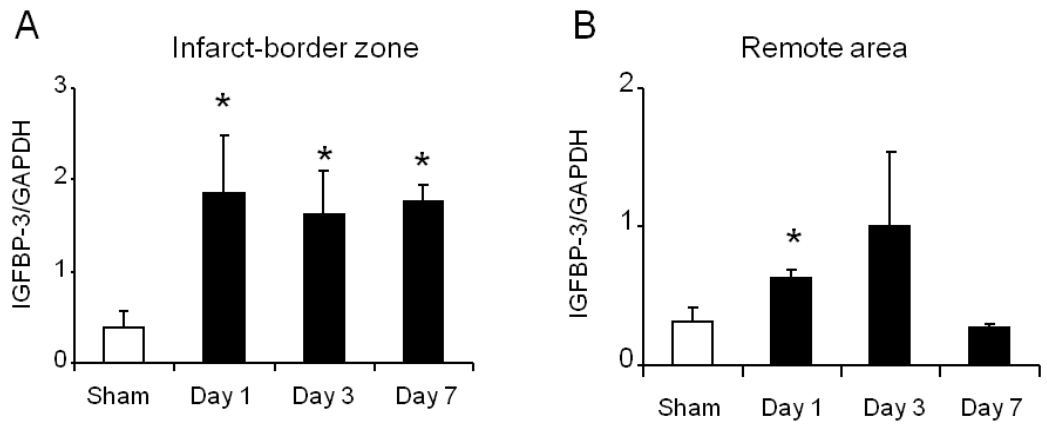

Figure 54: Measurement of IGFBP3 gene expression in post-MI myocardium (infarct/border zone and remote area) by qRT-PCR (n=3 for all). The expression of GAPDH was used for normalization. Error bars show s.e. * indicates $p<0.05$ for all samples day 1, day 3 and day 7 compared to sham.

6. Role of IGFBP4 in CSPs

- *Expression levels of IGFBP-4 in CSPs following treatment with Wnt3a-CM and BIO*

In a recent paper by Komuro *et al,* it was demonstrated that IGFBP4 promotes cardiomyogenic differentiation by blocking the Wnt signaling pathway [137]. Thus, I examined the expression and the role of IGFBP4 in CSPs following activation of the Wnt signaling

pathway. The expression levels of IGFBP-4 in CSPs were not up-regulated 1 day post-treatment with Wnt3a-CM, in comparison to vehicle-treated cells. However, IGFBP-4 mRNA levels were significantly increased 2 days and 3 days following treatment with Wnt3a-CM, by approximately 2-fold and 2.5-fold respectively, in comparison to vehicle-treated cells (Figure 55).

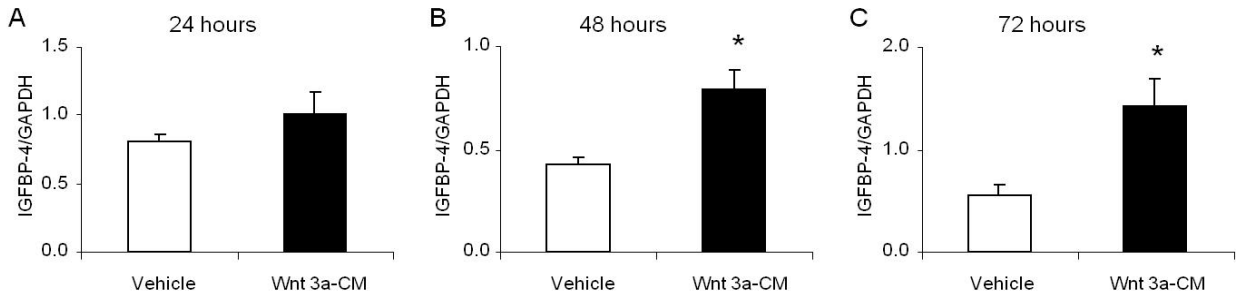

Figure 55: Measurement of IGFBP4 gene expression in post-MI myocardium (infarct/border zone and remote area) by qRT-PCR (n=3 for all). The expression of GAPDH was used for normalization. Error bars show s.e. * indicates $p<0.05$ for all samples day 1, day 3 and day 7 to sham.

BIO (GSK3β-inhibitor) mimics the effects of canonical Wnt ligands and activates the canonical Wnt signaling pathway, as described above. By using qRT-PCR we investigated the effects of BIO (2μM and 5μM) on the expression of IGFBP-4 in CSPs. As shown in Figure 56, treatment of CSPs with BIO (2μM and 5μM) increased significantly the expression of IGFBP4 by approximately 30-40%.

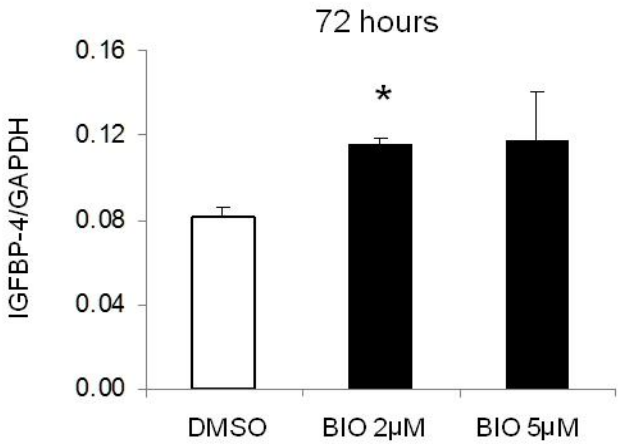

Figure 56: Measurement of IGFBP4 gene expression in CSPs following treatment with BIO (2μM and 5μM) for 72 hours, by quantitative RT-PCR (n=3 for all). The expression of GAPDH was used for normalization. Error bars show s.e. * indicates $p<0.05$ for all samples vs vehicle.

- *Expression levels of IGFBP-4 in post-MI myocardium*

In parallel, I measured the expression levels of IGFBP-4 in post-MI myocardium (infarct-border zone and remote area) at 1, 3 and 7 days post-injury. In the infarct-border zone, the expression of IGFBP-4 was not altered at 1 and 3 days post-MI but it was significantly elevated at 7 days post-MI, by approximately 4-fold (Figure 57A), in comparison to sham operated animals. In the remote area the expression levels of IGFBP-4 were transiently elevated at day 1 and day 3, without reaching statistical significance and at day 7 the levels of IGFBP-4 were restored back to baseline (Figure 57B).

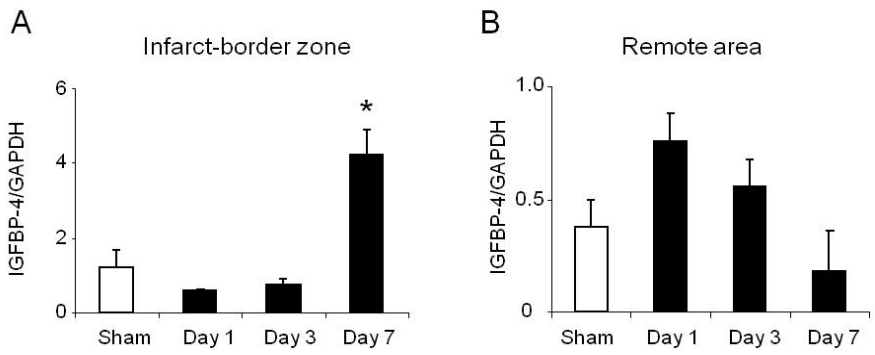

Figure 57: Measurement of IGFBP4 gene expression in post-MI myocardium in A) infarct/border zone and B) remote area by qRT-PCR (n=3 for all). The expression of GAPDH was used for normalization. Error bars show s.e. * indicates $p<0.05$ for all samples day 1, day 3 and day 7 to sham.

- *Over-expression of IGFBP-4 decreases the proliferation capacity of CSPs*

In order to study the effects of IGFBP-4 on the proliferation of CSPs I constructed a lentivirus (backbone LSLV-88 was kindly provided by Dr. Karen Westerman from Brigham and Women's Hospital) that expresses mouse IGFBP-4 under the constitutively active promoter Ef1α. CSPs over-expressing IGFBP-4 exhibited decreased proliferation capacity when compared to mock infected CSPs (Figure 58).

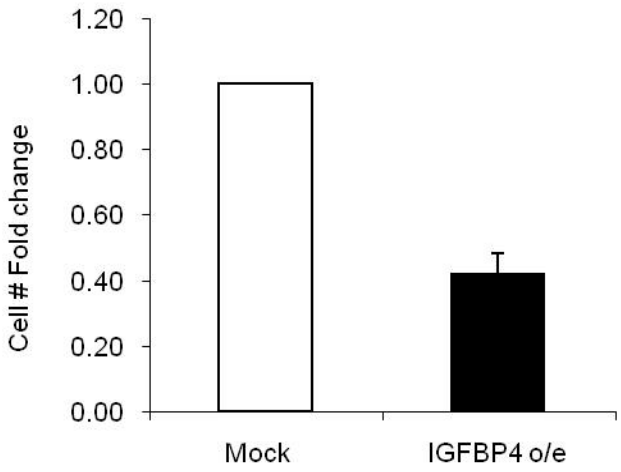

Figure 58: Effects of lentivirus mediated over-expression of IGFBP4 on the proliferation of CSPs. The diagram presents cell number fold change of mock and IGFBP4 expressing CSPs cultured for 5 days (n=2). Error bars show s.e.

- *Effects of IGFBP-4 and IGFBP3 on activation of canonical Wnt signaling*

Next, I investigated the role of IGFBP4 as well as IGFBP3 as modulators (activators or repressors) of the Wnt activity. I utilized a HEK293 cell line stably-infected with a TCF-lentivirus reporter (HEK293-Tcf-Luc cells) in order to monitor the activation status of the Wnt signaling pathway. HEK293-Tcf-Luc cells were treated with either recombinant IGFBP3 or IGFBP4 protein, in the presence of either 25% vehicle-CM or Wnt3a-CM. As expected treatment of HEK293 cells with Wnt3a-CM increased significantly the TCF activity as measured by the TCF-luciferase reporter (Figure 59) compared to vehicle treated HEK293-Tcf-Luc cells. Supplementation of the culture medium with 500ng/ml or 1 μg/ml of human recombinant IGFBP3 (h-r-BP3) or IGFBP-4 (h-r-BP4) did not alter the baseline activity of the TCF-luciferase reporter (Figure 59) in the presence of vehicle-CM. Similarly, none of the above doses of h-r-

BP3 and h-r-BP4 blocked or decreased the activation of the TCF-luciferase reporter in the presence of Wnt3a-CM (Figure 59).

In order to avoid any competition between the Wnt3a ligands and the h-r-BP3 or h-r-BP4 we pre-treated the HEK293-Tcf-Luc cells with the indicated doses of h-r-BP3 and h-r-BP4 for a period of 24 hours. At this time point HEK293-Tcf-Luc cells were treated for additional 24 hours with vehicle-CM or Wnt3a-CM containing 500ng/ml or 1 μg/ml of (h-r-BP3) or (h-r-BP4). As presented in Figure 60, pretreatment of HEK293-Tcf-Luc cells with either IGFBP did not prevent or attenuate the activation of the TCF-luciferase reporter system.

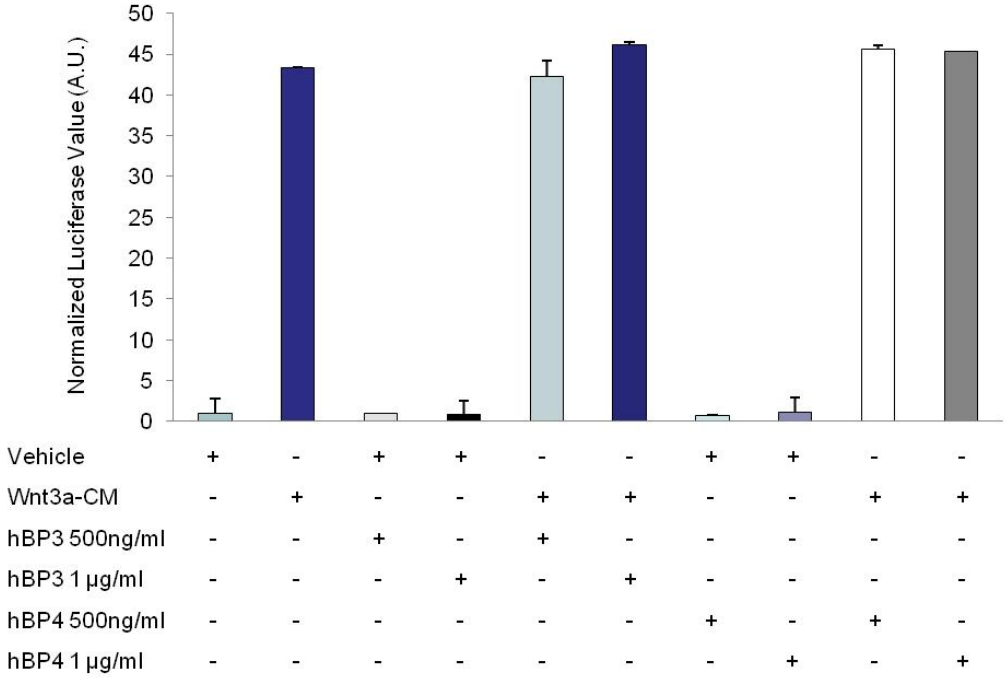

Figure 59: Effects of IGFBP4 and IGFBP-3 in the activation status of canonical Wnt signaling. Luciferase assay (TCF-activity) of HEK293 cells following treatment (24 hours) with human r-IGFBP3 (hBP3) and rIGFBP4 (hBP4) (500ng/ml or 1μg/ml) in the presence of Wnt3a-CM (25%) or vehicle medium. HEK293 cells were not pre-treated with hBP3 or hBP4. Error bars show s.e.

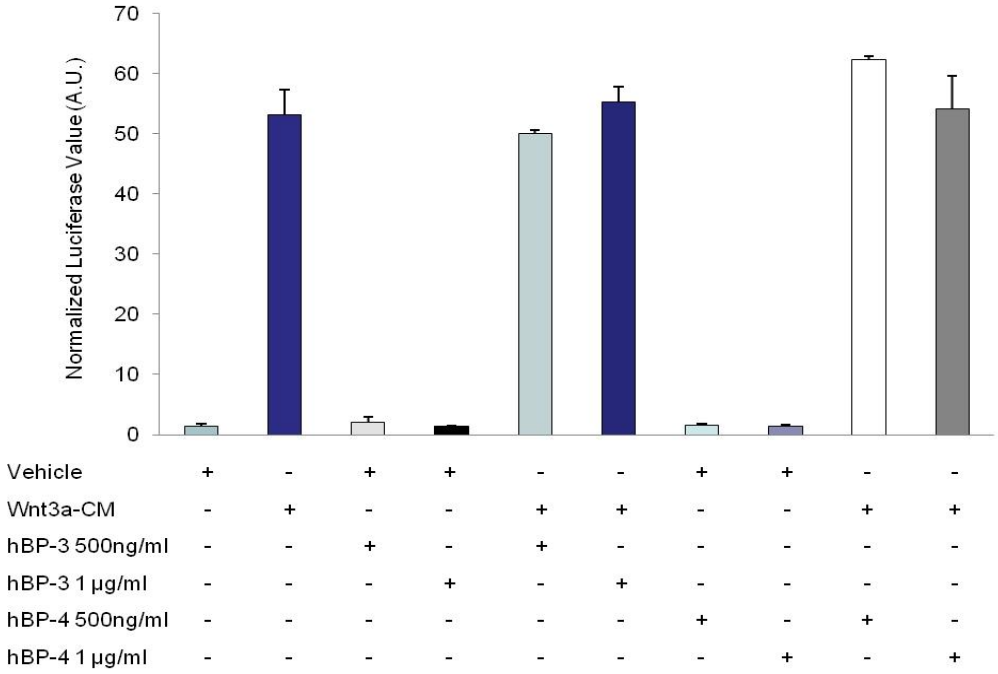

Figure 60: Effects of IGFBP4 and IGFBP-3 on the activation status of canonical Wnt signaling. Luciferase assay (TCF-activity) of HEK293 cells following treatment (48 hours) with human r-IGFBP3 (hBP3) and rIGFBP4 (hBP4) (500ng/ml or 1µg/ml) in the presence of Wnt3a-CM (25%) or vehicle medium. HEK293 cells were pre-treated with hBP3 or hBP4 for 24 hours and subsequently they were stimulated for another 24 hours with Wnt3a-CM or vehicle medium containing hBP3 or hBP4 respectively. Error bars show s.e.

- *Effects of IGFBP-4 on the cardiomyogenic differentiation of CSPs*

Finally, I sought to examine the role of IGFBP-4 on the cardiomyogenic differentiation of CSPs. By utilizing our well established co-culture system, I seeded 10000 GFP^{+}CSPs on top of a layer of neonatal rat ventricular cardiomyocytes (NRVM). CSPs were treated with 800 ng/ml of either mouse or human origin recombinant IGFBP-4 protein for a period of 3 days. The cardiomyogenic differentiation of co-cultured CSPs was evaluated through immunostaining for

the presence of α-sarcomeric-actinin, a marker of mature cardiomyocytes (Figure 61). Blind scoring of co-cultures treated with mouse (1.78%) and human (2.10%) originated IGFBP3 changed significantly the amount of GFP^+ α-sarcomeric-$actinin^+$ CSPs, compared to vehicle (2.10%). Representative examples of differentiated (GFP+ a-sarcomeric-actinin+) CSPs, in low and high magnification, from each experimental condition are presented in Figure 61.

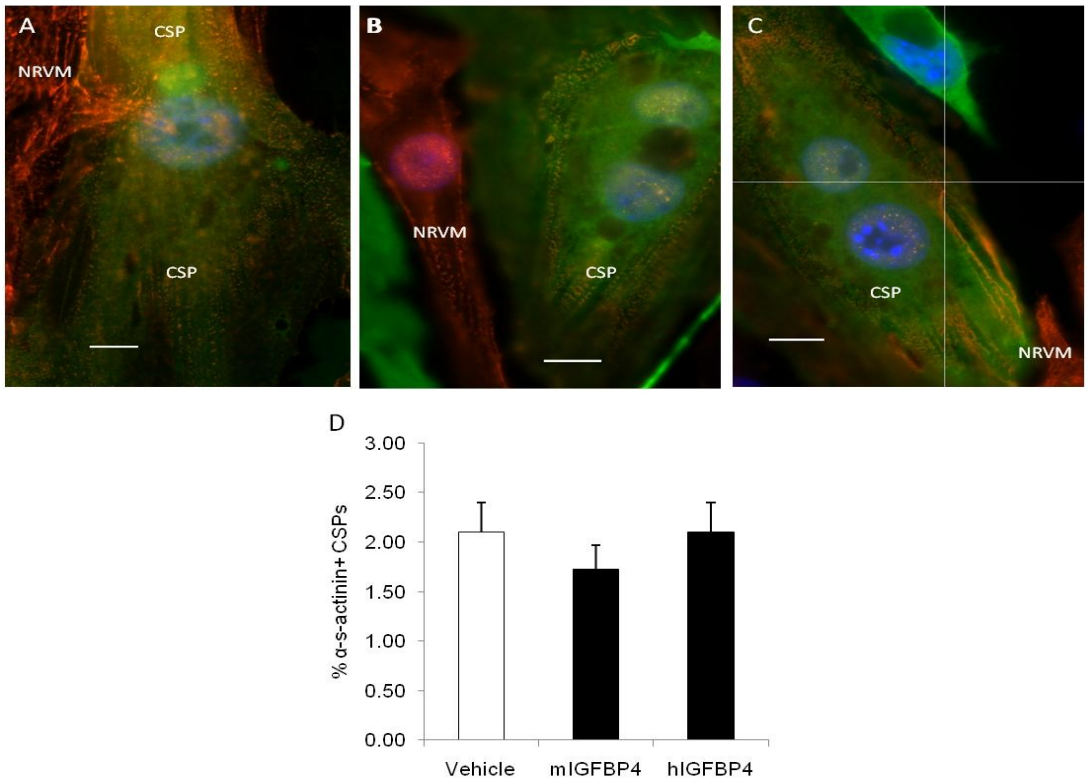

Figure 61: Effects of IGFBP4 on cardiomyogenic differentiation of CSPs. (A-E) Representative images of vehicle (PBS) treated CSPs (A), mouse derived IGFBP4 (mIGFBP4) (B) and human derived IGFBP4 (hIGFBP4) (C) treated CSPs, in co-culture with NRVM. GFP expression (green) identifies CSPs, α-sarcomeric-actinin (red) shows NRVM and differentiated CSPs. Nuclei are stained with DAPI (blue). The diagram presents the quantification of CSP cell differentiation. Error bars show s.e.

following direct intra-myocardial administration of purified recombinant-Wnt3a ligand (r-Wnt3a) were investigated. Thus, in the absence of ischemic injury, 400 ng of r-Wnt3a or vehicle (PBS) were injected in the cardiac free-wall (left ventricle) of female mice, according to the experimental plan shown in Figure 62.

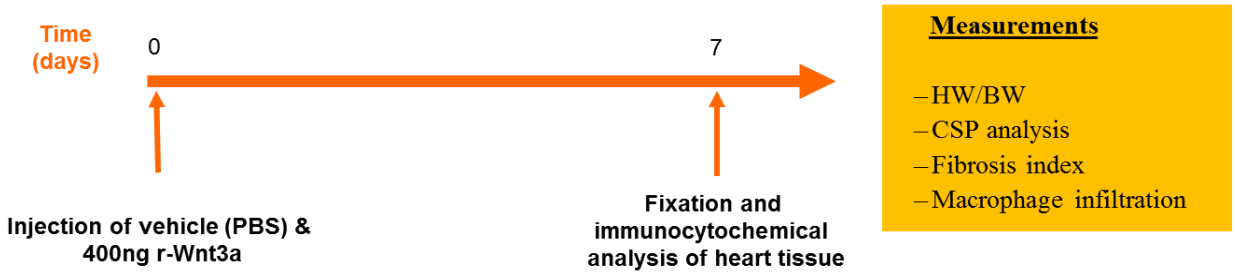

Figure 62: Schematic illustration of the experimental plan for the injection of r-Wnt3a in mouse myocardium in the absence of ischemic injury.

In the hearts that received r-Wnt3a, a "hematoma-like" area was detected in the free-wall (injection site), compared to the vehicle-injected hearts (Figure 63).

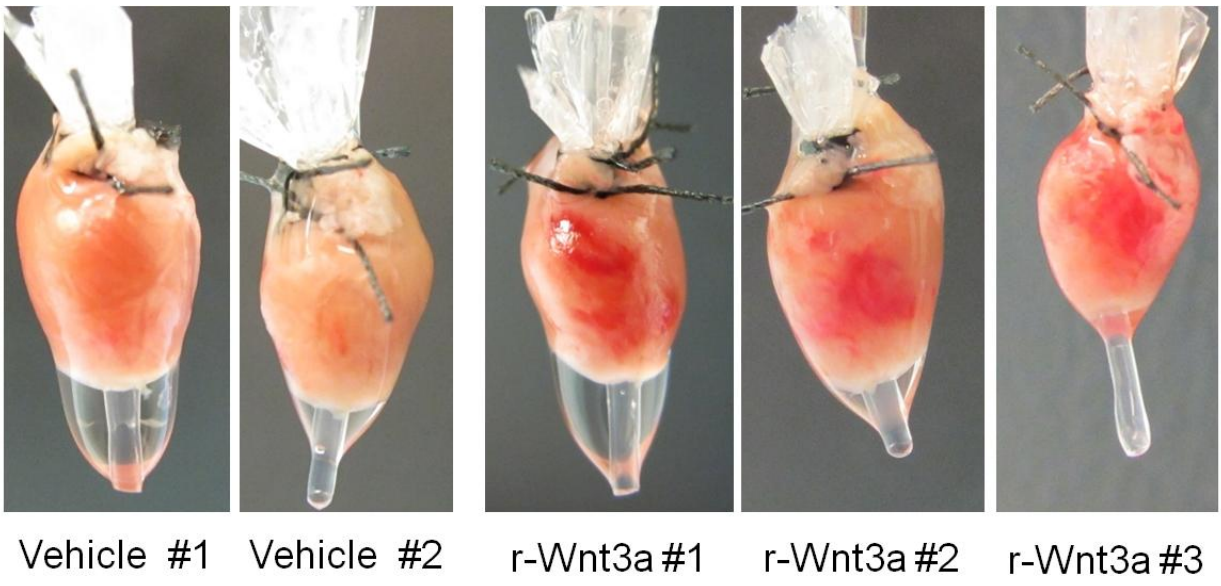

Figure 63: Injection of r-Wnt3a protein generated "hematoma-like" areas (shown in red in the above pictures. Vehicle injected hearts showed only mild demonstrations of these hematomas. Pictures were taken during fixation of the hearts using a perfusion system.

Moreover, administration of r-Wnt3a increased significantly the free-wall weight to body weight ratio (FWW/BW) as well as the total heart weight to body weight ratio (HW/BW) by approximately 11% and 17% respectively (Figure 64A-B). The heart weight to body weight ratio remained unchanged in the areas that were not injected with r-Wnt3a (atria, septum and right ventricle) between the experimental treatments (Figure 64C). Histological examination revealed no difference in the level of macrophage infiltration the vehicle and r-Wnt3a protein injected hearts (Figure 65). Moreover, picrosirius red staining revealed increased levels of collagen deposition in the r-Wtnt3a injected hearts, in comparison to vehicle injected hearts (Figure 66).

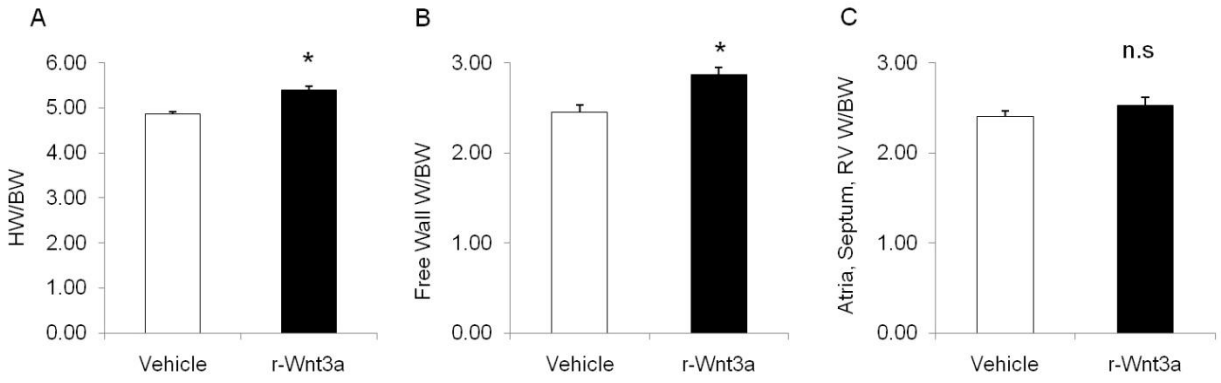

Figure 64: Heart weight to body weight ratios following injection of r-Wnt3a protein (n=8) or vehicle (PBS) (N=11). (A) Total heart weight to body weight ratio, (B) Free wall (injection site) weight to body weight ratio and (C) atria, RV and septum weight to body weight ratio. Error bars show s.e. * indicates $p<0.05$ for r-Wnt3a vs vehicle.

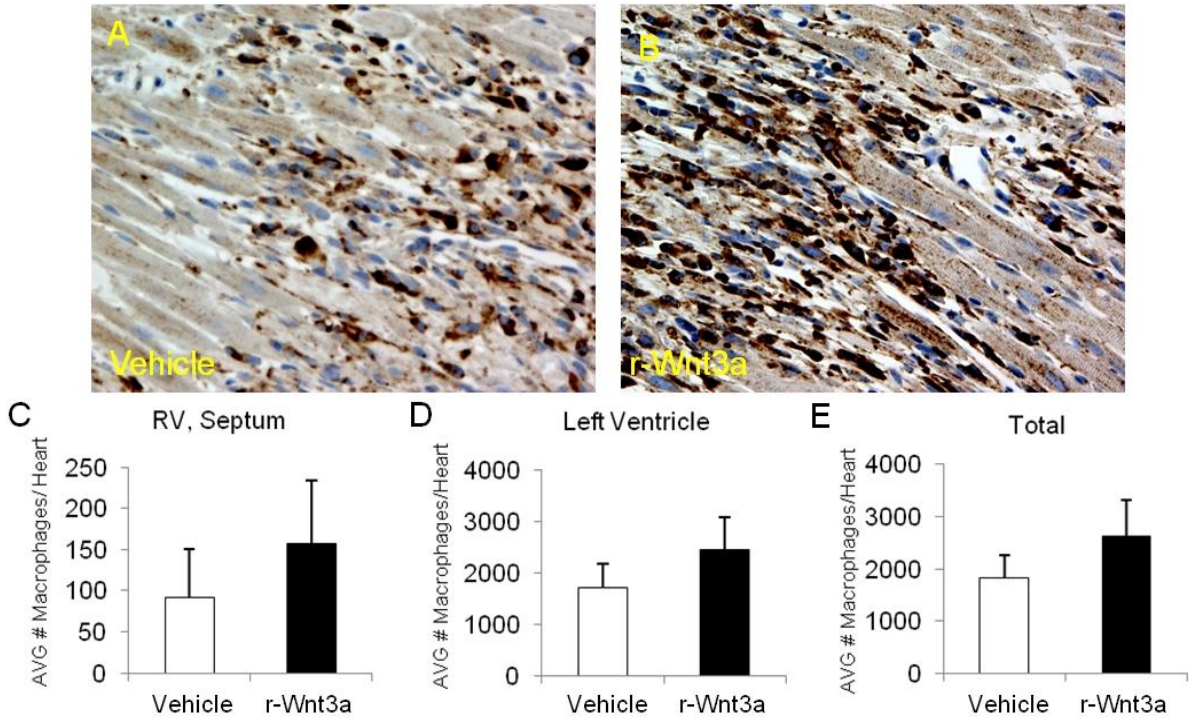

Figure 65: Estimation of macrophage infiltration in vehicle (A) and r-Wnt3a (B) injected hearts. Quantification of macrophage cells in the RV and the septum (C), the left ventricle (D) and in the whole heart (E) of vehicle and r-Wnt3a treated hearts (n=3 for vehicle and r-Wnt3a). Error bars show s.e.

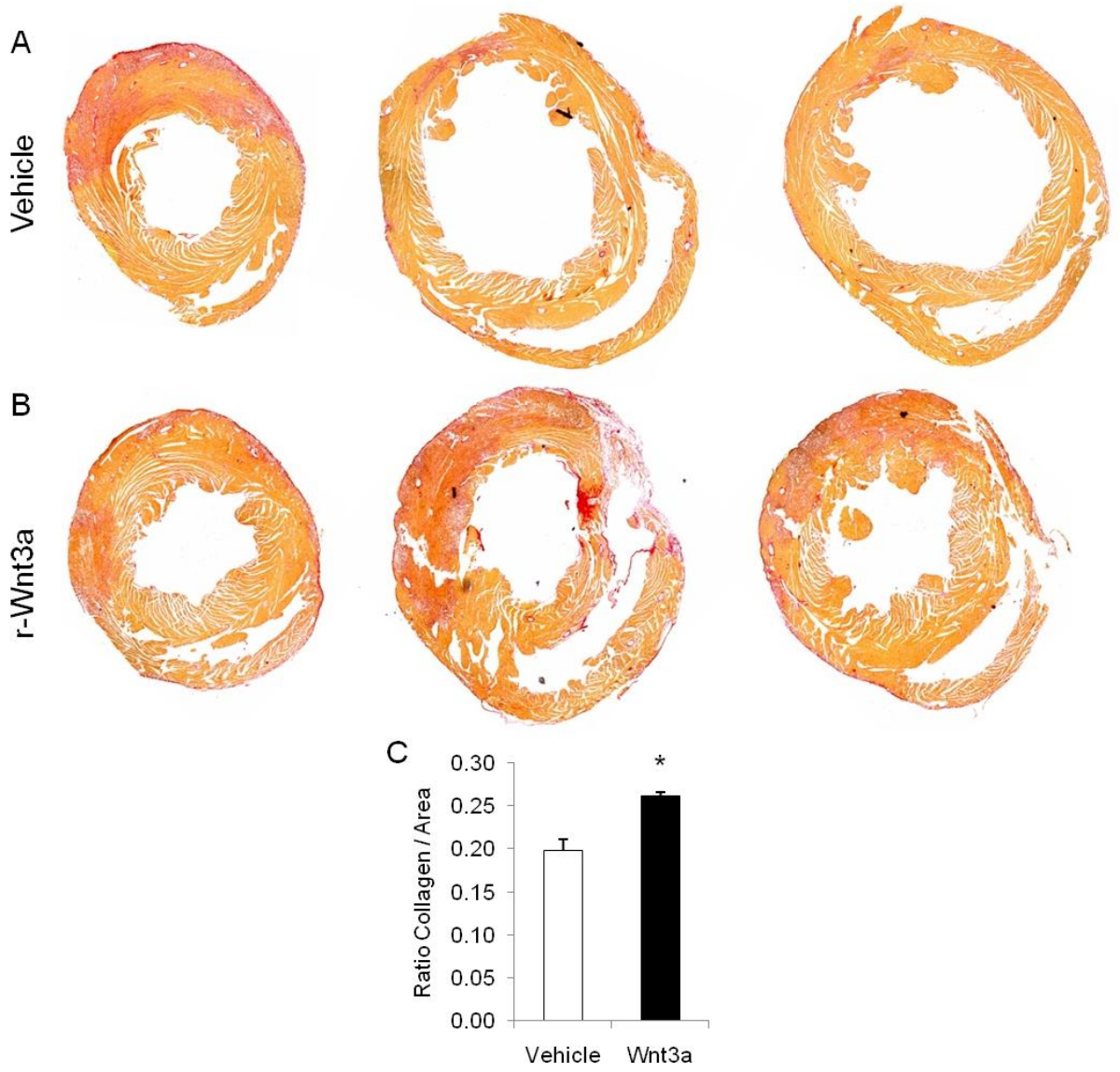

Figure 66: Evaluation of collagen deposition in vehicle (A) and r-Wnt3a (B) injected hearts. Quantification of collagen deposition in the whole heart (C) (n=4 for vehicle and n=3 for r-Wnt3a). Error bars show s.e. * indicates $p<0.05$ for r-Wnt3a vs vehicle.

Prior to staining with Hoechst dye the total number of cardiomyocyte-depleted mononuclear cells was determined in both areas of each heart. Treatment with r-Wnt3a increased the absolute number of the mononuclear cells only in the injected areas, by approximately 2-fold, in comparison to vehicle treated hearts (3 million cells versus 1.49 million

cells respectively) (Figure 67A). The number of mononuclear cells remained unaffected in the non injected areas of both Wnt3a and vehicle-injected animals (1.04 million cells versus 0.93 million cells respectively) (Figure 67B).

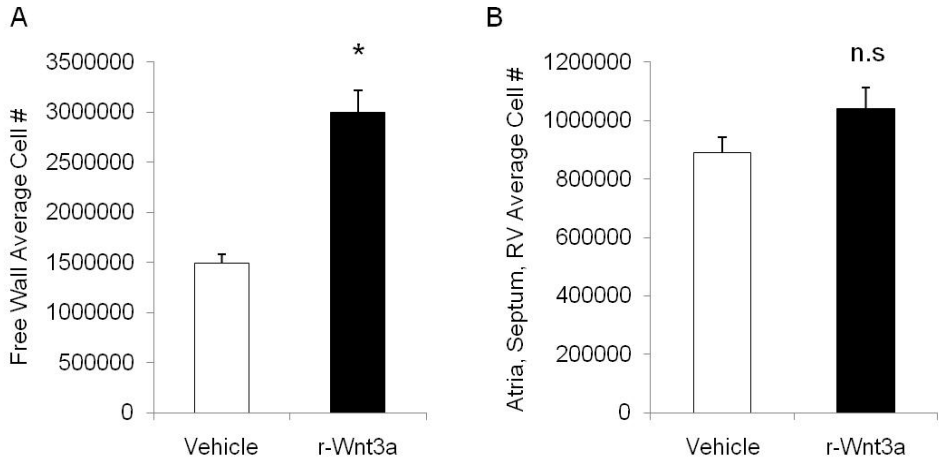

Figure 67: Quantification of total mononuclear cells in the injection site (free wall) (A) (vehicle n=8, r-Wmt3a n=11) and (B) the non-injected area (atria, RV, septum) (vehicle n=8, r-Wmt3a n=11). Error bars show s.e. * indicates $p<0.05$ for r-Wnt3a vs vehicle.

The percentage and the absolute number of CSPs were decreased in r-Wnt3a injected areas and not in non-injected areas. We determined the proportion of CSPs in the injection site (free wall) as well as in the non-injected sites (atria, septum and right ventricle). Administration of r-Wnt3a decreases significantly the percentage of CSPs only in the injected areas (free wall) and not in the non-injected areas (atria, septum, and right ventricle). The fraction of CSPs in the r-Wnt3a injection sites dropped significantly by 2.75-fold in comparison to the vehicle-treated hearts (0.65% versus 1.80% respectively) (Figure 68A). However, the percentage of CSPs remained unchanged (mild decrease) in the non-injected areas of r-Wnt3a and vehicle treated animals (0.90% versus 1.09% respectively) (Figure 68B). Representative examples of CSP cell

analysis from the injected and the non injected areas of r-Wtn3a and vehicle treated hearts are shown in figure 69.

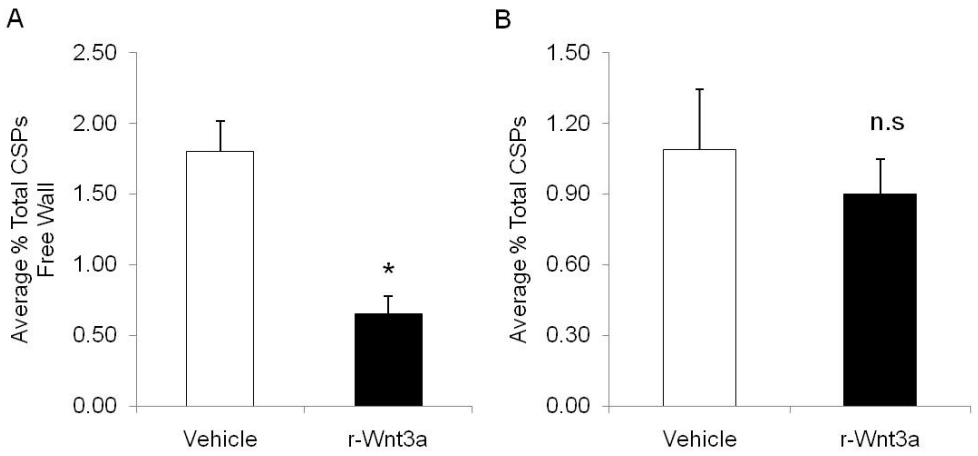

Figure 68: *In vivo* effects of r-Wnt3a in the amount of total CSPs. (A) Injection of r-Wnt3a (n=11) in the free wall decreased the amount of total CSPs compared to injection of vehicle (n=8). (B) In the non-injected area of Wnt3a-treated animals (n=11) the amount of total CSPs remained unchanged, in comparison to vehicle treated animals (n=8). Error bars show s.e. * indicates $p<0.05$ for r-Wnt3a vs vehicle.

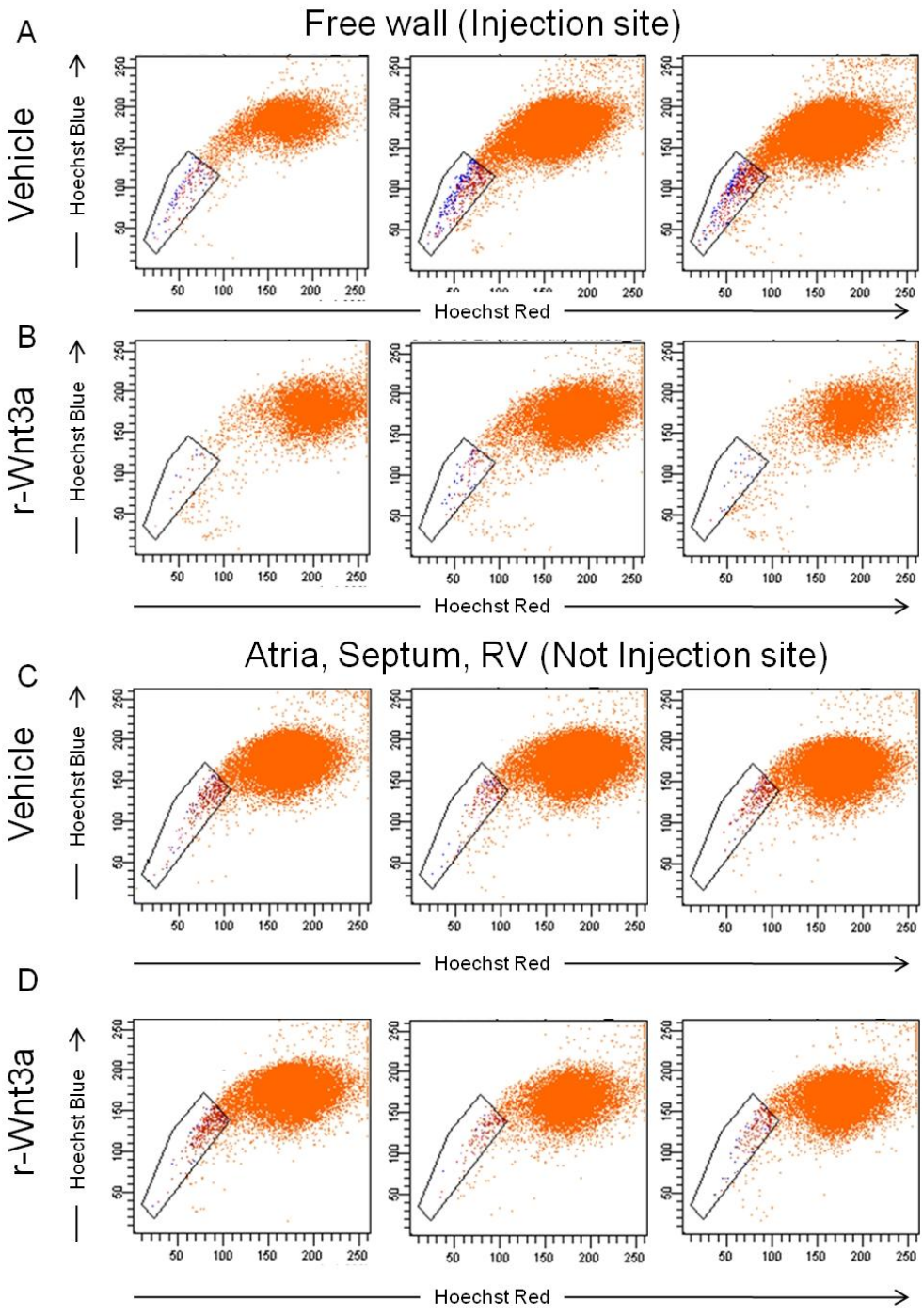

Figure 69: Representative examples of CSPs isolated from the (A) free wall of vehicle injected hearts, (B) the free wall of r-Wnt3a hearts, (C) atria, septum and RV of vehicle injected hearts and (D) the atria, septum, RV of the r-Wnt3a injected hearts.

wa

cells respectively) (Figure 70A). In contrast, the average absolute number of sorted cells in the non-injected areas remained unchanged in both r-Wnt3a and vehicle treated animals (3158 cells versus 2922 cells respectively) (Figure 70B).

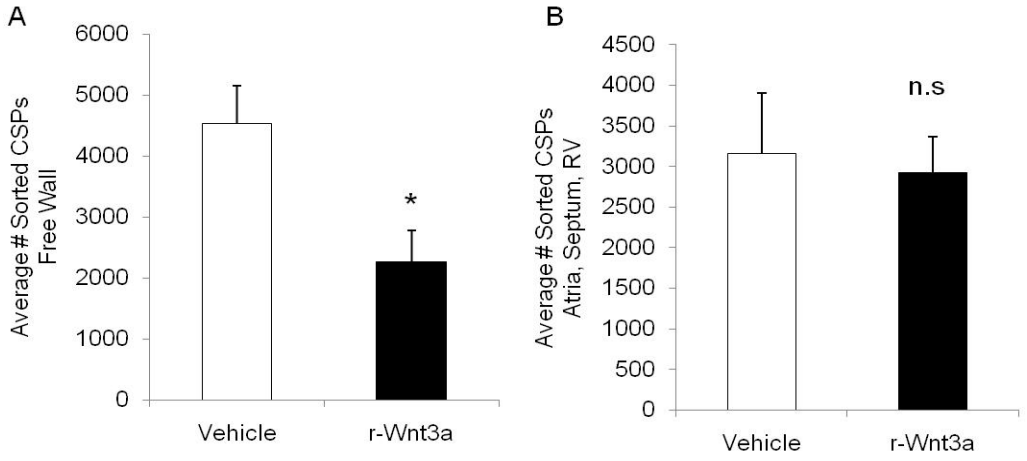

Figure 70: Quantification of total sorted CSPs cells in the injection site (free wall) (A) (vehicle n=8, r-Wmt3a n=11) and (B) the non-injected area (atria, RV, septum) (vehicle n=8, r-Wmt3a n=11). Error bars show s.e. * indicates $p<0.05$ for r-Wnt3a to vehicle.

Sorted CSPs from the injection areas (free wall) and from the non injection sites (atria, septum and right ventricle) were analyzed for the expression of the proliferation marker Ki67. No differences were observed in the proportion of $Ki67^+$ CSPs in the free wall of r-Wnt3a and of vehicle treated hearts (1.74% versus 1.41% respectively). Similarly, there was no difference in the percentage of $Ki67^+$ CSPs isolated from the non injected areas of r-Wnt3a and vehicle treated animals (5.4% versus 5.2% respectively). Correspondingly, the amount of total (isolated from the injected and the non injected areas) $Ki67^+$ CSPs was similar between the r-Wnt3a and vehicle treated hearts (2.86% versus 3.05% respectively) (Figure 71).

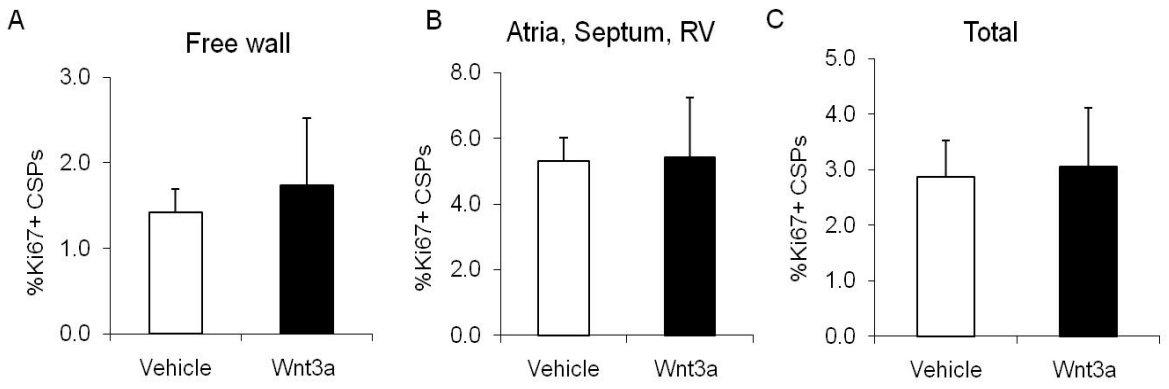

Figure 71: Quantification of $Ki67^+$ CSPs isolated from (A) the injection site (free wall) (vehicle n=8, r-Wmt3a n=11) and (B) the non-injected area (atria, RV, septum) (vehicle n=8, r-Wmt3a n=11). (C) Total $Ki67^+$ CSPs from both areas. Error bars show s.e. * indicates $p<0.05$ for r-Wnt3a vs vehicle.

r-Wnt3a treatment decreased both $CD31^-/Sca\text{-}1^+$/CSPs as well as $CD31^+/Sca\text{-}1^+$/CSPs. The fraction of the $CD31^-/Sca\text{-}1^+$/CSPs in the r-Wnt3a injected site was significantly lower (2.54-fold), in comparison to the vehicle-injected hearts (0.54% versus 1.37% respectively) (Figure 72A). Similarly, the percentage of the $CD31^+/Sca\text{-}1^+$/CSPs in the r-Wnt3a injected site was significantly lower (2.78-fold), in comparison to the vehicle-injected hearts (0.82% versus 2.28% respectively) (Figure 73A). The percentages of both the above populations of CSPs remained unaffected in the non-injected areas of r-Wnt3a and vehicle treated animals ($CD31^-/Sca\text{-}1^+$/CSPs: 0.28% versus 0.40% respectively) ($CD31^+/Sca\text{-}1^+$/CSPs: 1.08% versus 1.08% respectively) (Figures 72B and 73B).

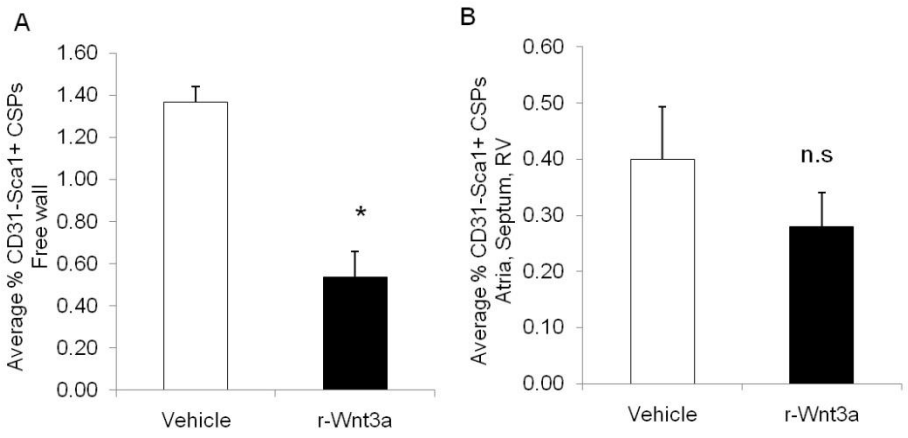

Figure 72: Quantification of $CD31^{-}Sca1^{+}$ CSPs isolated from (A) the injection site (free wall) and (B) the non-injected area (atria, RV, septum) (vehicle n=8, r-Wmt3a n=11). Error bars show s.e. * indicates $p<0.05$ for r-Wnt3a vs vehicle.

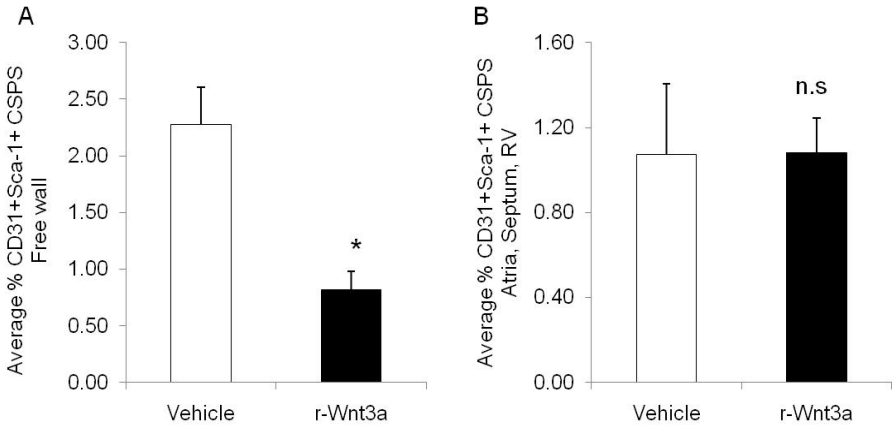

Figure 73: Quantification of $CD31^{+}Sca1^{+}$ CSPs isolated from (A) the injection site (free wall) and (B) the non-injected area (atria, RV, septum) (vehicle n=8, r-Wmt3a n=11). Error bars show s.e. * indicates $p<0.05$ for r-Wnt3a to vehicle.

Finally, the distribution of $CD31^+$ and $Sca\text{-}1^+$ cells, within each population of CSPs isolated from the vehicle or r-Wnt3a injected heart, remained unchanged. Namely, the amount of $CD31^-Sca\text{-}1^+$, $CD31^+Sca\text{-}1^+$, $CD31^+Sca1^-$ and $CD31^-Sca1^-$ cells of CSPs remained unchanged at approximately 18%, 69%, 1% and 22% respectively in the injected areas of the heart. Likewise, there was no difference in the amount of the same sub-populations within each population of CPSs isolated from the non injected areas of the r-Wnt3a and vehicle treated hearts. Specifically, the amount of $CD31^-Sca\text{-}1^+$, $CD31^+Sca\text{-}1^+$, $CD31^+Sca1^-$ and $CD31^-Sca1^-$ cells of CSPs remained unchanged at approximately 9%, 81%, 3% and 7% respectively in the non-injected areas of the heart.

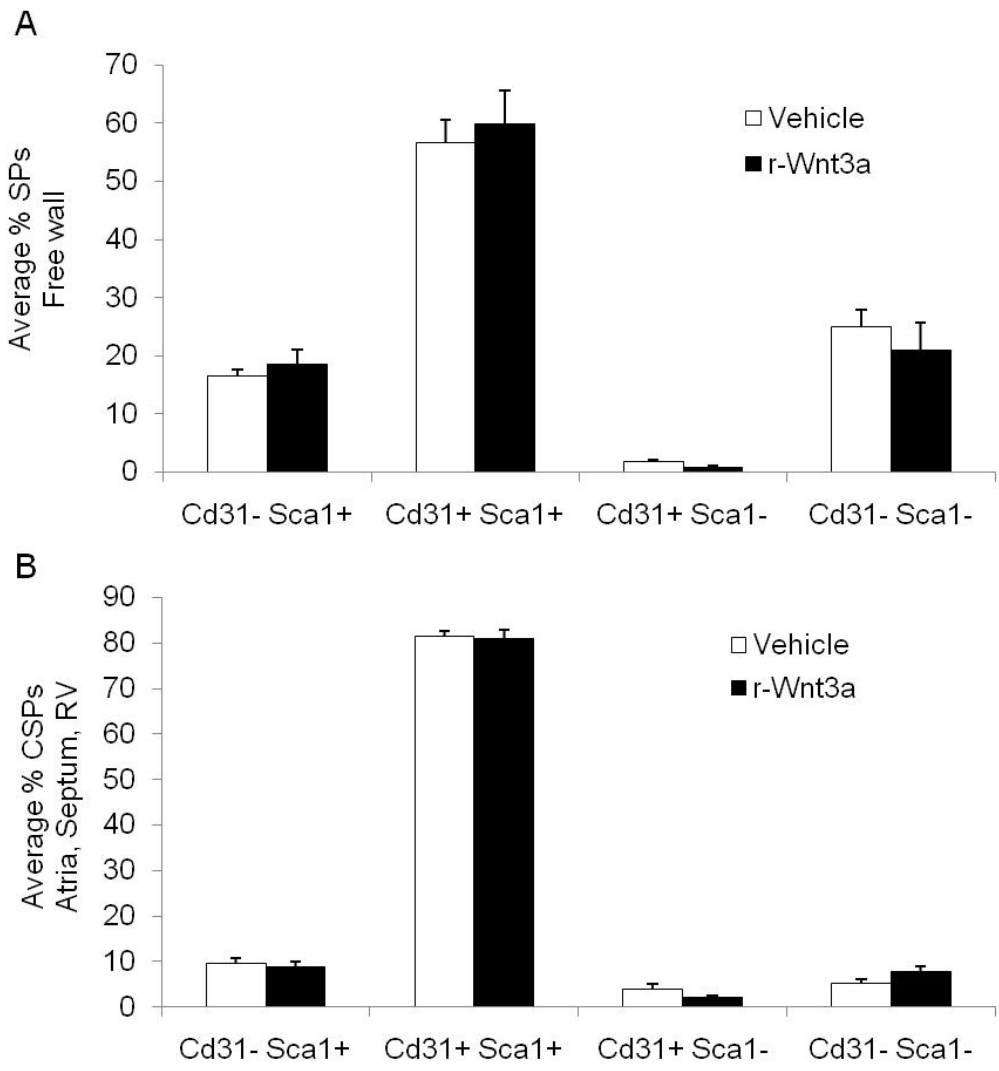

Figure 74: Effects of r-Wnt3a injection on the distribution of the sub-populations of CSPs isolated from (A) the injection site (free wall) and (B) the non-injected site (Atria, Septum, RV). (r-Wnt3a (n=11) and vehicle (n=8)). Error bars show s.e. * indicates $p<0.05$ for r-Wnt3a vs vehicle.

- *Effects of Wnt3a protein on post-MI cardiac remodeling*

My next step was to examine the effects of canonical Wnt signaling pathway on post-MI remodeling of the cardiac tissue. Thus, r-Wnt3a protein (400ng/ animal) was injected directly in the free wall of the myocardium, immediately after permanent occlusion of the left ascending coronary artery, according to the experimental plan showed in Figure 75.

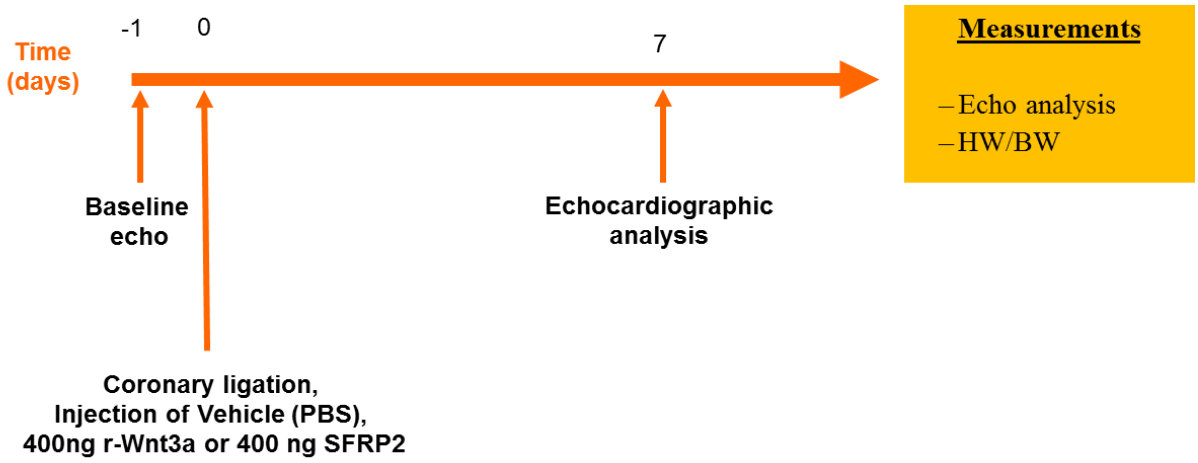

Figure 75: Schematic illustration of the experimental plan for the injection of r-Wnt3a or SFRP2 following myocardial infarction.

Administration of r-Wnt3a protein increased significantly (1.24-fold) the ratio of the heart weigh to the body weight, in comparison to vehicle (PBS) injected hearts (Figure 76A). Similar results were obtained when the ratio of heart weight to tibia length was examined as shown in Figure 76B.

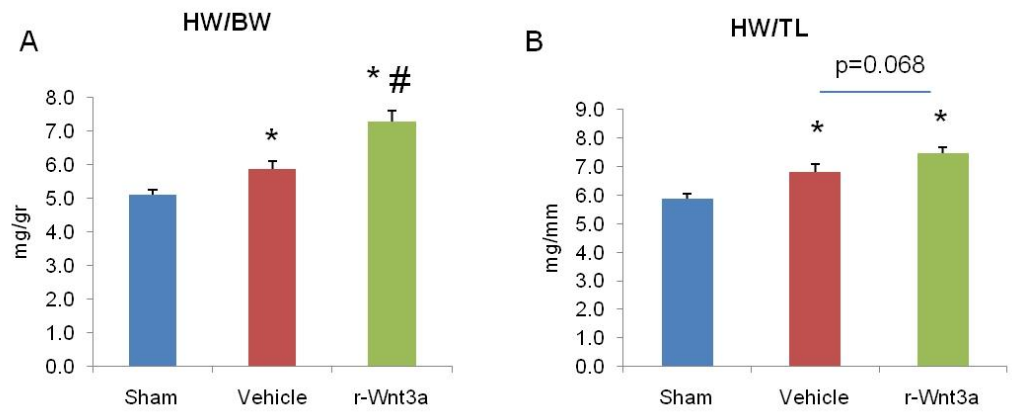

Figure 76: Morphometric measurements of mouse hearts injected with r-Wnt3a (n=10) or vehicle (n=9) following MI and from sham mice (n=7). Error bars show s.e. * indicates $p<0.05$ for vehicle and r-Wnt3a vs sham, # indicates $p<0.05$ for vehicle vs r-Wnt3a.

Echocardiographic analysis at 1 week post-MI revealed that the cardiac performance following injection of r-Wnt3a, was deteriorated. Administration of r-Wnt3a decreased significantly the thickness of the intra-ventricular septum, measured in both systole and diastole (IVS;s and IVS;d respectively), compared to vehicle injected hearts (Figure 77A and D). Furthermore, injection of r-Wnt3a increased significantly the left ventricular intra-ventricular dimension measured in systole (LVID;s) as well in diastole (LVID;d), compared to vehicle injected hearts (Figure 77B and E). Moreover, administration of r-Wnt3a increased the thickness of the left ventricular posterior wall when measured only in systole (LVPW;s), compared to vehicle injected hearts (Figure 77C and F). Moreover, injection of r-Wnt3a decreased significantly the fractional area change (FAC) in comparison to vehicle injected hearts (Figure 77G). Consequently, both the indexes of ejection fraction (%EF) as well as of fractional shortening (FS) were significantly diminished in r-Wnt3a treated animals, compared to vehicle

treated mice (Figure 77H and I). Overall, the above data strongly suggest that supplementation of Wnt3a ligand following MI deteriorates the cardiac performance by causing ventricular wall thinning and chamber dilatation.

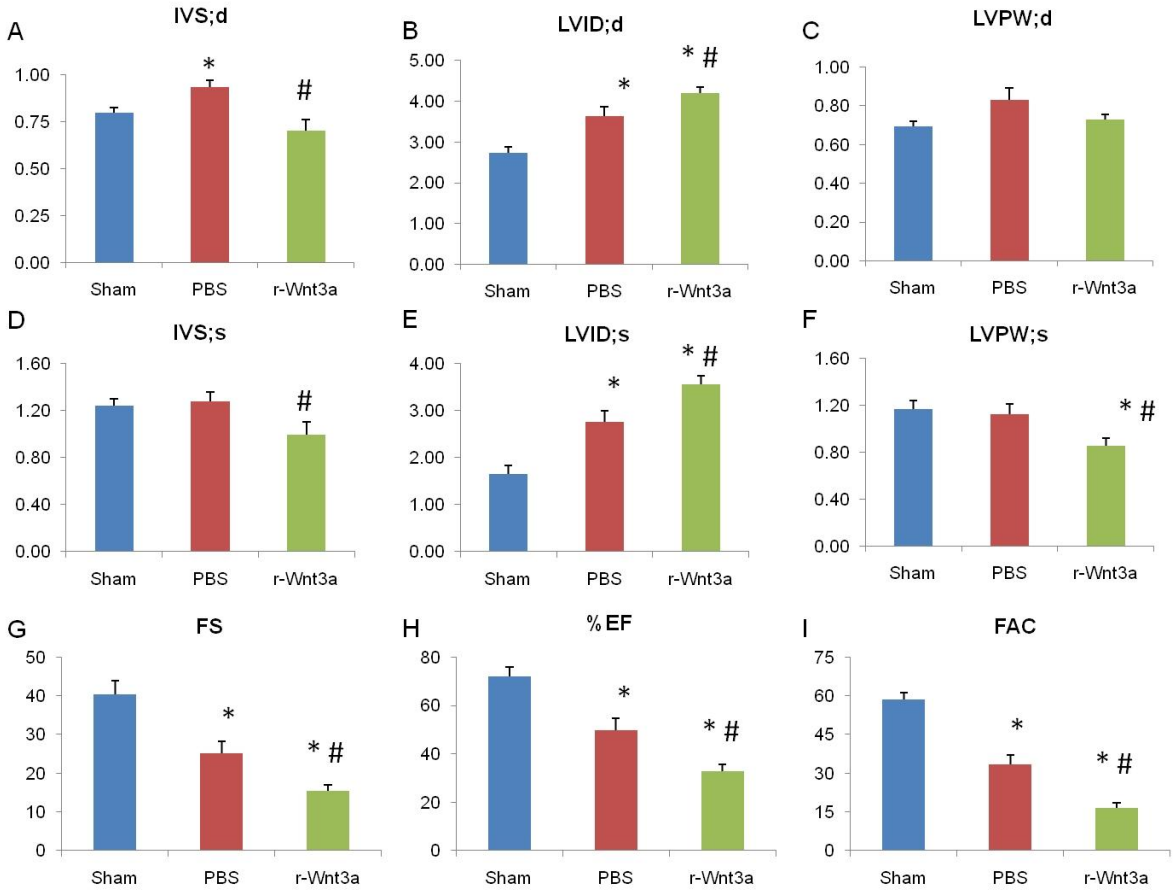

Figure 77: Echocardiographic analysis of r-Wnt3a-injected (n=10) and vehicle-injected (n=9) hearts post-MI compared to sham-operated hearts (n=7). Error bars show s.e. * indicates $p<0.05$ for MI vehicle and r-Wnt3a vs shams, # indicates $p<0.05$ for PBS vs r-Wnt3a.

- *Effects of SFRP-2 protein on post-MI cardiac remodeling*

In parallel with the above study, I also tested the effects of SFRP-2, a known Wnt inhibitor, in cardiac remodeling following cardiac infarction. Therefore, SFRP-2 protein (400ng/ animal) was injected directly in the free wall of the cardiac muscle immediately after permanent occlusion of the left ascending coronary artery as shown in Figure 75. Administration of SFRP-2 did not alter the ratio of heart weight to body weight nor of heart weight to tibia length (Figure 78A and B respectively).

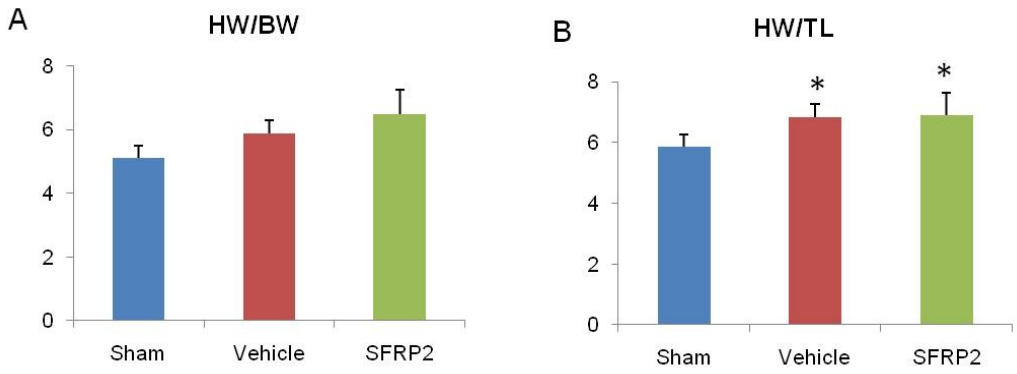

Figure 78: Morphometric measurements from mice injected with SFRP2 (n=7) or vehicle (n=9) following MI and from sham mice (n=7). Error bars show s.e. * indicates $p<0.05$ for vehicle and SFRP2 vs sham.

Moreover, SFRP-2 did not change any other functional parameter of the hearts as measured by echocardiography. Thus, the dimensions of the wall thickness (IVS;s, IVS;d, LVPW;s and LVPW;d) and the chamber dilatation (LVID;s, LVID;d) remained unchanged in SFRP-2 injected animals, compared to vehicle (PBS) treated mice (Figure 79), in either systole or diastole. Consequently, injection of SFRP-2 did not change the indexes of ejection fraction,

fractional shortening and the total fractional area change, compared to vehicle treated mice (Figure 79).

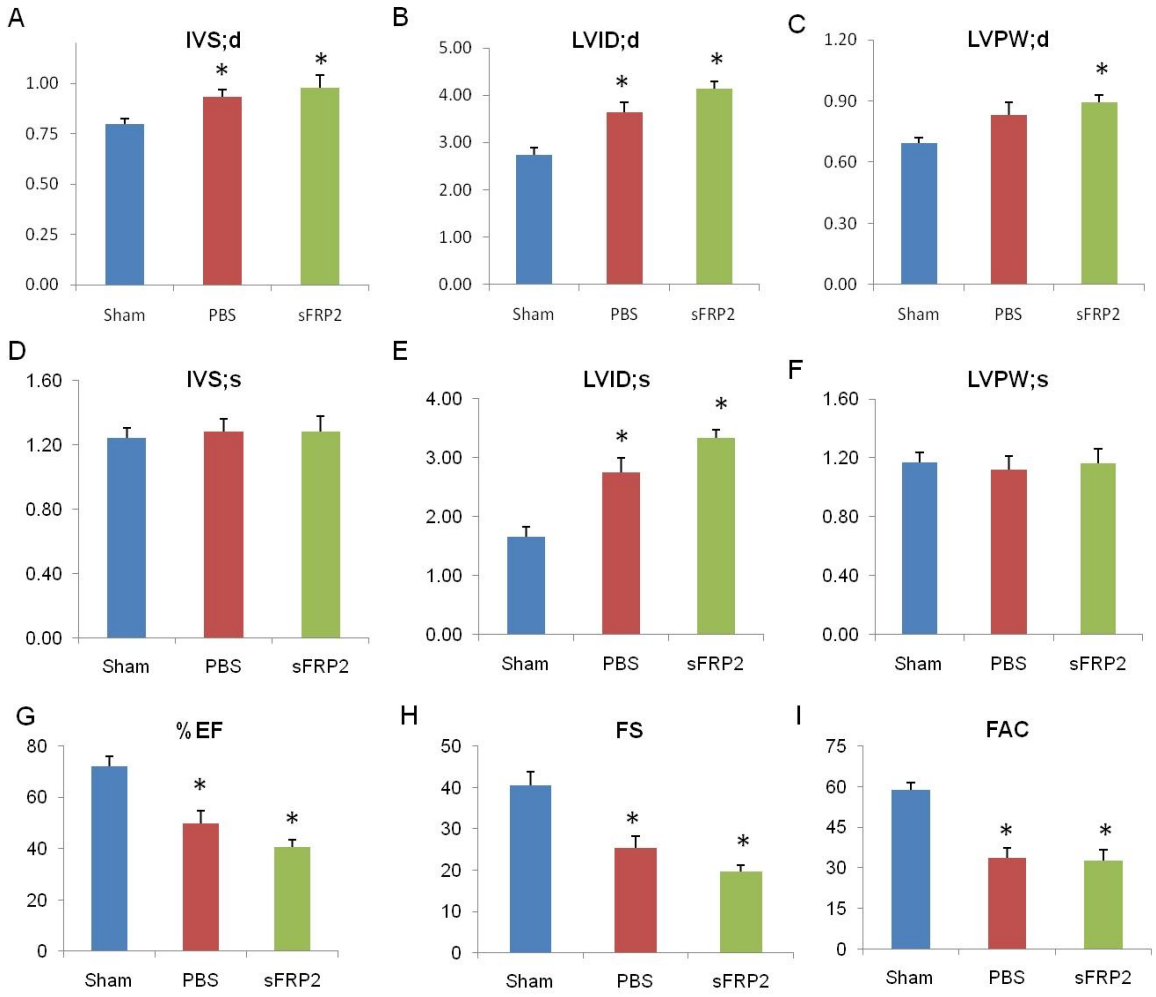

Figure 79: Echocardiographic analysis of MI operated SFRP2 injected (n=7), vehicle-injected (n=9) and sham-operated hearts (n=7). Error bars show s.e. * indicates $p<0.05$ for vehicle and SFRP2 vs sham.

6. Discussion

1. Overview

The post-natal heart is no longer viewed as a terminally differentiated organ, due to the identification of exogenous but mainly endogenous cardiac progenitor cells. Until today, utilization of different molecular markers has led to the identification of several cell populations that possess characteristics of cardiac precursors. Due to the increasing demand for alternative therapies for heart failure, a great interest has been focused on these populations. Detailed knowledge of the molecular and cellular mechanisms that control their cell fate and self-renewal is of paramount importance for the design of novel cell-based therapies against heart failure. My efforts concentrated on the examination of the canonical Wnt signaling pathway in CSPs. Currently, the role of canonical Wnt signaling pathway in the adult heart and especially in the homeostasis of cardiac stem/progenitor cells remains unknown. This work presents for the first time the effects of canonical Wnt signaling in cSPs as well as in the heart under normal and disease conditions.

2. Effects of Wnt signaling on CSPs proliferation capacity

One of the main goals of this thesis was to examine the role of canonical Wnt signaling on the proliferation of CSPs. By utilizing various methodologies I demonstrated that activation of the canonical Wnt signaling pathway leads to decreased proliferation of CSPs by altering their cell cycle profile. Manipulation of Wnt signaling pathway by either application of various

activators (Wnt3a-CM, r-Wnt3a protein, BIO and GSK3β kinase inhibitor) consistently blocked the expansion of CSPs. Moreover, application of Wnt pathway inhibitors (Dkk-1) promoted their proliferation. Dkk-1 is a well know inhibitor of the canonical Wnt signaling pathway, through promoting a clathrin-mediated internalization of the Wnt co-receptor LRP5/6 [138]. To our knowledge this is the first report revealing the effects of canonical Wnt signaling on adult populations of endogenous cardiac precursors.

The anti-proliferative effects of Wnt signaling can only be partially reversed by concurrent treatment of CSPs with Wnt3a-CM and Dkk-1-CM. Note that application of Dkk-1-CM, in the presence of Wnt3a-CM, decreases gradually but not completely the activation status of Wnt signaling pathway in CSPs. Similar results were reported in a recent study of the role of canonical Wnt signal transduction on the proliferation of malignant melanoma cells [139]. In this study, Chien *et al* demonstrated that treatment of melanoma cancer with Wnt3a protein resulted in decreased proliferation capacity. When Wnt3a-expressing melanoma B16 cells were implanted into mice they exhibited decreased tumor growth and metastasis ability. Moreover, activation of the canonical Wnt cascade resulted in up-regulation of the melanocyte differentiation gene program. Application of Dkk-1 could not rescue the decreased proliferation phenotype of melanoma cells. Overall, the above data suggest that the inability of Dkk-1 to fully rescue CSP proliferation capacity might reflect a permanent commitment of CSPs to an altered cell fate, which is consistent with the role of Wnt ligands as fate determinants [139]. My data support this hypothesis since treatment with Wtn3a-CM promoted their cardiomyogenic differentiation.

An alternative hypothesis is that Dkk-1 exerts its effects on Wnt signaling in a context dependent manner. Dkk-1 binds with high affinity to the Frizzled co-receptors LRP5/6 and thus it prevents the formation of a functional ligand-receptor complex (Wnt-Frizzled-LRP5/6). The exact molecular mechanism of Dkk-1-mediated inhibition of Wnt signaling remains unknown. In a recent paper, Hassler *et al* demonstrated that an additional protein, Kremen, binds to LRP5/6 in the absence of Dkk-1 and that it promotes the cell surface localization of LRP6 [83, 140]. In the presence of Dkk-1, Kremen proteins augment Dkk-1-mediated Wnt inhibition by promoting the endocytosis of LRP5/6. The authors proposed a model in which Kremen protein functions as a switch that regulates Wnt signaling activation through determining the cellular localization of LRP5/6. It is likely that high levels of Kremen protein expression in CSPs antagonize the inhibitory action of Dkk-1 and prevent a complete block of the Wnt pathway.

My data also indicate that in addition to CSPs, cardiac c-kit^{+} progenitors responded similarly to Wnt3a-CM treatment. Moreover, proliferation assays using neonatal CSPs treated with Wnt3a-CM and vehicle medium showed that Wnt signaling decreases their proliferation as well. In order to examine the extent and the specificity of this anti-proliferative phenotype I treated HEK293 cells with the same Wnt3a-CM and vehicle medium. In contrast to the data from CSPs and c-kit^{+} cells, activation of the Wnt signaling cascade augmented the proliferation of HEK293 cells. Thus, this anti-proliferative response to Wnt3a-CM is not media-dependent and it might represent a general reaction of adult cardiac progenitors to canonical Wnt3a ligands.

It was not until recently that several studies indicated that canonical Wnt signals control the proliferation and self-renewal of cardiac progenitors that belong primarily to the second heart field (SHF). The exact role of Wnt signal cascade in the proliferation and homeostasis of adult

cardiac progenitors is currently unknown. Several lines of evidence suggest that Wnt ligands determine not only the initial steps of cardiac formation but also the later steps of cardiac specification and maturation. Kwon *et al* demonstrated that activation of canonical Wnt signaling through genetic stabilization of β-catenin increases the size of the right ventricle (RV) in mice [141]. In addition, genetic ablation of β-catenin leads to severe hypoplasia of RV. In a series of consecutive reports it was further demonstrated that activation of the canonical Wnt signaling pathway leads to expansion of Islet-1^+ cardiac progenitor cells and that interruption of the Wnt signal cascade causes defects in the RV and the outflow track [73, 142-144]. It is noteworthy that none of these studies detected defects in the formation and maturation of the left ventricle (LV). Islet-1 represents a very well documented marker of the SHF cardiac progenitors, which are found predominantly in embryonic and neonatal hearts and in low abundance in adult myocardium [71]. Thus, the distinct response of CSPs as well as c-kit^+ cells and Islet-1^+ cells to canonical Wnt signals is most likely attributed to intrinsic differences between each examined cell population. The developmental relation between the Islet-1^+ cells and the CSPs / c-kit^+ cells remains largely unknown. Most likely Wnt signaling plays a different role during distinct developmental windows, initially acting as a growth stimulus and later on as an anti-proliferative factor. Additional studies are required to obtain more detailed knowledge about the different cellular effects of Wnt signaling on the various cardiac progenitor cells in order to fully understand the role of this developmental signaling pathway.

3. Effects of Wnt signaling on the cell cycle properties of CSPs

Subsequently, I focused on the effects of Wnt signaling pathway on the cell-cycle properties of CSPs. Utilization of well-established methodologies like BrdU incorporation assay, immunocytochemical detection of p-H3 and propidium iodide analysis revealed that activation of Wnt signal cascade causes a withdrawal of CSPs from the S and G2/M cell-cycle phases and their accumulation in the early G0/G1 cell-cycle phases. Furthermore, by combining the PI analysis with the Ki67 immunostaining, it was shown that withdrawal of CSPs from the later, more proliferative cell cycle phases (S and G2/M) is not accompanied by a permanent exit from the cell-cycle, towards the more quiescent phenotype (G0 phase).

Although all the utilized methods for the study of the cell cycle status point out to the same direction (Wnt signals delay the progression of CSPs cell-cycle), there are some differences in the actual values obtained from each assay. First of all, the amount of mitotic CSPs measured by PI staining is higher than the amount of pH-3^+ CSPs, measured by immunocytochemistry. This is due to the fact that pH-3 predominantly is a marker of mitotic cells and less of cells residing in the G2 cell cycle phase. From the other hand, PI staining labels all the cells with duplicated genetic material including those in G2-cell cycle phase as well as in the M-phase. Thus, quantification of p-$H3^+$ cells does not lead to the total amount of cells with duplicated DNA and it cannot be considered equivalent to the PI staining for G2/M cell cycle phases.

Another discrepancy is observed between the amount of CSPs residing in the S-phase when this value is calculated through BrdU incorporation experiments or PI analysis. Namely, following Wnt3a-CM treatment, the amount of CSPs which are located in the S-phase is higher

according to the PI analysis in comparison to the proportion measured by BrdU immunostaining. Technical issues in both assays are considered rather minimal and they cannot contribute substantially to the observed discrepancy. PI analysis represents a snapshot of the cell cycle profile at a specific time point. However, BrdU analysis is based on the duration of the pulsing with the nucleotide analog, and thus it is linked to the duration of the examined cell cycle. Here, CSPs were pulsed with BrdU uniformly for only 1 hour, whereas treatment with Wnt3a-CM prolonged extensively the duration of the cell cycle in CSPs, compared to vehicle treated cells. We believe that this led to underestimation of the proportion of cells that integrated BrdU following application of Wnt3a.

4. Effects of Wnt signaling on the regulation of the cell cycle of CSPs

My next step was to analyze the expression of various cell cycle related genes in CSPs, following treatment with Wnt3a-CM or vehicle. By utilizing a cell-cycle focused gene array I examined the expression of numerous markers or regulators of the cell cycle at 8 hours and 48 hours post-treatment with Wnt3a-CM and vehicle medium. This analysis revealed that activation of the canonical Wnt signaling pathway altered substantially the expression profile of various cell cycle regulators in CSPs. The anti-proliferative action of Wnt signaling pathway is mediated on CSPs as early as 8 hours post-treatment as indicated by the fact that well established proliferation markers such as Ki67 and PCNA were significantly down-regulated. Additionally, at the same time point negative regulators such as p16 and Gadd45 were markedly increased. Prolonged treatment (48 hours) of CSPs with Wnt3a-CM modulated the expression of the various additional cell cycle markers/regulators. Several positive cell cycle regulators such as

cyclin B1, Cyclin F1, Mcm2, Mcm3, Myb, Chek1, Cdk4, Cdc25, E2f2 and others were found to be substantially down-regulated. These genes changes clearly suggest that the canonical Wnt ligands induce alterations in the expression of critical regulators of the cell cycle progression.

These results suggest that activation of Wnt signaling in CSPs promotes cell cycle arrest without promoting exit from the cell cycle, towards the non-proliferative-quiescent G0 phase. As shown by flow-cytometric analysis, there is no difference in the $Ki67^{+}$ CSPs, following treatment with Wnt3a-CM or vehicle. Ki67 has been found to be expressed throughout all phases of the cell cycle, but not in the resting phase G0 [136]. In other words, the fraction of $Ki67^{+}$ cells represents the growing part of the examined *in vitro* or *in vivo* cell population. The exact function of Ki67 remains poorly understood and only few studies have proposed that is involved in the early steps of polymerase I rRNA synthesis [145, 146]. Overall my data suggest that treatment of CSPs with Wnt3a-CM although decreases the expression levels of Ki67 (mRNA levels), it does not decreases the growing fraction of CSPs, by promoting accumulation of cells in the G0 phase.

Another very interesting finding is that prolonged treatment of CSPs with Wnt3a-CM results in the profound down-regulation of p-63 (tumor protein p73-like, TP73L, p53-related protein p63, p51, KET, p40 and NBP). p63 does not represent an early direct or indirect target of the Wnt signaling pathway, as it is not affected following 8 hours of treatment but only following 48 hours of treatment with Wnt3a-CM. p63 belongs to the p53-protein family and has two major isoforms, the TAp63 (trans-activation domain) and the ΔNp63 (lack of trans-activation domain). Emerging evidence about the role of each isoform suggest that while the Tap63 isoform acts like a tumor suppressor gene, the ΔNp63 isoform functions as a potential oncogene [147]. ΔNp63

has been rarely found mutated in tumors, while it is often over-expressed in many types of cancer [148]. Furthermore, it was demonstrated that ΔNp73 and especially ΔNp63 are able to regulate the expression of various genes implicated in the G1-S and G2-M transitions of the cell cycle [149]. Thus, it is possible that activation of the Wnt signaling pathway in CSPs causes depletion of several positive cell cycle regulators through down-regulation of the expression levels of p63.

The above results strongly suggest that the canonical Wnt signaling pathway decreases the proliferation capacity of CSPs by promoting cell-cycle arrest. Until recently, numerous studies have implicated Wnt signaling in the progression of diverse types of malignancies, especially in epithelial cancer types. My findings are in agreement with emerging data that propose a novel non-oncogenic role for canonical Wnt signaling pathway in various forms of human cancers. Thus, the exact role of Wnt signaling is not uniform in all biological environments, as initially was considered [80, 150] but it rather depends on the specific developmental window [151] as well as the examined tissue or cell type [139].

5. IGFBP-3 is a major mediator of Wnt signaling-mediated anti-proliferative effects on CSPs

Subsequently, I focused my efforts on revealing potential mediators of the negative effects of Wnt signaling cascade on the proliferation of CSPs. I utilized a qRT-PCR gene array in order to measure the expression of numerous representative genes involved in different signaling pathways. Several interesting genes found to be substantially altered in the Wnt3a-treatment and among them IGFBP-3 was the most profoundly up-regulated. Follow up

experiments at different time points (8 hours, 24 hours, 48 hours and 72 hours) revealed that the earliest time point that increased expression of IGFBP3 was observed, was at 24 hours and that following this time point the expression of IGFBP3 was continually up-regulated. The above data clearly demonstrate that IGFBP-3 is steadily up-regulated by Wnt3a ligands in a time dependent fashion. Since I did not detect IGFBP3 up-regulation following 8 hours of Wnt3a treatment I assumed that IGFBP3 does not represent a direct transcriptional target of Wnt signaling pathway. Subsequent *in silico* analysis of the IGFBP3 promoter region (2 kilo bases upstream of the transcriptional starting point) revealed the existence of several conserved binding sites of transcription factors, as E2F, ARNT, p53, EF1 and AHRANT. However, no binding sites for the TCF transcription factors in the examined IGFBP3 promoter area were identified.

Before the significance of IGFBP3 in CSPs is further discussed, it is worthy to focus on the other examined genes of the pathway finder array, that were found to be substantially altered (more than 6-fold), following application of Wnt3a ligands. Treatment of CSPs with Wnt3a-CM resulted in up-regulation of Wnt2, Tcf7 and Lef1. All three genes represent important mediators of the canonical Wnt signaling and they provide further support that the treatment with Wnt3a-CM activates the canonical Wnt signaling cascade in CSPs. Moreover, the over-expression of p16 (Cdkn2a) and p15 (Cdkn2b) even at this time-point (6 days) suggest that Wnt signaling clearly augments the expression of well established cell cycle inhibitors. Another well studied gene that is up-regulated in my system is Fas, which is involved in TNF-mediated cell death. As presented above treatment with Wnt3a-CM resulted in increased apoptotic cell death. Fas might represent a potent mediator of these effects although it is unknown if it is a direct transcriptional

target of canonical Wnt ligands. Treatment of CSPs with Wnt3a-CM promotes the expression of various other genes, which are involved in diverse biological procedures and additional studies are required to unravel their functional role.

Through loss and gain of function approaches, I provide strong evidence that IGFBP3 represents a major mediator of the anti-proliferative action of Wnt signal cascade, via an IGF-dependent mechanism. IGFBP3 mimicked the effects of Wnt3a ligands on the proliferation capacity of CSPs when it was over-expressed through a lentivirus-vector or when it was added as a recombinant protein. The above conclusion was further confirmed by the finding that IGFBP3 over-expression or application of Wnt3a-CM regulated the gene expression profile of numerous cell cycle regulators in CSPs in a comparable manner.

Additionally, shRNA-mediated down-regulation of IGFBP3 in CSPs, granted them resistance to the anti-proliferative actions of Wnt3a ligands. Moreover, down–regulation of IGFBP3 expression reversed the effects of Wnt signaling on the expression profile of various cell cycle regulators. Finally, proliferation assays with CSPs over-expressing a mutated form of IGFBP3, which lacks the IGF-binding ability, showed that IGFBP3 exerts mainly its effects on CSPs by sequestering the IGF growth factor.

My data revealed an additional finding regarding the role of IGFBP3 on CSPs. ShRNA-mediated down-regulation of IGFBP3 decreased the proliferation of CSPs independent of the presence of Wnt3a ligands, suggesting the existence of a dual role for IGFBP3 in CSPs. IGFBP3 can rescue the proliferation capacity of CSPs in the presence of Wnt3a but in the absence of Wnt3a it causes a decrease in their growth. A dual role for IGFBP3 has been previously reported in HUVEC cells, where it was found to have both pro- and anti-apoptotic

function depending on the culture conditions [152]. Additionally, in a gastrointestinal tumor cell line both loss and over-expression of IGFBP3 decreased cell viability [153]. Additional experiments are required in order to explore this dual role of IGFBP3 in CSPs.

Currently, there is very limited knowledge regarding the relation of signaling provoked by IGFBP proteins and canonical Wnt ligands. The only documented direct connection between these diverse stimuli was published in a recent report by Zhu *et al [137]*. In this work it was demonstrated that IGFBP-4 promotes the cardiomyogenic differentiation of P19CL6 cells as well as embryonic stem cells through inhibition of the canonical Wnt signaling pathway. IGFBP-4 disrupts the formation of a functional ligand-receptor complex, through direct interaction with the Frizzled receptor and especially the LRP-6 co-receptor. Importantly, IGFBP-3 failed to decrease the activation of the canonical Wnt signaling pathway in a similar manner with IGFBP4.

This study reveals a previously unidentified role of IGFBP3 as a mediator of Wnt signaling effects on the proliferation capacity of CSPs. There are several important differences between the present study and the one published by Zhou *et al.* In our case I utilized an established population of adult cardiac progenitor cells instead of a population of cells that does not correspond to endogenous cardiac precursors, despite their use as a model of cardiomyogenic differentiation. Another distinction between the two studies is that here I activated the canonical Wnt pathway whereas in the study by Zhou *et al* they block the same signaling cascade by providing IGFBP4. Furthermore, in my hands both IGFBP3 and IGFBP4 failed to block the activation of canonical Wnt signaling pathway and they both caused similar effects on CSPs cell proliferation. In general there are several important differences between the two studies and it is

rather difficult to directly compare them. Further studies are needed to identify in more details the exact biological relationship between the IGFBP proteins and the Wnt ligands.

Overall, my data suggest that Wnt signaling pathway decreases the proliferation capacity of CSPs through up-regulation of IGFBP3, which most likely reduces the amount of available IGF-I growth factors. My work reveals a previously unknown functional connection between IGFBP3 and Wnt signaling pathway, as they both affect similarly numerous cell cycle regulators in CSPs. Additional experiments are required in order to identify the detailed mechanism as well as the connection between IGFBP3 and Wnts. Identification of the genes that are affected by both IGFBP3 protein and Wnt ligands, through microarray analysis, will provide critical information) about the relation of these stimuli.

6. Effects of Wnt signaling on the myocardium

Subsequently, I decided to examine the *in vivo* functional significance of Wnt signaling in the adult heart. Thus, the Wnt signaling cascade was activated by direct injection of recombinant Wnt3a protein (r-Wnt3a) in the left ventricle. Administration of r-Wnt3a in the myocardium resulted in an increased heart weight to body weight ratio and an increased number of mononuclear cells in the r-Wnt3a-injected areas. The increased amount of mononuclear cells in the r-WNt3a hearts cannot be attributed to recruitment of $CD45^{+}$ bone marrow derived cells or macrophage infiltration.

Intramyocardial delivery of r-Wnt3a resulted in a profound decrease in the percentage and the absolute number of total CSPs. These effects were mediated by the administered r-Wnt3a protein, as the respective values in the non-injected parts of the heart (atria, right ventricle

and septum) were unchanged. Moreover, administration of r-Wnt3a did not change the amount of total CSPs which are expressing the proliferation marker $Ki67^{+}$. These results are in agreement with my *in vitro* data, as in both cases Wnt3a ligands cause a decrease in the numbers of CSPs. Additionally, as shown by Ki67 immunostaining, in both cases, activation of Wnt signaling pathway does not promote cell cycle exit towards the resting G0 phase. To the best of our knowledge this is the first attempt to study the effects of canonical Wnt signaling on adult cardiac precursors, by direct administration of Wnt3a ligands. Additional experiments are required to clarify the molecular mechanisms which are involved in the decrease of the CSP cell number *in vivo*.

Although Wnt signaling has a well established role during development in various organs and especially the heart, its exact functions in post-natal tissues remain largely unknown. However, there are several studies proposing an unexpected role for canonical Wnt signaling pathway in stem cell renewal and aging. In a recent study, it was demonstrated that direct injection of r-Wnt3a protein in the skeletal muscle of young and aged mice 1 day following injury, augments the formation of fibrotic tissue while decreasing the proliferation index in the muscle [154]. Moreover in the same report, it was demonstrated that the serum of aged animals contained unknown Wnt-activating factors in comparison to the serum of young mice [154]. In another report published the same year, it was demonstrated that increased Wnt signaling is associated with decreased numbers of long-term BrdU-retaining cells and also decreased ability of satellite cells to maintain their myogenic capacity [155]. Furthermore, two additional reports have demonstrated that constitutively active canonical Wnt signaling can lead to depletion of hematopoietic stem cells [156, 157]. My results are in agreement with the above reports and it is

likely that long term activated Wnt signaling reduces the number of available cardiac progenitors in the adult myocardium. Moreover, it is possible that intramyocardial injection of r-Wnt3a may promote the proliferation of myofibroblasts and increase collagen deposition. Additional studies are required to examine this hypothesis and explain in greater detail the role of Wnt signaling in the adult heart.

7. Effects of Wnt signaling on post-MI cardiac remodeling

As mentioned previously, the role of Wnt signaling in the homeostasis of postnatal and especially injured cardiac muscle remains poorly understood. Thus, I decided to utilize a model of direct intramyocardial injection of r-Wnt3a following myocardial infarction, in order to examine the effects of Wnt signaling on the cardiac healing and performance. Administration of r-Wnt3a caused deterioration of cardiac function as evidenced by several critical markers including BW/HW ratio, chamber dilatation, LV wall thickness, fractional shortening, fractional area change and ejection fraction.

My results are in agreement with several previous reports that highlight the importance of GSK-3β in cardiac hypertrophy. GSK-3β can be inhibited by mediators of both physiologic (Akt kinase) and pathologic (Ga_q) hypertrophy [112]. However, over-expression of GSK-3β in transgenic mice resulted in smaller hearts with decreased contractility [158]. In addition, activated GSK-3β is an important anti-hypertrophic kinase, which mediates its beneficial effects in a Wnt-independent mechanism [113, 159]. Thus, it is possible that administration of r-Wnt3a deteriorates the cardiac function because it inhibits GSK-3β. Additional experiments are required to verify this hypothesis.

Furthermore, my results point to the same direction with several reports demonstrating the beneficial effects of several inhibitors of the canonical Wnt signaling pathway in cardiac performance following injury. Injection of Akt-over-expressing mesenchymal stem cells (Akt-MSC) in the myocardium following infarction resulted in improved heart function [122]. Akt-MSCs secrete SFRP2, a major paracrine factor. Transgenic mice over-expressing FrzA/SFRP1, a secreted Wnt antagonist, demonstrated reduced infarct size and improved cardiac function post-MI [118]. However, in my hands administration of 400 ng of recombinant SFRP2 protein (r-SFRP2) did not improved cardiac function following myocardial infarction, as none of the anatomical or functional parameters was recovered. It is likely that the injected amount of r-SFRP2 was insufficient to mediate any beneficial effects and that the administered dose needs to be increased.

Overall, the above data highlight the functional significance of canonical Wnt signaling pathway in cardiac performance. Activation of the canonical Wnt signaling pathway in post-MI myocardium deteriorates cardiac function by further inducing cardiac hypertrophy. Additional experiments are required to identify in greater detail the molecular mechanisms involved in this process. Canonical Wnt signaling exerts its effects through transcriptional up-regulation of numerous target genes that affect various biological processes. The "Wnt-targetome" includes a large number of genes and seems to be variable and dependent of the cellular context [160]. Thus, the discovery of novel mediators of the effects of Wnt signaling as well as inhibitors of the Wnt signal cascade is of great importance for the identification of new targets for future studies.

8. Status of Wnt signaling in post-MI heart tissue and CSPs

In the next series of experiments I investigated the activation status of Wnt signaling pathway in the cardiac tissue as well as in CSPs isolated following myocardial infarction. Various studies have utilized different types of markers of the Wnt signal cascade, but until today there is no solid evidence about the activation status of this pathway in normal and injured myocardium. According to studies using the TOP-GAL mouse, an *in vivo* Wnt reporter, there is very limited Wnt activity in the adult myocardium [100]. Gene expression studies suggest that the activity of Wnt signaling increases during MI. Various Wnt-related genes such as Frizzled-2, Wnt ligands and Dishevelled-1 are up-regulated following MI [106] [118] [161]. On the other hand, SFRP-2 a well established Wnt antagonist is also up-regulated in the infarcted heart [123].

By utilizing a Wnt-focused gene array I examined the expression of numerous genes related to Wnt signaling pathway in the infarct/border zone and in the remote area at different time points. There are several interesting observations derived from the expression profile of the Wnt-related genes. In the infarct/border zone area, myocardial infarction increases the expression of Frizzled-1, Frizzled-2 and Frizzled-5 receptors whereas in the remote area causes up-regulation of Frizzled-1 and Frizzled-2 and down-regulation of Frizzled-3, Frizzled-4, Frizzled-6 and Frizzled-8. These results suggest that there might be differential regulation of Wnt signaling between the infarct/border zone and the remote area.

The expression profile of the Wnt ligands is particularly interesting, as they represent the primary stimulus in the signaling cascade. Several Wnt ligands (Wnt3, Wnt3a, Wnt7b, Wnt8a and Wnt10a) are only expressed in the non-injured myocardium (sham animals) but not following myocardial infarction at all time points tested. The expression profile of the

remaining Wnt ligands provide additional evidence for differential regulation of Wnt signaling between the infarct/border zone and the remote area. In the infarct/border zone Wnt7a and Wnt16 are up-regulated whereas Wnt5, Wnt9, Wnt8a are all down-regulated. In contrast, in the remote area, Wnt2a, Wnt11 and Wnt 16 are down-regulated at various time points and no other Wnt ligand is up-regulated.

In both the infarct/border zone and the remote area there is a set of genes that was found to be steadily up-regulated at all time points. This set of genes is comprised by c-Myc, Ras and Wisp-1 (Wnt1 inducible signaling pathway protein 1), which are all targets of the canonical Wnt signaling pathway.

The gene-array data suggest that the canonical Wnt signaling pathway might be activated following myocardial infarction, primarily in the infarct/border zone and less in the remote area. However, the expression levels of SFRP1 but mainly of SFRP2 suggest that the activation status of Wnt signaling pathway in post-MI myocardium is not common for all cells. Although SFRP2 at day 1, was found to be slightly down-regulated its expression is robustly (more than 100-fold) up-regulated at a later time point (day 7), clearly suggesting that inhibition of Wnt signaling is critical for some aspects of cardiac remodeling.

Overall, the above results suggest that canonical Wnt signaling is involved in the process of cardiac remodeling and that it might be up-regulated following myocardial infarction. However, the activation status of Wnt signaling pathway differs in the various cell populations. Additional experiments are required to clarify the activation status of Wnt signaling pathway in different cell populations and the exact role of Wnt signaling cascade in cardiac remodeling.

Finally, my main interest was to examine the activation status of Wnt signaling pathway in CSPs derived from post-MI myocardium. By utilizing the same Wnt-related gene array I found that several positive regulators of the Wnt signaling pathway are significantly down-regulated, at day 3 and day 7 post-MI. The expression of Frizzled-5, Frizzled-6, Dishevelled-2, Tcf-3 and β-catenin was significantly decreased at the examined time points. Moreover, the expression of SFRP2 was significantly up-regulated at day 7 post-MI. These results suggest that in post-MI myocardium, Wnt signaling pathway in CSPs is silenced, despite that in the myocardium Wnt signaling seems to be activated. Thus, additional unknown mechanisms might create a special microenvironment for CSPs, in which the Wnt signaling pathway is differentially regulated from the rest of cardiac cells.

9. Conclusions

Cardiac stem/progenitor cells hold great potential for future therapeutic applications of heart failure, due to their potential to repopulate the damaged myocardium with newly formed cardiomyocytes. Detailed knowledge of the signaling pathways that control proliferation, differentiation and cell fate of cardiac progenitors is of paramount importance in the design of such cell therapy applications. The goal of this study was to examine the role of canonical Wnt signaling pathway in cardiac remodeling and in the self-renewal of CSPs.

Herein, I report that activation of Wnt signaling pathway in CSPs increases their cell size while decreasing dramatically their proliferation capacity, by altering their cell cycle properties. Similarly, Wnt signaling pathway decreases the percentage and the number of CSPs *in vivo.* I provide evidence that IGFBP3 acts as a major mediator of the *in vitro* anti-proliferative effects of

Wnt3a ligands in CSPs. Through site directed mutagenesis it was revealed that IGFBP3 mediates its effects on the proliferation of CSPs via an IGF-I-dependent mechanism. Furthermore, it is demonstrated that IGFB3 plays a dual role in CSPs as it can regulate their growth independent of Wnt signaling pathway. Additionally, I demonstrated that Wnt signaling affects the cardiac remodeling process. Administration of purified Wnt3a protein in the adult heart following myocardial infarction deteriorates the cardiac performance and decreases the cardiac output. My data reveal that Wnt signaling pathway controls various aspects in the adult myocardium. Thus besides its well established role in cardiac development, it possesses a less understood but critical role in the function and homeostasis of post-natal heart.

10. Future directions

Wnt signaling is a key developmental pathway that is actively involved in the formation and specification of the heart. The effects of Wnt signaling pathway on the various cardiac progenitor cells remain largely unknown. My data suggest that activation of Wnt signaling decreases their proliferation while increasing their cardiomyogenic differentiation. Additional experiments are required to examine if activation of Wnt signaling promotes cardiomyogenic differentiation *in vivo* and especially following cardiac injury. Moreover, it is necessary to analyze in more detail the molecular mechanisms of the Wnt-mediated anti-proliferative effects on CSPs. Identification of the direct and indirect Wnt target genes in CSPs through microarray experiments, would greatly serve this purpose.

Moreover, my study revealed a previously unknown connection between Wnt signaling and IGFBP3. Additional experiments are required to fully investigate the role of IGFBP3 in

CSPs as well as in the whole heart. Utilization of transgenic animals that over-express or lack IGFBP3 would be valuable tools in order to examine the role of this protein in the self-renewal of cardiac progenitors as well as in cardiac remodeling following injury.

Finally, my data demonstrate that activation of the canonical Wnt signaling pathway causes deterioration of cardiac function following myocardial infarction. Future studies should aim on the identification of the molecular mechanisms mediating the effects of Wnt on the cardiac function. Additionally, future studies of heart failure treatments could greatly benefit from the utilization of inhibitors of the canonical Wnt signaling pathway. Towards this goal, identification of novel chemical inhibitors of canonical Wnt signaling pathway will help in the design of such studies.

7. Bibliography

1. Lloyd-Jones, D., et al., *Heart disease and stroke statistics--2010 update: a report from the American Heart Association.* Circulation, 2010. **121**(7): p. e46-e215.
2. Jessup, M. and S. Brozena, *Heart failure.* N Engl J Med, 2003. **348**(20): p. 2007-18.
3. Hill, J.A. and E.N. Olson, *Cardiac plasticity.* N Engl J Med, 2008. **358**(13): p. 1370-80.
4. Mann, D.L., *Mechanisms and models in heart failure: A combinatorial approach.* Circulation, 1999. **100**(9): p. 999-1008.
5. Foody, J.M., M.H. Farrell, and H.M. Krumholz, *beta-Blocker therapy in heart failure: scientific review.* Jama, 2002. **287**(7): p. 883-9.
6. Cohn, J.N., *The management of chronic heart failure.* N Engl J Med, 1996. **335**(7): p. 490-8.
7. Ahuja, P., P. Sdek, and W.R. MacLellan, *Cardiac myocyte cell cycle control in development, disease, and regeneration.* Physiol Rev, 2007. **87**(2): p. 521-44.
8. Soonpaa, M.H. and L.J. Field, *Assessment of cardiomyocyte DNA synthesis in normal and injured adult mouse hearts.* Am J Physiol, 1997. **272**(1 Pt 2): p. H220-6.
9. Soonpaa, M.H., et al., *Cardiomyocyte DNA synthesis and binucleation during murine development.* Am J Physiol, 1996. **271**(5 Pt 2): p. H2183-9.
10. Anversa, P. and J. Kajstura, *Ventricular myocytes are not terminally differentiated in the adult mammalian heart.* Circ Res, 1998. **83**(1): p. 1-14.
11. Cheng, W., et al., *Down-regulation of the IGF-1 system parallels the attenuation in the proliferative capacity of rat ventricular myocytes during postnatal development.* Lab Invest, 1995. **72**(6): p. 646-55.
12. Marino, T.A., et al., *Proliferating cell nuclear antigen in developing and adult rat cardiac muscle cells.* Circ Res, 1991. **69**(5): p. 1353-60.
13. Dowell, R.T. and R.E. McManus, 3rd, *Pressure-induced cardiac enlargement in neonatal and adult rats. Left ventricular functional characteristics and evidence of cardiac muscle cell proliferation in the neonate.* Circ Res, 1978. **42**(3): p. 303-10.
14. Macdonald, R.A. and G.K. Mallory, *Autoradiography using tritiated thymidine. Detection of new cell formation in rat tissues.* Lab Invest, 1959. **8**: p. 1547-62.
15. Ring, P.A., *Myocardial regeneration in experimental ischaemic lesions of the heart.* J Pathol Bacteriol, 1950. **62**(1): p. 21-7.
16. Overy, H.R. and R.E. Priest, *Mitotic cell division in postnatal cardiac growth.* Lab Invest, 1966. **15**(6): p. 1100-3.
17. Beltrami, A.P., et al., *Evidence that human cardiac myocytes divide after myocardial infarction.* N Engl J Med, 2001. **344**(23): p. 1750-7.
18. Muller, P., et al., *Cardiomyocytes of noncardiac origin in myocardial biopsies of human transplanted hearts.* Circulation, 2002. **106**(1): p. 31-5.
19. Quaini, F., et al., *Chimerism of the transplanted heart.* N Engl J Med, 2002. **346**(1): p. 5-15.
20. Deb, A., et al., *Bone marrow-derived myofibroblasts are present in adult human heart valves.* J Heart Valve Dis, 2005. **14**(5): p. 674-8.
21. Minami, E., et al., *Extracardiac progenitor cells repopulate most major cell types in the transplanted human heart.* Circulation, 2005. **112**(19): p. 2951-8.
22. Glaser, R., et al., *Smooth muscle cells, but not myocytes, of host origin in transplanted human hearts.* Circulation, 2002. **106**(1): p. 17-9.

23. Bergmann, O., et al., *Evidence for cardiomyocyte renewal in humans.* Science, 2009. **324**(5923): p. 98-102.
24. Kajstura, J., et al., *Cardiomyogenesis in the adult human heart.* Circ Res, 2010. **107**(2): p. 305-15.
25. Hsieh, P.C., et al., *Evidence from a genetic fate-mapping study that stem cells refresh adult mammalian cardiomyocytes after injury.* Nat Med, 2007. **13**(8): p. 970-4.
26. Mikkers, H. and J. Frisen, *Deconstructing stemness.* EMBO J, 2005. **24**(15): p. 2715-9.
27. Alison, M.R., et al., *An introduction to stem cells.* J Pathol, 2002. **197**(4): p. 419-23.
28. Ramalho-Santos, M., et al., *"Stemness": transcriptional profiling of embryonic and adult stem cells.* Science, 2002. **298**(5593): p. 597-600.
29. Ivanova, N.B., et al., *A stem cell molecular signature.* Science, 2002. **298**(5593): p. 601-4.
30. Fortunel, N.O., et al., *Comment on " 'Stemness': transcriptional profiling of embryonic and adult stem cells" and "a stem cell molecular signature".* Science, 2003. **302**(5644): p. 393; author reply 393.
31. Li, L. and T. Xie, *Stem cell niche: structure and function.* Annu Rev Cell Dev Biol, 2005. **21**: p. 605-31.
32. Rietze, R.L., et al., *Purification of a pluripotent neural stem cell from the adult mouse brain.* Nature, 2001. **412**(6848): p. 736-9.
33. Jiang, Y., et al., *Pluripotency of mesenchymal stem cells derived from adult marrow.* Nature, 2002. **418**(6893): p. 41-9.
34. Overturf, K., et al., *Serial transplantation reveals the stem-cell-like regenerative potential of adult mouse hepatocytes.* Am J Pathol, 1997. **151**(5): p. 1273-80.
35. Beltrami, A.P., et al., *Adult cardiac stem cells are multipotent and support myocardial regeneration.* Cell, 2003. **114**(6): p. 763-76.
36. Urbanek, K., et al., *Stem cell niches in the adult mouse heart.* Proc Natl Acad Sci U S A, 2006. **103**(24): p. 9226-31.
37. Linke, A., et al., *Stem cells in the dog heart are self-renewing, clonogenic, and multipotent and regenerate infarcted myocardium, improving cardiac function.* Proc Natl Acad Sci U S A, 2005. **102**(25): p. 8966-71.
38. Bearzi, C., et al., *Human cardiac stem cells.* Proc Natl Acad Sci U S A, 2007. **104**(35): p. 14068-73.
39. Blume-Jensen, P. and T. Hunter, *Oncogenic kinase signalling.* Nature, 2001. **411**(6835): p. 355-65.
40. Pouly, J., et al., *Cardiac stem cells in the real world.* J Thorac Cardiovasc Surg, 2008. **135**(3): p. 673-8.
41. Oh, H., et al., *Cardiac progenitor cells from adult myocardium: homing, differentiation, and fusion after infarction.* Proc Natl Acad Sci U S A, 2003. **100**(21): p. 12313-8.
42. Holmes, C. and W.L. Stanford, *Concise review: stem cell antigen-1: expression, function, and enigma.* Stem Cells, 2007. **25**(6): p. 1339-47.
43. Wang, X., et al., *The role of the sca-1+/CD31- cardiac progenitor cell population in postinfarction left ventricular remodeling.* Stem Cells, 2006. **24**(7): p. 1779-88.
44. Matsuura, K., et al., *Adult cardiac Sca-1-positive cells differentiate into beating cardiomyocytes.* J Biol Chem, 2004. **279**(12): p. 11384-91.
45. Smits, A.M., et al., *Human cardiomyocyte progenitor cells differentiate into functional mature cardiomyocytes: an in vitro model for studying human cardiac physiology and pathophysiology.* Nat Protoc, 2009. **4**(2): p. 232-43.
46. Hierlihy, A.M., et al., *The post-natal heart contains a myocardial stem cell population.* FEBS Lett, 2002. **530**(1-3): p. 239-43.

47. Goodell, M.A., et al., *Isolation and functional properties of murine hematopoietic stem cells that are replicating in vivo.* J Exp Med, 1996. **183**(4): p. 1797-806.
48. Challen, G.A. and M.H. Little, *A side order of stem cells: the SP phenotype.* Stem Cells, 2006. **24**(1): p. 3-12.
49. Martin, C.M., et al., *Persistent expression of the ATP-binding cassette transporter, Abcg2, identifies cardiac SP cells in the developing and adult heart.* Dev Biol, 2004. **265**(1): p. 262-75.
50. Asakura, A. and M.A. Rudnicki, *Side population cells from diverse adult tissues are capable of in vitro hematopoietic differentiation.* Exp Hematol, 2002. **30**(11): p. 1339-45.
51. Pfister, O., et al., *CD31- but Not CD31+ cardiac side population cells exhibit functional cardiomyogenic differentiation.* Circ Res, 2005. **97**(1): p. 52-61.
52. Pfister, O., et al., *Isolation of resident cardiac progenitor cells by Hoechst 33342 staining.* Methods Mol Biol, 2010. **660**: p. 53-63.
53. Srivastava, D. and E.N. Olson, *A genetic blueprint for cardiac development.* Nature, 2000. **407**(6801): p. 221-6.
54. Brown, C.O., 3rd, et al., *The cardiac determination factor, Nkx2-5, is activated by mutual cofactors GATA-4 and Smad1/4 via a novel upstream enhancer.* J Biol Chem, 2004. **279**(11): p. 10659-69.
55. Camargo, F.D., et al., *Hematopoietic stem cells do not engraft with absolute efficiencies.* Blood, 2006. **107**(2): p. 501-7.
56. Schinkel, A.H., et al., *Normal viability and altered pharmacokinetics in mice lacking mdr1-type (drug-transporting) P-glycoproteins.* Proc Natl Acad Sci U S A, 1997. **94**(8): p. 4028-33.
57. Zhou, S., et al., *The ABC transporter Bcrp1/ABCG2 is expressed in a wide variety of stem cells and is a molecular determinant of the side-population phenotype.* Nat Med, 2001. **7**(9): p. 1028-34.
58. Zhou, S., et al., *Bcrp1 gene expression is required for normal numbers of side population stem cells in mice, and confers relative protection to mitoxantrone in hematopoietic cells in vivo.* Proc Natl Acad Sci U S A, 2002. **99**(19): p. 12339-44.
59. Schinkel, A.H. and J.W. Jonker, *Mammalian drug efflux transporters of the ATP binding cassette (ABC) family: an overview.* Adv Drug Deliv Rev, 2003. **55**(1): p. 3-29.
60. Staud, F. and P. Pavek, *Breast cancer resistance protein (BCRP/ABCG2).* Int J Biochem Cell Biol, 2005. **37**(4): p. 720-5.
61. Krishnamurthy, P., et al., *The stem cell marker Bcrp/ABCG2 enhances hypoxic cell survival through interactions with heme.* J Biol Chem, 2004. **279**(23): p. 24218-25.
62. Lazarowski, A.J., et al., *Cardiomyocytes of chronically ischemic pig hearts express the MDR-1 gene-encoded P-glycoprotein.* J Histochem Cytochem, 2005. **53**(7): p. 845-50.
63. Johnstone, R.W., E. Cretney, and M.J. Smyth, *P-glycoprotein protects leukemia cells against caspase-dependent, but not caspase-independent, cell death.* Blood, 1999. **93**(3): p. 1075-85.
64. Smyth, M.J., et al., *The drug efflux protein, P-glycoprotein, additionally protects drug-resistant tumor cells from multiple forms of caspase-dependent apoptosis.* Proc Natl Acad Sci U S A, 1998. **95**(12): p. 7024-9.
65. Pfister, O. and R. Liao, *Pump to survive: novel cytoprotective strategies for cardiac progenitor cells.* Circ Res, 2008. **102**(9): p. 998-1001.
66. Martin, C.M., et al., *Hypoxia-inducible factor-2alpha transactivates Abcg2 and promotes cytoprotection in cardiac side population cells.* Circ Res, 2008. **102**(9): p. 1075-81.
67. Patrawala, L., et al., *Side population is enriched in tumorigenic, stem-like cancer cells, whereas ABCG2+ and ABCG2- cancer cells are similarly tumorigenic.* Cancer Res, 2005. **65**(14): p. 6207-19.

68. Pfister, O., et al., *Role of the ATP-binding cassette transporter Abcg2 in the phenotype and function of cardiac side population cells.* Circ Res, 2008. **103**(8): p. 825-35.
69. Mouquet, F., et al., *Restoration of cardiac progenitor cells after myocardial infarction by self-proliferation and selective homing of bone marrow-derived stem cells.* Circ Res, 2005. **97**(11): p. 1090-2.
70. Orlic, D., et al., *Bone marrow cells regenerate infarcted myocardium.* Nature, 2001. **410**(6829): p. 701-5.
71. Laugwitz, K.L., et al., *Postnatal isl1+ cardioblasts enter fully differentiated cardiomyocyte lineages.* Nature, 2005. **433**(7026): p. 647-53.
72. Moretti, A., et al., *Multipotent embryonic isl1+ progenitor cells lead to cardiac, smooth muscle, and endothelial cell diversification.* Cell, 2006. **127**(6): p. 1151-65.
73. Qyang, Y., et al., *The renewal and differentiation of Isl1+ cardiovascular progenitors are controlled by a Wnt/beta-catenin pathway.* Cell Stem Cell, 2007. **1**(2): p. 165-79.
74. Messina, E., et al., *Isolation and expansion of adult cardiac stem cells from human and murine heart.* Circ Res, 2004. **95**(9): p. 911-21.
75. Dettman, R.W., et al., *Common epicardial origin of coronary vascular smooth muscle, perivascular fibroblasts, and intermyocardial fibroblasts in the avian heart.* Dev Biol, 1998. **193**(2): p. 169-81.
76. Zhou, B., et al., *Epicardial progenitors contribute to the cardiomyocyte lineage in the developing heart.* Nature, 2008. **454**(7200): p. 109-13.
77. Cai, C.L., et al., *A myocardial lineage derives from Tbx18 epicardial cells.* Nature, 2008. **454**(7200): p. 104-8.
78. Christoffels, V.M., et al., *Tbx18 and the fate of epicardial progenitors.* Nature, 2009. **458**(7240): p. E8-9; discussion E9-10.
79. Chien, A.J., W.H. Conrad, and R.T. Moon, *A Wnt survival guide: from flies to human disease.* J Invest Dermatol, 2009. **129**(7): p. 1614-27.
80. Rijsewijk, F., et al., *The Drosophila homolog of the mouse mammary oncogene int-1 is identical to the segment polarity gene wingless.* Cell, 1987. **50**(4): p. 649-57.
81. Willert, K., et al., *Wnt proteins are lipid-modified and can act as stem cell growth factors.* Nature, 2003. **423**(6938): p. 448-52.
82. Nusse, R., *Wnt signaling and stem cell control.* Cell Res, 2008. **18**(5): p. 523-7.
83. Rao, T.P. and M. Kuhl, *An updated overview on Wnt signaling pathways: a prelude for more.* Circ Res, 2010. **106**(12): p. 1798-806.
84. Semenov, M.V., et al., *Head inducer Dickkopf-1 is a ligand for Wnt coreceptor LRP6.* Curr Biol, 2001. **11**(12): p. 951-61.
85. Semenov, M.V., X. Zhang, and X. He, *DKK1 antagonizes Wnt signaling without promotion of LRP6 internalization and degradation.* J Biol Chem, 2008. **283**(31): p. 21427-32.
86. Mao, B., et al., *Kremen proteins are Dickkopf receptors that regulate Wnt/beta-catenin signalling.* Nature, 2002. **417**(6889): p. 664-7.
87. Sakane, H., H. Yamamoto, and A. Kikuchi, *LRP6 is internalized by Dkk1 to suppress its phosphorylation in the lipid raft and is recycled for reuse.* J Cell Sci, 2010. **123**(Pt 3): p. 360-8.
88. Cselenyi, C.S. and E. Lee, *Context-dependent activation or inhibition of Wnt-beta-catenin signaling by Kremen.* Sci Signal, 2008. **1**(8): p. pe10.
89. Kawano, Y. and R. Kypta, *Secreted antagonists of the Wnt signalling pathway.* J Cell Sci, 2003. **116**(Pt 13): p. 2627-34.

90. Bovolenta, P., et al., *Beyond Wnt inhibition: new functions of secreted Frizzled-related proteins in development and disease.* J Cell Sci, 2008. **121**(Pt 6): p. 737-46.
91. Cadigan, K.M. and R. Nusse, *Wnt signaling: a common theme in animal development.* Genes Dev, 1997. **11**(24): p. 3286-305.
92. Olson, E.N. and M.D. Schneider, *Sizing up the heart: development redux in disease.* Genes Dev, 2003. **17**(16): p. 1937-56.
93. Buckingham, M., S. Meilhac, and S. Zaffran, *Building the mammalian heart from two sources of myocardial cells.* Nat Rev Genet, 2005. **6**(11): p. 826-35.
94. Srivastava, D., *Making or breaking the heart: from lineage determination to morphogenesis.* Cell, 2006. **126**(6): p. 1037-48.
95. Garry, D.J. and E.N. Olson, *A common progenitor at the heart of development.* Cell, 2006. **127**(6): p. 1101-4.
96. Gessert, S. and M. Kuhl, *The multiple phases and faces of wnt signaling during cardiac differentiation and development.* Circ Res, 2010. **107**(2): p. 186-99.
97. Kattman, S.J., T.L. Huber, and G.M. Keller, *Multipotent flk-1+ cardiovascular progenitor cells give rise to the cardiomyocyte, endothelial, and vascular smooth muscle lineages.* Dev Cell, 2006. **11**(5): p. 723-32.
98. Olson, E.N., *Gene regulatory networks in the evolution and development of the heart.* Science, 2006. **313**(5795): p. 1922-7.
99. Takeuchi, J.K. and B.G. Bruneau, *Directed transdifferentiation of mouse mesoderm to heart tissue by defined factors.* Nature, 2009. **459**(7247): p. 708-11.
100. Cohen, E.D., Y. Tian, and E.E. Morrisey, *Wnt signaling: an essential regulator of cardiovascular differentiation, morphogenesis and progenitor self-renewal.* Development, 2008. **135**(5): p. 789-98.
101. Rochais, F., K. Mesbah, and R.G. Kelly, *Signaling pathways controlling second heart field development.* Circ Res, 2009. **104**(8): p. 933-42.
102. Dyer, L.A. and M.L. Kirby, *The role of secondary heart field in cardiac development.* Dev Biol, 2009. **336**(2): p. 137-44.
103. Logan, C.Y. and R. Nusse, *The Wnt signaling pathway in development and disease.* Annu Rev Cell Dev Biol, 2004. **20**: p. 781-810.
104. Moon, R.T., et al., *WNT and beta-catenin signalling: diseases and therapies.* Nat Rev Genet, 2004. **5**(9): p. 691-701.
105. Blankesteijn, W.M., et al., *Increased expression of a homologue of drosophila tissue polarity gene "frizzled" in left ventricular hypertrophy in the rat, as identified by subtractive hybridization.* J Mol Cell Cardiol, 1996. **28**(5): p. 1187-91.
106. Blankesteijn, W.M., et al., *A homologue of Drosophila tissue polarity gene frizzled is expressed in migrating myofibroblasts in the infarcted rat heart.* Nat Med, 1997. **3**(5): p. 541-4.
107. van de Schans, V.A., et al., *Interruption of Wnt signaling attenuates the onset of pressure overload-induced cardiac hypertrophy.* Hypertension, 2007. **49**(3): p. 473-80.
108. van Gijn, M.E., et al., *The wnt-frizzled cascade in cardiovascular disease.* Cardiovasc Res, 2002. **55**(1): p. 16-24.
109. Malekar, P., et al., *Wnt signaling is critical for maladaptive cardiac hypertrophy and accelerates myocardial remodeling.* Hypertension, 2010. **55**(4): p. 939-45.
110. Kerkela, R., et al., *Deletion of GSK-3beta in mice leads to hypertrophic cardiomyopathy secondary to cardiomyoblast hyperproliferation.* J Clin Invest, 2008. **118**(11): p. 3609-18.

111. Antos, C.L., et al., *Activated glycogen synthase-3 beta suppresses cardiac hypertrophy in vivo.* Proc Natl Acad Sci U S A, 2002. **99**(2): p. 907-12.
112. van de Schans, V.A., J.F. Smits, and W.M. Blankesteijn, *The Wnt/frizzled pathway in cardiovascular development and disease: friend or foe?* Eur J Pharmacol, 2008. **585**(2-3): p. 338-45.
113. Haq, S., et al., *Stabilization of beta-catenin by a Wnt-independent mechanism regulates cardiomyocyte growth.* Proc Natl Acad Sci U S A, 2003. **100**(8): p. 4610-5.
114. Chen, X., et al., *The beta-catenin/T-cell factor/lymphocyte enhancer factor signaling pathway is required for normal and stress-induced cardiac hypertrophy.* Mol Cell Biol, 2006. **26**(12): p. 4462-73.
115. Qu, J., et al., *Cardiac-specific haploinsufficiency of beta-catenin attenuates cardiac hypertrophy but enhances fetal gene expression in response to aortic constriction.* J Mol Cell Cardiol, 2007. **43**(3): p. 319-26.
116. Baurand, A., et al., *Beta-catenin downregulation is required for adaptive cardiac remodeling.* Circ Res, 2007. **100**(9): p. 1353-62.
117. Hahn, J.Y., et al., *Beta-catenin overexpression reduces myocardial infarct size through differential effects on cardiomyocytes and cardiac fibroblasts.* J Biol Chem, 2006. **281**(41): p. 30979-89.
118. Barandon, L., et al., *Reduction of infarct size and prevention of cardiac rupture in transgenic mice overexpressing FrzA.* Circulation, 2003. **108**(18): p. 2282-9.
119. Barandon, L., et al., *Involvement of FrzA/sFRP-1 and the Wnt/frizzled pathway in ischemic preconditioning.* Circ Res, 2005. **96**(12): p. 1299-306.
120. Mangi, A.A., et al., *Mesenchymal stem cells modified with Akt prevent remodeling and restore performance of infarcted hearts.* Nat Med, 2003. **9**(9): p. 1195-201.
121. Gnecchi, M., et al., *Paracrine action accounts for marked protection of ischemic heart by Akt-modified mesenchymal stem cells.* Nat Med, 2005. **11**(4): p. 367-8.
122. Mirotsou, M., et al., *Secreted frizzled related protein 2 (Sfrp2) is the key Akt-mesenchymal stem cell-released paracrine factor mediating myocardial survival and repair.* Proc Natl Acad Sci U S A, 2007. **104**(5): p. 1643-8.
123. Kobayashi, K., et al., *Secreted Frizzled-related protein 2 is a procollagen C proteinase enhancer with a role in fibrosis associated with myocardial infarction.* Nat Cell Biol, 2009. **11**(1): p. 46-55.
124. Pollak, M.N., E.S. Schernhammer, and S.E. Hankinson, *Insulin-like growth factors and neoplasia.* Nat Rev Cancer, 2004. **4**(7): p. 505-18.
125. Burger, A.M., et al., *Essential roles of IGFBP-3 and IGFBP-rP1 in breast cancer.* Eur J Cancer, 2005. **41**(11): p. 1515-27.
126. Hwa, V., Y. Oh, and R.G. Rosenfeld, *The insulin-like growth factor-binding protein (IGFBP) superfamily.* Endocr Rev, 1999. **20**(6): p. 761-87.
127. Yamada, P.M. and K.W. Lee, *Perspectives in mammalian IGFBP-3 biology: local vs. systemic action.* Am J Physiol Cell Physiol, 2009. **296**(5): p. C954-76.
128. Buckway, C.K., et al., *Mutation of three critical amino acids of the N-terminal domain of IGF-binding protein-3 essential for high affinity IGF binding.* J Clin Endocrinol Metab, 2001. **86**(10): p. 4943-50.
129. Pucci, A., et al., *Myocardial insulin-like growth factor-1 and insulin-like growth factor binding protein-3 gene expression in failing hearts harvested from patients undergoing cardiac transplantation.* J Heart Lung Transplant, 2009. **28**(4): p. 402-5.
130. Henson, M., et al., *Insulin-like growth factor-binding protein-3 induces fetalization in neonatal rat cardiomyocytes.* DNA Cell Biol, 2000. **19**(12): p. 757-63.

131. Murphy, L.J., et al., *Expression of human insulin-like growth factor-binding protein-3 in transgenic mice.* J Mol Endocrinol, 1995. **15**(3): p. 293-303.
132. Ning, Y., et al., *Diminished growth and enhanced glucose metabolism in triple knockout mice containing mutations of insulin-like growth factor binding protein-3, -4, and -5.* Mol Endocrinol, 2006. **20**(9): p. 2173-86.
133. Jain, M., et al., *Cell therapy attenuates deleterious ventricular remodeling and improves cardiac performance after myocardial infarction.* Circulation, 2001. **103**(14): p. 1920-7.
134. Shi, J., et al., *Amyloidogenic light chains induce cardiomyocyte contractile dysfunction and apoptosis via a non-canonical p38alpha MAPK pathway.* Proc Natl Acad Sci U S A, 2010. **107**(9): p. 4188-93.
135. Perez-Cadahia, B., B. Drobic, and J.R. Davie, *H3 phosphorylation: dual role in mitosis and interphase.* Biochem Cell Biol, 2009. **87**(5): p. 695-709.
136. Yerushalmi, R., et al., *Ki67 in breast cancer: prognostic and predictive potential.* Lancet Oncol, 2010. **11**(2): p. 174-83.
137. Zhu, W., et al., *IGFBP-4 is an inhibitor of canonical Wnt signalling required for cardiogenesis.* Nature, 2008. **454**(7202): p. 345-9.
138. Yamamoto, H., et al., *Wnt3a and Dkk1 regulate distinct internalization pathways of LRP6 to tune the activation of beta-catenin signaling.* Dev Cell, 2008. **15**(1): p. 37-48.
139. Chien, A.J., et al., *Activated Wnt/beta-catenin signaling in melanoma is associated with decreased proliferation in patient tumors and a murine melanoma model.* Proc Natl Acad Sci U S A, 2009. **106**(4): p. 1193-8.
140. Hassler, C., et al., *Kremen is required for neural crest induction in Xenopus and promotes LRP6-mediated Wnt signaling.* Development, 2007. **134**(23): p. 4255-63.
141. Kwon, C., K.R. Cordes, and D. Srivastava, *Wnt/beta-catenin signaling acts at multiple developmental stages to promote mammalian cardiogenesis.* Cell Cycle, 2008. **7**(24): p. 3815-8.
142. Cohen, E.D., et al., *Wnt/beta-catenin signaling promotes expansion of Isl-1-positive cardiac progenitor cells through regulation of FGF signaling.* J Clin Invest, 2007. **117**(7): p. 1794-804.
143. Kwon, C., et al., *Canonical Wnt signaling is a positive regulator of mammalian cardiac progenitors.* Proc Natl Acad Sci U S A, 2007. **104**(26): p. 10894-9.
144. Lin, L., et al., *Beta-catenin directly regulates Islet1 expression in cardiovascular progenitors and is required for multiple aspects of cardiogenesis.* Proc Natl Acad Sci U S A, 2007. **104**(22): p. 9313-8.
145. Rahmanzadeh, R., et al., *Chromophore-assisted light inactivation of pKi-67 leads to inhibition of ribosomal RNA synthesis.* Cell Prolif, 2007. **40**(3): p. 422-30.
146. Bullwinkel, J., et al., *Ki-67 protein is associated with ribosomal RNA transcription in quiescent and proliferating cells.* J Cell Physiol, 2006. **206**(3): p. 624-35.
147. Flores, E.R., *The roles of p63 in cancer.* Cell Cycle, 2007. **6**(3): p. 300-4.
148. Finlan, L.E. and T.R. Hupp, *p63: the phantom of the tumor suppressor.* Cell Cycle, 2007. **6**(9): p. 1062-71.
149. Lefkimmiatis, K., et al., *p73 and p63 sustain cellular growth by transcriptional activation of cell cycle progression genes.* Cancer Res, 2009. **69**(22): p. 8563-71.
150. Giles, R.H., J.H. van Es, and H. Clevers, *Caught up in a Wnt storm: Wnt signaling in cancer.* Biochim Biophys Acta, 2003. **1653**(1): p. 1-24.
151. Ueno, S., et al., *Biphasic role for Wnt/beta-catenin signaling in cardiac specification in zebrafish and embryonic stem cells.* Proc Natl Acad Sci U S A, 2007. **104**(23): p. 9685-90.
152. Granata, R., et al., *Dual effects of IGFBP-3 on endothelial cell apoptosis and survival: involvement of the sphingolipid signaling pathways.* FASEB J, 2004. **18**(12): p. 1456-8.

153. Dupart, J.J., et al., *Insulin-like growth factor binding protein-3 has dual effects on gastrointestinal stromal tumor cell viability and sensitivity to the anti-tumor effects of imatinib mesylate in vitro.* Mol Cancer, 2009. **8**: p. 99.
154. Brack, A.S., et al., *Increased Wnt signaling during aging alters muscle stem cell fate and increases fibrosis.* Science, 2007. **317**(5839): p. 807-10.
155. Liu, H., et al., *Augmented Wnt signaling in a mammalian model of accelerated aging.* Science, 2007. **317**(5839): p. 803-6.
156. Kirstetter, P., et al., *Activation of the canonical Wnt pathway leads to loss of hematopoietic stem cell repopulation and multilineage differentiation block.* Nat Immunol, 2006. **7**(10): p. 1048-56.
157. Scheller, M., et al., *Hematopoietic stem cell and multilineage defects generated by constitutive beta-catenin activation.* Nat Immunol, 2006. **7**(10): p. 1037-47.
158. Michael, A., et al., *Glycogen synthase kinase-3beta regulates growth, calcium homeostasis, and diastolic function in the heart.* J Biol Chem, 2004. **279**(20): p. 21383-93.
159. Haq, S., et al., *Glycogen synthase kinase-3beta is a negative regulator of cardiomyocyte hypertrophy.* J Cell Biol, 2000. **151**(1): p. 117-30.
160. Vlad, A., et al., *The first five years of the Wnt targetome.* Cell Signal, 2008. **20**(5): p. 795-802.
161. Chen, L., et al., *Expression of Dishevelled-1 in wound healing after acute myocardial infarction: possible involvement in myofibroblast proliferation and migration.* J Cell Mol Med, 2004. **8**(2): p. 257-64.

8. List of tables of qRT-PCR arrays:

- *Table 1A: Wnt signaling pathway array-Infarct/border zone post-MI day 1*

Wnt signaling qRT-PCR array (infarct/border zone)				
Description	**Symbol**	**Day 1 (AVG ÄCt)**		
		Sham	**post-MI**	**Fold change**
Myelocytomatosis oncogene	**Myc**	**7.44**	**4.16**	**9.75***
WNT1 inducible signaling pathway protein 1	**Wisp1**	**10.25**	**8.29**	**3.89***
Fos-like antigen 1	**Fosl1**	**8.38**	**6.70**	**3.21***
Ras homolog gene family, member U	**Rhou**	**8.32**	**7.05**	**2.41***
Lymphoid enhancer binding factor 1	Lef1	14.94	12.80	4.43
Fibroblast growth factor 4	Fgf4	14.41	13.17	2.38
Casein kinase 1, delta	Csnk1d	5.06	3.99	2.11
Cyclin D1	Ccnd1	3.75	2.70	2.08
Solute carrier family 9 (sodium/hydrogen exchanger), member 3 regulator 1	Slc9a3r1	6.54	5.50	2.06
Wingless-related MMTV integration site 1	Wnt1	13.97	12.95	2.02
Forkhead box N1	Foxn1	14.23	13.26	1.96
Frizzled homolog 1 (Drosophila)	Fzd1	6.07	5.25	1.77
Wingless-related MMTV integration site 4	Wnt4	10.48	9.71	1.71
B-cell CLL/lymphoma 9	Bcl9	6.56	5.84	1.64
Jun oncogene	Jun	3.02	2.35	1.60
Casein kinase 1, alpha 1	Csnk1a1	2.26	1.59	1.59
Beta-transducin repeat containing protein	Btrc	5.43	4.81	1.55
Wingless-related MMTV integration site 6	Wnt6	11.63	11.06	1.49
Wingless-related MMTV integration site 7A	Wnt7a	14.72	15.27	1.47
Axin 1	Axin1	5.88	5.38	1.41
Cyclin D3	Ccnd3	3.40	2.92	1.40
F-box and WD-40 domain protein 11	Fbxw11	3.99	3.56	1.35
Frizzled homolog 2 (Drosophila)	Fzd2	7.40	6.97	1.35
Dishevelled 2, dsh homolog (Drosophila)	Dvl2	7.63	7.30	1.26
Transcription factor 7, T-cell specific	Tcf7	10.26	9.93	1.26
F-box and WD-40 domain protein 2	Fbxw2	4.16	3.84	1.25
Dishevelled, dsh homolog 1 (Drosophila)	Dvl1	11.14	10.87	1.21
Frizzled homolog 5 (Drosophila)	Fzd5	8.56	8.30	1.20

Cyclin D2	Ccnd2	2.75	2.51	1.19
Paired-like homeodomain transcription factor 2	Pitx2	12.19	11.97	1.17
Wingless-related MMTV integration site 2	Wnt2	12.01	11.78	1.17
SUMO/sentrin specific peptidase 2	Senp2	6.12	5.91	1.16
C-terminal binding protein 2	Ctbp2	4.87	4.66	1.15
Frizzled homolog 3 (Drosophila)	Fzd3	8.62	8.44	1.13
E1A binding protein p300	Ep300	6.35	6.22	1.09
C-terminal binding protein 1	Ctbp1	2.66	2.58	1.06
Frizzled homolog 8 (Drosophila)	Fzd8	10.06	10.03	1.02
SRY-box containing gene 17	Sox17	6.79	6.79	1.00
Secreted frizzled-related protein 2	**Sfrp2**	**7.17**	**8.85**	**-3.20***
Secreted frizzled-related protein 1	**Sfrp1**	**5.15**	**6.71**	**-2.95***
Wnt inhibitory factor 1	**Wif1**	**8.46**	**10.01**	**-2.93***
Pygopus 1	**Pygo1**	**5.64**	**7.15**	**-2.83***
Secreted frizzled-related protein 4	**Sfrp4**	**11.80**	**13.05**	**-2.38***
Wingless-related MMTV integration site 5B	**Wnt5b**	**7.05**	**8.05**	**-2***
Porcupine homolog (Drosophila)	**Porcn**	**7.09**	**8.06**	**-1.95***
Naked cuticle 1 homolog (Drosophila)	Nkd1	8.11	10.81	-6.52
Wingless related MMTV integration site 2b	Wnt2b	11.95	14.15	-4.61
Wingless related MMTV integration site 8b	Wnt8b	12.70	14.87	-4.51
Brachyury	T	10.54	12.52	-3.93
Nemo like kinase	Nlk	5.71	6.99	-2.43
Frizzled homolog 4 (Drosophila)	Fzd4	3.45	4.68	-2.35
Transducin-like enhancer of split 2, homolog of Drosophila E(spl)	Tle2	6.35	7.57	-2.33
Frizzled-related protein	Frzb	10.18	11.28	-2.14
Wingless-related MMTV integration site 11	Wnt11	7.94	9.04	-2.14
Frizzled homolog 6 (Drosophila)	Fzd6	4.97	6.03	-2.08
Kringle containing transmembrane protein 1	Kremen1	1.46	2.48	-2.03
Catenin (cadherin associated protein), beta 1	Ctnnb1	0.82	1.84	-2.02
Wingless-related MMTV integration site 16	Wnt16	14.03	14.95	-1.90
Frequently rearranged in advanced T-cell lymphomas	Frat1	8.01	8.84	-1.78
Wingless-related MMTV integration site 5A	Wnt5a	8.59	9.42	-1.78
Catenin beta interacting protein 1	Ctnnbip1	7.54	8.34	-1.74
Protein phosphatase 2, regulatory subunit B (B56), delta isoform	Ppp2r5d	3.68	4.41	-1.65
Follicle stimulating hormone beta	Fshb	11.71	12.41	-1.62
Low density lipoprotein receptor-related protein 6	Lrp6	3.45	4.11	-1.57
F-box and WD-40 domain protein 4	Fbxw4	3.34	3.90	-1.47
Transcription factor 3	Tcf3	10.84	11.38	-1.45

DIX domain containing 1	Dixdc1	6.26	6.73	-1.39
Transducin-like enhancer of split 1, homolog of Drosophila E(spl)	Tle1	5.26	5.59	-1.25
Frizzled homolog 7 (Drosophila)	Fzd7	7.35	7.64	-1.22
Protein phosphatase 2 (formerly 2A), regulatory subunit A (PR 65), alpha isoform	Ppp2r1a	1.42	1.69	-1.21
Glycogen synthase kinase 3 beta	Gsk3b	2.56	2.82	-1.20
Adenomatosis polyposis coli	Apc	5.11	5.31	-1.15
Dishevelled associated activator of morphogenesis 1	Daam1	2.66	2.81	-1.11
Amino-terminal enhancer of split	Aes	1.46	1.60	-1.10
Dickkopf homolog 1 (Xenopus laevis)	Dkk1	13.76	13.89	-1.09
Wingless-type MMTV integration site 9A	Wnt9a	9.76	9.89	-1.09
Low density lipoprotein receptor-related protein 5	Lrp5	4.46	4.57	-1.08
Protein phosphatase 2 (formerly 2A), catalytic subunit, alpha isoform	Ppp2ca	1.22	1.27	-1.03
Casein kinase 2, alpha 1 polypeptide	Csnk2a1	4.62	4.63	-1.01
Wingless related MMTV integration site 10a	Wnt10a	N/A	N/A	N/A
Wingless-related MMTV integration site 3	Wnt3	N/A	N/A	N/A
Wingless-related MMTV integration site 3A	Wnt3a	N/A	N/A	N/A
Wingless-related MMTV integration site 7B	Wnt7b	N/A	N/A	N/A
Wingless-related MMTV integration site 8A	Wnt8a	N/A	N/A	N/A

- *Table 1B: Wnt signaling pathway array- infarct area post-MI day 3*

Wnt signaling qRT-PCR array (Infarct/border zone)				
Gene description	**Symbol**	**Day 3 (AVG ÄCt)**		
		Sham	**post-MI**	**Fold change**
Wingless-related MMTV integration site 7A	**Wnt7a**	**15.27**	**10.71**	**23.57***
WNT1 inducible signaling pathway protein 1	**Wisp1**	**10.25**	**6.82**	**10.82***
Myelocytomatosis oncogene	**Myc**	**7.44**	**5.14**	**4.95***
Ras homolog gene family, member U	**Rhou**	**8.32**	**6.66**	**3.16***
Frizzled homolog 2 (Drosophila)	**Fzd2**	**7.40**	**5.91**	**2.83***
Secreted frizzled-related protein 1	**Sfrp1**	**5.15**	**4.14**	**2.02***
B-cell CLL/lymphoma 9	Bcl9	6.56	4.70	**3.62**
Wingless-related MMTV integration site 1	Wnt1	13.97	12.45	**2.86**
Cyclin D1	Ccnd1	3.75	2.43	**2.51**

Beta-transducin repeat containing protein	Btrc	5.43	4.12	**2.49**
Secreted frizzled-related protein 2	Sfrp2	7.17	5.98	**2.28**
Fibroblast growth factor 4	Fgf4	14.41	13.24	**2.25**
Frizzled homolog 5 (Drosophila)	Fzd5	8.56	7.51	**2.06**
Lymphoid enhancer binding factor 1	Lef1	14.94	14.00	**1.93**
C-terminal binding protein 2	Ctbp2	4.87	4.01	**1.81**
Frizzled homolog 1 (Drosophila)	Fzd1	6.07	5.28	**1.74**
Axin 1	Axin1	5.88	5.10	**1.72**
Solute carrier family 9 (sodium/hydrogen exchanger), member 3 regulator 1	Slc9a3r1	6.54	5.78	**1.70**
Casein kinase 1, delta	Csnk1d	5.06	4.32	**1.67**
Jun oncogene	Jun	3.02	2.56	**1.38**
Cyclin D3	Ccnd3	3.40	3.02	**1.30**
Cyclin D2	Ccnd2	2.75	2.45	**1.24**
Amino-terminal enhancer of split	Aes	1.46	1.17	**1.23**
Fos-like antigen 1	Fosl1	8.38	8.09	**1.23**
Dishevelled, dsh homolog 1 (Drosophila)	Dvl1	11.14	10.88	**1.20**
F-box and WD-40 domain protein 11	Fbxw11	3.99	3.76	**1.18**
Dishevelled 2, dsh homolog (Drosophila)	Dvl2	7.63	7.43	**1.15**
Adenomatosis polyposis coli	Apc	5.11	4.93	**1.13**
Wingless-related MMTV integration site 4	Wnt4	10.48	10.34	**1.11**
Paired-like homeodomain transcription factor 2	Pitx2	12.19	12.06	**1.10**
Wingless-related MMTV integration site 6	Wnt6	11.63	11.59	**1.03**
C-terminal binding protein 1	Ctbp1	2.66	2.63	**1.02**
Casein kinase 1, alpha 1	Csnk1a1	2.26	2.26	**1.00**
Wingless related MMTV integration site 8b	**Wnt8b**	**12.70**	**15.83**	**-8.76***
DIX domain containing 1	**Dixdc1**	**6.26**	**8.11**	**-3.61***
Pygopus 1	**Pygo1**	**5.64**	**6.99**	**-2.55***
Transducin-like enhancer of split 2, homolog of Drosophila E(spl)	**Tle2**	**6.35**	**7.30**	**-1.93***
Wingless-type MMTV integration site 9A	**Wnt9a**	**9.76**	**10.71**	**-1.92***
Transducin-like enhancer of split 1, homolog of Drosophila E(spl)	**Tle1**	**5.26**	**6.20**	**-1.91***
Naked cuticle 1 homolog (Drosophila)	Nkd1	8.11	11.77	-12.62
Brachyury	T	10.54	12.78	-4.70
Kringle containing transmembrane protein 1	Kremen1	1.46	3.21	-3.34
Nemo like kinase	Nlk	5.71	7.34	-3.08
Forkhead box N1	Foxn1	14.23	15.68	-2.73
Wnt inhibitory factor 1	Wif1	8.46	9.84	-2.61
Wingless-related MMTV integration site 5A	Wnt5a	8.59	9.97	-2.59
Wingless-related MMTV integration site 2	Wnt2	12.01	13.35	-2.54

Frizzled homolog 6 (Drosophila)	Fzd6	4.97	6.15	-2.26
Wingless-related MMTV integration site 16	Wnt16	14.03	15.11	-2.12
Porcupine homolog (Drosophila)	Porcn	7.09	8.12	-2.03
Transcription factor 3	Tcf3	10.84	11.80	-1.94
Frequently rearranged in advanced T-cell lymphomas	Frat1	8.01	8.93	-1.89
Wingless-related MMTV integration site 5B	Wnt5b	7.05	7.95	-1.86
Frizzled homolog 4 (Drosophila)	Fzd4	3.45	4.30	-1.81
Dickkopf homolog 1 (Xenopus laevis)	Dkk1	13.76	14.60	-1.78
Catenin (cadherin associated protein), beta 1	Ctnnb1	0.82	1.62	-1.74
Follicle stimulating hormone beta	Fshb	11.71	12.51	-1.74
Dishevelled associated activator of morphogenesis 1	Daam1	2.66	3.35	-1.61
Low density lipoprotein receptor-related protein 6	Lrp6	3.45	4.11	-1.58
Glycogen synthase kinase 3 beta	Gsk3b	2.56	3.17	-1.52
SRY-box containing gene 17	Sox17	6.79	7.37	-1.49
E1A binding protein p300	Ep300	6.35	6.86	-1.42
Frizzled homolog 8 (Drosophila)	Fzd8	10.06	10.56	-1.41
Protein phosphatase 2 (formerly 2A), regulatory subunit A (PR 65), alpha isoform	Ppp2r1a	1.42	1.90	-1.40
Protein phosphatase 2 (formerly 2A), catalytic subunit, alpha isoform	Ppp2ca	1.22	1.70	-1.39
Frizzled-related protein	Frzb	10.18	10.63	-1.37
Frizzled homolog 7 (Drosophila)	Fzd7	7.35	7.78	-1.34
Low density lipoprotein receptor-related protein 5	Lrp5	4.46	4.81	-1.27
SUMO/sentrin specific peptidase 2	Senp2	6.12	6.43	-1.24
Casein kinase 2, alpha 1 polypeptide	Csnk2a1	4.62	4.91	-1.22
F-box and WD-40 domain protein 4	Fbxw4	3.34	3.59	-1.19
F-box and WD-40 domain protein 2	Fbxw2	4.16	4.40	-1.18
Transcription factor 7, T-cell specific	Tcf7	10.26	10.45	-1.14
Catenin beta interacting protein 1	Ctnnbip1	7.54	7.61	-1.05
Secreted frizzled-related protein 4	Sfrp4	11.80	11.87	-1.05
Wingless related MMTV integration site 2b	Wnt2b	11.95	12.02	-1.05
Protein phosphatase 2, regulatory subunit B (B56), delta isoform	Ppp2r5d	3.68	3.73	-1.03
Frizzled homolog 3 (Drosophila)	Fzd3	8.62	8.65	-1.02
Wingless-related MMTV integration site 11	Wnt11	7.94	7.97	-1.02
Wingless related MMTV integration site 10a	Wnt10a	N/A	N/A	N/A
Wingless-related MMTV integration site 3	Wnt3	N/A	N/A	N/A
Wingless-related MMTV integration site 3A	Wnt3a	N/A	N/A	N/A
Wingless-related MMTV integration site 7B	Wnt7b	N/A	N/A	N/A
Wingless-related MMTV integration site 8A	Wnt8a	N/A	N/A	N/A

- *Table 1C: Wnt signaling pathway array- infarct area post-MI day 7*

Wnt signaling qRT-PCR array (Infarct/border zone)				
Gene description	**Symbol**	**Day 7 (AVG ÄCt)**		
		Sham	**post-MI**	**Fold change**
Secreted frizzled-related protein 2	**Sfrp2**	**7.17**	**0.33**	**114.25***
WNT1 inducible signaling pathway protein 1	**Wisp1**	**10.25**	**3.89**	**81.91***
Wingless-related MMTV integration site 16	**Wnt16**	**14.03**	**10.04**	**15.88***
Secreted frizzled-related protein 1	**Sfrp1**	**5.15**	**1.32**	**14.18***
Frizzled homolog 5 (Drosophila)	**Fzd5**	**8.56**	**5.62**	**7.67***
Frizzled homolog 2 (Drosophila)	**Fzd2**	**7.4**	**4.49**	**7.51***
Ras homolog gene family, member U	**Rhou**	**8.32**	**5.67**	**6.26***
Wingless-related MMTV integration site 7A	**Wnt7a**	**15.27**	**12.74**	**5.76***
Frizzled homolog 1 (Drosophila)	**Fzd1**	**6.07**	**4**	**4.20***
Secreted frizzled-related protein 4	**Sfrp4**	**11.8**	**9.95**	**3.60***
Frizzled homolog 8 (Drosophila)	**Fzd8**	**10.06**	**8.37**	**3.21***
Wingless-related MMTV integration site 11	**Wnt11**	**7.94**	**6.31**	**3.09***
Myelocytomatosis oncogene	**Myc**	**7.44**	**6**	**2.72***
Solute carrier family 9 (sodium/hydrogen exchanger), member 3 regulator 1	**Slc9a3r1**	**6.54**	**5.09**	**2.72***
Frizzled-related protein	Frzb	10.18	6.18	16.03
Wingless-related MMTV integration site 4	Wnt4	10.48	7.58	7.46
Lymphoid enhancer binding factor 1	Lef1	14.94	12.07	7.32
Wingless-related MMTV integration site 1	Wnt1	13.97	11.85	4.34
Wingless related MMTV integration site 2b	Wnt2b	11.95	9.89	4.17
Dishevelled, dsh homolog 1 (Drosophila)	Dvl1	11.14	9.5	3.12
Transcription factor 3	Tcf3	10.84	9.39	2.73
Transcription factor 7, T-cell specific	Tcf7	10.26	8.81	2.72
Forkhead box N1	Foxn1	14.23	12.87	2.56
C-terminal binding protein 2	Ctbp2	4.87	3.74	2.18
Casein kinase 1, delta	Csnk1d	5.06	3.99	2.10
Follicle stimulating hormone beta	Fshb	11.71	10.78	1.90
B-cell CLL/lymphoma 9	Bcl9	6.56	5.77	1.72
Dishevelled 2, dsh homolog (Drosophila)	Dvl2	7.63	6.91	1.65
Frizzled homolog 7 (Drosophila)	Fzd7	7.35	6.63	1.65
Frizzled homolog 3 (Drosophila)	Fzd3	8.62	7.96	1.58
Axin 1	Axin1	5.88	5.3	1.49

Low density lipoprotein receptor-related protein 5	Lrp5	4.46	3.95	1.43
Catenin beta interacting protein 1	Ctnnbip1	7.54	7.06	1.40
Dickkopf homolog 1 (Xenopus laevis)	Dkk1	13.76	13.3	1.38
E1A binding protein p300	Ep300	6.35	5.88	1.38
Casein kinase 2, alpha 1 polypeptide	Csnk2a1	4.62	4.2	1.34
Jun oncogene	Jun	3.02	2.63	1.31
Frequently rearranged in advanced T-cell lymphomas	Frat1	8.01	7.71	1.23
Fos-like antigen 1	Fosl1	8.38	8.1	1.22
Cyclin D3	Ccnd3	3.4	3.17	1.17
Wingless-related MMTV integration site 6	Wnt6	11.63	11.41	1.16
Adenomatosis polyposis coli	Apc	5.11	4.91	1.15
Wingless-type MMTV integration site 9A	Wnt9a	9.76	9.59	1.12
F-box and WD-40 domain protein 2	Fbxw2	4.16	4.02	1.10
Wingless-related MMTV integration site 5A	Wnt5a	8.59	8.45	1.10
Wingless-related MMTV integration site 5B	Wnt5b	7.05	6.93	1.09
Wingless related MMTV integration site 8b	**Wnt8b**	**12.7**	**15.84**	**-8.80***
Wnt inhibitory factor 1	**Wif1**	**8.46**	**10.05**	**-3.01***
SUMO/sentrin specific peptidase 2	**Senp2**	**6.12**	**6.16**	**-1.03***
Brachyury	T	10.54	13.38	-7.15
Nemo like kinase	Nlk	5.71	7.47	-3.39
Transducin-like enhancer of split 2, homolog of Drosophila E(spl)	Tle2	6.35	8.05	-3.26
F-box and WD-40 domain protein 4	Fbxw4	3.34	4.86	-2.87
Kringle containing transmembrane protein 1	Kremen1	1.46	2.9	-2.71
Glycogen synthase kinase 3 beta	Gsk3b	2.56	3.92	-2.57
Fibroblast growth factor 4	Fgf4	14.41	15.72	-2.47
Paired-like homeodomain transcription factor 2	Pitx2	12.19	13.33	-2.20
Wingless-related MMTV integration site 2	Wnt2	12.01	13.1	-2.14
Amino-terminal enhancer of split	Aes	1.46	2.38	-1.88
Pygopus 1	Pygo1	5.64	6.5	-1.81
SRY-box containing gene 17	Sox17	6.79	7.58	-1.73
Frizzled homolog 4 (Drosophila)	Fzd4	3.45	4.21	-1.70
Protein phosphatase 2, regulatory subunit B (B56), delta isoform	Ppp2r5d	3.68	4.43	-1.67
Protein phosphatase 2 (formerly 2A), regulatory subunit A (PR 65), alpha isoform	Ppp2r1a	1.42	1.99	-1.49
F-box and WD-40 domain protein 11	Fbxw11	3.99	4.56	-1.48
DIX domain containing 1	Dixdc1	6.26	6.81	-1.46
Frizzled homolog 6 (Drosophila)	Fzd6	4.97	5.48	-1.43
Catenin (cadherin associated protein), beta 1	Ctnnb1	0.82	1.33	-1.42
Dishevelled associated activator of morphogenesis 1	Daam1	2.66	3.09	-1.35
Naked cuticle 1 homolog (Drosophila)	Nkd1	8.11	8.44	-1.26

Cyclin D2	Ccnd2	2.75	3.05	-1.23
Porcupine homolog (Drosophila)	Porcn	7.09	7.38	-1.22
Casein kinase 1, alpha 1	Csnk1a1	2.26	2.53	-1.20
Cyclin D1	Ccnd1	3.75	4	-1.18
Protein phosphatase 2 (formerly 2A), catalytic subunit, alpha isoform	Ppp2ca	1.22	1.42	-1.15
C-terminal binding protein 1	Ctbp1	2.66	2.81	-1.11
Low density lipoprotein receptor-related protein 6	Lrp6	3.45	3.59	-1.10
Beta-transducin repeat containing protein	Btrc	5.43	5.56	-1.09
Transducin-like enhancer of split 1, homolog of Drosophila E(spl)	Tle1	5.26	5.32	-1.04
Wingless related MMTV integration site 10a	Wnt10a	N/A	N/A	N/A
Wingless-related MMTV integration site 3	Wnt3	N/A	N/A	N/A
Wingless-related MMTV integration site 3A	Wnt3a	N/A	N/A	N/A
Wingless-related MMTV integration site 7B	Wnt7b	N/A	N/A	N/A
Wingless-related MMTV integration site 8A	Wnt8a	N/A	N/A	N/A

- *Table 2A: Wnt signaling pathway array- remote area post-MI day 1*

Wnt signaling qRT-PCR array (Remote area)				
Gene description	**Symbol**	**Day 1 (AVG ÄCt)**		
		Sham	**post-MI**	**Fold change**
Myelocytomatosis oncogene	**Myc**	**8.86**	**6.92**	**3.84***
WNT1 inducible signaling pathway protein 1	**Wisp1**	**7.83**	**6.4**	**2.68***
Frizzled homolog 1 (Drosophila)	**Fzd1**	**6.4**	**5.79**	**1.53***
Ras homolog gene family, member U	**Rhou**	**8.3**	**7.85**	**1.36***
Solute carrier family 9 (sodium/hydrogen exchanger), member 3 regulator 1	Slc9a3r1	7.84	6.87	1.97
Beta-transducin repeat containing protein	Btrc	7.09	6.5	1.51
Wingless-related MMTV integration site 4	Wnt4	10.8	10.24	1.43
Fos-like antigen 1	Fosl1	6.57	6.06	1.42
Secreted frizzled-related protein 1	Sfrp1	6.82	6.33	1.40
Frizzled-related protein	Frzb	4.98	4.63	1.28
Cyclin D1	Ccnd1	4.9	4.62	1.22
Casein kinase 1, alpha 1	Csnk1a1	1.96	1.73	1.17
Kringle containing transmembrane protein 1	Kremen1	1.52	1.29	1.17

Casein kinase 1, delta	Csnk1d	3.68	3.48	1.15
Jun oncogene	Jun	2.53	2.35	1.13
F-box and WD-40 domain protein 11	Fbxw11	6	5.85	1.11
Frizzled homolog 2 (Drosophila)	Fzd2	7.36	7.2	1.11
Frizzled homolog 4 (Drosophila)	Fzd4	4.59	4.53	1.05
Axin 1	Axin1	4.77	4.73	1.03
Dishevelled, dsh homolog 1 (Drosophila)	Dvl1	5.91	5.88	1.03
B-cell CLL/lymphoma 9	Bcl9	5.24	5.22	1.01
Frizzled homolog 7 (Drosophila)	Fzd7	8.05	8.04	1.01
Secreted frizzled-related protein 2	Sfrp2	5.61	5.59	1.01
Frequently rearranged in advanced T-cell lymphomas	**Frat1**	**6.85**	**8.23**	**-2.6***
Wingless related MMTV integration site 2b	**Wnt2b**	**6.42**	**7.63**	**-2.3***
Amino-terminal enhancer of split	**Aes**	**0.43**	**1.36**	**-1.9***
Wingless-related MMTV integration site 11	**Wnt11**	**6.9**	**7.84**	**-1.93***
Casein kinase 2, alpha 1 polypeptide	**Csnk2a1**	**1.55**	**2.35**	**-1.73***
Wingless-related MMTV integration site 16	**Wnt16**	**10.3**	**11.03**	**-1.68***
Frizzled homolog 3 (Drosophila)	**Fzd3**	**7.65**	**8.38**	**-1.66***
Wingless related MMTV integration site 8b	Wnt8b	12.5	15.04	-5.88
Follicle stimulating hormone beta	Fshb	12.3	14.4	-4.38
Forkhead box N1	Foxn1	12.1	14.14	-4.21
Pygopus 1	Pygo1	4.71	6.05	-2.52
Wingless-related MMTV integration site 7A	Wnt7a	13.4	14.5	-2.20
Secreted frizzled-related protein 4	Sfrp4	11.3	12.17	-1.86
Wingless-related MMTV integration site 2	Wnt2	12	12.84	-1.78
Wingless-related MMTV integration site 5A	Wnt5a	8.44	9.23	-1.73
Wingless-related MMTV integration site 1	Wnt1	13	13.79	-1.72
Wingless-type MMTV integration site 9A	Wnt9a	8.69	9.47	-1.72
Dishevelled associated activator of morphogenesis 1	Daam1	1.6	2.36	-1.69
Transducin-like enhancer of split 2, homolog of Drosophila E(spl)	Tle2	8.79	9.54	-1.68
Protein phosphatase 2, regulatory subunit B (B56), delta isoform	Ppp2r5d	4.22	4.93	-1.63
DIX domain containing 1	Dixdc1	5.45	6.11	-1.58
Low density lipoprotein receptor-related protein 6	Lrp6	3.16	3.81	-1.57
Wingless-related MMTV integration site 6	Wnt6	11.7	12.26	-1.50
Catenin (cadherin associated protein), beta 1	Ctnnb1	1.54	2.11	-1.49
Catenin beta interacting protein 1	Ctnnbip1	5.24	5.81	-1.48
Frizzled homolog 8 (Drosophila)	Fzd8	9.09	9.63	-1.45
Paired-like homeodomain transcription factor 2	Pitx2	11.9	12.41	-1.45

Transcription factor 7, T-cell specific	Tcf7	7.69	8.19	-1.41
C-terminal binding protein 1	Ctbp1	2.02	2.48	-1.37
F-box and WD-40 domain protein 2	Fbxw2	3.01	3.47	-1.37
Glycogen synthase kinase 3 beta	Gsk3b	5.78	6.22	-1.36
Dishevelled 2, dsh homolog (Drosophila)	Dvl2	6.64	7.05	-1.32
Wnt inhibitory factor 1	Wif1	6.18	6.58	-1.32
Frizzled homolog 6 (Drosophila)	Fzd6	5.35	5.74	-1.31
Cyclin D2	Ccnd2	2.63	3	-1.29
Lymphoid enhancer binding factor 1	Lef1	10.4	10.8	-1.29
Protein phosphatase 2 (formerly 2A), catalytic subunit, alpha isoform	Ppp2ca	0.66	1.02	-1.29
SUMO/sentrin specific peptidase 2	Senp2	6.39	6.75	-1.28
Wingless-related MMTV integration site 5B	Wnt5b	6.11	6.47	-1.28
Low density lipoprotein receptor-related protein 5	Lrp5	4.27	4.62	-1.27
F-box and WD-40 domain protein 4	Fbxw4	5.59	5.89	-1.23
Adenomatosis polyposis coli	Apc	4.23	4.52	-1.22
Transducin-like enhancer of split 1, homolog of Drosophila E(spl)	Tle1	5.68	5.95	-1.20
Protein phosphatase 2 (formerly 2A), regulatory subunit A (PR 65), alpha isoform	Ppp2r1a	1.26	1.47	-1.15
Porcupine homolog (Drosophila)	Porcn	6.92	7.11	-1.14
C-terminal binding protein 2	Ctbp2	2.87	3.04	-1.13
SRY-box containing gene 17	Sox17	7.31	7.49	-1.13
Frizzled homolog 5 (Drosophila)	Fzd5	6.6	6.73	-1.10
Nemo like kinase	Nlk	7.57	7.69	-1.09
Transcription factor 3	Tcf3	6.32	6.42	-1.07
Cyclin D3	Ccnd3	2.8	2.86	-1.05
E1A binding protein p300	Ep300	4.79	4.83	-1.03
Naked cuticle 1 homolog (Drosophila)	Nkd1	7.78	7.81	-1.02
Dickkopf homolog 1 (Xenopus laevis)	Dkk1	N/A	N/A	N/A
Fibroblast growth factor 4	Fgf4	N/A	N/A	N/A
Brachyury	T	N/A	N/A	N/A
Wingless related MMTV integration site 10a	Wnt10a	N/A	N/A	N/A
Wingless-related MMTV integration site 3	Wnt3	N/A	N/A	N/A
Wingless-related MMTV integration site 3A	Wnt3a	N/A	N/A	N/A
Wingless-related MMTV integration site 7B	Wnt7b	N/A	N/A	N/A
Wingless-related MMTV integration site 8A	Wnt8a	N/A	N/A	N/A

- *Table 2B: Wnt signaling pathway array- remote area post-MI day 3*

Wnt signaling qRT-PCR array (Remote area)				
Gene description	**Symbol**	**Day 3 (AVG ÄCt)**		
		Sham	**post-MI**	**Fold change**
WNT1 inducible signaling pathway protein 1	**Wisp1**	**7.83**	**4.95**	**7.33***
Secreted frizzled-related protein 1	**Sfrp1**	**6.82**	**5.15**	**3.18***
Secreted frizzled-related protein 2	**Sfrp2**	**5.61**	**4.43**	**2.27***
Ras homolog gene family, member U	**Rhou**	**8.3**	**7.35**	**1.92***
Wingless-related MMTV integration site 7A	Wnt7a	13.4	11.35	4.03
Wingless-related MMTV integration site 1	Wnt1	13	11.68	2.53
Solute carrier family 9 (sodium/hydrogen exchanger), member 3 regulator 1	Slc9a3r1	7.84	6.6	2.37
Wingless-related MMTV integration site 4	Wnt4	10.8	10	1.69
Frizzled-related protein	Frzb	4.98	4.33	1.57
Frizzled homolog 1 (Drosophila)	Fzd1	6.4	5.84	1.47
Frizzled homolog 2 (Drosophila)	Fzd2	7.36	7.13	1.17
Fos-like antigen 1	Fosl1	6.57	6.44	1.10
Cyclin D1	Ccnd1	4.9	4.89	1.01
Follicle stimulating hormone beta	**Fshb**	**12.3**	**16.11**	**-14.31***
DIX domain containing 1	**Dixdc1**	**5.45**	**7.58**	**-4.38***
Transducin-like enhancer of split 2, homolog of Drosophila E(spl)	**Tle2**	**8.79**	**10.82**	**-4.09***
Myelocytomatosis oncogene	**Myc**	**8.86**	**6.83**	**4.09***
Frequently rearranged in advanced T-cell lymphomas	**Frat1**	**6.85**	**8.81**	**-3.89***
Pygopus 1	**Pygo1**	**4.71**	**6.49**	**-3.43***
Amino-terminal enhancer of split	**Aes**	**0.43**	**2.18**	**-3.36***
Wingless related MMTV integration site 2b	**Wnt2b**	**6.42**	**8.08**	**-3.15***
SRY-box containing gene 17	**Sox17**	**7.31**	**8.92**	**-3.05***
Dishevelled associated activator of morphogenesis 1	**Daam1**	**1.6**	**3.08**	**-2.80***
Frizzled homolog 4 (Drosophila)	**Fzd4**	**4.59**	**6.02**	**-2.69***
Cyclin D2	**Ccnd2**	**2.63**	**4.04**	**-2.66***
Frizzled homolog 6 (Drosophila)	**Fzd6**	**5.35**	**6.74**	**-2.63***
Casein kinase 2, alpha 1 polypeptide	**Csnk2a1**	**1.55**	**2.83**	**-2.42***
Frizzled homolog 8 (Drosophila)	**Fzd8**	**9.09**	**10.35**	**-2.39***
C-terminal binding protein 1	**Ctbp1**	**2.02**	**3.22**	**-2.30***
Porcupine homolog (Drosophila)	**Porcn**	**6.92**	**8.03**	**-2.15***
Dishevelled, dsh homolog 1 (Drosophila)	**Dvl1**	**5.91**	**7**	**-2.12***
Catenin beta interacting protein 1	**Ctnnbip1**	**5.24**	**6.21**	**-1.96***
Frizzled homolog 3 (Drosophila)	**Fzd3**	**7.65**	**8.62**	**-1.95***

Low density lipoprotein receptor-related protein 6	**Lrp6**	**3.16**	**4.12**	**-1.94***
F-box and WD-40 domain protein 2	**Fbxw2**	**3.01**	**3.96**	**-1.93***
Glycogen synthase kinase 3 beta	**Gsk3b**	**5.78**	**6.73**	**-1.93***
Catenin (cadherin associated protein), beta 1	**Ctnnb1**	**1.54**	**2.42**	**-1.84***
Protein phosphatase 2 (formerly 2A), catalytic subunit, alpha isoform	**Ppp2ca**	**0.66**	**1.43**	**-1.71***
Axin 1	**Axin1**	**4.77**	**5.48**	**-1.63***
C-terminal binding protein 2	**Ctbp2**	**2.87**	**3.51**	**-1.56***
Transducin-like enhancer of split 1, homolog of Drosophila E(spl)	**Tle1**	**5.68**	**6.28**	**-1.52***
Adenomatosis polyposis coli	**Apc**	**4.23**	**4.83**	**-1.51***
E1A binding protein p300	**Ep300**	**4.79**	**5.35**	**-1.48***
Low density lipoprotein receptor-related protein 5	**Lrp5**	**4.27**	**4.84**	**-1.48***
SUMO/sentrin specific peptidase 2	**Senp2**	**6.39**	**6.96**	**-1.48***
Wingless related MMTV integration site 8b	Wnt8b	12.5	15.58	-8.57
Forkhead box N1	Foxn1	12.1	14.75	-6.45
Paired-like homeodomain transcription factor 2	Pitx2	11.9	13.38	-2.83
Wingless-type MMTV integration site 9A	Wnt9a	8.69	10.17	-2.79
Wnt inhibitory factor 1	Wif1	6.18	7.53	-2.56
Wingless-related MMTV integration site 2	Wnt2	12	13.35	-2.54
Wingless-related MMTV integration site 16	Wnt16	10.3	11.45	-2.24
Wingless-related MMTV integration site 6	Wnt6	11.7	12.8	-2.18
Wingless-related MMTV integration site 5A	Wnt5a	8.44	9.51	-2.10
Beta-transducin repeat containing protein	Btrc	7.09	8.1	-2.01
Dishevelled 2, dsh homolog (Drosophila)	Dvl2	6.64	7.58	-1.91
Protein phosphatase 2, regulatory subunit B (B56), delta isoform	Ppp2r5d	4.22	5.15	-1.90
B-cell CLL/lymphoma 9	Bcl9	5.24	6.09	-1.80
F-box and WD-40 domain protein 4	Fbxw4	5.59	6.39	-1.74
Nemo like kinase	Nlk	7.57	8.37	-1.74
Wingless-related MMTV integration site 11	Wnt11	6.9	7.59	-1.61
Frizzled homolog 7 (Drosophila)	Fzd7	8.05	8.68	-1.54
Naked cuticle 1 homolog (Drosophila)	Nkd1	7.78	8.4	-1.54
Protein phosphatase 2 (formerly 2A), regulatory subunit A (PR 65), alpha isoform	Ppp2r1a	1.26	1.81	-1.46
Wingless-related MMTV integration site 5B	Wnt5b	6.11	6.62	-1.42
Casein kinase 1, alpha 1	Csnk1a1	1.96	2.45	-1.40
Kringle containing transmembrane protein 1	Kremen1	1.52	1.94	-1.34
Cyclin D3	Ccnd3	2.8	3.2	-1.32
Transcription factor 7, T-cell specific	Tcf7	7.69	8.07	-1.30
F-box and WD-40 domain protein 11	Fbxw11	6	6.37	-1.29
Transcription factor 3	Tcf3	6.32	6.67	-1.27

Jun oncogene	Jun	2.53	2.86	-1.25
Secreted frizzled-related protein 4	Sfrp4	11.3	11.49	-1.16
Casein kinase 1, delta	Csnk1d	3.68	3.83	-1.11
Frizzled homolog 5 (Drosophila)	Fzd5	6.6	6.71	-1.08
Lymphoid enhancer binding factor 1	Lef1	10.4	10.53	-1.07
Dickkopf homolog 1 (Xenopus laevis)	Dkk1	N/A	N/A	N/A
Fibroblast growth factor 4	Fgf4	N/A	N/A	N/A
Brachyury	T	N/A	N/A	N/A
Wingless related MMTV integration site 10a	Wnt10a	N/A	N/A	N/A
Wingless-related MMTV integration site 3	Wnt3	N/A	N/A	N/A
Wingless-related MMTV integration site 3A	Wnt3a	N/A	N/A	N/A
Wingless-related MMTV integration site 7B	Wnt7b	N/A	N/A	N/A
Wingless-related MMTV integration site 8A	Wnt8a	N/A	N/A	N/A

- *Table 2C: Wnt signaling pathway array- remote area post-MI day 7*

Wnt signaling qRT-PCR array (Remote area)				
Gene description	**Symbol**	**Day 7 (AVG ÄCt)**		
		Sham	**post-MI**	**Fold change**
Cyclin D1	**Ccnd1**	**4.9**	**2.81**	**4.25***
Secreted frizzled-related protein 2	**Sfrp2**	**5.61**	**3.89**	**3.28***
Myelocytomatosis oncogene	**Myc**	**8.86**	**7.68**	**2.26***
Frizzled homolog 2 (Drosophila)	**Fzd2**	**7.36**	**6.63**	**1.66***
Ras homolog gene family, member U	**Rhou**	**8.3**	**7.82**	**1.39***
Beta-transducin repeat containing protein	Btrc	7.09	5.67	2.66
Solute carrier family 9 (sodium/hydrogen exchanger), member 3 regulator 1	Slc9a3r1	7.84	6.91	1.91
Wingless-related MMTV integration site 1	Wnt1	13.01	12.25	1.70
Glycogen synthase kinase 3 beta	Gsk3b	5.78	5.02	1.68
WNT1 inducible signaling pathway protein 1	Wisp1	7.83	7.1	1.66
F-box and WD-40 domain protein 11	Fbxw11	6	5.28	1.65
Frizzled homolog 1 (Drosophila)	Fzd1	6.4	5.79	1.53
Cyclin D3	Ccnd3	2.8	2.35	1.36
F-box and WD-40 domain protein 4	Fbxw4	5.59	5.2	1.31
Amino-terminal enhancer of split	Aes	0.43	0.11	1.24
Cyclin D2	Ccnd2	2.63	2.42	1.15
Jun oncogene	Jun	2.53	2.35	1.13
Nemo like kinase	Nlk	7.57	7.44	1.09

Frizzled homolog 4 (Drosophila)	Fzd4	4.59	4.47	1.08
Casein kinase 1, alpha 1	Csnk1a1	1.96	1.86	1.07
B-cell CLL/lymphoma 9	Bcl9	5.24	5.19	1.04
Wingless-related MMTV integration site 16	**Wnt16**	**10.28**	**11.96**	**-3.21***
DIX domain containing 1	**Dixdc1**	**5.45**	**7.11**	**-3.16***
Frequently rearranged in advanced T-cell lymphomas	**Frat1**	**6.85**	**8.4**	**-2.92***
Secreted frizzled-related protein 1	**Sfrp1**	**6.82**	**5.37**	**2.73***
Pygopus 1	**Pygo1**	**4.71**	**6.13**	**-2.67***
Wingless-related MMTV integration site 11	**Wnt11**	**6.9**	**7.86**	**-1.96***
Frizzled homolog 6 (Drosophila)	**Fzd6**	**5.35**	**5.95**	**-1.52***
Dishevelled, dsh homolog 1 (Drosophila)	Dvl1	5.91	9.06	-8.86
Wingless related MMTV integration site 2b	Wnt2b	6.42	9.36	-7.68
Transcription factor 3	Tcf3	6.32	8.66	-5.07
Follicle stimulating hormone beta	Fshb	12.27	14.31	-4.11
Forkhead box N1	Foxn1	12.06	13.94	-3.67
Wingless related MMTV integration site 8b	Wnt8b	12.48	14.25	-3.40
Transcription factor 7, T-cell specific	Tcf7	7.69	9.39	-3.24
Casein kinase 2, alpha 1 polypeptide	Csnk2a1	1.55	3.02	-2.76
Wingless-related MMTV integration site 7A	Wnt7a	13.36	14.79	-2.70
Frizzled-related protein	Frzb	4.98	6.39	-2.66
Paired-like homeodomain transcription factor 2	Pitx2	11.87	13.27	-2.64
Wingless-related MMTV integration site 6	Wnt6	11.67	12.96	-2.45
Wingless-type MMTV integration site 9A	Wnt9a	8.69	9.95	-2.41
Naked cuticle 1 homolog (Drosophila)	Nkd1	7.78	9.01	-2.34
Frizzled homolog 8 (Drosophila)	Fzd8	9.09	10.28	-2.29
Wnt inhibitory factor 1	Wif1	6.18	7.26	-2.13
Lymphoid enhancer binding factor 1	Lef1	10.43	11.45	-2.03
Dishevelled associated activator of morphogenesis 1	Daam1	1.6	2.58	-1.98
Fos-like antigen 1	Fosl1	6.57	7.51	-1.92
Protein phosphatase 2 (formerly 2A), catalytic subunit, alpha isoform	Ppp2ca	0.66	1.59	-1.91
F-box and WD-40 domain protein 2	Fbxw2	3.01	3.75	-1.67
E1A binding protein p300	Ep300	4.79	5.49	-1.63
Secreted frizzled-related protein 4	Sfrp4	11.28	11.98	-1.62
Protein phosphatase 2 (formerly 2A), regulatory subunit A (PR 65), alpha isoform	Ppp2r1a	1.26	1.95	-1.61
Axin 1	Axin1	4.77	5.44	-1.59
Frizzled homolog 5 (Drosophila)	Fzd5	6.6	7.26	-1.59
C-terminal binding protein 2	Ctbp2	2.87	3.52	-1.58
Wingless-related MMTV integration site 2	Wnt2	12.01	12.65	-1.56
Wingless-related MMTV integration site 5A	Wnt5a	8.44	9.01	-1.49

Wingless-related MMTV integration site 5B	Wnt5b	6.11	6.68	-1.48
Porcupine homolog (Drosophila)	Porcn	6.92	7.47	-1.47
Low density lipoprotein receptor-related protein 6	Lrp6	3.16	3.71	-1.46
Frizzled homolog 3 (Drosophila)	Fzd3	7.65	8.17	-1.43
Kringle containing transmembrane protein 1	Kremen1	1.52	1.97	-1.37
SRY-box containing gene 17	Sox17	7.31	7.77	-1.37
Protein phosphatase 2, regulatory subunit B (B56), delta isoform	Ppp2r5d	4.22	4.67	-1.36
Dishevelled 2, dsh homolog (Drosophila)	Dvl2	6.64	7.06	-1.33
SUMO/sentrin specific peptidase 2	Senp2	6.39	6.8	-1.32
Catenin (cadherin associated protein), beta 1	Ctnnb1	1.54	1.91	-1.29
C-terminal binding protein 1	Ctbp1	2.02	2.33	-1.24
Adenomatosis polyposis coli	Apc	4.23	4.53	-1.23
Catenin beta interacting protein 1	Ctnnbip1	5.24	5.5	-1.19
Casein kinase 1, delta	Csnk1d	3.68	3.81	-1.09
Transducin-like enhancer of split 1, homolog of Drosophila E(spl)	Tle1	5.68	5.78	-1.07
Frizzled homolog 7 (Drosophila)	Fzd7	8.05	8.11	-1.04
Wingless-related MMTV integration site 4	Wnt4	10.76	10.77	-1.01
Low density lipoprotein receptor-related protein 5	Lrp5	4.27	4.27	-1.00
Transducin-like enhancer of split 2, homolog of Drosophila E(spl)	Tle2	8.79	8.79	-1.00
Dickkopf homolog 1 (Xenopus laevis)	Dkk1	N/A	N/A	N/A
Fibroblast growth factor 4	Fgf4	N/A	N/A	N/A
Brachyury	T	N/A	N/A	N/A
Wingless related MMTV integration site 10a	Wnt10a	N/A	N/A	N/A
Wingless-related MMTV integration site 3	Wnt3	N/A	N/A	N/A
Wingless-related MMTV integration site 3A	Wnt3a	N/A	N/A	N/A
Wingless-related MMTV integration site 7B	Wnt7b	N/A	N/A	N/A
Wingless-related MMTV integration site 8A	Wnt8a	N/A	N/A	N/A

- *Table 3A: Wnt signaling pathway array- CSP cells post-MI day 1*

Wnt signaling qRT-PCR array (CSP cells)				
Gene description	**Symbol**	**Day 1 (AVG ÄCt)**		
		Sham	**post-MI**	**Fold change**
Casein kinase 1, delta	**Csnk1d**	***2.59***	***3.22***	**-1.55***

Jun oncogene	Jun	*-2.42*	*-2.38*	-1.02
F-box and WD-40 domain protein 11	Fbxw11	*5.69*	*5.72*	-1.02
Secreted frizzled-related protein 4	Sfrp4	*5.67*	*5.72*	-1.03
Amino-terminal enhancer of split	Aes	*3.42*	*3.48*	-1.04
Cyclin D3	Ccnd3	*2.18*	*2.24*	-1.04
Transducin-like enhancer of split 1, homolog of Drosophila E(spl)	Tle1	*4.56*	*4.69*	-1.09
Casein kinase 1, alpha 1	Csnk1a1	*2.04*	*2.18*	-1.10
Frizzled homolog 1 (Drosophila)	Fzd1	*2.86*	*3.01*	-1.10
Low density lipoprotein receptor-related protein 6	Lrp6	*2.76*	*2.92*	-1.11
Protein phosphatase 2a, regulatory subunit A (PR 65)	Ppp2r1a	*1.53*	*1.71*	-1.12
Casein kinase 2, alpha 1 polypeptide	Csnk2a1	*2.48*	*2.64*	-1.12
Protein phosphatase 2 (formerly 2A), catalytic subunit, alpha isoform	Ppp2ca	*1.39*	*1.58*	-1.14
Dishevelled 2, dsh homolog (Drosophila)	Dvl2	*4.31*	*4.52*	-1.15
Kringle containing transmembrane protein 1	Kremen1	*2.43*	*2.67*	-1.17
C-terminal binding protein 1	Ctbp1	*1.62*	*1.90*	-1.21
Wingless-related MMTV integration site 4	Wnt4	*5.44*	*5.72*	-1.21
Secreted frizzled-related protein 2	Sfrp2	*2.07*	*2.37*	-1.22
Ras homolog gene family, member U	Rhou	*4.83*	*5.14*	-1.24
Secreted frizzled-related protein 1	Sfrp1	*3.66*	*4.00*	-1.26
Fos-like antigen 1	Fosl1	*2.72*	*3.08*	-1.27
Dishevelled, dsh homolog 1 (Drosophila)	Dvl1	*5.01*	*5.37*	-1.28
Catenin (cadherin associated protein), beta 1	Ctnnb1	*0.37*	*0.78*	-1.33
SUMO/sentrin specific peptidase 2	Senp2	*5.31*	*5.72*	-1.33
Low density lipoprotein receptor-related protein 5	Lrp5	*2.51*	*2.97*	-1.37
Frizzled homolog 7 (Drosophila)	Fzd7	*3.80*	*4.26*	-1.37
Frizzled homolog 2 (Drosophila)	Fzd2	*5.67*	*5.20*	1.38
Transcription factor 3	Tcf3	*4.69*	*5.17*	-1.39
Frizzled homolog 4 (Drosophila)	Fzd4	*3.50*	*3.98*	-1.39
C-terminal binding protein 2	Ctbp2	*1.93*	*2.41*	-1.39
Protein phosphatase 2d, regulatory subunit B (B56)	Ppp2r5d	*3.18*	*3.70*	-1.43
Axin 1	Axin1	*3.51*	*4.13*	-1.53

Catenin beta interacting protein 1	Ctnnbip1	*4.56*	*5.22*	-1.57
WNT1 inducible signaling pathway protein 1	Wisp1	*5.02*	*5.72*	-1.63
Frizzled homolog 5 (Drosophila)	Fzd5	*4.04*	*4.78*	-1.67
E1A binding protein p300	Ep300	*4.61*	*5.37*	-1.68
Cyclin D1	Ccnd1	*4.52*	*5.27*	-1.68
Frizzled homolog 6 (Drosophila)	Fzd6	*4.48*	*5.28*	-1.73
Naked cuticle 1 homolog (Drosophila)	Nkd1	*3.89*	*4.87*	-1.98
Adenomatosis polyposis coli	Apc	*4.03*	*5.24*	-2.30
Solute carrier family 9 (sodium/hydrogen exchanger), member 3 regulator 1	Slc9a3r1	*5.53*	*5.53*	1.00
Myelocytomatosis oncogene	Myc	*2.90*	*2.89*	1.00
F-box and WD-40 domain protein 2	Fbxw2	*3.22*	*3.20*	1.01
B-cell CLL/lymphoma 9	Bcl9	*5.76*	*5.72*	1.02
Lymphoid enhancer binding factor 1	Lef1	*5.76*	*5.72*	1.02
Frizzled homolog 8 (Drosophila)	Fzd8	*5.77*	*5.72*	1.03
Cyclin D2	Ccnd2	*2.72*	*2.65*	1.05
SRY-box containing gene 17	Sox17	*3.75*	*3.66*	1.06
Wingless-type MMTV integration site 9A	Wnt9a	*5.81*	*5.72*	1.06
Pygopus 1	Pygo1	*5.69*	*5.59*	1.07
Wingless-related MMTV integration site 11	Wnt11	*4.33*	*4.23*	1.07
Dishevelled associated activator of morphogenesis 1	Daam1	*3.57*	*3.45*	1.08
Wingless related MMTV integration site 2b	Wnt2b	*5.15*	*5.00*	1.10
F-box and WD-40 domain protein 4	Fbxw4	*5.87*	*5.72*	1.10
Frizzled homolog 3 (Drosophila)	Fzd3	*5.89*	*5.72*	1.12
DIX domain containing 1	Dixdc1	*5.61*	*5.40*	1.15
Glycogen synthase kinase 3 beta	Gsk3b	*5.97*	*5.72*	1.18
Beta-transducin repeat containing protein	Btrc	*6.03*	*5.72*	1.23
Frizzled-related protein	Frzb	*2.15*	*1.81*	1.26
Porcupine homolog (Drosophila)	Porcn	*6.03*	*5.64*	1.30
Wingless-related MMTV integration site 5B	Wnt5b	*5.56*	*5.16*	1.32
Wingless-related MMTV integration site 5A	Wnt5a	*6.15*	*5.72*	1.34
Transcription factor 7, T-cell specific	Tcf7	*5.86*	*5.21*	1.57
Follicle stimulating hormone beta	Fshb	*6.17*	*5.51*	1.58
Wingless-related MMTV integration site 16	Wnt16	*6.17*	*5.44*	1.65
Wnt inhibitory factor 1	Wif1	*4.42*	*3.08*	2.52
Dickkopf homolog 1 (Xenopus laevis)	Dkk1	N/A	N/A	N/A

Fibroblast growth factor 4	Fgf4	N/A	N/A	N/A
Forkhead box N1	Foxn1	N/A	N/A	N/A
Frequently rearranged in advanced T-cell lymphomas	Frat1	N/A	N/A	N/A
Nemo like kinase	Nlk	N/A	N/A	N/A
Paired-like homeodomain transcription factor 2	Pitx2	N/A	N/A	N/A
Brachyury	T	N/A	N/A	N/A
Transducin-like enhancer of split 2, homolog of Drosophila E(spl)	Tle2	N/A	N/A	N/A
Wingless-related MMTV integration site 1	Wnt1	N/A	N/A	N/A
Wingless related MMTV integration site 10a	Wnt10a	N/A	N/A	N/A
Wingless-related MMTV integration site 2	Wnt2	N/A	N/A	N/A
Wingless-related MMTV integration site 3	Wnt3	N/A	N/A	N/A
Wingless-related MMTV integration site 3A	Wnt3a	N/A	N/A	N/A
Wingless-related MMTV integration site 6	Wnt6	N/A	N/A	N/A
Wingless-related MMTV integration site 7A	Wnt7a	N/A	N/A	N/A
Wingless-related MMTV integration site 7B	Wnt7b	N/A	N/A	N/A
Wingless-related MMTV integration site 8A	Wnt8a	N/A	N/A	N/A
Wingless related MMTV integration site 8b	Wnt8b	N/A	N/A	N/A

- *Table 3B: Wnt signaling pathway array- CSP cells post-MI day 3*

Wnt signaling qRT-PCR array (CSP cells)				
Gene description	**Symbol**	**Day 3 (AVG ÄCt)**		**Fold change**
		Sham	**post-MI**	
Frizzled homolog 6 (Drosophila)	**Fzd6**	***4.48***	***6.44***	**-3.89***
SRY-box containing gene 17	**Sox17**	***3.75***	***5.44***	**-3.23***
Secreted frizzled-related protein 4	**Sfrp4**	***5.66***	***7.29***	**-3.00***
E1A binding protein p300	**Ep300**	***4.61***	***6.02***	**-2.66***
Transcription factor 3	**Tcf3**	***4.68***	***6.09***	**-2.65***
Amino-terminal enhancer of split	**Aes**	***3.42***	***4.75***	**-2.52***
Dishevelled 2, dsh homolog (Drosophila)	**Dvl2**	***4.30***	***5.47***	**-2.25***
Adenomatosis polyposis coli	**Apc**	***4.03***	***5.07***	**-2.07***

Frizzled homolog 5 (Drosophila)	**Fzd5**	***4.03***	***5.03***	**-1.99***
Ras homolog gene family, member U	Rhou	*4.83*	*4.84*	-1.00
Frizzled-related protein	Frzb	*2.15*	*2.18*	-1.01
Frizzled homolog 1 (Drosophila)	Fzd1	*2.86*	*2.91*	-1.03
Casein kinase 1, alpha 1	Csnk1a1	*2.04*	*2.23*	-1.13
Wingless-related MMTV integration site 11	Wnt11	*4.33*	*4.52*	-1.14
Transducin-like enhancer of split 1, homolog of Drosophila E(spl)	Tle1	*4.56*	*4.79*	-1.16
Myelocytomatosis oncogene	Myc	*2.90*	*3.16*	-1.19
Secreted frizzled-related protein 1	Sfrp1	*3.66*	*3.96*	-1.22
Cyclin D1	Ccnd1	*4.52*	*4.85*	-1.25
Protein phosphatase 2a, regulatory subunit A (PR 65)	Ppp2r1a	*1.53*	*1.91*	-1.29
F-box and WD-40 domain protein 2	Fbxw2	*3.22*	*3.61*	-1.30
Wnt inhibitory factor 1	Wif1	*4.42*	*4.85*	-1.34
SUMO/sentrin specific peptidase 2	Senp2	*5.31*	*5.74*	-1.34
Fos-like antigen 1	Fosl1	*2.72*	*3.19*	-1.38
C-terminal binding protein 1	Ctbp1	*1.62*	*2.10*	-1.39
Low density lipoprotein receptor-related protein 6	Lrp6	*2.76*	*3.26*	-1.40
Dishevelled associated activator of morphogenesis 1	Daam1	*3.57*	*4.12*	-1.45
Transcription factor 7, T-cell specific	Tcf7	*5.86*	*6.42*	-1.47
F-box and WD-40 domain protein 11	Fbxw11	*5.69*	*6.32*	-1.54
Axin 1	Axin1	*3.51*	*4.15*	-1.55
Catenin (cadherin associated protein), beta 1	Ctnnb1	*0.37*	*1.03*	-1.57
Kringle containing transmembrane protein 1	Kremen1	*2.43*	*3.13*	-1.61
Frizzled homolog 2 (Drosophila)	Fzd2	*5.67*	*6.36*	-1.61
Casein kinase 1, delta	Csnk1d	*2.59*	*3.31*	-1.63
Solute carrier family 9 (sodium/hydrogen exchanger), member 3 regulator 1	Slc9a3r1	*5.53*	*6.25*	-1.64
C-terminal binding protein 2	Ctbp2	*1.93*	*2.72*	-1.72
Glycogen synthase kinase 3 beta	Gsk3b	*5.97*	*6.76*	-1.73
Wingless related MMTV integration site 2b	Wnt2b	*5.15*	*5.94*	-1.73

Cyclin D3	Ccnd3	*2.18*	*2.99*	-1.74
Wingless-related MMTV integration site 4	Wnt4	*5.44*	*6.25*	-1.75
Dishevelled, dsh homolog 1 (Drosophila)	Dvl1	*5.01*	*5.82*	-1.75
Casein kinase 2, alpha 1 polypeptide	Csnk2a1	*2.48*	*3.30*	-1.76
Low density lipoprotein receptor-related protein 5	Lrp5	*2.51*	*3.34*	-1.77
Wingless-related MMTV integration site 5A	Wnt5a	*6.15*	*7.00*	-1.80
Cyclin D2	Ccnd2	*2.72*	*3.59*	-1.82
Frizzled homolog 3 (Drosophila)	Fzd3	*5.89*	*6.83*	-1.91
Jun oncogene	Jun	*-2.42*	*-1.47*	-1.92
Porcupine homolog (Drosophila)	Porcn	*6.03*	*7.00*	-1.96
Frizzled homolog 8 (Drosophila)	Fzd8	*5.77*	*6.76*	-1.97
Frizzled homolog 7 (Drosophila)	Fzd7	*3.80*	*4.85*	-2.06
F-box and WD-40 domain protein 4	Fbxw4	*5.87*	*6.95*	-2.11
Wingless-type MMTV integration site 9A	Wnt9a	*5.81*	*6.90*	-2.11
Catenin beta interacting protein 1	Ctnnbip1	*4.56*	*5.70*	-2.20
Wingless-related MMTV integration site 5B	Wnt5b	*5.56*	*6.71*	-2.21
B-cell CLL/lymphoma 9	Bcl9	*5.76*	*6.94*	-2.25
Frizzled homolog 4 (Drosophila)	Fzd4	*3.50*	*4.69*	-2.27
Naked cuticle 1 homolog (Drosophila)	Nkd1	*3.89*	*5.07*	-2.27
DIX domain containing 1	Dixdc1	*5.61*	*6.81*	-2.28
Beta-transducin repeat containing protein	Btrc	*6.03*	*7.23*	-2.29
Lymphoid enhancer binding factor 1	Lef1	*5.76*	*7.15*	-2.61
Pygopus 1	Pygo1	*5.69*	*7.16*	-2.76
Secreted frizzled-related protein 2	Sfrp2	*2.07*	*1.57*	1.41
WNT1 inducible signaling pathway protein 1	Wisp1	*5.02*	*4.71*	1.23
Protein phosphatase 2d, regulatory subunit B (B56)	Ppp2r5d	*3.18*	*3.03*	1.11
Protein phosphatase 2 (formerly 2A), catalytic subunit, alpha isoform	Ppp2ca	*1.39*	*1.27*	1.08
Dickkopf homolog 1 (Xenopus laevis)	Dkk1	N/A	N/A	N/A

Fibroblast growth factor 4	Fgf4	N/A	N/A	N/A
Forkhead box N1	Foxn1	N/A	N/A	N/A
Frequently rearranged in advanced T-cell lymphomas	Frat1	N/A	N/A	N/A
Follicle stimulating hormone beta	Fshb	N/A	N/A	N/A
Nemo like kinase	Nlk	N/A	N/A	N/A
Paired-like homeodomain transcription factor 2	Pitx2	N/A	N/A	N/A
Brachyury	T	N/A	N/A	N/A
Transducin-like enhancer of split 2, homolog of Drosophila E(spl)	Tle2	N/A	N/A	N/A
Wingless-related MMTV integration site 1	Wnt1	N/A	N/A	N/A
Wingless related MMTV integration site 10a	Wnt10a	N/A	N/A	N/A
Wingless-related MMTV integration site 16	Wnt16	N/A	N/A	N/A
Wingless-related MMTV integration site 2	Wnt2	N/A	N/A	N/A
Wingless-related MMTV integration site 3	Wnt3	N/A	N/A	N/A
Wingless-related MMTV integration site 3A	Wnt3a	N/A	N/A	N/A
Wingless-related MMTV integration site 6	Wnt6	N/A	N/A	N/A
Wingless-related MMTV integration site 7A	Wnt7a	N/A	N/A	N/A
Wingless-related MMTV integration site 7B	Wnt7b	N/A	N/A	N/A
Wingless-related MMTV integration site 8A	Wnt8a	N/A	N/A	N/A
Wingless related MMTV integration site 8b	Wnt8b	N/A	N/A	N/A

- *Table 3C: Wnt signaling pathway array- CSP cells post-MI day 7*

Wnt signaling qRT-PCR array (CSP cells)				
Gene description	**Symbol**	**Day 7 (AVG ÄCt)**		**Fold change**
		Sham	**post-MI**	
Amino-terminal enhancer of split	Aes	2.77	4.74	**-3.91***
Cyclin D2	Ccnd2	2.13	3.58	**-2.74***
Casein kinase 1, alpha 1	Csnk1a1	1.99	2.87	**-1.83***

Wnt inhibitory factor 1	Wif1	3.50	4.34	**-1.78***
C-terminal binding protein 1	Ctbp1	1.73	2.36	**-1.54***
Catenin (cadherin associated protein), beta 1	Ctnnb1	0.09	0.47	**-1.30***
Protein phosphatase 2a, regulatory subunit A (PR 65)	Ppp2r1a	1.79	1.80	**-1.00**
Frizzled homolog 1 (Drosophila)	Fzd1	3.11	3.13	**-1.01**
Pygopus 1	Pygo1	5.13	5.17	**-1.02**
Transcription factor 3	Tcf3	4.80	4.84	**-1.02**
Casein kinase 2, alpha 1 polypeptide	Csnk2a1	2.83	2.88	**-1.03**
Solute carrier family 9 (sodium/hydrogen exchanger), member 3 regulator 1	Slc9a3r1	4.94	5.02	**-1.05**
Frizzled-related protein	Frzb	2.12	2.23	**-1.07**
Frizzled homolog 5 (Drosophila)	Fzd5	4.11	4.22	**-1.07**
Wingless-related MMTV integration site 11	Wnt11	4.53	4.66	**-1.09**
Dishevelled 2, dsh homolog (Drosophila)	Dvl2	4.16	4.31	**-1.10**
Frizzled homolog 3 (Drosophila)	Fzd3	5.09	5.34	**-1.18**
Myelocytomatosis oncogene	Myc	3.08	3.32	**-1.18**
Frizzled homolog 8 (Drosophila)	Fzd8	5.01	5.27	**-1.19**
Frizzled homolog 4 (Drosophila)	Fzd4	3.14	3.41	**-1.20**
Secreted frizzled-related protein 1	Sfrp1	3.78	4.06	**-1.21**
Secreted frizzled-related protein 4	Sfrp4	5.04	5.34	**-1.22**
Protein phosphatase 2d, regulatory subunit B (B56)	Ppp2r5d	3.04	3.37	**-1.24**
C-terminal binding protein 2	Ctbp2	1.86	2.25	**-1.31**
Casein kinase 1, delta	Csnk1d	2.82	3.26	**-1.35**
Low density lipoprotein receptor-related protein 6	Lrp6	2.57	3.01	**-1.35**
B-cell CLL/lymphoma 9	Bcl9	4.88	5.34	**-1.36**
Naked cuticle 1 homolog (Drosophila)	Nkd1	3.72	4.16	**-1.36**
F-box and WD-40 domain protein 2	Fbxw2	2.66	3.12	**-1.37**
E1A binding protein p300	Ep300	4.21	4.69	**-1.38**
SRY-box containing gene 17	Sox17	2.71	3.19	**-1.39**
Transcription factor 7, T-cell specific	Tcf7	4.37	4.85	**-1.39**
Kringle containing transmembrane protein 1	Kremen1	2.47	2.96	**-1.40**

Low density lipoprotein receptor-related protein 5	Lrp5	2.10	2.63	**-1.44**
Porcupine homolog (Drosophila)	Porcn	4.79	5.34	**-1.45**
Frizzled homolog 7 (Drosophila)	Fzd7	3.93	4.49	**-1.47**
Wingless-related MMTV integration site 5A	Wnt5a	4.72	5.29	**-1.48**
Jun oncogene	Jun	-2.87	-2.22	**-1.57**
SUMO/sentrin specific peptidase 2	Senp2	4.24	4.93	**-1.60**
Ras homolog gene family, member U	Rhou	4.11	4.80	**-1.61**
Frizzled homolog 2 (Drosophila)	Fzd2	4.63	5.34	**-1.62**
Catenin beta interacting protein 1	Ctnnbip1	3.96	4.74	**-1.71**
Cyclin D3	Ccnd3	1.33	2.12	**-1.72**
Wingless related MMTV integration site 2b	Wnt2b	4.05	4.85	**-1.73**
Adenomatosis polyposis coli	Apc	3.79	4.64	**-1.80**
Fos-like antigen 1	Fosl1	3.24	4.17	**-1.90**
Cyclin D1	Ccnd1	3.46	4.41	**-1.92**
Axin 1	Axin1	3.45	4.47	**-2.01**
Dishevelled associated activator of morphogenesis 1	Daam1	3.15	4.20	**-2.06**
Dishevelled, dsh homolog 1 (Drosophila)	Dvl1	3.91	5.06	**-2.21**
Secreted frizzled-related protein 2	Sfrp2	3.07	1.66	**2.66***
Transducin-like enhancer of split 1, homolog of Drosophila E(spl)	Tle1	5.04	4.21	**1.77**
Wingless-related MMTV integration site 5B	Wnt5b	4.70	4.44	**1.19**
Protein phosphatase 2 (formerly 2A), catalytic subunit, alpha isoform	Ppp2ca	1.42	1.28	**1.09**
WNT1 inducible signaling pathway protein 1	Wisp1	5.13	5.01	**1.09**
Wingless-related MMTV integration site 4	Wnt4	5.13	5.00	**1.09**
Frizzled homolog 6 (Drosophila)	Fzd6	3.97	3.96	**1.00**
Glycogen synthase kinase 3 beta	Gsk3b	5.13	5.12	**1.00**
Beta-transducin repeat containing protein	Btrc	N/A	N/A	N/A
DIX domain containing 1	Dixdc1	N/A	N/A	N/A

Dickkopf homolog 1 (Xenopus laevis)	Dkk1	N/A	N/A	N/A
F-box and WD-40 domain protein 11	Fbxw11	N/A	N/A	N/A
F-box and WD-40 domain protein 4	Fbxw4	N/A	N/A	N/A
Fibroblast growth factor 4	Fgf4	N/A	N/A	N/A
Forkhead box N1	Foxn1	N/A	N/A	N/A
Frequently rearranged in advanced T-cell lymphomas	Frat1	N/A	N/A	N/A
Follicle stimulating hormone beta	Fshb	N/A	N/A	N/A
Lymphoid enhancer binding factor 1	Lef1	N/A	N/A	N/A
Nemo like kinase	Nlk	N/A	N/A	N/A
Paired-like homeodomain transcription factor 2	Pitx2	N/A	N/A	N/A
Brachyury	T	N/A	N/A	N/A
Transducin-like enhancer of split 2, homolog of Drosophila E(spl)	Tle2	N/A	N/A	N/A
Wingless-related MMTV integration site 1	Wnt1	N/A	N/A	N/A
Wingless related MMTV integration site 10a	Wnt10a	N/A	N/A	N/A
Wingless-related MMTV integration site 16	Wnt16	N/A	N/A	N/A
Wingless-related MMTV integration site 2	Wnt2	N/A	N/A	N/A
Wingless-related MMTV integration site 3	Wnt3	N/A	N/A	N/A
Wingless-related MMTV integration site 3A	Wnt3a	N/A	N/A	N/A
Wingless-related MMTV integration site 6	Wnt6	N/A	N/A	N/A
Wingless-related MMTV integration site 7A	Wnt7a	N/A	N/A	N/A
Wingless-related MMTV integration site 7B	Wnt7b	N/A	N/A	N/A
Wingless-related MMTV integration site 8A	Wnt8a	N/A	N/A	N/A
Wingless related MMTV integration site 8b	Wnt8b	N/A	N/A	N/A
Wingless-type MMTV integration site 9A	Wnt9a	N/A	N/A	N/A

- *Table 4: Cell cycle array- Vehicle and Wnt3a medium treated CSP-8hrs and 48hrs*

Cell cycle qRT-PCR							
Description	**Symbol**	**8 hours (AVG ÄCt)**		***Fold change***	***48 hours (AVG ÄCt)***		***Fold change***
		Vehicle	**Wnt3a**		***Vehicle***	***Wnt3a***	
Integrin beta 1 (fibronectin receptor beta)	Itgb1	*-1.87*	*-2.28*	***1.33***	*-0.14*	*-1.36*	***2.33****
Cyclin-dependent kinase inhibitor 2A	Cdkn2a	*5.09*	*4.08*	***2.00****	*2.52*	*1.49*	***2.04****
Cyclin-dependent kinase inhibitor 1A (P21)	Cdkn1a	*0.17*	*0.34*	***-1.12***	*1.60*	*1.23*	***1.30***
Peripheral myelin protein 22	Pmp22	*3.11*	*2.99*	**1.08**	*1.94*	*1.63*	**1.24**
Cyclin D1	Ccnd1	*3.37*	*3.28*	**1.06**	*2.49*	*2.23*	**1.20**
Transformed mouse 3T3 cell double minute 2	Mdm2	*2.61*	*2.64*	**-1.01**	*1.65*	*1.39*	**1.20**
DNA-damage inducible transcript 3	Ddit3	*4.47*	*4.26*	**1.15**	*4.82*	*4.61*	**1.16**
Protein phosphatase 2 (formerly 2A), regulatory subunit B", alpha	Ppp2r3a	*9.88*	*9.90*	**-1.01**	*10.09*	*9.92*	**1.12**
Adenylate kinase 1	Ak1	*1.85*	*1.67*	**1.13**	*2.82*	*2.68*	**1.10**
Protein phosphatase 1D magnesium-dependent, delta isoform	Ppm1d	*4.91*	*5.06*	**-1.10**	*4.24*	*4.74*	**-1.41***
Structural maintenance of chromosomes 1A	Smc1a	*4.70*	*4.62*	**1.05**	*3.99*	*4.48*	**-1.41***
Nucleophosmin/nucleoplasmin 2	Npm2	*9.83*	*9.90*	**-1.04**	*9.46*	*9.98*	**-1.43***
Cell division cycle 25 homolog A (S. pombe)	Cdc25a	*3.36*	*3.55*	**-1.14**	*4.36*	*4.88*	**-1.44***
Transcription factor Dp 1	Tfdp1	*1.33*	*1.38*	**-1.03**	*1.04*	*1.60*	**-1.48***
Stromal antigen 1	Stag1	*5.04*	*5.51*	**-1.38**	*4.78*	*5.39*	**-1.52***
Telomeric repeat binding factor 1	Terf1	*6.22*	*6.54*	**-1.24**	*4.71*	*5.34*	**-1.54***
Cyclin B1	Ccnb1	*4.54*	*4.46*	**1.05**	*3.17*	*3.80*	**-1.55***

Proliferating cell nuclear antigen	Pcna	*1.71*	*2.03*	**-1.25***	*0.92*	*1.57*	**-1.57***
Protein phosphatase 3, catalytic subunit, alpha isoform	Ppp3ca	*4.67*	*5.07*	**-1.31**	*4.08*	*4.77*	**-1.62***
RAD21 homolog (S. pombe)	Rad21	*4.71*	*5.01*	**-1.22**	*1.95*	*2.65*	**-1.62***
Cyclin-dependent kinase 4	Cdk4	*2.13*	*2.47*	**-1.26**	*1.20*	*1.91*	**-1.63***
Inhibin alpha	Inha	*8.30*	*8.48*	**-1.13**	*7.77*	*8.47*	**-1.63***
Mdm2, transformed 3T3 cell double minute p53 binding protein	Mtbp	*8.32*	*8.67*	**-1.27**	*5.13*	*5.84*	**-1.63***
Minichromosome maintenance deficient 3 (S. cerevisiae)	Mcm3	*2.95*	*3.10*	**-1.11**	*2.86*	*3.57*	**-1.64***
MutS homolog 2 (E. coli)	Msh2	*4.23*	*4.23*	**-1.00**	*3.80*	*4.54*	**-1.66***
Checkpoint kinase 1 homolog (S. pombe)	Chek1	*5.53*	*6.15*	**-1.53**	*5.48*	*6.22*	**-1.67***
RAD9 homolog (S. pombe)	Rad9	*5.62*	*5.90*	**-1.21**	*5.19*	*5.97*	**-1.72***
NIMA (never in mitosis gene a)-related expressed kinase 2	Nek2	*N/A*	*N/A*	*N/A*	*4.28*	*5.07*	**-1.73***
RAD51 homolog (S. cerevisiae)	Rad51	*6.23*	*6.86*	**-1.55**	*4.99*	*5.81*	**-1.77***
MAD2 mitotic arrest deficient-like 1 (yeast)	Mad2l1	*3.91*	*4.21*	**-1.2**	*3.28*	*4.12*	**-1.79***
Transformation related protein 53	Trp53	*2.98*	*3.15*	**-1.12**	*1.83*	*2.68*	**-1.81***
Retinoblastoma-like 1 (p107)	Rbl1	*5.51*	*5.96*	**-1.37**	*5.69*	*6.57*	**-1.85***
Myeloblastosis oncogene	Myb	*N/A*	*N/A*	*N/A*	*12.28*	*13.25*	**-1.96***
Breast cancer 2	Brca2	*6.72*	*8.67**	**-3.88***	*6.67*	*7.70*	**-2.04***
WEE 1 homolog 1 (S. pombe)	Wee1	*5.16*	*5.53*	**-1.29**	*5.24*	*6.27*	**-2.04***
Breast cancer 1	Brca1	*6.20*	*6.73*	**-1.44**	*5.58*	*6.62*	**-2.06***
Cyclin F	Ccnf	*4.40*	*4.32*	**1.06**	*3.71*	*4.76*	**-2.06***

Minichromosome maintenance deficient 2 mitotin (S. cerevisiae)	Mcm2	*4.23*	*4.47*	**-1.18**	*2.75*	*3.81*	**-2.07***
Antigen identified by monoclonal antibody Ki67	Mki67	*5.02*	*6.59*	**-2.96***	*2.94*	*4.07*	**-2.19***
Transformation related protein 63	Trp63	*10.02*	*9.90*	**1.08**	*10.58*	*13.40*	**-7.09***
Calcium/calmodulin-dependent protein kinase II alpha	Camk2a	*N/A*	*N/A*	*N/A*	*9.14*	*9.14*	**-1.00**
Polycystic kidney disease 1 homolog	Pkd1	*4.06*	*3.80*	**1.20**	*3.74*	*3.76*	**-1.01**
Notch gene homolog 2 (Drosophila)	Notch2	*6.57*	*6.80*	**-1.17**	*5.23*	*5.29*	**-1.04**
Microtubule-actin crosslinking factor 1	Macf1	*2.53*	*2.61*	**-1.05**	*3.01*	*3.12*	**-1.07**
Amyloid beta (A4) precursor protein-binding, family B, member 1	Apbb1	*9.45*	*8.78*	**1.59**	*8.76*	*8.87*	**-1.08**
Cyclin C	Ccnc	*6.36*	*6.59*	**-1.17**	*7.30*	*7.44*	**-1.10**
Tumor susceptibility gene 101	Tsg101	*6.80*	*6.51*	**1.22**	*7.03*	*7.17*	**-1.10**
Nuclear factor of activated T-cells, cytoplasmic, calcineurin-dependent 1	Nfatc1	*2.99*	*3.02*	**-1.01**	*4.46*	*4.63*	**-1.12**
RAD17 homolog (S. pombe)	Rad17	*5.93*	*5.90*	**1.01**	*4.81*	*4.99*	**-1.13**
SMT3 suppressor of mif two 3 homolog 1 (yeast)	Sumo1	*2.24*	*2.37*	**-1.09**	*2.10*	*2.28*	**-1.13**
TAF10 RNA polymerase II, TATA box binding protein (TBP)-associated factor	Taf10	*2.37*	*2.36*	**1.00**	*1.31*	*1.53*	**-1.16**
G protein-coupled receptor 132	Gpr132	*N/A*	*N/A*	*N/A*	*12.38*	*12.60*	**-1.17**
Sestrin 2	Sesn2	*7.65*	*7.39*	**1.19**	*5.57*	*5.80*	**-1.17**
RAN, member RAS oncogene family	Ran	*-1.57*	*-1.44*	**-1.09**	*-1.58*	*-1.33*	**-1.19**
CDK5 regulatory subunit associated protein 1	Cdk5rap1	*7.71*	*7.14*	**1.48**	*7.76*	*8.03*	**-1.2**
C-abl oncogene 1, receptor tyrosine kinase	Abl1	*N/A*	*N/A*	*N/A*	*9.49*	*9.76*	**-1.21**
E2F transcription factor 4	E2f4	*2.73*	*2.93*	**-1.15**	*3.96*	*4.25*	**-1.22**

Pescadillo homolog 1, containing BRCT domain (zebrafish)	Pes1	*3.67*	*3.86*	**-1.13**	*2.20*	*2.50*	**-1.23**
DnaJ (Hsp40) homolog, subfamily C, member 2	Dnajc2	*3.39*	*3.47*	**-1.05**	*3.22*	*3.54*	**-1.25**
Dystonin	Dst	*4.79*	*4.75*	**1.02**	*3.12*	*3.44*	**-1.25**
Protamine 1	Prm1	*N/A*	*N/A*	*N/A*	*13.23*	*13.57*	**-1.26**
Retinoblastoma-like 2	Rbl2	*6.52*	*6.78*	**-1.19**	*5.31*	*5.64*	**-1.26**
Growth arrest and DNA-damage-inducible 45 alpha	Gadd45a	*6.55*	*5.96*	**1.50***	*5.06*	*5.42*	**-1.28**
Cyclin-dependent kinase 2	Cdk2	*4.61*	*5.06*	**-1.36**	*3.62*	*4.01*	**-1.31**
Caspase 3	Casp3	*4.88*	*5.05*	**-1.12**	*4.79*	*5.20*	**-1.32**
E2F transcription factor 3	E2f3	*6.44*	*6.56*	**-1.08**	*5.85*	*6.30*	**-1.36**
Src homology 2 domain-containing transforming protein C1	Shc1	*2.93*	*2.88*	**1.03**	*3.85*	*4.30*	**-1.36**
Stratifin	Sfn	*7.34*	*6.98*	**1.28**	*8.39*	*8.85*	**-1.37**
Cyclin E1	Ccne1	*6.99*	*6.98*	**1.00**	*5.01*	*5.47*	**-1.38**
Proteasome (prosome, macropain) assembly chaperone 2	Psmg2	*4.83*	*5.23*	**-1.32**	*3.07*	*3.56*	**-1.4**
E2F transcription factor 1	E2f1	*6.53*	*6.71*	**-1.12**	*5.48*	*5.98*	**-1.41**
CDC28 protein kinase 1b	Cks1b	*2.16*	*2.09*	**1.04**	*3.01*	*3.56*	**-1.46**
Cyclin-dependent kinase inhibitor 1B	Cdkn1b	*5.93*	*5.92*	**1.00**	*3.79*	*4.36*	**-1.48**
S-phase kinase-associated protein 2 (p45)	Skp2	*5.60*	*6.07*	**-1.37**	*5.42*	*6.00*	**-1.49**
Ataxia telangiectasia mutated homolog (human)	Atm	*5.42*	*6.23*	**-1.75**	*5.56*	*6.14*	**-1.50**
Meiotic recombination 11 homolog A (S. cerevisiae)	Mre11a	*5.78*	*5.71*	**1.04**	*5.10*	*5.68*	**-1.50**
Hus1 homolog (S. pombe)	Hus1	*5.41*	*5.58*	**-1.11**	*6.29*	*6.94*	**-1.57**
Calcium/calmodulin-dependent protein kinase II, beta	Camk2b	*10.02*	*9.90*	**1.08**	*11.89*	*12.55*	**-1.58**
Cyclin A2	Ccna2	*3.89*	*4.09*	**-1.15**	*3.55*	*4.25*	**-1.62**
Cyclin B2	Ccnb2	*6.37*	*6.39*	**-1.01**	*4.10*	*4.91*	**-1.74**

Minichromosome maintenance deficient 4 homolog (S. cerevisiae)	Mcm4	*2.34*	*2.54*	**-1.14**	*2.32*	*3.18*	**-1.82**
E2F transcription factor 2	E2f2	*N/A*	*N/A*	*N/A*	*11.09*	*12.32*	**-2.35**
Cyclin A1	Ccna1	*N/A*	*N/A*	*N/A*	*N/A*	*N/A*	*N/A*
Schlafen 1	Slfn1	*N/A*	*N/A*	*N/A*	*N/A*	*N/A*	*N/A*

- *Table 5: Pathway finder array-Vehicle and Wnt3a medium treated CSPs-6days*

Pathway finder qRT-PCR				
Description	**Gene Symbol**	**AVG ÄCt**		**Fold change**
		Vehicle	**Wnt3a**	
Insulin-like growth factor binding protein 3	Igfbp3	*10.01*	*5.08*	**43.44***
Wingless-related MMTV integration site 2	Wnt2	*10.1*	*6.55*	**13.94***
Fas (TNF receptor superfamily member 6)	Fas	*8.08*	*5.15*	**10.14***
Transcription factor 7, T-cell specific	Tcf7	*8.47*	*5.55*	**9.81***
Cyclin-dependent kinase inhibitor 2A (p16)	Cdkn2a	*3.18*	*0.19*	**9.11***
Lymphoid enhancer binding factor 1	Lef1	*8.02*	*4.97*	**8.52***
Prostate transmembrane protein, androgen induced 1	Tmepai	*7.18*	*4.49*	**6.88***
Etoposide induced 2.4 mRNA	Ei24	*4.21*	*3.36*	**1.92***
Heat shock protein 1	Hspb1	*0.26*	*-0.63*	**1.92***
Cyclin-dependent kinase inhibitor 2B (p15, inhibits CDK4)	Cdkn2b	*5.94*	*2.46*	**12.33**
Intercellular adhesion molecule 1	Icam1	*9.85*	*6.24*	**12.17**
Fatty acid synthase	Fasn	*9.41*	*7.32*	**9.91**
FBJ osteosarcoma oncogene	Fos	*9.12*	*7.07*	**9.83**
Bone morphogenetic protein 4	Bmp4	*8.79*	*7.06*	**9.73**
Prostaglandin-endoperoxide synthase 2	Ptgs2	*6.54*	*4.43*	**9.42**
Chemokine (C-C motif) ligand 2	Ccl2	*6.9*	*6.87*	**8.74**
Baculoviral IAP repeat-containing 5	Birc5	*6.33*	*7.85*	**8.61**
Myelocytomatosis oncogene	Myc	*6.21*	*6.01*	**6.43**
Baculoviral IAP repeat-containing 2	Birc2	*7.92*	*6.38*	**6.28**
B-cell leukemia/lymphoma 2	Bcl2	*7.31*	*6.31*	**6.09**
WNT1 inducible signaling pathway protein 1	Wisp1	*4.96*	*2.87*	**5.90**
Nuclear receptor interacting protein 1	Nrip1	*7.93*	*6.37*	**4.71**
Transformed mouse 3T3 cell double minute 2	Mdm2	*4.5*	*2.82*	**3.45**

Retinol binding protein 1, cellular	Rbp1	*2.34*	*1.5*	**3.41**
Telomerase reverse transcriptase	Tert	*8.16*	*6.66*	**3.34**
Cyclin-dependent kinase inhibitor 1A (P21)	Cdkn1a	*0.88*	*-0.23*	**3.08**
Baculoviral IAP repeat-containing 3	Birc3	*6.56*	*5.47*	**2.96**
Breast cancer 1	Brca1	*6.82*	*7.74*	**2.85**
Patched homolog 1	Ptch1	*6.35*	*4.98*	**2.84**
Homeo box A1	Hoxa1	*7.48*	*6.32*	**2.77**
Jun oncogene	Jun	*5.65*	*4.6*	**2.76**
TRAF family member-associated Nf-kappa B activator	Tank	*5.97*	*5.66*	**2.75**
Peroxisome proliferator activated receptor gamma	Pparg	*6.8*	*6.29*	**2.41**
Inhibitor of kappaB kinase beta	Ikbkb	*6.73*	*5.97*	**2.36**
Transferrin receptor	Tfrc	*5.58*	*5.44*	**2.34**
Cyclin-dependent kinase 2	Cdk2	*5.53*	*5.79*	**2.05**
Early growth response 1	Egr1	*5.37*	*6.19*	**1.88**
Hexokinase 2	Hk2	*4.76*	*4.2*	**1.55**
Bcl2-associated X protein	Bax	*1.16*	*0.58*	**1.53**
Heat shock factor 1	Hsf1	*4.37*	*3.84*	**1.52**
Ngfi-A binding protein 2	Nab2	*5.53*	*5.36*	**1.49**
Vascular cell adhesion molecule 1	Vcam1	*5.27*	*5.67*	**1.49**
Nuclear factor of kappa light polypeptide gene enhancer in B-cells inhibitor, alpha	Nfkbia	*4.97*	*4.48*	**1.44**
Growth arrest and DNA-damage-inducible 45 alpha	Gadd45a	*4.69*	*4.36*	**1.43**
Insulin-like growth factor binding protein 4	Igfbp4	*2.75*	*2.27*	**1.43**
Interferon regulatory factor 1	Irf1	*5.86*	*5.4*	**1.43**
Cyclin-dependent kinase inhibitor 1B	Cdkn1b	*6.77*	*7.02*	**1.33**
Bcl2-like 1	Bcl2l1	*5.24*	*5.45*	**1.23**
Glycogen synthase 1, muscle	Gys1	*4.86*	*4.65*	**1.20**
Vascular endothelial growth factor A	Vegfa	*4.66*	*4.51*	**1.12**
Ornithine decarboxylase, structural 1	Odc1	*2.11*	*2.14*	**1.05**
Activating transcription factor 2	Atf2	*3.55*	*4.46*	**1.04**
Transformation related protein 53	Trp53	*2.48*	*2.48*	**1.02**
Cyclin D1	Ccnd1	*2.9*	*3.21*	**1.02**
Interleukin 4 receptor, alpha	Il4ra	*6.09*	*6.67*	**0.73**
Fibronectin 1	Fn1	*-1.26*	*-0.41*	**0.63**
CCAAT/enhancer binding protein (C/EBP), beta	Cebpb	*1.68*	*2.55*	**0.60**
Bone morphogenetic protein 2	Bmp2	N/A	N/A	N/A
Chemokine (C-C motif) ligand 20	Ccl20	N/A	N/A	N/A
CD5 antigen	Cd5	N/A	N/A	N/A

Cadherin 1	Cdh1	N/A	N/A	N/A
Colony stimulating factor 2 (granulocyte-macrophage)	Csf2	N/A	N/A	N/A
Chemokine (C-X-C motif) ligand 1	Cxcl1	N/A	N/A	N/A
Chemokine (C-X-C motif) ligand 9	Cxcl9	N/A	N/A	N/A
Cytochrome P450, family 19, subfamily a, polypeptide 1	Cyp19a1	N/A	N/A	N/A
Engrailed 1	En1	N/A	N/A	N/A
Fas ligand (TNF superfamily, member 6)	Fasl	N/A	N/A	N/A
Fibroblast growth factor 4	Fgf4	N/A	N/A	N/A
Forkhead box A2	Foxa2	N/A	N/A	N/A
Gene regulated by estrogen in breast cancer protein	Greb1	N/A	N/A	N/A
Hedgehog-interacting protein	Hhip	N/A	N/A	N/A
Interleukin 1 alpha	Il1a	N/A	N/A	N/A
Interleukin 2	Il2	N/A	N/A	N/A
Interleukin 2 receptor, alpha chain	Il2ra	N/A	N/A	N/A
Leptin	Lep	N/A	N/A	N/A
Lymphotoxin A	Lta	N/A	N/A	N/A
Matrix metallopeptidase 10	Mmp10	N/A	N/A	N/A
Matrix metallopeptidase 7	Mmp7	N/A	N/A	N/A
NLR family, apoptosis inhibitory protein 1	Naip1	N/A	N/A	N/A
Nitric oxide synthase 2, inducible	Nos2	N/A	N/A	N/A
Selectin, endothelial cell	Sele	N/A	N/A	N/A
Selectin, platelet	Selp	N/A	N/A	N/A
Tumor necrosis factor	Tnf	N/A	N/A	N/A
Wingless-related MMTV integration site 1	Wnt1	N/A	N/A	N/A

- *Table 6: Cell cycle array comparison- Vehicle and Wnt3a medium treated CSPs (48hours) to mock and IGFBP3 over-expressing CSPs*

Symbol	**Wnt3a treatment (48 hours)**			**IGFBP3 over-expression**		
	AVG ÄCt		**Fold change**	**AVG ÄCt**		**Fold change**
	Vehicle	**Wnt3a**	**Wnt3a/Vehicle**	**Mock**	**IGFBP3 over-expression**	**IGFBP3-over-expression/Mock**
Itgb1	*-0.14*	*-1.36*	**2.33**	*-1.32*	*-1.63*	**1.24**

Cdkn2a	*2.52*	*1.49*	**2.04**	*1.14*	*0.49*	**1.56**
Cdkn1a	*1.6*	*1.23*	**1.3**	*0.57*	*-0.01*	**1.49**
Pmp22	*1.94*	*1.63*	**1.24**	*0.83*	*0.39*	**1.35**
Ccnd1	*2.49*	*2.23*	**1.20**	*0.95*	*0.7*	**1.19**
Mdm2	*1.65*	*1.39*	**1.20**	*0.88*	*0.76*	**1.09**
Ddit3	*4.82*	*4.61*	**1.16**	*2.9*	*2.75*	**1.11**
Ak1	*2.82*	*2.68*	**1.10**	*1.21*	*0.79*	**1.33**
Notch2	*5.23*	*5.29*	**-1.04**	*4.23*	*4.67*	**-1.36**
Macf1	*3.01*	*3.12*	**-1.07**	*2.22*	*2.27*	**-1.04**
Rad17	*4.81*	*4.99*	**-1.13**	*4.1*	*4.36*	**-1.2**
Taf10	*1.31*	*1.53*	**-1.16**	*0.57*	*0.85*	**-1.22**
Sesn2	*5.57*	*5.8*	**-1.17**	*4.25*	*4.27*	**-1.01**
Ran	*-1.58*	*-1.33*	**-1.19**	*-1.45*	*-1.06*	**-1.31**
Cdk5rap1	*7.76*	*8.03*	**-1.20**	*6.79*	*6.84*	**-1.04**
E2f4	*3.96*	*4.25*	**-1.22**	*3.14*	*3.41*	**-1.21**
Pes1	*2.2*	*2.5*	**-1.23**	*2.01*	*2.29*	**-1.22**
Dnajc2	*3.22*	*3.54*	**-1.25**	*2.74*	*3.09*	**-1.28**
Rbl2	*5.31*	*5.64*	**-1.26**	*4.55*	*5.42*	**-1.83**
Cdk2	*3.62*	*4.01*	**-1.31**	*3.83*	*4*	**-1.12**
E2f3	*5.85*	*6.3*	**-1.36**	*5.3*	*5.33*	**-1.02**
Shc1	*3.85*	*4.3*	**-1.36**	*2.63*	*2.76*	**-1.10**
Sfn	*8.39*	*8.85*	**-1.37**	*7.06*	*7.1*	**-1.03**
Ccne1	*5.01*	*5.47*	**-1.38**	*5.11*	*5.24*	**-1.09**
Psmg2	*3.07*	*3.56*	**-1.40**	*3.13*	*3.24*	**-1.08**

E2f1	*5.48*	*5.98*	**-1.41**	*4.57*	*4.76*	**-1.14**
Ppm1d	*4.24*	*4.74*	**-1.41**	*3.76*	*4.13*	**-1.29**
Smc1a	*3.99*	*4.48*	**-1.41**	*3.31*	*3.79*	**-1.40**
Npm2	*9.46*	*9.98*	**-1.43**	*8.65*	*8.75*	**-1.07**
Cdc25a	*4.36*	*4.88*	**-1.44**	*3.68*	*3.99*	**-1.25**
Cks1b	*3.01*	*3.56*	**-1.46**	*2.58*	*3.07*	**-1.41**
Cdkn1b	*3.79*	*4.36*	**-1.48**	*2.5*	*3.11*	**-1.52**
Tfdp1	*1.04*	*1.6*	**-1.48**	*1.08*	*1.42*	**-1.27**
Skp2	*5.42*	*6*	**-1.49**	*6.31*	*6.77*	**-1.37**
Atm	*5.56*	*6.14*	**-1.50**	*4.83*	*5.25*	**-1.34**
Mre11a	*5.1*	*5.68*	**-1.50**	*5.87*	*5.95*	**-1.06**
Stag1	*4.78*	*5.39*	**-1.52**	*3.86*	*4.37*	**-1.43**
Terf1	*4.71*	*5.34*	**-1.54**	*4.7*	*5.29*	**-1.51**
Ccnb1	*3.17*	*3.8*	**-1.55**	*3.11*	*4.38*	**-2.42**
Hus1	*6.29*	*6.94*	**-1.57**	*6.08*	*6.76*	**-1.60**
Pcna	*0.92*	*1.57*	**-1.57**	*1.33*	*2.25*	**-1.89**
Ccna2	*3.55*	*4.25*	**-1.62**	*2.79*	*4.22*	**-2.69**
Ppp3ca	*4.08*	*4.77*	**-1.62**	*2.86*	*3.16*	**-1.23**
Rad21	*1.95*	*2.65*	**-1.62**	*1.4*	*2.05*	**-1.57**
Cdk4	*1.2*	*1.91*	**-1.63**	*0.63*	*0.87*	**-1.18**
Inha	*7.77*	*8.47*	**-1.63**	*6.97*	*7.05*	**-1.06**
Mtbp	*5.13*	*5.84*	**-1.63**	*4.99*	*5.51*	**-1.43**
Mcm3	*2.86*	*3.57*	**-1.64**	*3.13*	*3.98*	**-1.80**
Msh2	*3.8*	*4.54*	**-1.66**	*3.71*	*4.12*	**-1.33**
Chek1	*5.48*	*6.22*	**-1.67**	*5.8*	*6.76*	**-1.95**
Rad9	*5.19*	*5.97*	**-1.72**	*4.73*	*5.23*	**-1.41**

Nek2	*4.28*	*5.07*	**-1.73**	*4.87*	*6.22*	**-2.55**
Ccnb2	*4.1*	*4.91*	**-1.74**	*4.1*	*5.13*	**-2.04**
Rad51	*4.99*	*5.81*	**-1.77**	*5.45*	*6.73*	**-2.42**
Mad2l1	*3.28*	*4.12*	**-1.79**	*3.27*	*4.4*	**-2.19**
Trp53	*1.83*	*2.68*	**-1.81**	*1.85*	*2.64*	**-1.72**
Mcm4	*2.32*	*3.18*	**-1.82**	*2.77*	*3.39*	**-1.54**
Rbl1	*5.69*	*6.57*	**-1.85**	*5.21*	*6.09*	**-1.85**
Brca2	*6.67*	*7.7*	**-2.04**	*5.97*	*6.64*	**-1.59**
Wee1	*5.24*	*6.27*	**-2.04**	*5.58*	*5.94*	**-1.28**
Brca1	*5.58*	*6.62*	**-2.06**	*5.7*	*7.24*	**-2.91**
Ccnf	*3.71*	*4.76*	**-2.06**	*3.47*	*4.78*	**-2.49**
Mcm2	*2.75*	*3.81*	**-2.07**	*3.15*	*4.42*	**-2.42**
Mki67	*2.94*	*4.07*	**-2.19**	*1.75*	*3.49*	**-3.34**
E2f2	*11.09*	*12.32*	**-2.35**	*11.35*	*11.75*	**-1.32**
Trp63	*10.58*	*13.4*	**-7.09**	*11.7*	*11.79*	**-1.06**
Ppp2r3a	*10.09*	*9.92*	**1.12**	*8.83*	*9.05*	**-1.17**
Camk2a	*9.14*	*9.14*	**-1.00**	*8.09*	*6.95*	**2.2**
Pkd1	*3.74*	*3.76*	**-1.01**	*2.73*	*2.43*	**1.23**
Apbb1	*8.76*	*8.87*	**-1.08**	*6.27*	*6.22*	**1.04**
Ccnc	*7.3*	*7.44*	**-1.10**	*5.99*	*5.82*	**1.13**
Tsg101	*7.03*	*7.17*	**-1.10**	*6.54*	*6.52*	**1.02**
Nfatc1	*4.46*	*4.63*	**-1.12**	*2.93*	*2.91*	**1.01**
Sumo1	*2.1*	*2.28*	**-1.13**	*1.76*	*1.61*	**1.11**
Gpr132	*12.38*	*12.6*	**-1.17**	*11.95*	*11.79*	**1.12**

Abl1	*9.49*	*9.76*	**-1.21**	*8.13*	*7.72*	**1.33**
Dst	*3.12*	*3.44*	**-1.25**	*2.2*	*2.07*	**1.09**
Prm1	*13.23*	*13.57*	**-1.26**	*12.07*	*11.79*	**1.21**
Gadd45a	*5.06*	*5.42*	**-1.28**	*4.41*	*3.51*	**1.86**
Casp3	*4.79*	*5.2*	**-1.32**	*3.98*	*3.86*	**1.09**
Ccna1	*13.27*	*13.75*	**-1.39**	*12.07*	*11.79*	**1.21**
Slfn1	*13.27*	*13.75*	**-1.39**	*12.07*	*11.79*	**1.21**
Camk2b	*11.89*	*12.55*	**-1.58**	*10.26*	*9.78*	**1.40**
Myb	*12.28*	*13.25*	**-1.96**	*11.85*	*11.79*	**1.04**

*****: The genes that were significantly changed are indicated with bold and asterisk in all the above tables.

9. PUBLICATION

Role of the ATP-Binding Cassette Transporter Abcg2 in the Phenotype and Function of Cardiac Side Population Cells

Otmar Pfister, Angelos Oikonomopoulos, Konstantina-Ioanna Sereti, Regina L. Sohn, Darragh Cullen, Gabriel C. Fine, Frédéric Mouquet, Karen Westerman and Ronglih Liao

Circ. Res. 2008;103;825-835; originally published online Sep 11, 2008;
DOI: 10.1161/CIRCRESAHA.108.174615
Circulation Research is published by the American Heart Association. 7272 Greenville Avenue, Dallas, TX 72514
 Print ISSN: 0009-7330. Online ISSN: 1524-4571

Role of the ATP-Binding Cassette Transporter *Abcg2* in the Phenotype and Function of Cardiac Side Population Cells

Otmar Pfister,* Angelos Oikonomopoulos,* Konstantina-Ioanna Sereti,* Regina L. Sohn, Darragh Cullen, Gabriel C. Fine, Frédéric Mouquet, Karen Westerman, Ronglih Liao

Abstract—Recently, the side population (SP) phenotype has been introduced as a reliable marker to identify subpopulations of cells with stem/progenitor cell properties in various tissues. We and others have identified SP cells from postmitotic tissues, including adult myocardium, in which they have been suggested to contribute to cellular regeneration following injury. SP cells are identified and characterized by a unique efflux of Hoechst 33342 dye. *Abcg2* belongs to the ATP-binding cassette (ABC) transporter superfamily and constitutes the molecular basis for the dye efflux, hence the SP phenotype, in hematopoietic stem cells. Although *Abcg2* is also expressed in cardiac SP (cSP) cells, its role in regulating the SP phenotype and function of cSP cells is unknown. Herein, we demonstrate that regulation of the SP phenotype in cSP cells occurs in a dynamic, age-dependent fashion, with *Abcg2* as the molecular determinant of the cSP phenotype in the neonatal heart and another ABC transporter, *Mdr1,* as the main contributor to the SP phenotype in the adult heart. Using loss- and gain-of-function experiments, we find that *Abcg2* tightly regulates cell fate and function. Adult cSP cells isolated from mice with genetic ablation of *Abcg2* exhibit blunted proliferation capacity and augmented cell death. Conversely, overexpression of *Abcg2* is sufficient to enhance cell proliferation, although with a limitation of cardiomyogenic differentiation. In summary, for the first time, we reveal a functional role for *Abcg2* in modulating the proliferation, differentiation, and survival of adult cSP cells that goes beyond its distinct role in Hoechst dye efflux. **(*Circ Res*. 2008;103:825-835.)**

Key Words: *Abcg2* ■ *Mdr1* ■ progenitor cells ■ proliferation ■ SP cells

Recently, the side population (SP) phenotype has been introduced as a reliable marker to identify subpopulations of cells with stem/progenitor cell properties in various tissues including the heart.[1] On the molecular level, the SP phenotype is linked to the presence of ATP-binding cassette (ABC) transporters with the ability to efficiently efflux the DNA binding dye Hoechst 33342.[2] This ABC transporter–dependent Hoechst efflux phenomenon confers the characteristic fluorescent-activated cell sorting (FACS) profile of SP cells as a Hoechst-low "side population" located to the periphery of the Hoechst-high main population.[2]

Among the various members of the ABC transporter superfamily, *Abcg2* (also referred to as breast cancer resistance protein 1 [*Bcrp1*]) and *Mdr1* (also referred to as P-glycoprotein [*p-gp*] or *Abcb1*) have been shown to efficiently efflux Hoechst 33342 and thereby confer the SP phenotype.[3] Although both transporters are highly expressed in bone marrow (BM)SP cells, studies performed in mice with targeted disruption of the *Mdr1a* and *Mdr1b* genes, the murine homologs of the human Abcb1/Mdr1 gene, demonstrated that *Abcg2* is the sole molecular determinant of the SP phenotype in hematopoietic stem cells.[4] Moreover, *Abcg2* expression is conserved in SP cells from a wide range of tissues including blood, gonad, lung, skeletal muscle and the retina, suggesting an important role of *Abcg2* in stem cells.[4–7]

We and others have characterized SP cells isolated from adult myocardium.[8–11] These cardiac (c)SP cells are phenotypically distinct from BMSP cells, in that they are not hematopoietic but exhibit the potential to differentiate into functional cardiomyocytes.[10] As in SP cells from the bone marrow, *Abcg2* is expressed in SP cells from the heart.[9] The contribution of *Abcg2* to the cSP phenotype and its biological significance in cSP progenitor cells, however, remain unknown. In this study, we find that the contribution of *Abcg2* to the SP phenotype in the heart exists in an age-dependent manner, with *Abcg2* as the molecular determinant of the SP phenotype in the neonatal heart and *Mdr1* as the basis for the SP phenotype in the adult heart. In addition, we demonstrate

Original received February 25, 2008; revision received August 27, 2008; accepted August 28, 2008.

From the Cardiac Muscle Research Laboratory (O.P., A.O., K.-I.S., R.L.S., D.C., G.C.F., F.M., R.L.), Cardiovascular Division, Department of Medicine; and Department of Anesthesia (K.W.), Brigham and Women's Hospital, Harvard Medical School, Boston, Mass; School of Medicine (A.O., K.-I.S.), University of Crete, Greece; and University of Washington School of Medicine (G.C.F.), Seattle. Present address for O.P.: Myocardial Research, Department of Biomedicine, and Division of Cardiology, University Hospital Basel, Switzerland. Present address for F.M.: Cardiologie C, Lille University Hospital, France.

*These authors contributed equally to this work.

Correspondence to Dr Ronglih Liao, Division of Cardiology, Department of Medicine, Brigham and Women's Hospital, Harvard Medical School, 77 Ave Louis Pasteur, NRB 431, Boston, MA 02115. E-mail rliao@rics.bwh.harvard.edu

Circulation Research **is available at http://circres.ahajournals.org** **DOI: 10.1161/CIRCRESAHA.108.174615**

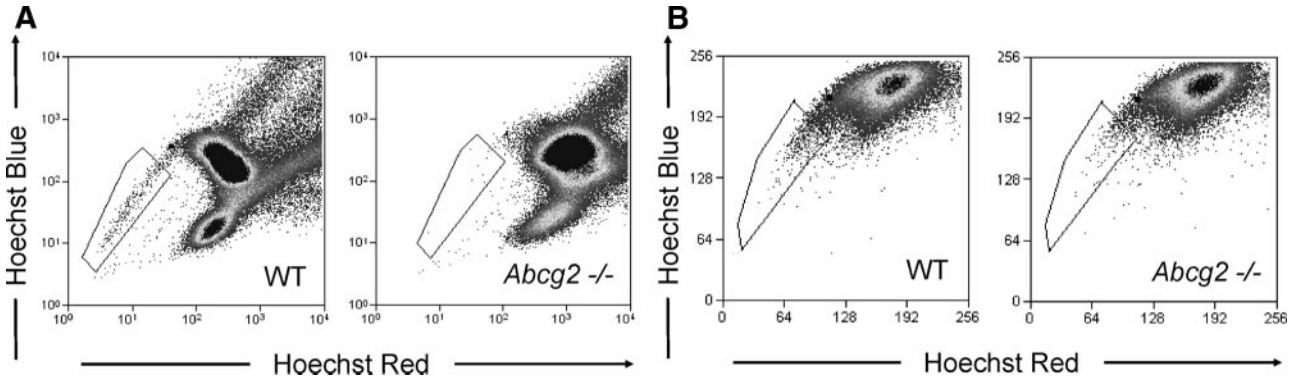

Figure 1. The role of *Abcg2* in mediating the SP cell phenotype in bone marrow and cardiac cells. FACS analyses carried out on Hoechst-stained bone marrow and cardiac cells from WT and *Abcg2*$^{-/-}$ mice. Hoechst-extruding SP cells are located in the boxed area. Compared to WT cells, bone marrow cells from *Abcg2*$^{-/-}$ mice lack a detectable SP cell population (A), whereas cardiac cells from *Abcg2*$^{-/-}$ mice exhibit a clearly detectable SP cell population (B).

that *Abcg2* plays a crucial role in the maintenance of cSP progenitor cells by promoting cell proliferation and survival, while inhibiting lineage commitment. Intriguingly, for the first time, we reveal a functional role of *Abcg2* in modulating proliferation, differentiation, and survival of cSP cells that goes beyond its distinct role of Hoechst dye efflux.

Materials and Methods

Animals

Male mice with genetic ablation of *Abcg2* (*Abcg2*$^{-/-}$) or *Mdr1a/b* (*Mdr1a/b*$^{-/-}$) were purchased from Taconic (catalog nos. 002767-M and 001487-MM; Germantown, NY). Age-matched FVB mice were also purchased from Taconic to serve as wild-type (WT) control. Mice were studied at postnatal day (p)3, p14, and p21 and between 8 and 12 weeks of age (adult). All animal studies strictly adhered to the guidelines of the Harvard Medical School, the Institutional Animal Care and Use Committee of the Longwood Medical Area, and the National Society for Medical Research.

Cardiac and BMSP Cell Preparation

Cardiomyocyte-depleted mononuclear cell suspensions were prepared as previously described to obtain cSP cells.[10] (For details, see the expanded Materials and Methods section in the online data supplement, available at http://circres.ahajournals.org.) BMSP cells were isolated form the tibia and femur as previously described.[1]

Cell Viability Assay

Cell death was determined by an annexin V kit (Abcam) using FACS analysis, and cell viability was determined by CellTiter-Glo and CellTiter-Blue (Promega) using a luminescence/fluorescence plate reader, respectively, according to the instructions of the manufacturer.

cSP Expansion and Lentiviral Infection

Freshly isolated cSP cells were cultured in expansion medium (α-MEM culture medium supplemented with 20% FBS, 2 mmol/L L-glutamine, and 1% penicillin/streptomycin). Vector pSPORT1 (American Type Culture Collection vector no. 10471063) was enzymatically digested with *Bam*HI, and the resulting Abcg2 cDNA was blunted and subsequently cloned into the HPV-422 lentivirus vector (kindly provided by Dr P. Allen, Brigham and Women's Hospital, Harvard Medical School, Boston, Mass). The bicistronic vector HPV-422 encodes the Abcg2 and IRES-GFP under the promoter EF1a. WT cSP cells from passage 4 to 6 were infected with the *Abcg2*-IRES-GFP lentivirus, and 48 hours postinfection green fluorescent protein–positive (GFP^{+}) cSP cells were sorted and further expanded. Culture medium was replaced every 72 hours.

Proliferation Assays

The proliferative capacity of cSP cells was determined in expanded passage 4 to 6 cSP cells using total cell number, expression of Ki67 and phospho-histone H_3, total protein, and total DNA. For detailed protocols, see the online data supplement.

Cardiomyogenic Differentiation Capacity

The role of *Abcg2* in regulating the ability of cSP cells to undergo cardiomyogenic differentiation was determined in our established coculture system.[10] cSP cells were transfected with GFP-expressing lentivirus, and cocultures were stained for α-sarcomeric actinin (Sigma). (For details, see the online data supplement.)

Statistical Analysis

Statistical differences between groups were evaluated using Student's unpaired *t* test or ANOVA, as appropriate. All data are presented as means±SEM. A probability value of <0.05 was considered statistically significant.

Results

Abcg2 Regulates the SP Phenotype in cSP Cells in an Age-Dependent Manner

Given published data suggesting that *Abcg2* is the sole molecular determinant of the SP cell phenotype in bone marrow cells, we first sought to determine whether *Abcg2* also regulates the SP phenotype in cardiac cells. To establish the role of *Abcg2* in mediating the SP cell phenotype, bone marrow and cardiac cell suspensions were isolated from 8- to 12-week-old age-matched mice with genetic ablation of *Abcg2* (*Abcg2*$^{-/-}$) and WT counterparts. FACS analysis of bone marrow cell suspensions from *Abcg2*$^{-/-}$ mice demonstrated a complete lack of BMSP cells (WT: 0.20±0.05%; *Abcg2*$^{-/-}$: 0.02±0.02%) compared to WT mice, suggesting that *Abcg2* is indeed required for conferring the SP phenotype in bone marrow cells (Figure 1A). In contrast, cSP cells from *Abcg2*$^{-/-}$ hearts revealed a clearly detectable, although significantly reduced, SP population (WT: 0.8±0.1%; *Abcg2*$^{-/-}$: 0.46±0.1%) (Figure 1B).

To confirm the correct FACS gating of SP cells (Figure 2A and 2B), we used 2 potent inhibitors of ABC transporters, verapamil and fumitremorgin C (FTC). Treatment of cells with verapamil or FTC completely abolished the SP cell band in both WT and *Abcg2*$^{-/-}$ cardiac cell suspensions (Figure 2C and 2F). To further verify that Hoechst dye efflux in *Abcg2*$^{-/-}$

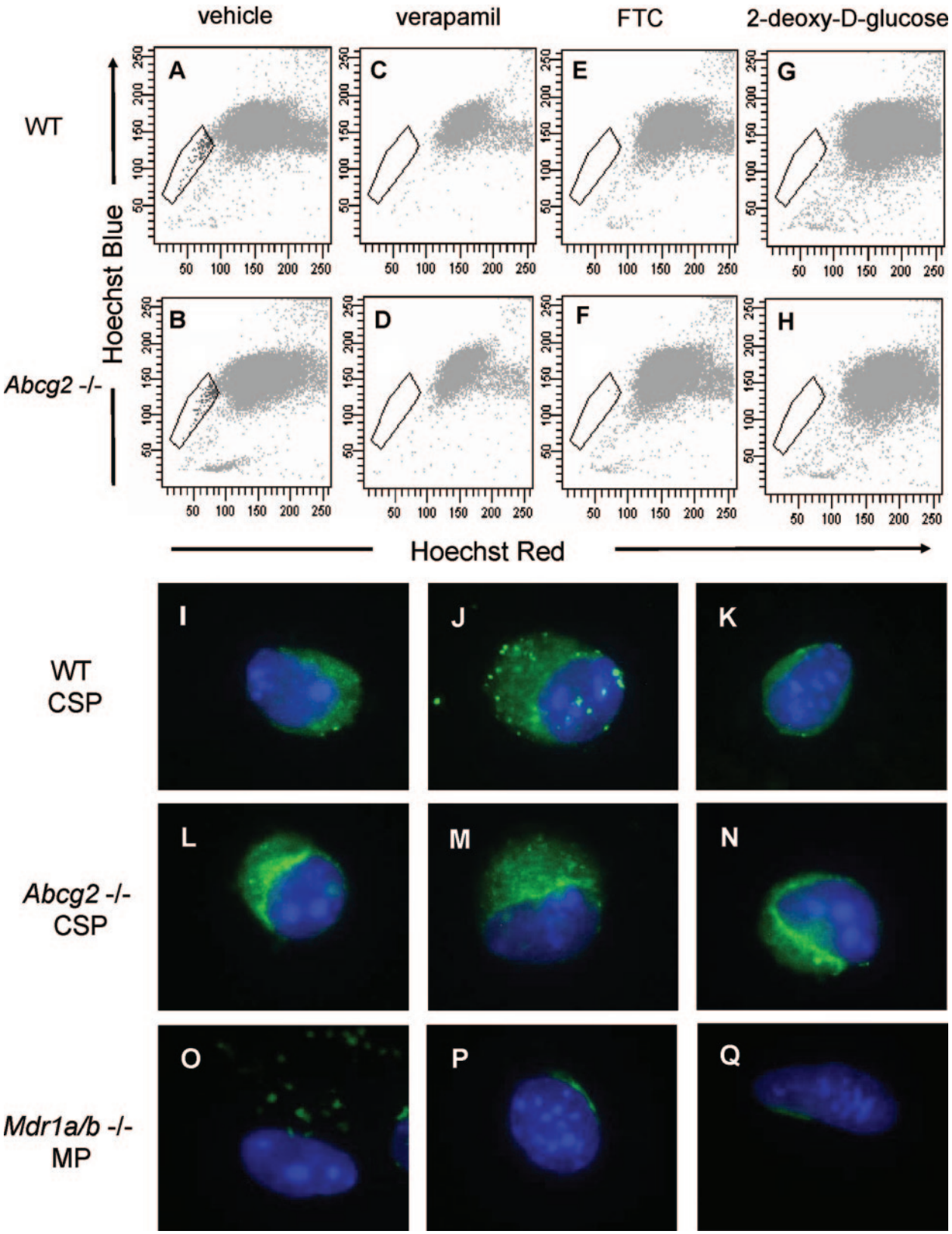

Figure 2. Hoechst dye efflux in *Abcg2*$^{-/-}$ cardiac cells is mediated by ATP-dependent ABC transporter function. FACS analyses of Hoechst-stained cardiac cells from WT and *Abcg2*$^{-/-}$ mice pretreated with either vehicle (A and B), the ABC transporter inhibitors verapamil (C and D), or FTC (E and F) or after ATP depletion with 2-deoxy-D-glucose (G and H). Similar to WT cardiac cells, inhibition of ABC-transporter function, as well as ATP depletion, completely abolishes the SP phenotype in *Abcg2*$^{-/-}$ cardiac cells, indicating that dye efflux in *Abcg2*$^{-/-}$ cardiac cell suspensions is mediated via ABC transporter activity. Immunocytochemical analysis demonstrates the expression of *Mdr1a/b* in freshly isolated WT and *Abcg2*$^{-/-}$ cSP cells (I through N). The lack of *Mdr1a/b* expression seen in *Mdr1a/b*$^{-/-}$ main population (MP) cells serves as negative control (O through Q).

Table. Cell Surface Marker Expression in WT and *Abcg2*$^{-/-}$ Cardiac SP Cells

Surface Marker	WT (%)	*Abcg2*$^{-/-}$ (%)
Sca-1	90±1	89±2
CD31	80±2	79±3
CD45	≤1	≤1

hearts was mediated via ABC transport, cardiac cell suspensions were preincubated with 2-deoxyglucose to deplete ATP and thereby inactivate ATP-dependent transporter function. Depletion of ATP also resulted in a complete loss of SP cells in both WT and *Abcg2*$^{-/-}$ cell suspensions, indicating that dye efflux in *Abcg2*$^{-/-}$ cell suspensions is indeed mediated in an ATP-dependent manner (Figure 2G and 2H).

We and others have previously shown that cSP cells express high levels of stem cell antigen 1 (Sca-1) and moderate levels of CD31 but lack the pan-hematopoietic marker CD45.[10] To further immunophenotypically characterize *Abcg2*$^{-/-}$ cSP cells, we compared the expression of cell surface markers, Sca-1, CD31 and CD45, in *Abcg2*$^{-/-}$ and WT cSP cells using FACS analysis. As shown in the Table, deficiency of *Abcg2* did not alter the expression pattern of Sca-1, CD31, and CD45, as compared to WT cSP cells, further suggesting that lacking *Abcg2* does not alter the expression pattern of major cell surface markers in adult cSP cells.

In addition to *Abcg2*, another member of the ABC transporter superfamily, the P-glycoprotein *Mdr1*, has been demonstrated to exhibit the capacity to efflux the Hoechst 33342 dye.[12] We therefore hypothesized that *Mdr1* may be involved in the regulation of the cSP phenotype in the adult heart. Quantitative RT-PCR analysis (Figure I in the online data supplement) and immunocytochemistry (Figure 2I through 2Q) in WT and *Abcg2*$^{-/-}$ cSP cells confirmed the expression of *Mdr1a* and *Mdr1b* genes and proteins independent of the expression of *Abcg2*.

To determine the contribution of *Mdr1* to the Hoechst 33342 efflux phenotype in the adult heart, cSP cells were isolated from hearts of adult mice with targeted disruption of *Mdr1a/b* genes. Strikingly, *Mdr1a/b*$^{-/-}$ hearts exhibited a severe depletion of cSP (Figure 3A). In contrast, bone marrow from *Mdr1a/b*$^{-/-}$ animals exhibited normal BMSP cell numbers (data not shown). To ensure that the limited number of cSP cells observed in *Mdr1a/b*$^{-/-}$ hearts was not attributable to experimental variables, in particular Hoechst concentration, cell ratio, and staining duration, we used an internal control by mixing 1 part of cardiomyocyte-depleted mononuclear cells ubiquitously expressing enhanced green fluorescent protein (GFP$^+$ control cells) with 3 parts of non-GFP, *Mdr1a/b*$^{-/-}$, or WT cardiomyocyte-depleted mononuclear cells (Figure 3B). Indeed, analysis of these cell mixtures revealed almost exclusively GFP$^+$ cells among the cSP cells (>98%), with no significant contribution from *Mdr1a/b*$^{-/-}$ cells to the SP band, thereby confirming the severely impaired Hoechst efflux capacity in *Mdr1a/b*$^{-/-}$ cSP cells (Figure 3B). In contrast, 1:3 cell mixtures of GFP$^+$ control cells and WT cardiac cells revealed only ≈25% GFP$^+$ control cells within the SP cell population, confirming the dye efflux competence of WT cardiac cells (Figure 3B).

Whereas *Abcg2* is enriched in early neonatal cSP cells, its expression level is markedly decreased postnatally.[9] To determine whether ABC-transporter expression in the heart is age-dependent, quantitative RT-PCR analysis for *Abcg2* and *Mdr1a/b* was performed in neonatal and adult mouse hearts. These analyses confirmed profound downregulation of *Abcg2* gene expression in the adult cSP cells as compared to the neonatal cSP cells. In contrast, *Mdr1a/b* expression levels demonstrated a reverse pattern with low expression in the neonatal cSP cells and high expression in the adult cSP cells (supplemental Figure II). To determine whether *Abcg2* and *Mdr1a/b* mediate the SP phenotype in cSP cells in an age-dependent manner, cSP cells were isolated from *Abcg2*$^{-/-}$, *Mdr1a/b*$^{-/-}$, and age-matched WT mice at p3, p14, and p21 and 8 to 12 weeks (adult) of age (Figure 4A through 4D). In contrast to adult hearts, early postnatal (p3) *Abcg2*$^{-/-}$ hearts demonstrated almost no detectable cSP cells, whereas a similar number of SP cells was observed in *Mdr1a/b*$^{-/-}$ and WT hearts (Figure 4A). The lack of Hoechst dye efflux was confirmed in cSP cells from *Abcg2*$^{-/-}$ hearts at p3 using GFP-mixing studies, similar to those described above (data not shown). A gradual decrease in cSP cells from p3 (9.4±1.2%) to adulthood (0.8±0.1%) was noted in WT hearts. *Abcg2*$^{-/-}$ hearts, however, demonstrated a gradual increase in cSP cells from day 3 postnatally (0.18±0.1%) to adult (0.46±0.1%) and thereafter maintained cSP cell levels into adulthood. The opposite profile was observed in *Mdr1a/b*$^{-/-}$ hearts, with cSP cell numbers dropping dramatically within the first 3 weeks of postnatal life and being barely detectable in adulthood. Taken together, these data demonstrate that the cSP cell phenotype is mediated by *Abcg2* and *Mdr1a/b* in an age-dependent fashion.

Abcg2 Regulates cSP Cell Proliferation

Expression of *Abcg2* has been associated with cellular proliferation in cancer cell lines.[13] Using gain- and loss-of-function approaches, we investigated the role of *Abcg2* in the regulation of cSP cell proliferation. cSP cells isolated from adult age-matched *Abcg2*$^{-/-}$ and WT mouse hearts were subjected to proliferation assays. As shown in Figure 5A, the proliferation capacity, as determined by total cell number, was markedly decreased in cSP cells lacking *Abcg2*. Consistent with the decrease in cell proliferation, the expression of the cell cycle markers Ki67 that identifies cells in G_1, S, G_2, and M phases (Figure 5B) and phospho-histone H_3 (Figure 5C and 5D) that identifies cells in M phase were decreased by ≈50% and ≈70%, respectively, in *Abcg2*$^{-/-}$ cSP cells when compared to WT cSP cells. Likewise, total protein and DNA content were significantly decreased in *Abcg2*$^{-/-}$ cSP cells cultured in the expansion media, thus further supporting impaired cell proliferation seen in *Abcg2*$^{-/-}$ cSP cells (Figure 5E and 5F). Conversely, the proliferation capacity was significantly enhanced in cSP cells following overexpression of *Abcg2* via lentiviral-mediated gene transfer, with an increase in both total cell number (Figure 5G) and expression of Ki67 (data not shown) as compared to WT cSP cells.

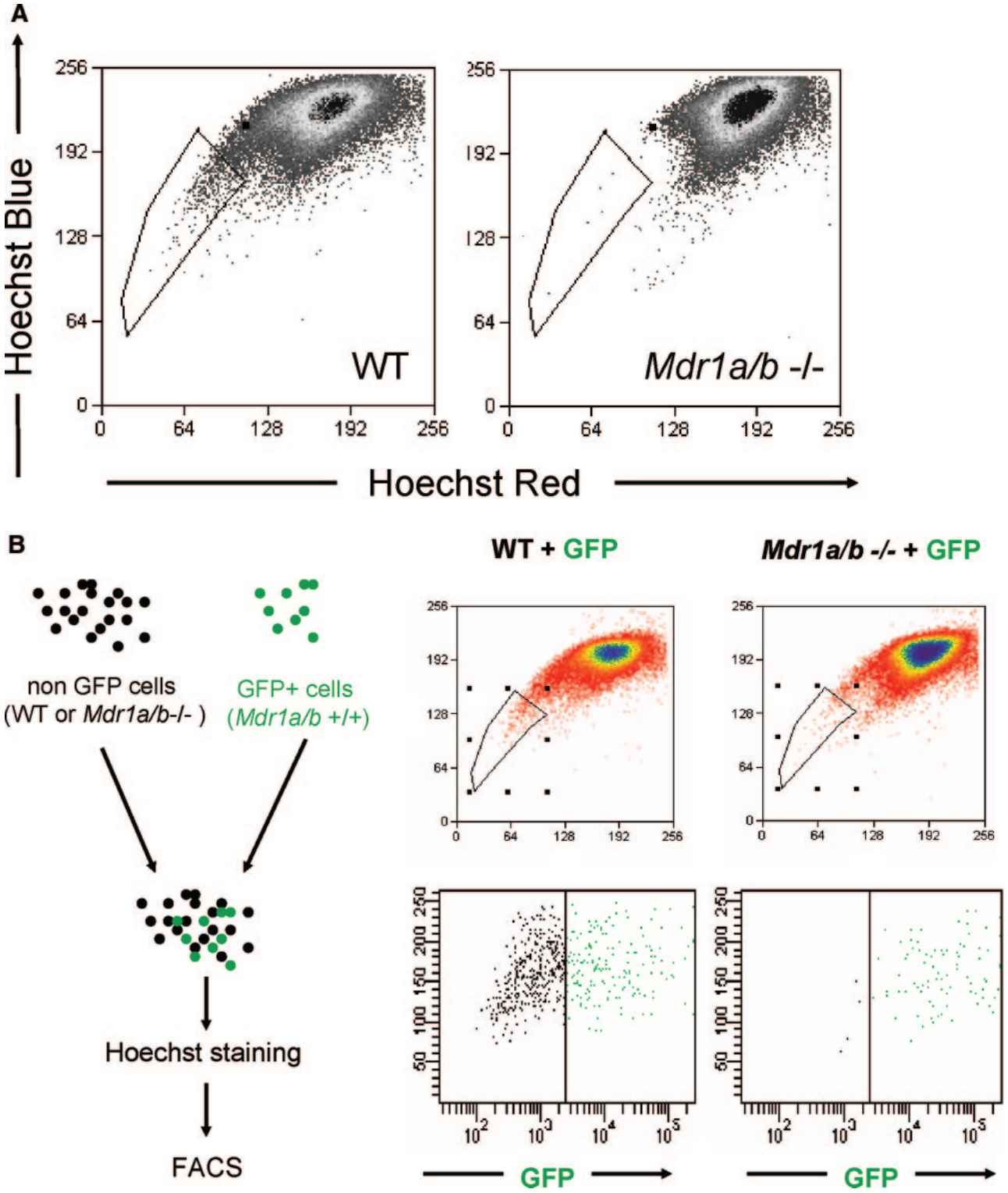

Figure 3. The ABC transporter *Mdr1a/b* mediates the Hoechst efflux phenotype of cSP cells in the adult heart. SP cell analyses of cardiac cells from WT and *Mdr1a/b*$^{-/-}$ mice. A, Compared to WT cells, *Mdr1a/b*$^{-/-}$ mononuclear cells almost completely lack cSP cells. B, SP cell analyses of cell mixtures containing 1 part of WT mononuclear cells expressing GFP and 3 parts of either WT or *Mdr1a/b*$^{-/-}$ mononuclear cells not expressing GFP. In cell mixtures containing WT cells, GFP^{+} cells account for ≈25% of total SP cells, thus reflecting the 1:3 ratio of the cell mixture. In cell mixtures containing GFP^{+} control and *Mdr1a/b*$^{-/-}$ cells, however, SP cells are almost exclusively GFP-positive, implicating a dominant role of *Mdr1a/b* in the mediation of the cSP cell phenotype in adult hearts.

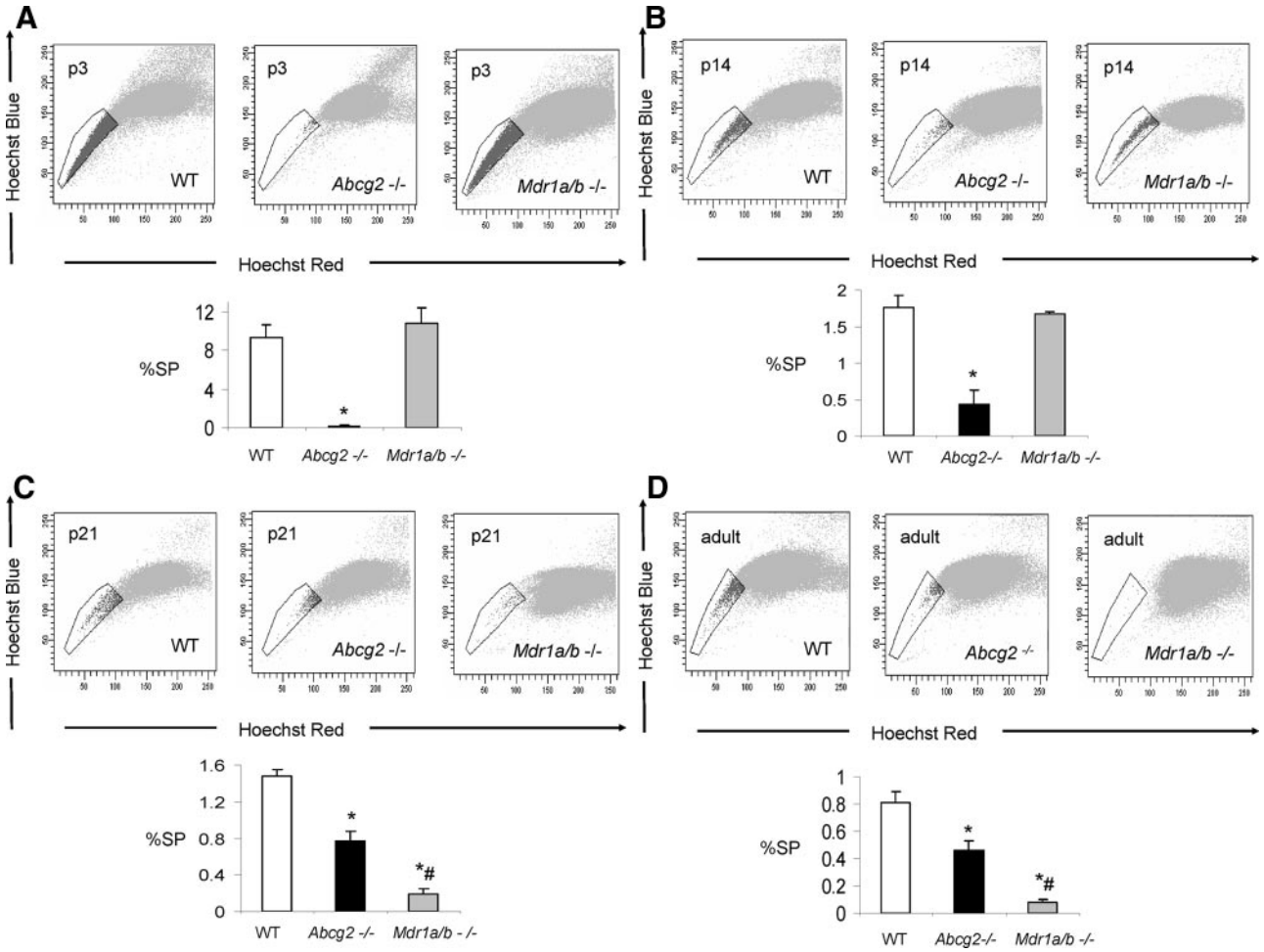

Figure 4. Age-dependent regulation of the cSP phenotype by *Abcg2* and *Mdr1a/b*. SP cell analyses of cardiac cells isolated from *Abcg2*$^{-/-}$, *Mdr1a/b*$^{-/-}$, and age-matched WT mice at p3, p14, and p21 and 8 to 12 weeks (adult) (A through D). A gradual decrease in cSP cells from early postnatal life through adulthood is evident in WT hearts. In contrast to WT hearts, early postnatal (p3) *Abcg2*$^{-/-}$ hearts demonstrate almost no detectable cSP cells, whereas similar numbers of SP cells are observed between *Mdr1a/b*$^{-/-}$ and WT hearts (A). During postnatal development, *Abcg2*$^{-/-}$ hearts demonstrate a steady increase in cSP cells from early postnatal into early adulthood (A through C) and maintain significant SP cell numbers throughout adulthood (D), whereas SP cell numbers of *Mdr1a/b*$^{-/-}$ hearts dramatically drop within the first 3 weeks of postnatal life and are barely detectable in adulthood (B through D).

Taken together, these data demonstrate a functional role of *Abcg2* in facilitating proliferation of cSP cells.

Regulation of cSP Cell Survival by *Abcg2*

Emerging evidence also suggests that *Abcg2* may play a critical role in protecting primitive cells from cellular injury.[14,15] To date, it is unclear whether *Abcg2* also exerts cell protective effects on cSP cells. To determine whether *Abcg2* is implicated in cSP cell survival, we first assessed apoptosis and necrosis in cSP cells under normal culture conditions using annexin V and propidium iodide staining, respectively. As illustrated in Figure 6A and 6B, even under normal culture conditions, significantly elevated numbers of both apoptotic and necrotic cells were observed in cSP cells lacking *Abcg2* as compared to WT cells. In addition, cell viability assays measuring cellular metabolic capacity by means of ATP quantitation (CellTiter-Glo, Promega) or conversion of the redox dye resazurin to the fluorescent end product resorufin (CellTiter-Blue, Promega) demonstrated significantly decreased metabolic capacity in *Abcg2*$^{-/-}$ cSP cells (Figure 6C and 6D), thus further confirming impaired viability.

Because oxidative stress is a common mediator of cell death in myocardial injury of various causes, we further investigated oxidative stress–induced cell death in WT and *Abcg2*$^{-/-}$ cSP cells after exposing cSP cell cultures to 200 μmol/L H_2O_2. In this model, oxidative stress–induced cell death was significantly higher in cSP cells lacking *Abcg2* as compared to WT cSP cells (Figure 6E). Taken together, our data indicate a protective role of *Abcg2* in cSP cells under normal culture (21% O_2) and H_2O_2-induced oxidative stress conditions.

Overexpression of *Abcg2* Impairs the Ability of cSP Cells to Undergo Cardiomyogenic Differentiation

Regulation of proliferation and differentiation maintains progenitor cell homeostasis. We have found that *Abcg2* is an essential regulator of cSP cell proliferation. We next sought to determine whether *Abcg2* mediates cardiomyogenic differentiation of cSP cells. Using a previously described coculture

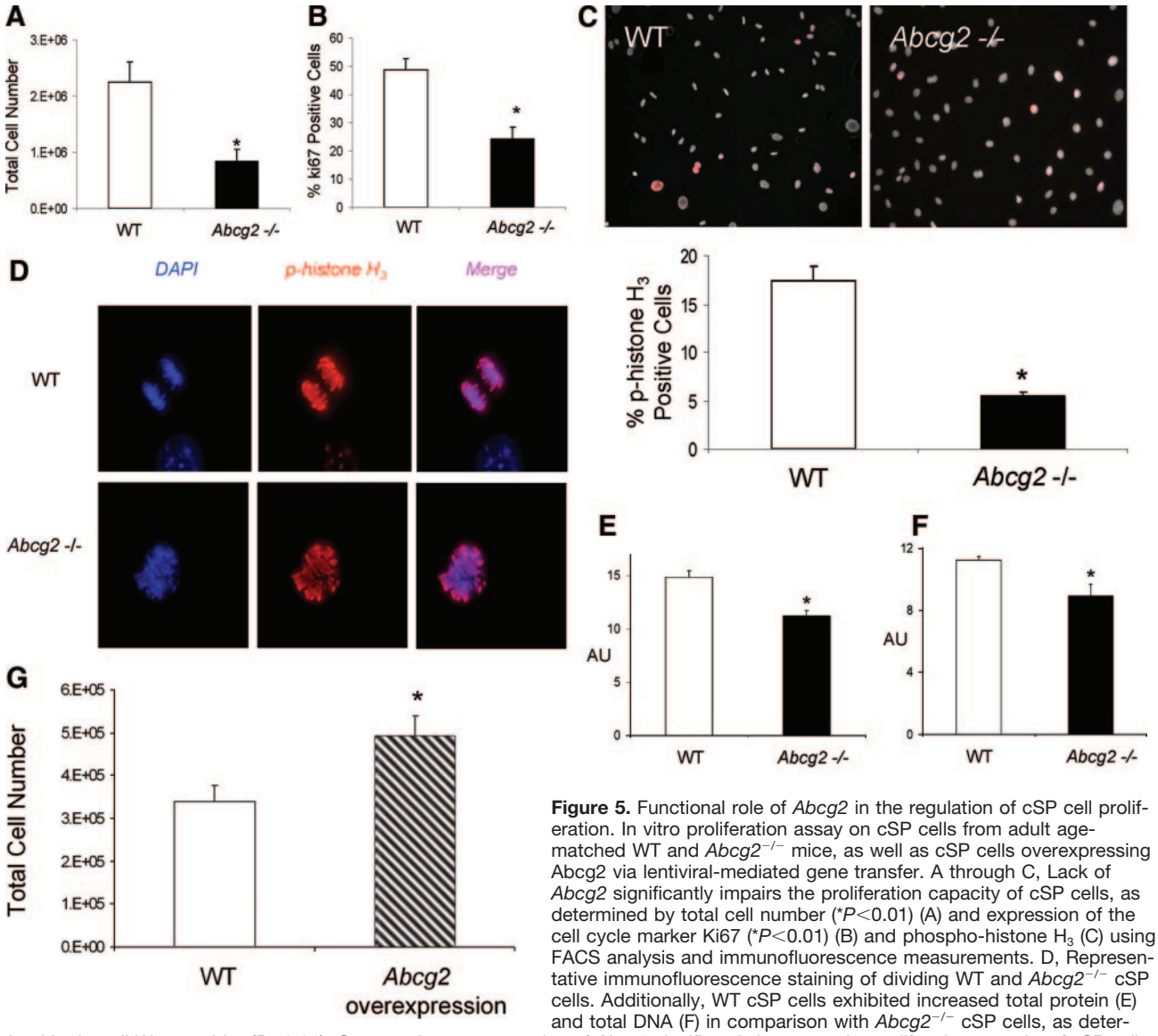

Figure 5. Functional role of *Abcg2* in the regulation of cSP cell proliferation. In vitro proliferation assay on cSP cells from adult age-matched WT and *Abcg2*$^{-/-}$ mice, as well as cSP cells overexpressing Abcg2 via lentiviral-mediated gene transfer. A through C, Lack of *Abcg2* significantly impairs the proliferation capacity of cSP cells, as determined by total cell number (*$P<0.01$) (A) and expression of the cell cycle marker Ki67 (*$P<0.01$) (B) and phospho-histone H_3 (C) using FACS analysis and immunofluorescence measurements. D, Representative immunofluorescence staining of dividing WT and *Abcg2*$^{-/-}$ cSP cells. Additionally, WT cSP cells exhibited increased total protein (E) and total DNA (F) in comparison with *Abcg2*$^{-/-}$ cSP cells, as determined by in-cell Western blot ($P<0.01$). Conversely, overexpression of *Abcg2* significantly increases the proliferation capacity of cSP cells in terms of (G) total cell number ($P<0.05$).

system with adult rat cardiomyocytes, cardiomyogenic differentiation was assessed in WT and *Abcg2*$^{-/-}$ cSP cells, as well as in *Abcg2*-overexpressing cSP cells (Figure 7A through 7I). To track the cell fate of cells in coculture, cSP cells were infected with lentivirus expressing GFP. Genetic deficiency of *Abcg2* did not limit the cardiomyogenic differentiation of cSP cells (Figure 7D through 7F). Overexpression of *Abcg2* via lentiviral-mediated gene transfer significantly decreased cardiomyogenic differentiation of cSP cells (Figure 7G through 7I). Moreover, overexpression of *Abcg2* maintained cSP cells in a proliferative state even under conditions promoting cardiomyogenic differentiation.

Discussion

Since the first isolation of BMSP cells more than a decade ago,[2] the SP phenotype has been widely used to identify stem/progenitor cells in various tissues.[2,7,16–19] More recently, the ABC transporter *Abcg2* has been identified as the sole molecular determinant of the SP phenotype in bone marrow cells.[4] However, the role of ABC transporters in the regulation of SP phenotype and function of cSP cells remains unknown. Herein, we demonstrate not only a dynamic, age-dependent regulation of the cSP phenotype by *Abcg2* but also a functional role of *Abcg2* in modulating proliferation, differentiation, and survival of cSP cells that goes beyond its distinct role in Hoechst dye efflux.

Role of *Abcg2* in Conferring the SP Phenotype in the Heart

Although *Abcg2* and *Mdr1* are both expressed in hematopoietic stem cells identified by the SP phenotype, *Abcg2* was shown to be the sole molecular determinant of the SP phenotype in bone marrow cells.[4] These findings in the bone marrow led to the assumption that *Abcg2* may also be

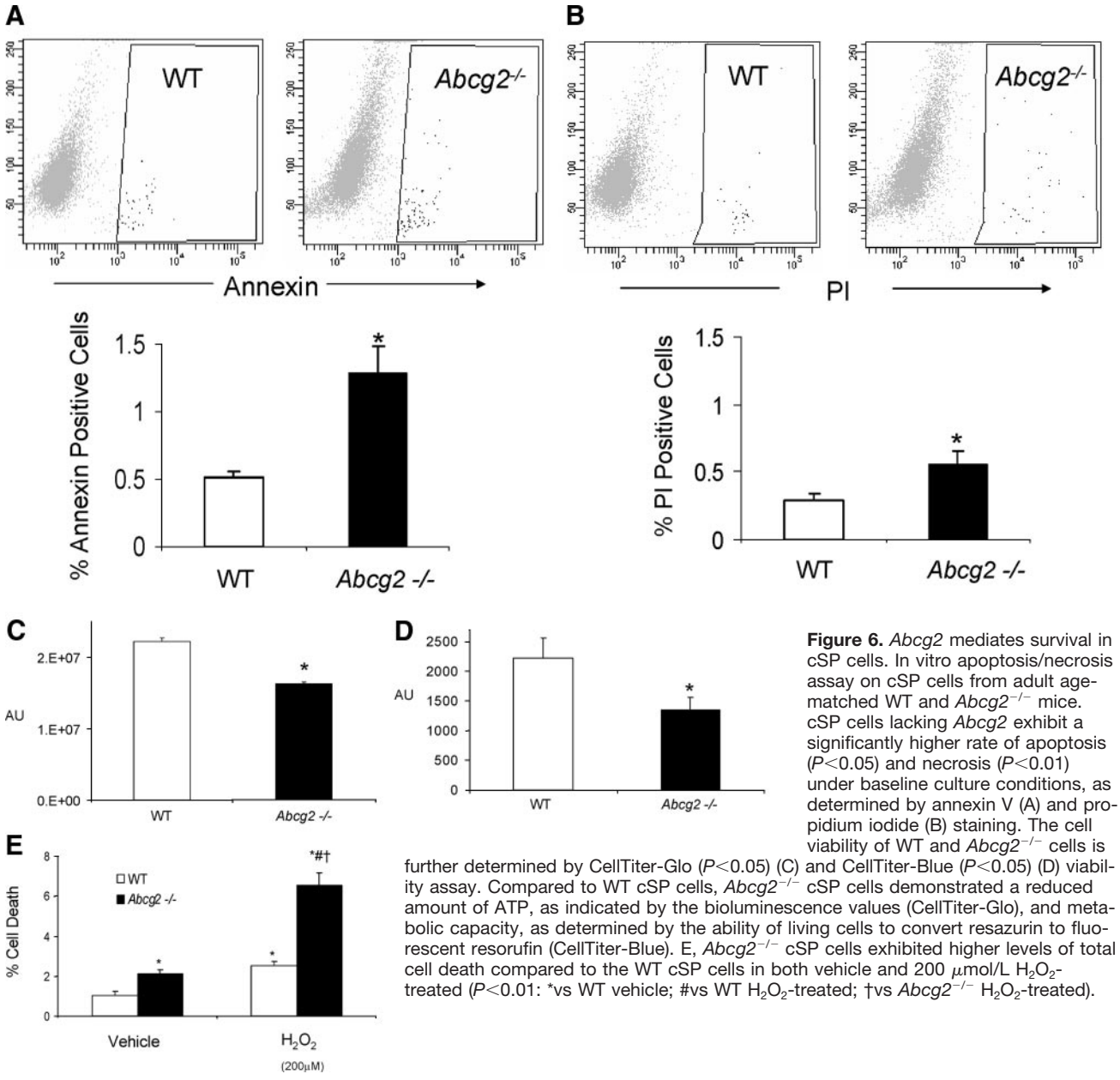

Figure 6. *Abcg2* mediates survival in cSP cells. In vitro apoptosis/necrosis assay on cSP cells from adult age-matched WT and *Abcg2*$^{-/-}$ mice. cSP cells lacking *Abcg2* exhibit a significantly higher rate of apoptosis ($P<0.05$) and necrosis ($P<0.01$) under baseline culture conditions, as determined by annexin V (A) and propidium iodide (B) staining. The cell viability of WT and *Abcg2*$^{-/-}$ cells is further determined by CellTiter-Glo ($P<0.05$) (C) and CellTiter-Blue ($P<0.05$) (D) viability assay. Compared to WT cSP cells, *Abcg2*$^{-/-}$ cSP cells demonstrated a reduced amount of ATP, as indicated by the bioluminescence values (CellTiter-Glo), and metabolic capacity, as determined by the ability of living cells to convert resazurin to fluorescent resorufin (CellTiter-Blue). E, *Abcg2*$^{-/-}$ cSP cells exhibited higher levels of total cell death compared to the WT cSP cells in both vehicle and 200 μmol/L H_2O_2-treated ($P<0.01$: *vs WT vehicle; #vs WT H_2O_2-treated; †vs *Abcg2*$^{-/-}$ H_2O_2-treated).

responsible for the dye efflux observed in SP cells isolated from other tissues, particularly given the preferential expression pattern of *Abcg2* in SP cells as compared to main population cells. Similar to their expression in bone marrow, *Abcg2* and *Mdr1* were shown to be expressed in the heart, although their contribution to the cSP phenotype remained to be elucidated. Using mouse models with targeted gene ablation of either *Abcg2* or *Mdr1*, we demonstrate that the cSP cell phenotype is not governed by a single ABC transporter but rather is regulated in an age-dependent manner by both *Abcg2* and *Mdr1*. Our findings show that during early postnatal development, *Abcg2* represents the main transporter responsible for dye efflux in cardiac cells and thus constitutes the molecular basis for the SP phenotype in the neonatal and early postnatal heart. This is in accordance with the role of *Abcg2* in bone marrow–derived cells and may indicate that cSP cells of the early postnatal heart share phenotypic characteristics of bone marrow–derived SP cells. Whether cSP cells developmentally originate from blood-borne cells, however, remains to be determined. It is important to point out that our present data provide no evidence to either support or dispute such notion. Prior data from our laboratory using labeled bone marrow transplantation, however, suggest that extracardiac stem cells only contribute to the maintenance of resident cSP cell pools following injury, with little role in the maintenance of cSP cell numbers under normal physiological conditions.[20]

Although our results agree with previous reports of persistent *Abcg2* expression in cSP cells throughout adulthood,[9] we find that the contribution of *Abcg2* to the SP phenotype diminishes in the adult heart. Our results show that very limited cSP cells can be detected in early neonatal *Abcg2*$^{-/-}$ hearts, with

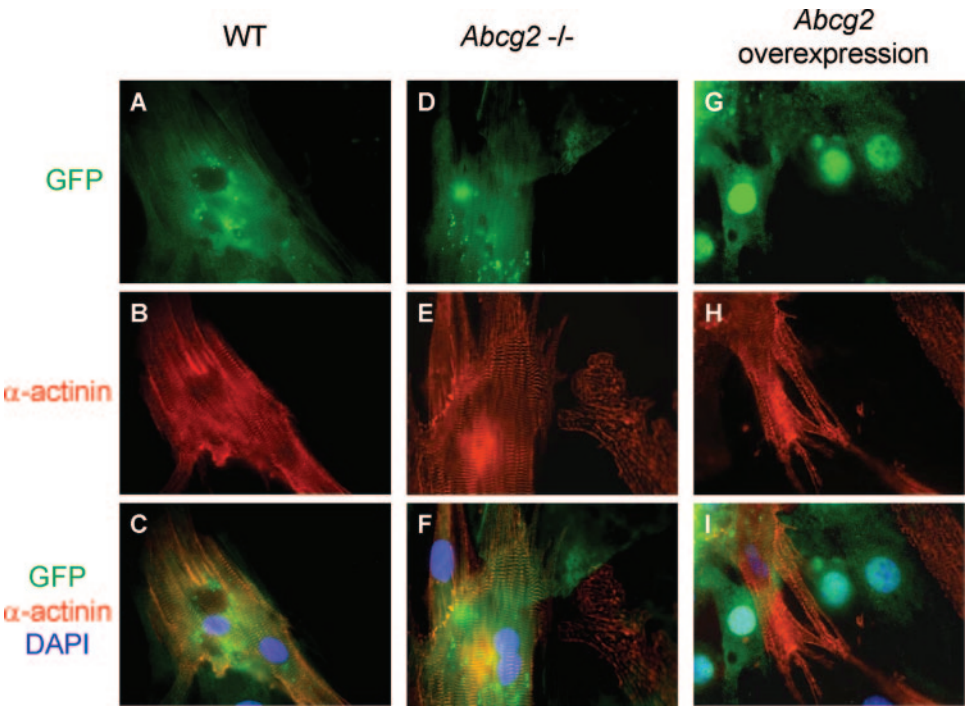

Figure 7. *Abcg2* overexpression prevents cardiomyogenic differentiation of cSP cells. Fluorescence images of WT (A through C), *Abcg2*$^{-/-}$ (D through F), and *Abcg2*-overexpressing (G through I) cSP cells in coculture with adult rat cardiomyocytes. Green fluorescence corresponds to GFP expression that identifies respective cSP cells (upper row). Red fluorescence corresponds to the expression of α-actinin, a marker of cardiomyogenic differentiation (middle row). Merged images show areas of colocalization of GFP and α-actinin in yellow (bottom row). In this differentiation assay, lack of *Abcg2* does not limit the cardiomyogenic differentiation of cSP cells, as demonstrated by α-actinin expression and appearance of clearly organized sarcomeric structures in differentiated *Abcg2*$^{-/-}$ cSP cells (D through F), similar to that seen in WT cells (A through C). *Abcg2* overexpression, however, prevents cSP cells from undergoing cardiomyogenic differentiation, as demonstrated by lack of α-actinin expression in *Abcg2*-overexpressing cSP cells cocultured with cardiomyocytes (G through I).

clearly detectable cSP cells in adult *Abcg2*$^{-/-}$ hearts, albeit at a lower total number as compared to WT hearts. These *Abcg2*$^{-/-}$ cSP cells are sensitive to verapamil, FTC, and 2-deoxyglucose treatment, thus suggesting that their Hoechst-extruding ability is mediated through another ABC transporter. Analyses of mice completely lacking *Mdr1* identified the P-glycoprotein as the essential ABC transporter for Hoechst efflux in adult cSP cells. It is important to note that the putative *Abcg2* inhibitor FTC, which was previously shown to have no effect on *Mdr1*-mediated mitoxantrone efflux in mitoxantrone-resistance-selected human colon carcinoma cell lines,[21] did inhibit *Mdr1*-mediated Hoechst efflux in cSP cells, suggesting that the specificity of FTC may depend on the cell type and the substrate.

Interestingly, this regulatory role of *Mdr1* in the cSP phenotype is limited to cSP cells from mice older than 3 weeks of age, with limited contribution of *Mdr1* to the SP phenotype in early neonatal mouse hearts. Although the origin of cardiac stem/progenitor cells and their relationship with bone marrow–derived stem cells remains speculative at this time, our data suggest that BMSP cells do not significantly contribute to the maintenance of cSP cells under physiological conditions, as evidenced by the lack of SP cells in adult *Mdr1a/b*$^{-/-}$ hearts, whereas *Mdr1a/b*$^{-/-}$ bone marrow contains normal SP cells. Thus, the present data are consistent with our previous findings demonstrating that BMSP cells only contribute to the maintenance of cSP cells following cardiac injury such as myocardial infarction.[20]

Our data dispute the perception that a single universal ABC transporter is responsible for the SP phenotype and suggest that developmental status and local microenvironment dictate the relative contribution of ABC transporters to the SP phenotype at the given tissue. In line with this observation is the recent demonstration of contribution of both *Mdr1* and *Abcg2* transporters to the SP phenotype in mammary glands.[22]

Role of *Abcg2* in Regulating the Function of cSP Cells

Abcg2 has been found to be highly expressed in various proliferating stem/progenitor cells and tumor cell lines, although its role in the regulation of SP cell proliferation and differentiation remains unknown. Using gain- and loss-of function approaches, we demonstrate that overexpression of *Abcg2* is sufficient to increase the proliferative capacity of cSP cells, whereas lack of *Abcg2* expression markedly impairs their expandability in vitro. The marked decrease in cells being in M phase of the cell cycle, as measured by phospho-histone H_3 expression, suggests that the absence of *Abcg2* may hamper cell cycle progression. This association of *Abcg2* expression with cell proliferation is in line with the findings in cancer cells, where *Abcg2* identified mainly fast cycling tumor progenitor cells.[13] Our data provide convincing evidence demonstrating that *Abcg2* may play a functional role in regulating the proliferation capacity of cSP cells, although the precise mechanisms are unknown. Further investigation, therefore, is warranted to dissect the molecular mechanisms by which *Abcg2* facilitates the cell cycle progression in cardiac progenitor cells.

In addition to enhancing cell proliferation, we show that *Abcg2* expression is necessary for protecting cSP cells from undergoing apoptosis and necrosis, specifically under condi-

tions of increased oxidative stress. A similar prosurvival effect of *Abcg2* was identified in trophoblast and hematopoietic stem cells.[14,23] Moreover, Martin et al recently demonstrated that expression of *Abcg2* induced low levels of oxidative stress in C2C12 myoblasts, which resulted in upregulation of cytoprotective and oxidative stress pathways.[15] The cytoprotective effect of such *Abcg2*-mediated ROS preconditioning was also confirmed in mouse embryonic fibroblasts that displayed reduced oxidative stress–induced cell death, when transfected with *Abcg2*.[15] Our data are in complete agreement with this concept by demonstrating increased tolerance of oxidative stress in *Abcg2*-competent WT cSP cells as compared to cSP cells lacking *Abcg2*.

Consistent with the notion that *Abcg2* maintains progenitor cells in a proliferative stage and is downregulated during lineage-specific differentiation, overexpression of *Abcg2* prevented cSP cells from undergoing cardiomyogenic differentiation. Our data are supported by the recently published work in hematopoietic and retinal stem cells demonstrating highly regulated *Abcg2* expression during stem cell differentiation with a sharp decline during lineage commitment.[4,5] In contrast, overexpression of *Abcg2* blocks the differentiation of hematopoietic and retinal stem cells, indicating a functional role of *Abcg2* in the maintenance of the stem cell pool.[4,5] In both cell types, overexpression of *Abcg2* leads to increased cell expansion and adversely affects their lineage commitment.

We have shown that overexpression of *Abcg2* not only promotes proliferation and survival of cSP cells but, at the same time, also inhibits cellular differentiation. Taken together, our data suggest that *Abcg2* is essential to the fate and function of cSP cells. As such, the tight regulation of *Abcg2* expression may be critical for maintaining progenitor cells in either a proproliferative or prodifferentiation state. Moreover, such regulation may be especially essential following tissue injury, during which a rapid increase in cSP cell proliferation is observed to replenish tissue SP cell pools.[20] Dysregulation of *Abcg2* expression may also result in uncontrolled cell growth or cell death. To date, the exact mechanism by which *Abcg2* prevents stem cells from lineage commitment remains to be elucidated. Considering the primary function of *Abcg2* as a detoxifying transmembrane pump, however, it is tempting to speculate that active extrusion of key molecules of the differentiation-promoting pathway might be involved in this process.

In summary, our study highlights the importance of *Abcg2* in regulating the function and homeostasis of cSP cells that goes beyond its traditional role as dye efflux transporter. Manipulation of *Abcg2* expression and function may be of particular importance in promoting cardiac regeneration following injury by both endogenous and exogenously delivered cSP cells. Given the role of *Abcg2* in the proliferation of cancer cells, as well as cSP cells, there is great potential for cardiac toxicity with emerging chemotherapeutic agents specifically targeting *Abcg2*. Further investigation into the role of *Abcg2* in cSP cells is of clinical importance to limit cancer drug–induced cardiac toxicity and to promote cardiac regeneration.

Acknowledgments

We thank Drs Richard C. Mulligan and Alejandro B. Balazs for help in the purification of SP cells and for useful discussions. Grigoriy Losyev at the Brigham and Women's Hospital Cardiovascular and Laura B. Prickett at the Massachusetts General Hospital FACS Cores are acknowledged for assistance with cell sorting.

Sources of Funding

This work was supported by NIH grants HL71775, HL86967, HL73756, and HL 88533 (to R.L.). A.O. and G.C.F. were supported by an American Heart Association Northeast Affiliate Predoctoral Fellowship and a Sarnoff Cardiovascular Research Foundation Fellowship, respectively.

Disclosures

None.

References

1. Challen GA, Little MH. A side order of stem cells: the SP phenotype. *Stem Cells*. 2006;24:3–12.
2. Goodell MA, Brose K, Paradis G, Conner AS, Mulligan RC. Isolation and functional properties of murine hematopoietic stem cells that are replicating in vivo. *J Exp Med*. 1996;183:1797–1806.
3. Bunting KD. ABC transporters as phenotypic markers and functional regulators of stem cells. *Stem Cells*. 2002;20:11–20.
4. Zhou S, Schuetz JD, Bunting KD, Colapietro AM, Sampath J, Morris JJ, Lagutina I, Grosveld GC, Osawa M, Nakauchi H, Sorrentino BP. The ABC transporter Bcrp1/ABCG2 is expressed in a wide variety of stem cells and is a molecular determinant of the side-population phenotype. *Nat Med*. 2001;7:1028–1034.
5. Bhattacharya S, Das A, Mallya K, Ahmad I. Maintenance of retinal stem cells by Abcg2 is regulated by notch signaling. *J Cell Sci*. 2007;120:2652–2662.
6. Lassalle B, Bastos H, Louis JP, Riou L, Testart J, Dutrillaux B, Fouchet P, Allemand I. 'Side Population' cells in adult mouse testis express Bcrp1 gene and are enriched in spermatogonia and germinal stem cells. *Development*. 2004;131:479–487.
7. Summer R, Kotton DN, Sun X, Ma B, Fitzsimmons K, Fine A. Side population cells and Bcrp1 expression in lung. *Am J Physiol Lung Cell Mol Physiol*. 2003;285:L97–L104.
8. Hierlihy AM, Seale P, Lobe CG, Rudnicki MA, Megeney LA. The post-natal heart contains a myocardial stem cell population. *FEBS Lett*. 2002;530:239–243.
9. Martin CM, Meeson AP, Robertson SM, Hawke TJ, Richardson JA, Bates S, Goetsch SC, Gallardo TD, Garry DJ. Persistent expression of the ATP-binding cassette transporter, Abcg2, identifies cardiac SP cells in the developing and adult heart. *Dev Biol*. 2004;265:262–275.
10. Pfister O, Mouquet F, Jain M, Summer R, Helmes M, Fine A, Colucci WS, Liao R. CD31- but Not CD31+ cardiac side population cells exhibit functional cardiomyogenic differentiation. *Circ Res*. 2005;97:52–61.
11. Oyama T, Nagai T, Wada H, Naito AT, Matsuura K, Iwanaga K, Takahashi T, Goto M, Mikami Y, Yasuda N, Akazawa H, Uezumi A, Takeda S, Komuro I. Cardiac side population cells have a potential to migrate and differentiate into cardiomyocytes in vitro and in vivo. *J Cell Biol*. 2007;176:329–341.
12. Bunting KD, Zhou S, Lu T, Sorrentino BP. Enforced P-glycoprotein pump function in murine bone marrow cells results in expansion of side population stem cells in vitro and repopulating cells in vivo. *Blood*. 2000;96:902–909.
13. Patrawala L, Calhoun T, Schneider-Broussard R, Zhou J, Claypool K, Tang DG. Side population is enriched in tumorigenic, stem-like cancer cells, whereas ABCG2+ and ABCG2− cancer cells are similarly tumorigenic. *Cancer Res*. 2005;65:6207–6219.
14. Krishnamurthy P, Ross DD, Nakanishi T, Bailey-Dell K, Zhou S, Mercer KE, Sarkadi B, Sorrentino BP, Schuetz JD. The stem cell marker Bcrp/ABCG2 enhances hypoxic cell survival through interactions with heme. *J Biol Chem*. 2004;279:24218–24225.
15. Martin CM, Ferdous A, Gallardo T, Humphries C, Sadek H, Caprioli A, Garcia JA, Szweda LI, Garry MG, Garry DJ. Hypoxia-inducible factor-

2alpha transactivates Abcg2 and promotes cytoprotection in cardiac side population cells. *Circ Res*. 2008;102:1075–1081.
16. Behbod F, Xian W, Shaw CA, Hilsenbeck SG, Tsimelzon A, Rosen JM. Transcriptional profiling of mammary gland side population cells. *Stem Cells*. 2006;24:1065–1074.
17. Hishikawa K, Marumo T, Miura S, Nakanishi A, Matsuzaki Y, Shibata K, Ichiyanagi T, Kohike H, Komori T, Takahashi I, Takase O, Imai N, Yoshikawa M, Inowa T, Hayashi M, Nakaki T, Nakauchi H, Okano H, Fujita T. Musculin/MyoR is expressed in kidney side population cells and can regulate their function. *J Cell Biol*. 2005;169:921–928.
18. Kotton DN, Fabian AJ, Mulligan RC. A novel stem-cell population in adult liver with potent hematopoietic-reconstitution activity. *Blood*. 2005; 106:1574–1580.
19. Rivier F, Alkan O, Flint AF, Muskiewicz K, Allen PD, Leboulch P, Gussoni E. Role of bone marrow cell trafficking in replenishing skeletal muscle SP and MP cell populations. *J Cell Sci*. 2004;117: 1979–1988.
20. Mouquet F, Pfister O, Jain M, Oikonomopoulos A, Ngoy S, Summer R, Fine A, Liao R. Restoration of cardiac progenitor cells after myocardial infarction by self-proliferation and selective homing of bone marrow-derived stem cells. *Circ Res*. 2005;97:1090–1092.
21. Rabindran SK, He H, Singh M, Brown E, Collins KI, Annable T, Greenberger LM. Reversal of a novel multidrug resistance mechanism in human colon carcinoma cells by fumitremorgin C. *Cancer Res*. 1998;58: 5850–5858.
22. Jonker JW, Freeman J, Bolscher E, Musters S, Alvi AJ, Titley I, Schinkel AH, Dale TC. Contribution of the ABC transporters Bcrp1 and Mdr1a/1b to the side population phenotype in mammary gland and bone marrow of mice. *Stem Cells*. 2005;23:1059–1065.
23. Evseenko DA, Murthi P, Paxton JW, Reid G, Emerald BS, Mohankumar KM, Lobie PE, Brennecke SP, Kalionis B, Keelan JA. The ABC transporter BCRP/ABCG2 is a placental survival factor, and its expression is reduced in idiopathic human fetal growth restriction. *FASEB J*. 2007;21: 3592–3605.

Supplemental Materials and Methods

Isolation of cardiac and bone marrow SP cells.

Minced cardiac tissue was digested with 0.1% collagenase B (Roche Molecular Biochemicals), 2.4 U/ml dispase II (Roche Molecular Biochemicals), and 2.5 mmol/L $CaCl_2$ at 37°C for 30 minutes, filtered through 70 μm and 40 μm filters, and washed with HBSS buffer supplemented with 2% fetal calf serum and 10 mmol/L HEPES. Cardiomyocyte depleted mononuclear cell suspensions were incubated with Hoechst 33342 (5 μg/ml) (Sigma) at 37°C for 90 minutes in Dulbecco's modified Eagle's medium (DMEM) (Invitrogen) (2% fetal calf serum, 10 mmol/L HEPES) at a concentration of 10^6 nucleated cells/mL. Verapamil (50 mmol/L), fumitremorgin C (FTC, 1 μmol/L) and 2-deoxyglucose (50 mmol/L) were used as inhibitors of the Hoechst 33342 dye efflux ability. Bone marrow SP cells were isolated form the tibia and femur as previously described [1]. Cell Surface antigen staining was performed at 4° C for 30 minutes using fluorochrome-conjugated monoclonal rat anti-mouse antibodies reactive to Sca-1, CD31, and CD45 (Pharmingen). Respective isotype controls (Pharmingen) were used as negative controls. Propidium iodide (PI) (2 μg/mL) was added prior to FACS to exclude dead cells.

FACS analysis.

FACS was performed using MoFlo (Cytomation Inc.) and FACSAria (BD) both equipped with triple lasers. Acquired data were analyzed using Summit software (Cytomation, Inc.) and BD FACSDIVA software (BD Biosciences). SP cells were identified as Hoechst-low cells as previously described [1]. Samples co-incubated with Hoechst and verapamil were used as negative controls to set the threshold of the respective SP gate as previously described [1].

Experiments defining the proliferative capacity of cSP cells.

Total cell number. Twenty thousand WT and *Abcg2 -/-* or ten thousand WT and *Abcg2* overexpressing cSP cells from passage 4-6 were plated onto culture dishes. Cardiac SP cells were trypsinized and the cell number was calculated using a hematocytometer at day 9 or 6 for *Abcg2 -/-* or *Abcg2* overexpressing, respectively. Culture medium was replaced every 72 hours.

Immunocytochemistry for phospho-histone H_3. cSP cells from passage 4-6 were plated and cultured in proliferation media for 5 days. Cells were washed twice with PBS, fixed with 4% paraformaldehyde solution and permeabilized with methanol. cSP cells were subsequently incubated in 1% BSA solution for one hour and then stained with a primary antibody against phospho-histone H_3 (Abcam) for 2 hours followed by 2 hours staining with secondary antibody (Alexa-555, Molecular probes) at room temperature. Coverslips were mounted on the slides using a DAPI-containing mounting medium (Vector Vectashield). Cells were visualized using Zeiss epi-fluorescent microscopy (Zeiss, Axiovert 200M).

Expression of Ki67 via FACS analysis. cSP cells were fixed (4% paraformaldehyde), permeabilized (Perm/Wash solution, BD Biosciences) and stained with FITC-conjugated polyclonal Ki67 antibody (Santa Cruz). Respective isotype control (BD Biosciences) was used as negative control.

***In cell western for total protein and DNA*.** Equal numbers of WT and Abcg2 -/- cSP cells from passages 4-6 were cultured in the proliferation media. Two days following culture, cSP cells were fixed with 4% paraformaldehyde and permeabilized with 0.2% Triton X-100 in PBS. Total protein was measured by the staining of Alexa-680 conjugated antibody against succinimidyl ester (Molecular probes, 1:50000 for 15min). The total DNA content was determined by nuclear staining with the TOPRO-3 DNA dye (Molecular probes, 1:2500 for 1hr). The in-cell Western analysis was performed in the Licor Odyssey infrared imager.

Co-culture experiments.

Adult rat cardiomyocytes were isolated from male Wistar rats as described previously [2]. The isolated cardiomyocytes were seeded at low density onto

laminin-coated culture dishes or coverslips. Cardiomyocytes were maintained in DMEM culture medium supplemented with creatine (5 mmol/L), L-carnitine (2 mmol/L), taurine (5 mmol/L), penicillin/streptomycin (1 %), FBS (7%) and bromodeoxyuridine (BrdU, 100 µmol/L) and the culture medium was replaced every 72 hours. For co-culture experiments cardiac SP cells were transfected with either GFP-lentivirus (control) or GFP-Abcg2-lentivirus (sample). GFP-positive cardiac SP cells were added onto the cardiomyocyte feeder layer at a ratio of 1:10 at day 10 and maintained for additional 10-12 days. The cardiomyogenic differentiation of cSP cells was evaluated by Immunocytochemical staining for a-sarcomeric actinin, as previously described (Otmar's paper). Nuclear staining was performed by supplementation of 4, 6-diamidino-2-phenylindole (DAPI).

Quantitative RT-PCR.

Total RNA was extracted from freshly isolated CSP cells and CDNA was synthesized using the iScript cDNA synthesis kit from BIO-RAD. Real-time PCR (BioRad-MyIQ) was performed using the following primers:

GADPH: 5'-TCACCACCATGGAGAAGGC-3'

and 3'-GCTAAGCAGTTGGTGGTGCA-5',

Abcg2: 5'-GAACTCCAGAGCCGTTAGGAC-3'

and 3'-CAGAATAGCATTAAGGCCAGG-5',

Mdr1a: 5'-TGGGTGCAGCTTTTCTCCTTA-3'

And 3'-CAGTGAGCACTTGTCCAATAGAG-5'

Mdr1b: 5'-CTG TTGGCGTATTTGGGATGT-3,'

and 3'-CAGCATCAAGAGGGGAAGTAATG-5'.

Data analysis was performed based on the standard curve method. Starting quantity (SQ) of Abcg2, Mdr1a and Mdr1b genes were compared to SQ of GAPDH.

Immunocytochemistry.

cSP cells were cyto-spinned (500rpm for 5min) onto slides at a concentration of 5000 cells/slide (Shandon Cytopsin 3). Cells were fixed immediately in 4% paraformaldehyde and permeabilized with methanol. Subsequently cSP cells were incubated for 1 hr with 1% BSA solution and were stained for Mdr1 (Santa Cruz, clone C-19, FITC-conjugated) for 2hr at room temperature. Coverslips were mounted on the slides as described above.

References.

1. Pfister O, Mouquet F, Jain M, Summer R, Helmes M, Fine A, Colucci WS, Liao R. CD31- but Not CD31+ cardiac side population cells exhibit functional cardiomyogenic differentiation. *Circ Res*. 2005;97:52-61.
2. Lim CC, Zuppinger C, Guo X, Kuster GM, Helmes M, Eppenberger HM, Suter TM, Liao R, Sawyer DB. Anthracyclines induce calpain-dependent titin proteolysis and necrosis in cardiomyocytes. *J Biol Chem*. 2004;279:8290-9.

Online Figure I

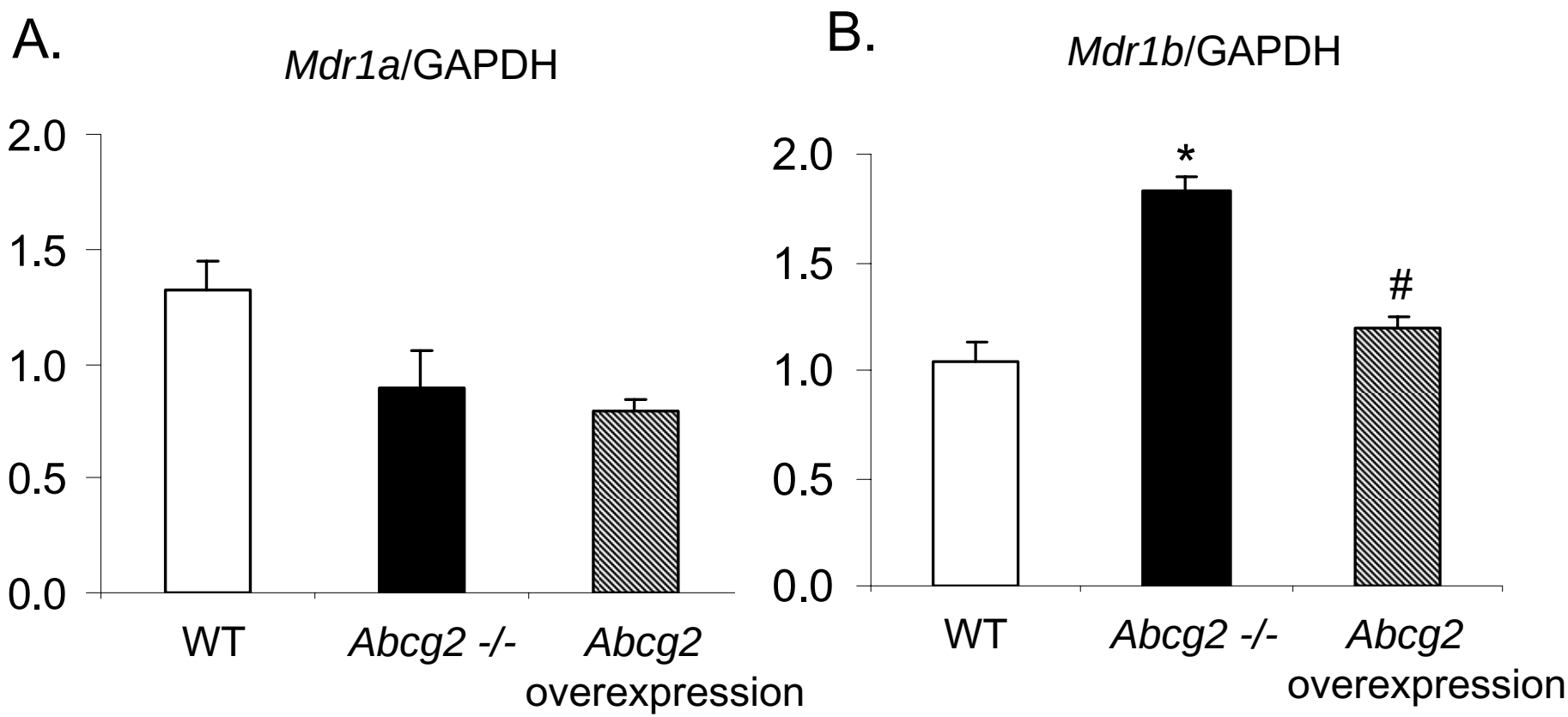

Online Figure II

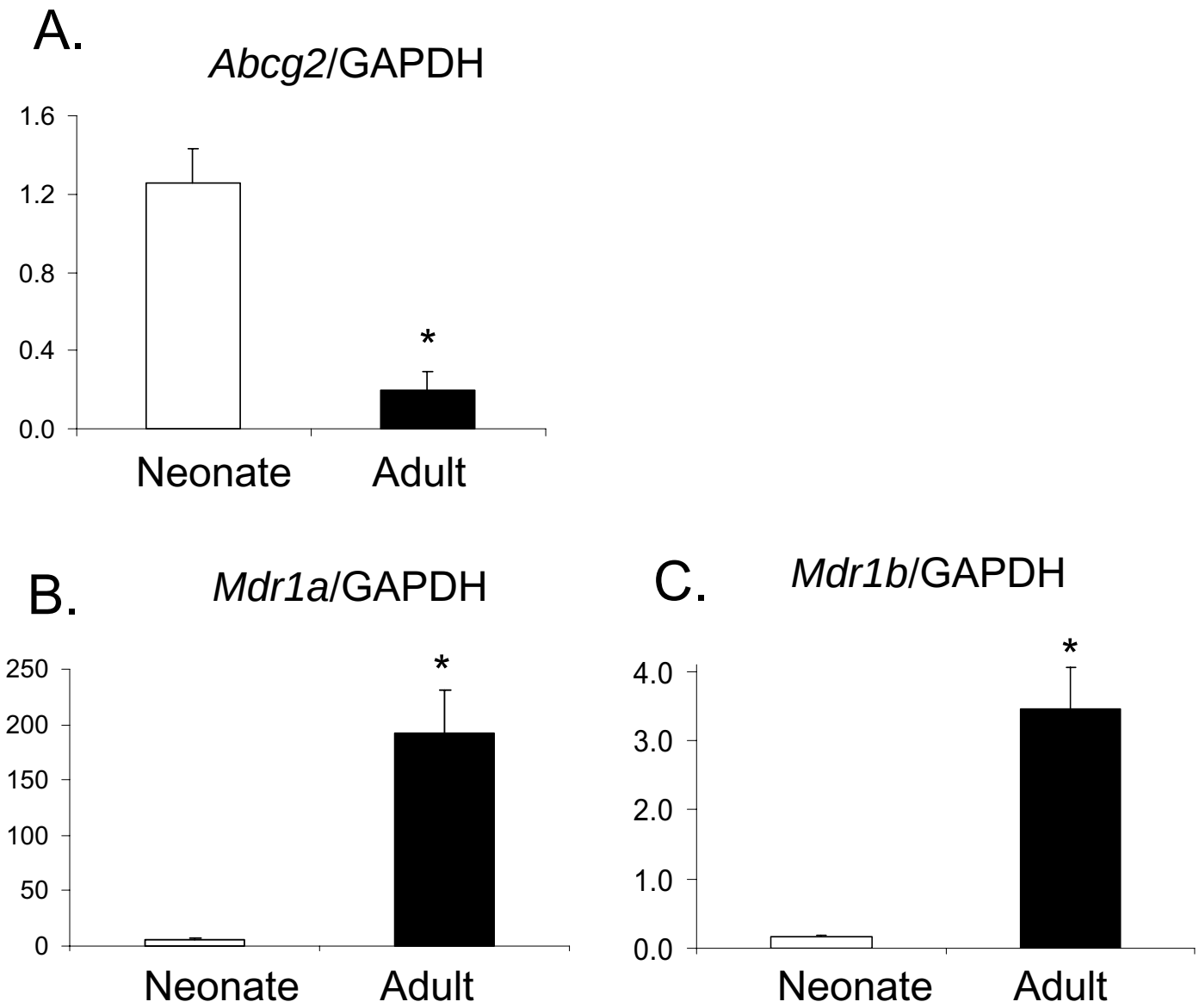

Online Figure I: Mdr1a/b gene expression in expanded WT, *Abcg2 -/-* and *Abcg2* over-expressing cSP cells. (A) *Mdr1a* and (B) *Mdr1b* mRNA levels normalized with GAPDH determined by quantitative RT-PCR (*, $p<0.05$ vs. WT, #, $p<0.05$ vs. *Abcg2 -/-*). Data are presented as relative fold changes to the WT cSP cells.

Online Figure II: *Abcg2 and Mdr1a/b gene expression is regulated in an age-dependent fashion.* **(A)** *Abcg2*, **(B)** *Mdr1a*, and **(C)** *Mdr1b* mRNA normalized to GAPDH using quantitative RT-PCR ($p < 0.05$).